UNIVERSITEIT VAN PRETORIA
UNIVERSITY OF PRETORIA
YUNIBESITHI YA PRETORIA
Denkleiers • Leading Minds • Dikgopolo tša Dihlalefi

Towards paper-based micro bio-sensing of biomarker anti-mycolic acid antibodies for TB diagnosis

by

Alma Truyts

Submitted in partial fulfilment of the requirements for the degree

Magister Scientiae

Biotechnology

In the Faculty of Natural & Agricultural Sciences

University of Pretoria

Pretoria

June 2019

Declaration of originality

I, Alma Truyts declare that the dissertation, which I hereby submit for the degree MSc (Biotechnology) at the University of Pretoria, is my own work and has not previously been submitted by me for a degree at this or any other tertiary institution.

Plagiarism declaration

1. I understand what plagiarism is and am aware of the University's policy in this regard.
2. I declare that this MSc dissertation is my own original work. Where other people's work has been used (either from a printed source, Internet or any other source), this has been properly acknowledged and referenced in accordance with departmental requirements.
3. I have not used work previously produced by another student or any other person to hand in as my own.
4. I have not allowed, and will not allow, anyone to copy my work with the intention of passing it off as his or her own work.

SIGNATURE: Alma Truyts

DATE: 20 June 2019

Acknowledgements

Jesus Christ In whom I live and move and have my being. My Glorious

Father who's faithful,
Jesus who's able,
who by His Spirit,
guided me into his light.
© Mary De Kock – Hatfield Christian Church, 'Come and have your way' 2014

Then, I am the most privileged MSc candidate ever as I had whole heaps of people with higher degrees and lofty titles helping me and giving me regular input throughout. As such I have a very lengthy acknowledgements list! A huge thank you then,

Primarily to my Supervisors: **Prof Jan Verschoor, Dr Yolandy Lemmer and Shavon David** for all their feedback, help and encouragement throughout. You are truly the best supervisors I've heard of!

Prof – thank you especially for pushing me to communicate clearly what I mean and for finding positives even when that required 'liquid courage' assistance.

Yolandy – veral vir "Jy sukkel mooi!" en al die aanmoediging. Also for teaching me so so many things I needed to do this and will need to be in this field.

And Shavon – In general for your open door and essential help throughout. If ever there was an uncited reference you are it!

Also to my pseudo-supervisor **Dr Kevin Land** – Thank you for insisting on pictures and managing the great team I got to be a part of. Thank you also for reviewing parts of this document.

Then the MALIA project team in which soil this MSc grew:

Dr Heena Ranchod – for teaching me so many things I needed to know and for writing the paper that is the cornerstone for much of my work. Also for expressing and purifying gallibodies for me.

Arthessa Ragavaloo, Mosa Molatseli – a huge thank you for all your work expressing and purifying gallibodies and purifying MA for me and for all the commiseration along the journey.

Thabang Noge, Ilse Du Preez, Lonji Kalombo – For diverse sets of help, in the lab, for reagents, for advice and ideas. I am super grateful!

Prof Anton Stolz – Thank you for making me feel like my enthusiasm covered over some of my sins and for encouraging that.

Kruger Goosen – For introducing me to and supplying the casein that had an enormous impact on my work, thank you.

Also to everyone else that attended and gave input and discussion in our fortnightly meetings. It has been an honour to work on this project.

And then to the wider ecosystem of people at the university, CSIR and elsewhere who were essential help at critical points especially…

Dr James Wesley-Smith – For your willing and expert help on the TEM visualisation and sample preparation. Especially for those beautifully smooth carbon coated grids which hereby receive due acknowledgement!

Christa Marais – For your help with the patent searches, you found me some golden references. Thank you.

Sandra van Wyngaardt – vir al die hulp met die liposome en andersins- baie dankie!

Susan Wemmer – For providing the unrelated gallibodies for my controls. Thank you.

Patric, Vusi, Andri and my colleagues at P & C – for your help on the DLS and whenever you found me wandering around your corridors.

Abesach Motlatle – for your very necessary help, advice and reassurance with my DLS data.

Dr Maretha O'Kennedy and Dr Robyn Roth – for loaning me essential reagents and letting me use your sonicator.

Dr Henriette Hobbs – for loaning me reagents and being a soundboard when I got stuck.

Everyone in the MMM competency area – For all your support and help in general.

And a very special mention to the **Microsystems Group – Kevin, Suzanne, Petroné, Louis, Shavon, Phophi and Thabang** thank you for all the help, advice and support. You will do great things!

CSIR for funding my MSc studentship and the thematic grant for the project funding.

Then for all the emotional and moral support an enormous thank you to all my friends and family especially…

To the office mates of destiny, **Thabang and Phophi** and all former inhabitants of F66, and ‘the cool kids’ lunch crew: **Angus, Willis, Yurisha, John, Kshir, Dillon, Roy, Petroné and Jamie** (and all the honorary, temporary, new as well as former members) thank you for being a consistent light spot in my days.

Also my immediate family – **Mamma, Pappa**, **Carina** en **Theo:** Dankie vir julle amazing geloof in my werk en al die ondersteuning en liefde en sorg. Also **Clare** and **Joseph** thank you for your support and love from afar.

And also **Forum/Reverb and church fam in general** – Thank you for taking care of me and backing me and praying for and with me. Also for listening to me talk about TB all the time and keeping my priorities straight!

Summary

Accessible point of care diagnosis of Tuberculosis (TB) is an essential development to better manage the global epidemic that infects 10 million people annually. Current diagnostics are centralised, causing patient loss to follow up or delays in treatment. Although serological diagnosis using finger-prick blood has been historically insensitive in the diagnosis of TB, the detection of anti-mycolic acid (MA) antibodies in patient sera has been shown to allow accurate diagnosis in HIV-positive, previously infected and TB exposed patients. MA is a unique lipid antigen of mycobacteria with anti-MA antibodies being formed early upon infection in a T-cell independent pathway.

This work aimed to contribute towards the development of a lateral flow immunoassay termed MALIA (Mycolate Antibodies Lateral flow Immuno Assay). This diagnostic has the unique lipid antigen MA as the immobilised capture agent and custom developed monoclonal anti-MA chicken antibodies (gallibodies) as the labelled bio-recognition element.

Casein hydrolysate was newly applied as a blocker in enzyme-immuno assay (EIA) to characterise the functionality of the gallibodies in order to circumvent import restrictions on bovine milk products. MA dissolved in hexane and immobilised on nitrocellulose was not detected by the passively conjugated gold labelled gallibody conjugate in the lateral flow test (LFT) format, despite the confirmation with lipid staining and EIA that MA remained immobilised and antigenic on nitrocellulose. Various substrates, blockers and running buffers were explored for the LFT to attempt to detect MA.

The method of passive conjugation of the gallibodies to gold nanoparticles was chosen as this is a commonly successful and simple strategy for conjugate preparation in LFTs. Initial characterisation of gold labelled gallibody conjugate suggested that the orientation of the gallibody on the nanoparticle may be favourable for binding by anti-chicken antibody (the control) but not MA. The biological activity (MA binding) of the gold labelled conjugate was probed on alternative methods. The results showed that in EIA, gold labelling caused the loss of MA binding but not anti-chicken immunoglobulin binding. This is possibly due to the extra force in the wash steps caused by the presence of the gold nanoparticle. Interaction of gold labelled gallibody conjugate with antigenic MA nanoparticles in transmission electron microscopy showed loss of biological activity, while dynamic light scattering intensity measurement of the same interaction showed a weak interaction similar to that seen between gold labelled bovine serum albumin conjugate with fatty acid coated nanoparticles.

To address the challenges uncovered by this research, gallibodies can be re-engineered to increase functional affinity (by increasing the valency) to be able to compensate for activity losses due to labelling. In addition, labelling of MA, rather than gallibodies may result in a

successful, inverted MALIA to meet the ultimate aim to drastically change the face of the TB epidemic at the critical fault line – point of care diagnosis. The promising avenues uncovered by this key explorative research must be pursued to actualise this critically important and non-standard LFT technology.

Table of Contents

Declaration of originality ii
Plagiarism declaration ii
Acknowledgements iii
Summary vi
Table of Contents viii
List of Figures xii
List of Tables xv
List of Abbreviations xvi
Chapter 1: Introduction 1
1.1 Tuberculosis overview 1
1.2 TB treatment 2
1.3 TB prevention 3
1.4 TB diagnostics 4
1.4.1 Patient specimens 4
1.4.2 Sputum culture 4
1.4.3 Sputum smear microscopy 5
1.4.4 Cepheid Gene Xpert™/ Gene Xpert Ultra™ 6
1.4.5 Alere™ Determine™ TB LAM Ag test 7
1.4.6 Radiography/ empirical diagnosis 7
1.4.7 Immune response tests for TB 7
1.4.7.1 Interferon gamma release assay 8
1.4.7.2 Tuberculin skin test 8
1.5 TB diagnostic landscape 8
1.5.1 TB laboratory networks 8
1.5.2 Treatment monitoring/ detection of drug resistance 9
1.5.3 Diagnostic algorithm 9
1.6 TB diagnostic gap 10
1.6.1 Pre-treatment loss to follow up 10
1.6.2 Requirements for a point of care diagnostic 11
1.6.3 TB diagnostic tests in development 13
1.7 Problem statement 14
1.8 Significance 14
1.9 Proposed format 15

1.10 Research aim and objectives 16
1.11 Scope and assumptions 17
1.12 Chapter outlines 17
Chapter 2: Detection of mycolic acid by custom developed anti-mycolic acid antibodies 19
2.1 Introduction 19
2.1.1 Antigens for serodiagnosis of TB 19
2.1.2 Mycolic acids as antigens 20
2.1.3 Anti-mycolic acid antibodies as biomarkers for TB 23
2.1.4 Detection of anti-mycolic acid antibodies in serum 24
2.1.5 Chapter outline 25
2.2 Materials and methods 25
2.2.1 Materials 25
2.2.1.1 Custom developed monoclonal antibody 25
2.2.1.2 Self-isolated mycolic acid 26
2.2.2 Enzyme Linked Immuno Sorbent Assay 26
2.2.3 Immunoblot tests 28
2.3 Results and discussion 29
2.4 Conclusion 33
Chapter 3: Lateral flow test development 34
3.1 Introduction 34
3.1.1 Lateral flow test format 34
3.1.2 A case study of a successful lateral flow test 35
3.1.3 Lateral flow tests for TB 38
3.1.4 Why another attempt at a lateral flow test for TB? 39
3.1.5 Lateral flow tests development considerations 40
3.1.6 Use of lipids, liposomes and lipoidal antigens in lateral flow tests 43
3.1.7 Chapter outline 44
3.2 Materials and Methods 44
3.2.1 Materials 44
3.2.2 Salt test to assess the conjugate stability 45
3.2.3 Gold labelled gallibody conjugate preparation 45
3.2.4 Lateral flow test manufacture 46
3.2.5 Phosphomolybdic acid staining 48
3.2.6 Alternative substrate investigation 48
3.2.7 Alternative blocker investigation 50
3.3 Results and discussion 50

3.3.1 Probing of absence of anti-mycolic acid gallibody signal on the test line 51
3.3.2 Alternative substrate investigation 52
3.3.3 Membrane blocker investigation 56
3.3.4 Running buffer investigation 58
3.4 Conclusion 60
Chapter 4: Labelled gallibody evaluation and alternatives 61
4.1 Introduction 61
4.1.1 Antibodies 61
4.1.2 Colloidal gold nanoparticles 64
4.1.3 Colloidal gold conjugation 67
4.1.4 Conjugate characterisation in literature 68
4.1.4.1 Transmission Electron Microscopy 68
4.1.4.2 Enzyme Linked Immuno Sorbent Assay 71
4.1.4.3 Dynamic Light Scattering 72
4.1.5 Chapter outline 74
4.2 Materials and methods 74
4.2.1 Materials 74
4.2.2 Anti-chicken IgG (Fc) antibody controls 74
4.2.3 Visible spectrum salt tests 75
4.2.4 Enzyme Linked Immuno Sorbent Assay using gold labelled conjugate 76
4.2.5 Dynamic Light Scattering 77
4.2.6 Transmission Electron Microscopy 78
4.3 Results and discussion 79
4.3.1 Gold conjugate evaluation 79
4.3.1.1 The binding of gold labelled gallibody by anti-chicken IgG (Fc) antibody 79
4.3.1.2 The effect of coating conditions on gold labelled gallibody 82
4.3.2 Functional characterisation of gold labelled gallibody conjugate 89
4.3.2.1 Conjugate interaction with MA coated on a microtiter plate – ELISA 89
4.3.2.2 Conjugate interaction with MA nanoparticles – DLS 96
4.3.2.3 Conjugate interaction with MA nanoparticles – TEM 99
4.4 Conclusion 105
Chapter 5: Concluding Discussion 107
6. References 112
Appendix A 133

A1. LFT detection of *E. coli* 0157:H7 by gold labelled anti-*E. coli* antibody conjugate 133

Appendix B 134

B1. TEM images of conjugate interaction with MA nanoparticles..... 134

List of Figures

Figure 1.1: *Mycobacterium tuberculosis* visualised by sputum smear microscopy……..…6

Figure 1.2: WHO laboratory network classifications…….8

Figure 1.3: Simplified South African TB GeneXpert based diagnostic algorithm……...10

Figure 1.4: Proposed composition of MALIA……...16

Figure 2.1: Structures of the two types of vectors used for the gallibody engineering……26

Figure 2.2: Schematic of direct and indirect ELISA……...27

Figure 2.3: Direct ELISA to compare sports supplement and biochemical reagent casein blockers by titration of antibody coating concentration……..….29

Figure 2.4: Indirect ELISA to compare sports supplement and biochemical reagent casein blockers for detection of gallibodies on MA coated plate……..….30

Figure 2.5: Indirect ELISA to compare casein hydrolysate and biochemical reagent casein as blockers for detection of gallibodies on MA coated plate……...31

Figure 2.6: Immunoblot test to determine antigenicity of MA spotted on nitrocellulose membrane. ……..32

Figure 3.1: The standard lateral flow test format. ……...34

Figure 3.2: Mode of action of the sandwich (A) and competitive (B) formats of the lateral flow immunoassay. ……35

Figure 3.3 A: Schematic representation of the progressive development of the Rapid HIV test B: Example of test results for a fifth generation rapid HIV test. ……....37

Figure 3.4: Receiver operating characteristic curve showing the specificity and sensitivity scores of the 19 commercial rapid tests for the diagnosis of pulmonary TB……...….39

Figure 3.5: WHO ASSURED criteria for POC diagnostics: peak feature trade-off in resource constrained healthcare settings. ……..40

Figure 3.6: Composition of the lateral flow test (A) and the half test (B). ……46

Figure 3.7: Test manufacture alignment process. ……48

Figure 3.8: Composition and steps followed for the flow through test format. ……..….49

Figure 3.9: Examples of unsuccessful detection of coated MA by gold labelled gallibody conjugate. ……51

Figure 3.10: Phosphomolybdic acid staining to confirm presence of MA on nitrocellulose…...52

Figure 3.11: Nitrocellulose membrane investigation to compare the effect of membrane properties on gold labelled gallibody conjugate binding. ……..53

Figure 3.12: Flow through tests using direct washing comparing the effect of paper type and reaction time on signal intensity. ……..55

Figure 3.13: Flow through tests with gentle washing comparing the effect of paper type and reaction time on signal intensity. ……..….56

Figure 3.14: Half tests comparing commercial Invitrogen blocker to casein blockers by gold labelled gallibody conjugate binding. ……..…..57

Figure 3.15: LFTs comparing commercial Invitrogen blocker to casein hydrolysate by gold labelled gallibody conjugate binding. ……...58

Figure 3.16: Half tests comparing different running buffers by gold labelled gallibody conjugate binding. ……..……59

Figure 4.1: Labelled representation of the structure of an antibody. ……62

Figure 4.2: Multivalent antibody immunoglobulin (Ig) isotypes. ……...63

Figure 4.3: Bright red colour of differently sized colloidal gold nanoparticle suspensions. …...64

Figure 4.4: Visible absorbance spectra of colloidal gold nanoparticles of varying sizes. ……..65

Figure 4.5: Graphical representation of the electrical double layer describing the electrostatic potential (ψ) near a charged colloidal particle. ……66

Figure 4.6: Colloidal suspension stabilisation strategies. ……..66

Figure 4.7. Flocculation curves (absorbance at 580 nm) for colloidal gold (25 nm) sols stabilised with increasing concentrations of monoclonal (A) or polyclonal (B) antibodies…….68

Figure 4.8: Examples (A, B and C) of TEM images using gold nanoparticle labelling to enhance visualisation. ……...69

Figure 4.9: TEM visualisation of binding of differently sized gold labelled antibody conjugates in ELISA-like protocol. ……70

Figure 4.10: TEM visualisation of binding of differently sized gold labelled antibody conjugates incubated in liquid. ……..71

Figure 4.11: The effect of protein orientation on hydrodynamic diameter of conjugates……...73

Figure 4.12: LFTs comparing the signal intensity of gold labelled gallibody conjugate at a concentration range of immobilised anti-chicken Ig antibodies. ……..79

Figure 4.13: Half tests to compare binding of immobilised anti-chicken IgG (Fc) antibodies by gold labelled gallibody 18-2 and BSA conjugates. ……..…….…….80

Figure 4.14: Half tests comparing the signals obtained on immobilised anti-chicken IgG (Fc) antibodies and PBS using all six gallibodies conjugated to gold.……..…….81

Figure 4.15: Two dimensional representation of possible orientations of gallibody conjugated to gold nanoparticles. ……82

Figure 4.16: Visible wavelength absorbance spectra showing surface plasmon resonance bands of three conditions of colloidal gold suspensions: stable, conjugated to gallibody and aggregated. ……83

Figure 4.17: Visible wavelength absorbance spectra showing surface plasmon resonance bands of colloidal gold conjugated to a range of gallibody 12-2 concentrations: 1(A), 1.5(B), 10(C), 40(D) µg/mL. ……...84

Figure 4.18: Gold labelled gallibody 12-2 conjugate stability at varying gallibody concentration shown by: (I) conjugate colour after NaCl addition, absorbance curves at (II) 520 nm the plasmon resonance wavelength and at (III) 580 nm as an indicator of flocculation, and (IV) binding by immobilised anti-chicken IgG (Fc) antibodies. ……..……85

Figure 4.19: Gold labelled gallibody conjugate stability at varying pH shown by: (I) visible wavelength absorbance spectra at a range of gallibody 12-2 concentrations; (II) absorbance curves at 580 nm and 520 nm at varying gallibody 12-2 concentration and (III) binding of immobilised anti-chicken IgG (Fc) antibodies by gold labelled gallibody 18-2 conjugates…...88

Figure 4.20: Indirect ELISA system test using *E. coli* as antigen with gold labelled anti-*E. coli* antibody conjugate and anti-*E. coli* antibodies as primary antibody to establish the method of antibody functionality determination after gold conjugation. ……90

Figure 4.21: Sandwich ELISA control test using anti-chicken IgG (Fc) antibody as capture antibody with gold labelled gallibody 12-2 conjugate or gallibody 12-2 as antigen to be detected to confirm anti-chicken IgG (Fc) binding of gallibody after conjugation.……..92

Figure 4.22: Indirect ELISA test using MA as antigen with gold labelled gallibody 12-2 conjugate or gallibody 12-2 as primary antibody to determine MA binding functionality of gallibody after conjugation. ……...94

Figure 4.23: Hydrodynamic diameter distributions of PLGA nanoparticles with and without MA. ……..96

Figure 4.24: Hydrodynamic diameter distributions of gold labelled gallibody 18-2 conjugates (A) and uncoated colloidal gold (B). ……..97

Figure 4.25: Hydrodynamic diameter distributions of gold labelled gallibody conjugates (A) and uncoated gold (B) incubated with PLGA nanoparticles with and without MA. ……..……..98

Figure 4.26: TEM images of PLGA nanoparticles with MA (A) and without (B). ……..…100

Figure 4.27: TEM images of gold labelled gallibody 18-2 (A) and BSA (B) conjugates…...…101

Figure 4.28: TEM images of gold labelled gallibody 18-2 (top) and BSA (bottom) conjugates incubated with MA-PLGA nanoparticles (A) and PLGA nanoparticles (B). ……..102

Figure 4.29: TEM images of *E. coli* bacteria (A) and gold labelled anti-*E.coli* antibody conjugate (B). ……103

Figure 4.30: TEM images of *E. coli* bacteria incubated with gold labelled gallibody 18-2 conjugate (A); gold labelled BSA conjugate (B) and gold labelled anti-*E.coli* antibody conjugate (C). ……104

List of Tables

Table 1.1: Optimal and minimal requirements for a point of care TB diagnostic……....12

Table 1.2: POC tests assessed according to the ASSURED criteria……...13

Table 3.1: Nitrocellulose membrane properties…….……53

List of Abbreviations

BCG	Bacillus Calmette-Guerin
CDR	complementarity determining region
CF	cellulose fibre
CFU	colony forming units
C_H	constant heavy domain
C_H1-4	scaffold containing constant heavy domains 1 – 4
C_H2-4	scaffold containing constant heavy domains 2 – 4
DLS	dynamic light scattering
DNA	deoxy-ribonucleic acid
DOTS	directly observed short course
DST	drug-susceptibility testing
ELISA	enzyme linked immuno sorbent assay
Fab	fragment antigen binding
Fc	fragment crystallisable
FIND	Foundation for Innovative New Diagnostics
GXP	GeneXpert
HIV	human immunodeficiency virus
HRP	horse radish peroxidase
IGRA	interferon gamma release assay
K_A	association constant
K_D	dissociation constant
LAM	lipoarabinomannan
LED	light emitting diode
LFT	lateral flow test
LPA	line probe assay

MA	mycolic acid
MALIA	mycolate antibodies lateral flow immunoassay
MDR-TB	multiple drug resistant tuberculosis
MES	2-(N-morpholino) ethanesulfonic acid
Mtb	*Mycobacterium tuberculosis*
MTB/RIF	*Mycobacterium tuberculosis*/Rifampicin (GeneXpert test name)
NPV	negative predictive value
OD	optical density
PBS	phosphate buffered saline
PEG	poly-ethylene glycol
pI	iso-electric point
PLGA	poly$_{DL}$-lactic-co-glycolic acid
PMoA	phosphomolybdic acid
POC	point of care
PPV	positive predictive value
RIF	rifampicin
rpm	revolutions per minute
RT	room temperature
scFvs	single chain variable fragment (antigen binding antibody fragments)
SPR	surface plasmon resonance
TB	tuberculosis
TEM	transmission electron microscopy
TMB	tetramethylbenzidine
TPP	target product profile
TDR	Special programme for Research and Training in Tropical Diseases
TST	tuberculin skin test

USA	United States of America
VH	variable heavy domain
VL	variable light domain
Vis	Visible – referring to the visible light wavelengths
WHO	World Health Organisation

12-1	Gallibody clone number 12 engineered into C_H1-4 scaffold
12-2	Gallibody clone number 12 engineered into C_H2-4 scaffold
16-1	Gallibody clone number 16 engineered into C_H1-4 scaffold
16-2	Gallibody clone number 16 engineered into C_H2-4 scaffold
18-1	Gallibody clone number 18 engineered into C_H1-4 scaffold
18-2	Gallibody clone number 18 engineered into C_H2-4 scaffold

Chapter 1: Introduction

1.1 Tuberculosis overview

Tuberculosis (TB) is arguably the most successful human disease in existence. This infection, usually of the lungs, by the bacterium *Mycobacterium tuberculosis* (Mtb) has followed humanity for millennia [1]. The World Health Organisation (WHO) estimates that ten million people fell ill with TB in 2017 with ~ 1.6 million deaths resulting [2]. Despite the availability of treatment and a partially effective vaccine, TB is still the leading cause of death from a single infectious agent globally [2,3].

Many of the challenges in the control of Mtb relate to its slow growth – a doubling time of 12 – 24 hours under optimal laboratory conditions [4] and 25 – 32 hours within the (infected) macrophage [5]. The slow growth prolongs the time to diagnosis by culture to about two to six weeks by the reference standard solid culture based method [5]. Resultant delays to the start of treatment of patients naturally contribute to the spread of the disease.

The lethargic growth rate also makes the disease slow to treat as antibiotics tend to target active bacteria. Effective treatment requires intensive chemotherapy for at least six months but can increase to two years [5]. Patients begin to feel better long before the bacteria are eliminated, and the treatment has significant side effects; both of which contribute to patients defaulting (stopping treatment before completion) [6]. Patient defaulting allows the development of drug resistant bacteria – a further significant problem in the control of the disease [6].

A further weapon in the arsenal of this bacterium is its ability to persist in the human host in a dormant state – known as a latent infection. Tuberculosis is spread through bacteria in the air coughed up by people with pulmonary TB [2]. It is estimated that 1.7 billion people globally (~ 1/5th of the global population) are infected. However, only 5 – 10% of successfully infected people will develop TB symptoms [2,7]. High risk populations include patients that are human immuno-deficiency virus (HIV) positive, malnourished, diabetic, smokers or excessive alcohol consumers [5].

The picture is, however, more complex than just latent or active infections. Drain *et al.* [3] propose a continuous spectrum of disease states between latent and active (symptomatic) infection which they break down into five states. In the first state the patient is exposed to Mtb, but the infection is eliminated [3]. In the second state, latent TB infection, the patient has viable, persistent Mtb bacteria [3]. In the third state, incipient TB infection, the Mtb bacterium have "metabolic activity to indicate ongoing or impending progression of infection" [3]. In subclinical

TB disease, the fourth state, patients present with “radiographic abnormalities or microbiological evidence of active, viable Mtb” [3]. Finally in active TB, patients present with symptoms of TB disease [3]. Recently, Weiner *et al.* [8] found metabolomics signatures consistent with the development of subclinical disease before active TB in ‘progressing’ patients (household contacts of active TB patients followed for ~ two years).

These progressive states make it difficult to diagnose active TB, because active immune response to TB antigens, clinical TB symptoms and the detection of live mycobacteria could singly or combined not necessarily distinguish between latent or active infection with, or mere exposure to Mtb. Detection of these common biomarkers will then give false positive results. This makes diagnosis especially difficult in high disease burden populations [9].

A further challenge complicating the TB epidemic is the concurrent HIV epidemic. HIV positive patients are at high risk for infection due to their reduced immune function [5]. The WHO estimates that 300 000 HIV positive patients succumbed to TB in 2017 – the leading cause of death in HIV patients [2]. Diagnosis in these patients is also difficult as their infections are characterised by poor immune response – the main source for biomarkers of infection.

1.2 TB treatment

TB treatment is divided into two phases, an intensive phase and a continuation phase. In the case of drug susceptible TB these phases are two and four months long respectively [5]. In the intensive phase four TB drugs are taken daily while these are reduced to two during the continuation phase [5]. The TB drugs that are taken throughout the treatment are Rifampicin and Isoniazid [5]. The latter drug targets actively dividing bacteria while the former will also kill dormant cells [5]. The most commonly applied additional drugs (used only during the intensive phase) are Pyrazinamide and Ethambutol [5].

Due to the widespread problem of treatment non-compliance, health care practitioners are recommended to directly observe patients taking their medication, either through home visits by mobile units or daily clinic visits [5]. This strategy was named DOTS for directly observed treatment short-course [5].

In the case of drug resistant TB less effective, more toxic and more expensive drugs need to be used [6]. The newly diagnosed patient is started on a standardised regimen until (where available) the patient’s drug susceptibility tests are available to enable the design of a personalised treatment regimen [5]. Generally in the case of drug resistant TB the intensive phase lasts 6 months and the continuation phase 18 [6]. The intensive phase requires the observed administration of drugs, including injectable ones [6]. Patients with drug resistant TB

are admitted (if possible) to multiple drug resistant (MDR) TB hospitals for at least the intensive phase of treatment [6].

Even drug susceptible TB requires a minimum of six months of treatment and these drugs often have severe side-effects, not all of which can be treated or are reversible [5]. These side effects include, among other symptoms: peripheral nerve damage, nausea, joint pains, rashes, deafness, visual impairment and liver damage [5]. The South African National Department of Health TB guidelines (which are based on WHO recommendations) recommend the prescription of vitamin B6 to prevent/overcome nerve damage caused by isoniazid [5]. Other side effects such as nausea and visual impairment cease upon the cessation of treatment. Hearing loss, however, is permanent [5].

1.3 TB prevention

TB prevention interventions include the vaccination of children, the treatment of latently infected patients at high risk of progression and the prevention of transmission.

The only currently WHO approved vaccine against TB is the Bacillus Calmette-Guerin (BCG) vaccine that was introduced in the 1920s [10]. This vaccine is recommended for neonates to protect infants and children from more serious forms of TB such as TB meningitis and disseminated (non-pulmonary) TB [5]. However the vaccine does not prevent wider transmission of TB as it has poorly protective effects in adults [10].

As part of the strategy to disrupt TB transmission and reach the 2030 'End TB' goals the WHO has recommended the prophylactic treatment of latently infected TB patients and patients at risk of contracting active TB disease (such as HIV positive patients and household contacts of MDR-TB patients) [11]. Prophylactic treatment involves the use of one or two first-line TB drugs for three to six months based on the TB disease burden in that country [11].

Prevention of transmission involves administrative, environmental and personal infection protection measures especially in aggregate health care facilities to protect healthcare workers [2]. The WHO policy on TB infection control cites early and rapid diagnosis and management of TB patients as the bedrocks of infection control [12]. This policy emphasizes the need to reduce diagnostic delays and start treatment as quickly as possible in addition to measures such as ventilation, reduction of over-crowding (in congregate areas such as prisons) and particulate respirators for healthcare workers [12].

The risk of nosocomial infection is known to be very high in South Africa and infection control measures are not consistently applied or understood [13,14]. Healthcare workers in South Africa have an incidence rate of TB that is double that of the general population [15].

1.4 TB diagnostics

Due to the lack of a widely protective vaccine and the cost and health implications of prophylactic treatment the most essential tools in the current management of TB are diagnostics. Besides diagnosis, these tests are also used to monitor treatment success (and thus detect drug resistant strains). All diagnostic tests have advantages and disadvantages related to their features, where they can be used, the specimens they require etc. [16]. The currently employed TB diagnostics will be outlined hereafter followed by a description of the landscape these are used in.

1.4.1 Patient specimens

The most commonly used patient specimen for diagnosis is sputum. Sputum is not saliva or nasal secretions, it is a "thick, mucoid, white-yellow, and sometimes blood-tinged" specimen coughed up or 'expectorated' from the lower airways and lungs [17]. If a patient struggles to produce the desired specimen sputum can be induced by aerosol inhalation [17]. As can be deduced from this description, collection of sufficient quality (minimal salivary content) and quantity (2 – 3 mL) of sputum from a patient is an invasive and uncomfortable procedure and not usually feasible for children. This is significant as 10% of TB cases are in children globally [2]. The quality of the sputum also affects sensitivity of the test [18].

A sputum sample would also not allow diagnosis of extra-pulmonary TB [17]. This is important, as 14% of notified TB cases in 2017 were of non-pulmonary TB [2]. HIV co-infected patients are often sputum negative. As TB is the leading cause of death among people with HIV [2] the use of an alternative patient sample to sputum to diagnose TB in these patients would be needed.

1.4.2 Sputum culture

The reference standard against which all diagnostic tests are measured is bacterial cell culture (liquid or solid). This method involves a two to six week culturing step that must be carried out in a biosafety level 3 laboratory by trained technicians [19]. The time for culture depends on whether the bacteria are cultivated in liquid or solid media and the status of the sample (positive/negative) [5]. A positive sample may be detected in as little as ten days while a sample is declared negative only if no growth is present after six weeks [5].

Automated systems such as the BACTEC™ Mycobacteria Growth Indicator Tube (MGIT™) 960 system have been developed for the liquid culturing system to limit the technician contact time. In this method the patient sample is inoculated into a tube containing growth media, a growth enhancing supplement and a non-mycobacteria inhibition cocktail [19]. The detection is effected by depletion of the oxygen in the media resulting in an oxygen quenched fluorophore

fluorescing [19]. However, the inhibition cocktail is not fail proof resulting in contamination from other bacteria commonly present in patient samples [19].

In the case of solid media growth of mycobacterium, selective agar based media is inoculated with decontaminated and concentrated sputum specimens and grown for a number of weeks [17]. Use of solid media is cheaper and easier than liquid media and is also less prone to contamination. However, the system is prone to errors due to manual reading of the results [5]. This is done by looking at the plate and identifying characteristic Mtb colony formation and confluence followed by mycobacteria detection tests such as acid fact bacilli staining as used for sputum smear microscopy diagnosis [17].

It is important to note that although this is the reference standard method it is not 100% sensitive, because of the prevalence of contaminant bacteria in sputum and the need to inhibit these [16]. The culturing method often misdiagnoses TB in HIV positive patients, because Mtb from their sputum is often undetectable by culture [16]. In high HIV-TB coinfection prevalence populations, often associated with diagnostic resource constraints, HIV positive patients with TB symptoms are often treated without microbiological confirmation of their diagnosis (this is called empirical diagnosis). Positive symptomatic response to TB treatment despite a negative culture result must then be confirmed (by patient follow up) and recorded if patient specimens are to be used for the evaluation of diagnostic tests [20]. Thus patient response to treatment is the ultimate reference standard.

1.4.3 Sputum smear microscopy

The most widely used diagnostic near the point of care (POC) is sputum smear microscopy. 'Near' the POC denotes the possible use of this method in peripheral level laboratory facilities but not at the point of decision by the health care worker [21].

In this method the non-mycobacteria are killed and removed by centrifugation before the specific staining of the sample. The staining selectively stains acid-fast mycobacteria versus the other organisms and debris in the sample [17]. The stained bacteria are then examined under a microscope (figure 1.1) [17].

However, this method requires laboratory facilities and trained technicians and often results in false negatives in HIV patients. This method is also used to track treatment success to determine the presence of drug resistance [5].

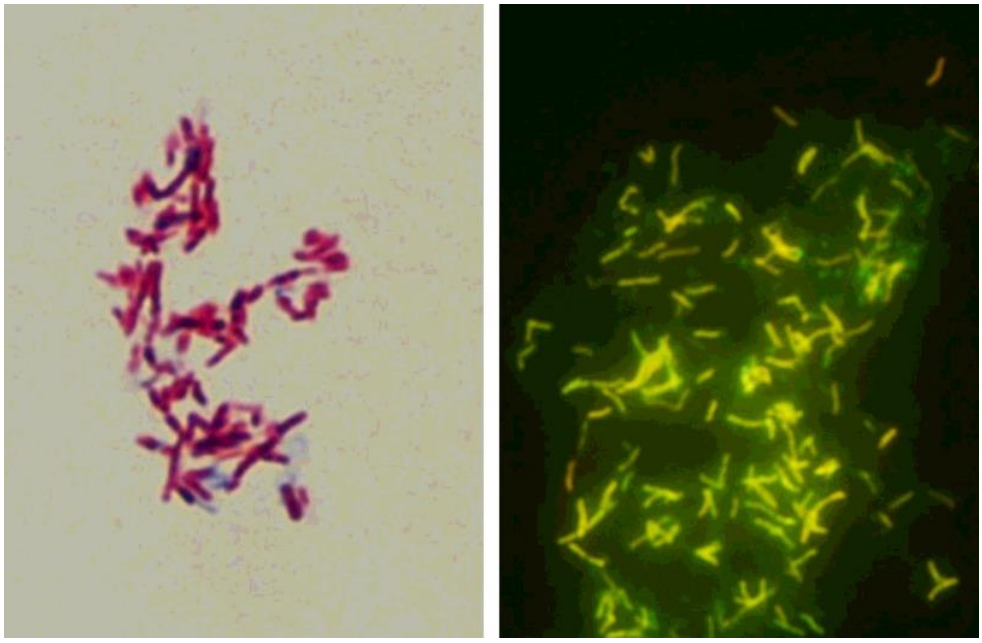

Figure 1.1: *Mycobacterium tuberculosis* visualised by sputum smear microscopy using the carbol fuchsin-based Kinyoun stain (left) and fluorescent auramine-rhodamine stain (right). Taken from Caulfield and Wengenack [22].

1.4.4 Cepheid Gene Xpert™/ Gene Xpert Ultra™

The best available 'rapid' diagnostic test, endorsed by the WHO [16] and the first line diagnostic test mandated by the South African National department of Health Guidelines is the Gene Xpert™ (GXP) [5]. This test is based on TB gene amplification usually from a patient sputum sample although other samples may be used (such as gastric aspirates, biopsies and bronchoalveolar lavages [23]).

The GXP has a sensitivity similar to that of liquid culture (~89%) and very high specificity (~99%)[16,24]. The GXP Ultra cartridge was introduced to overcome the comparatively lower sensitivity (~79%) [24] in HIV positive and smear negative patients. The sensitivity of the Ultra test is ~5% higher than the GXP, however as a trade-off the specificity is ~3.2% lower. Most notably the Ultra assay showed a pooled sensitivity improvement of 17% in smear negative patients [25,26]. Similar trends in comparing the Ultra to the GXP have been observed in the diagnosis of TB in children [27].

The specificity trade-off is especially prominent in patients with a history of TB infection. The GXP showed positive results almost a year after treatment completion [28] and lower specificity in relapse/repeat cases [29,30]. This has the effect of one in 40 – 70 false diagnoses and 10 – 500 unnecessary TB treatments per single TB death averted [25]. Given the severe side effects of TB treatment this is a significant drawback.

The GXP test is performed using disposable cartridges in an electricity dependent machine. As a result it is not generally affordable without concessional pricing, requires trademarked

components, air-conditioned laboratory facilities, skilled technicians and a minimum 0.5 mL patient sputum sample [21]. The GXP is considered a rapid test as results can be obtained in two hours, however this is only practical when a GXP instrument is available on site and minimal samples are collected at a time. Practically in South Africa samples are sent away to the nearest laboratory with GXP facilities and results are actioned in a target time of 48 hours [5]. This means that the problem of patient loss to follow up is not solved by this test [5].

1.4.5 Alere™ Determine™ TB LAM Ag test

This is a rapid lateral flow diagnostic that detects the presence of the glycolipid, lipoarabinomannan (LAM) in TB suspects' urine. LAM is present in the cell walls of mycobacteria and is detectable in the urine of patients with active TB infection. However, the accuracy of tests with LAM as a basis is poor when compared to currently used diagnostics except in patients with severe HIV infection where it performs better than the current diagnostics [31]. The WHO recently endorsed it for use only in diagnosing TB in "seriously ill" HIV positive patients with low CD4 cell counts [32]. Boyles *et al.* [33] found that it did not improve diagnostic yield where sputum induction was present but may still be considered for use due to cost savings.

1.4.6 Radiography/ empirical diagnosis

Chest x-rays are still widely used as an adjacent diagnostic test. Even though there is no absolutely diagnostic pattern, many visible effects are indicative of active or previous TB infection and taken with clinical symptoms is often considered sufficient to diagnose a patient [34]. This is called empiric diagnosis. Chest x-ray may be considered useful as an early diagnostic test but cannot be considered conclusive as normal x-rays are not uncommon in patients with active TB disease [34,35]. The use of chest x-ray to diagnose TB patients requires access to x-ray equipment and trained health care workers to interpret results.

1.4.7 Immune response tests for TB

Diagnostic tests measuring immune response biomarkers from patient serum are historically not successful for accurate diagnosis of active TB [9,16]. These tests include the Tuberculin Skin Test (TST) and the Interferon Gamma Release Assay (IGRA) and cannot distinguish between latent and active TB [5]. In high TB burden countries like South Africa, where most people would have a latent TB infection without any active disease symptoms or consequences, these tests would have little value [5]. These tests are not recommended by the WHO for use in low – middle income countries or for use in the diagnosis of active TB [9,16].

1.4.7.1 Interferon gamma release assay

IGRA measures T-cell response to TB in whole blood patient samples [9]. The result can be obtained in one visit and is not affected by BCG vaccination [9]. The test has low specificity and is recommended only to diagnose latent TB [9]. This test has not been able to predict progression to active disease [9]. A recent evaluation of available and second generation IGRA tests to diagnose active TB found that available IGRAs are not sufficiently sensitive to rule out TB, however second generation tests may be in a low incidence, high income setting [36].

1.4.7.2 Tuberculin skin test

This test cannot be used in previously diagnosed or vaccinated TB patients. It involves the injection of TB protein derivatives into a patient's skin and the size of the reaction (due to memory T-cell response) measured (in mm) two to three days thereafter [16,37]. This test is cheaper than the IGRA and so WHO does not recommend it be replaced by IGRA in low income or low incidence middle income countries [16,37].

1.5 TB diagnostic landscape

1.5.1 TB laboratory networks

The WHO sorts national TB laboratory networks into three tiers – peripheral, intermediate and central/reference levels (figure 1.2). These levels also mostly correspond to risk levels with peripheral laboratories associated with low risk and reference level with high risk – requiring conversant TB containment measures [16].

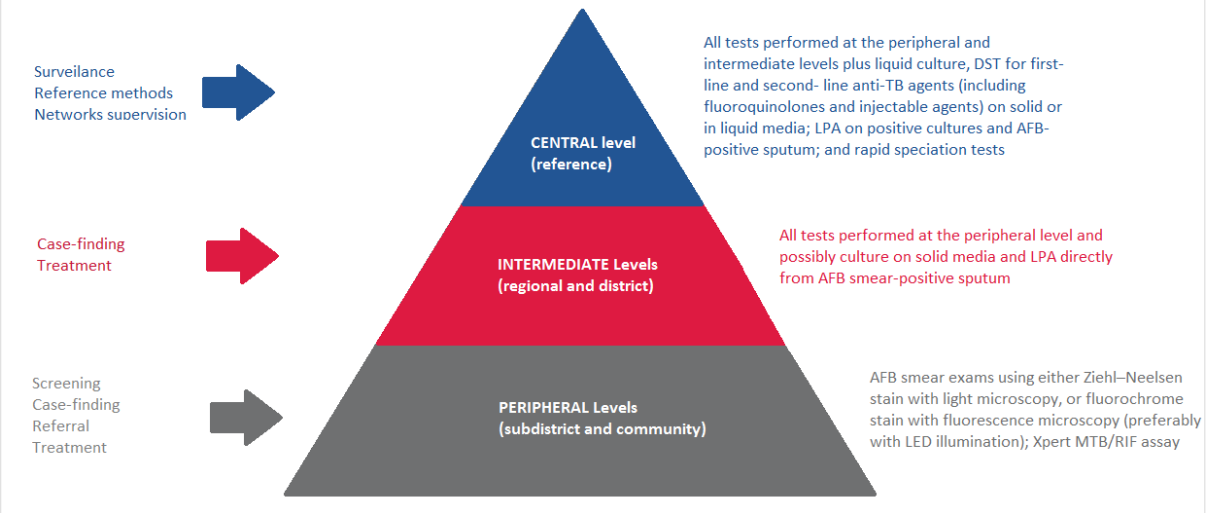

Figure 1.2: WHO laboratory network classifications. DST – drug-susceptibility testing, LPA – Line Probe Assay, AFB – Acid-fast bacteria, LED – Light emitting diode. Functions are given on the right and the tests that can be performed on the left. Adapted from the WHO policy framework for implementing TB diagnostics [16].

This sorting does not include that of the health post. This is the most decentralised location where many patients seek health care, like that of a local/rural clinic. The health post presumably serves about 60% of TB care seekers, does not have access to laboratory staff or equipment and often will lack access to electricity and water [38].

1.5.2 Treatment monitoring/ detection of drug resistance

A major problem in the management of the TB epidemic is drug resistance. Obviously, information about the susceptibility of a patient's TB strains to anti-TB medication will inform successful treatment regimes. However, these methods are not fail proof and add extra time to diagnosis.

Drug resistance can be detected by phenotypic or genotypic methods. In phenotypic methods culture grown from a patient specimen is inoculated into drug free and drug containing media and the viability of the culture is observed (called DST). Liquid culture systems are faster and considered more accurate for certain anti-TB agents than solid culture methods [5,16].

Genotypic methods involve the detection of resistance mutations in TB nucleic acid and provide results much faster than culturing methods. These tests are called Line Probe Assays (LPAs), are usable at lower biosafety level laboratories and are high through-put [16]. LPAs, however, cannot replace conventional DST for resistance to second line anti-TB drugs [16]. The GXP diagnostic test also simultaneously genotypically detects resistance to Rifampicin during diagnosis, however not all clinically relevant mutations are detected by this test [16].

1.5.3 Diagnostic algorithm

There is currently no diagnostic system capable of addressing each aspect of TB patient care. Such a diagnostic would need to allow fast and accurate diagnosis, treatment monitoring and drug susceptibility testing [16]. As a result WHO policy documents on the use of diagnostics are translated to a diagnostic algorithm that is specific to the local conditions. This algorithm is set up considering the prevalence of HIV-TB co-infection and drug resistant TB, the available (healthcare and laboratory) resources and the incidence and distribution of the disease at a national or regional level [16].

The inclusion of all these variables can be seen in the South African diagnostic algorithm in figure 1.3, taken from the most recently available National Department of Health TB management guidelines [5]. In South Africa, the GXP system has been widely deployed [39,40] leading to a GXP centric diagnostic algorithm. The South African National Department of Health TB management guidelines also sanction the use of sputum smear microscopy for diagnosis and treatment monitoring as well as culture (liquid and solid) for diagnosis and drug susceptibility testing [5].

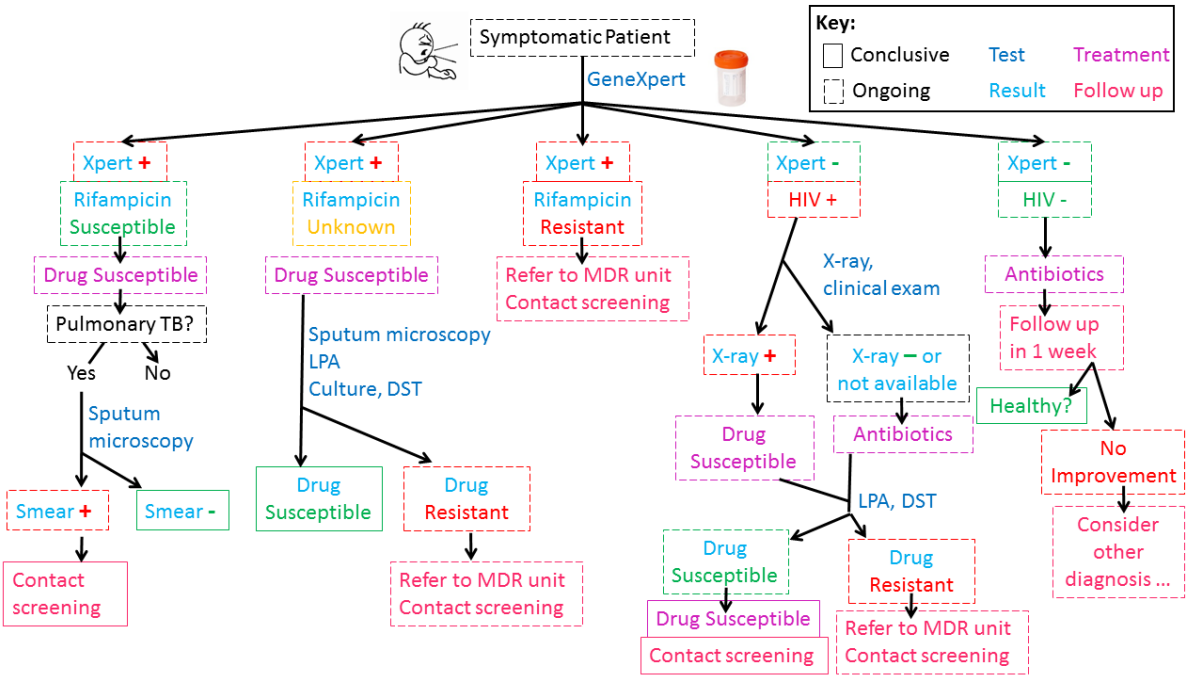

Figure 1.3: Simplified South African TB GeneXpert based diagnostic algorithm. LPA – Line Probe Assay, DST – Drug susceptibility test. A further case includes an unsuccessful GXP test whereupon another sample is collected from the patient and the cycle repeated. Adapted from South African National Tuberculosis Management Guidelines [5].

As can be seen in the algorithm even in the case of a negative GXP result in an HIV negative patient, further follow up is required to confirm the diagnosis. The algorithm also encourages the screening of persons who have been in contact with a positively diagnosed patient. Various algorithm approaches can be implemented to try to improve positive detection rates and decrease the number of diagnostic tests performed, but other trade-offs will be in play [35].

Despite the emphasis on the GXP test in the diagnostic algorithm (figure 1.3) many patients are still enrolled in treatment with only clinical evidence of disease, i.e. chest x-rays, symptoms, patient history etc. Empirical diagnosis is employed due to the high TB incidence rate and the likelihood of patient loss to follow up. A recent study in primary healthcare facilities in South Africa found that 15% of patients were started on TB treatment without laboratory evidence of TB and even for these cases the median number of visits prior to the start of treatment was three with almost four weeks between the first visit and the start of treatment [41].

1.6 TB diagnostic gap

1.6.1 Pre-treatment loss to follow up

In South Africa approximately 322 000 people fell ill with TB in 2017 of which approximately a third were not notified or not diagnosed according to the *2018 Global Tuberculosis report* [2]. A

2017 study in Indonesia on TB diagnosis and reporting found that 20% of new cases were not diagnosed “either because people do not access health care or because they are not diagnosed when they do” [2].

The WHO statistics reporting TB disease burden are the product of an informed estimation method. National TB incidence rates are determined by combining data from case notifications, TB prevalence surveys and research based or expert estimates of under-reporting and under-diagnosis [2]. The global estimate for TB incidence in 2017 is ten million cases, of which 67% were notified cases [2]. Furthermore of the 5.5 million notified cases of pulmonary TB, 56% were bacteriologically confirmed [2]. “A bacteriologically confirmed case is one from whom a biological specimen is positive by smear microscopy, culture or WHO recommended rapid diagnostic test, such as GXP MTB/RIF.” [2]. While these numbers paint a convincing picture of the gaps in TB surveillance and reporting they also allude to the lack of access to accurate diagnosis of this disease.

Pre-treatment loss to follow up of TB patients is a major problem facing the epidemic and centralised diagnosis a major factor in this problem [42]. Three quantitative studies in South Africa reported proportions of 22.5% [43], 33.7% [44] and 25% [45] of patients being lost to follow up. Qualitative studies investigating pre-treatment loss to follow up consistently find diagnostic delays and centralisation to be the main contributors to this problem [46,47]. In a study in Zimbabwe from 2012 – 2016 almost half of the patients lost to follow up (overall 20.8%) died [48]. This paints a strong picture of the still current requirement for a really deployable POC diagnostic in this field.

Another area of need is that of a screening test to conduct regular checks of people at increased risk of TB infection because of regular exposure/ higher than normal incidence rates such as healthcare workers, mineworkers, prisoners and families in contact with TB patients [49]. Screening tests are used before symptoms appear and can be an effective tool to prevent transmission- as applied in the case of the HIV epidemic [49]. The South African National TB management guidelines recommend stringent pre-placement screening and periodic medical examinations of all staff at healthcare facilities to attempt to reduce infection risk [5]. These screenings record previous as well as latent TB infections (from patient history as well as TSTs) and active TB symptoms, but only every six months [5].

1.6.2 Requirements for a point of care diagnostic

A serious gap in the current TB diagnostic landscape is a test that can be used at the so called health post level (i.e. POC) to immediately diagnose any TB patient using a non-invasively obtained sample [2].

The specific requirements for a POC TB diagnostic is outlined in the *High Priority Target Product Profile (TPP) for New Tuberculosis Diagnostics: Report of a Consensus Meeting* convened by the Global TB Programme of the World Health Organisation in April 2014 [50]. This product profile is expanded on and discussed by Denkinger *et al.* [51]. The summarised table from the consensus report is shown in table 1.1.

Table 1.1: Optimal and minimal requirements for a point of care TB diagnostic adapted from the *High Priority Target Product Profile for New Tuberculosis Diagnostics: report of a consensus meeting* convened by the Global TB Programme of the World Health Organisation in April 2014 [50].

Characteristic	**Optimal requirements**	**Minimal requirements**
Scope		
Goal	To develop a rapid biomarker-based test that can diagnose pulmonary TB and, ideally, also extra-pulmonary TB using non-sputum samples (such as, urine, blood, oral mucosal transudates, saliva, exhaled air) for the purpose of initiating TB treatment during the same clinical encounter or on the same day	
Target population	Target groups are adults and children including those who are HIV positive who are suspected of having active TB; this includes both pulmonary TB and extra-pulmonary TB in countries with a medium to a high prevalence of TB as defined by WHO (20 – 40/>40 cases per 100 000 population)	
Target user of test	Health-care workers with a minimum of training	Trained microscopy technicians
Setting (level of the healthcare system)	Health posts without attached laboratories (a level lower than microscopy centres)	Primary health clinics that have laboratories; peripheral microscopy centres

The general requirements for POC diagnostics in the developing world were recently updated to include ‘real-time connectivity’ and ‘ease of specimen collection’ to the ASSURED criteria (Affordable, Sensitive, Specific, User-friendly, Rapid and Robust, Equipment Free and environmentally friendly) to form the new acronym REASSURED [52]. Land *et al.* [52] assessed POC diagnostics in currently relevant infectious epidemics: HIV, Syphilis, Malaria, Chlamydia/Gonorrhoeae and TB shown in table 1.2. Except for TB all the POC diagnostics take the form of lateral flow tests (LFTs) demonstrating the excellent applicability of this technology in the diagnostic field. The TB diagnostic assessed here is the ‘near-POC’ GXP device with its limitations clearly evident in the ‘Rapid’ and ‘Deliverable’ fields [52].

Table 1.2: POC tests assessed according to the ASSURED criteria. Adapted from Land *et al.* [52]

Test Parameters	HIV	Malaria	Syphilis	Chlamydia/ Gonorrhoeae*	POC TB
Diagnostic target	Antibody	Antigen	Antibody	Antigen	DNA and RIF resistance
Test format	LFT	LFT	LFT	LFT with specimen processing	Nucleic acid amplification test
Affordable (US$)	1.00	0.50 – 0.75	6.00 – 7.00	6.00 – 7.00	10.00
Sensitive (%) **	>98		>75	>50	
Specific (%) **	>99.8		>92	>98	
User-friendly	3 steps	3 steps	3 steps	6-7 steps	Sample in, answer out
Rapid and Robust (min)	15-20	15-20	15-20	<60	90
Equipment Free	Yes	Yes	Yes	Yes	POC device
Deliverable	Yes	Yes	limited	Used in labs	Only with donor support

* *Chlamydia trachomatis/Neisseria gonorrhoeae*
**Compared to a laboratory-based reference standard assay.
LFT – lateral flow test, POC – point of care, DNA – deoxy-ribonucleic acid, RIF – Rifampicin.

In the ASSURED/REASSURED definitions, 'sensitive' is defined as a test with low false negatives and 'specific' as one with low false positives [52,53]. So an accurate test would have low false positives and negatives. The predictive value of a diagnostic test is then a measure of the probability of an accurate result. In the case of a negative (disease/condition absent) result, referred to as negative predictive value (NPV), a test with good NPV would have excellent sensitivity and could be used as a "rule-out" test. In the case of a positive (disease/condition present) result, referred to as positive predictive value (PPV) a test with good PPV would have excellent specificity and could be used as a "rule-in" test.

In the case of screening tests (used before symptoms appear) a rule out test is required, implying the need for good sensitivity. This is also true where the consequences of non-treatment far exceed those of incorrect treatment, in which case lower specificity can be tolerated [52]. However, the 'rapid test paradox' a term coined by Gift *et al.* [54] showed that an insensitive test that is deployable at the POC could have a higher diagnostic yield than a more accurate laboratory assay that requires patients to return to the healthcare facility for their results [52,54]. In cases where diagnosis has significant consequences in terms of treatment and lifestyle, such as for an incurable illness like HIV, high false positives are not acceptable and so these tests also require high specificity [55].

1.6.3 TB diagnostic tests in development

Improvements to current diagnostics to make them more deliverable or sensitive dominate the current pipeline. Cepheid is developing a battery powered version of the GXP with real-time

connectivity called the GXP Omni. This instrument is meant to allow decentralised testing for TB. However, this release has been delayed several times due to development challenges [56].

Some novel technologies have been identified by the Foundation for Innovative New Diagnostics (FIND) as at the proof of concept stage or beyond. FIND maintains a TB diagnostics pipeline status dashboard on their website [57]. The 'non-sputum' target product profile (table 1.1) for use at the community level (L0) is targeted by only two products in the FIND TB diagnostics pipeline. These tests are at the feasibility (level 1/8) and validation (level 3/8) status levels and involve technology to pre-concentrate urine samples for the more sensitive detection of Lf-LAM (section 1.4.5). [57] Patent searches of all the companies listed in the pipeline as targeting the TPP in table 1.1 did not yield any TB specific patents. This indicates a very non-diverse and thin pipeline targeting this essential TPP.

1.7 Problem statement

Current diagnostics for TB require invasive sample collection procedures and do not provide rapid results. As a result numerous patients are lost to follow up before they receive their diagnosis. In addition the WHO endorsed GXP system is generally not affordable without extensive sponsorship from international aid agencies and provides poor sensitivity in HIV-co-infected patients and children. Furthermore current diagnostics show a poor negative predictive value (i.e. even if the test is negative there is still a good chance the disease is present, shown in the prevalence of false negatives) with the result that minimal reliance can be placed on test results and further patient follow up is still required in the case of negative tests.

The proposed diagnostic method to overcome the above mentioned failings is a low cost rapid immunoassay for POC use with a novel competitive serodiagnosis methodology for detecting anti-lipid biomarker antibodies, unlike existing protein antigen-antibody based lateral flow technologies in the TB diagnostic field. This novelty is based on the use of custom made and unusual reagents in a competitive LFT. This project has investigated and developed methods to realise this diagnostic.

1.8 Significance

The realisation of a rapid and sensitive TB diagnostic that can be used at the POC by health workers has the potential to drastically change the face of the epidemic on a global scale by contributing to lessening the time to the start of treatment and consequently the further spread of the disease. In addition, the effectiveness of such a test in HIV positive patients could have

a concurrent impact on the HIV epidemic. Such a test would also address the current diagnostic gap in children as recognised by the WHO [21].

While the development, optimisation and testing of the complete device is outside the scope of an MSc, this project aims to make a practical contribution to the development of such a test by investigating and optimising methods which use novel and unusual reagents in a unique competitive model on a LFT.

1.9 Proposed format

The format and mode of action of the proposed test is outlined in figure 1.4. This test has been termed MALIA for mycolate antibody lateral flow immunoassay. The test relies on the detection of anti-mycolic acid (MA) biomarker antibodies in patient serum using a competitive LFT format. MAs are a lipid cell wall component of Mtb cells. Further discussion of the development and choice of the custom reagents and the rationale for their use will be laid out in subsequent chapters.

The proposed test will work as follows: in the case of a TB negative patient (top scenario, figure 1.4) the custom developed [58,59] gold labelled anti-MA chicken antibodies (gallibodies) will bind to the MAs on the test line and to the anti-chicken IgG (Fc) antibodies on the control line – forming two red lines. In the case of a positive TB patient (bottom scenario, figure 1.4) anti-MA antibodies in the serum will outcompete the labelled gallibodies for binding on the test line, reducing or removing its colour. A positive test will thus have only one line – the control line.

The functionality of the test hinges on the assumption that TB patient antibodies will have a stronger affinity for the MA antigen on the test line than the developed labelled gallibodies and will out compete them for binding on the test line, thus removing or reducing the colour. However, before this assumption can be interrogated the baseline (negative result) of the test needs to be established. The signal to be reduced must be clear and strong.

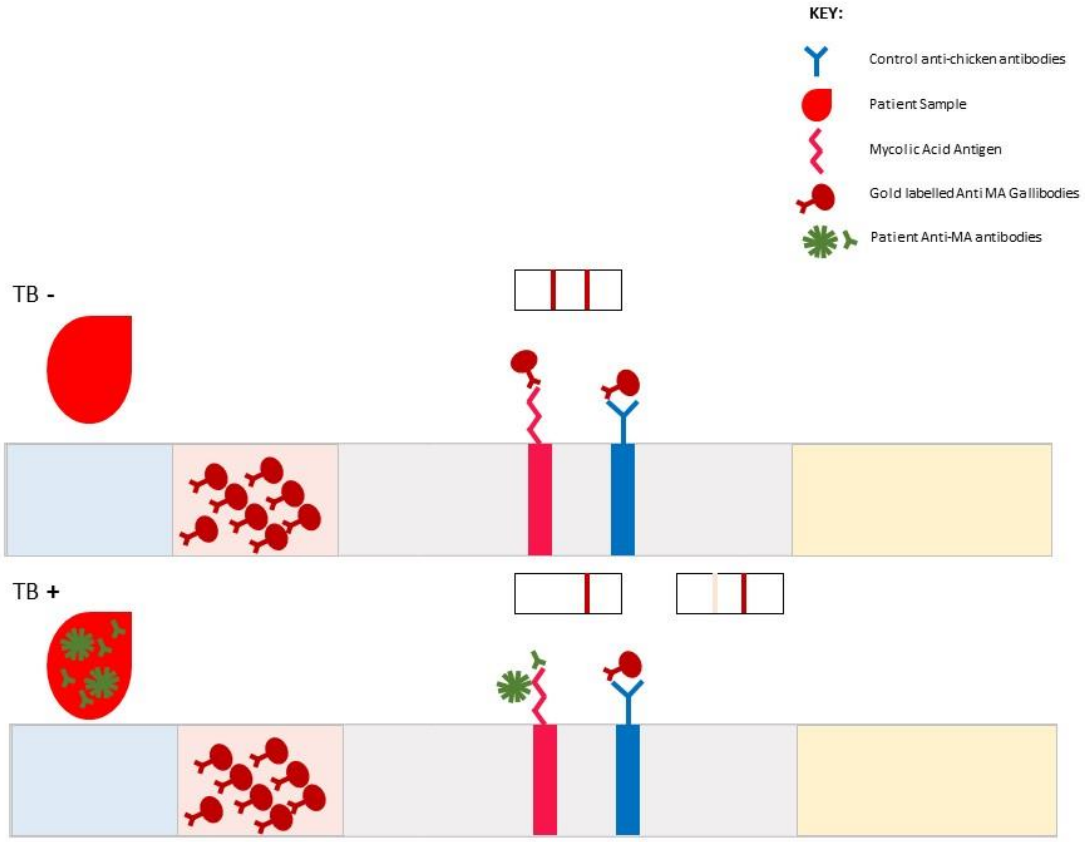

Figure 1.4: Proposed composition of MALIA. Custom developed reagent – monoclonal gallibodies to mycolic acids will be the conjugated labelled reagent (shown in maroon). Mycolic acid (MA) (pink) – the capture biomolecule – will capture the labelled monoclonal gallibodies in the absence of patient anti-MA antibodies. The labelled gallibodies will be captured by the control anti-chicken antibodies (blue) producing the second (control) line. Colours of the test and control lines are not representative. A sample from a TB negative patient (top) will produce two lines on the test. In a TB positive patient sample (bottom) anti-MA antibodies (green) will compete with the labelled gallibodies for binding to the immobilised MA, thus removing or reducing the colour of the test line. Free MA in patient blood will also prevent binding of the gallibodies to the test line. As such a TB positive sample will tend to produce only one line on the test.

The feasibility of this methodology will be evaluated in the course of this study. The primary source of novelty lies in the use of a lipid antigen, MA, on the test line and the exploitation of the relatively weak lipid antigen – antibody reaction in an otherwise standard competitive LFT architecture. In addition certain parameters are unknown due to the use of custom developed monoclonal antibodies.

1.10 Research aim and objectives

To determine specifications required to manufacture a POC, competitive lateral flow immunoassay that uses readily available and highly specialised reagents. These include a MA

(lipid) antigen as the capture agent and recombinant monoclonal chicken anti- MA antibodies as the detector.

The objectives to address this aim are to develop and evaluate:

1. the deposition of the mycolic acid antigen (lipid) test line and antibody (anti-chicken IgG (Fc) antibodies) control line on paper substrates and the adaptation of the conditions of the test
2. the process for labelling the recombinant monoclonal chicken anti-mycolic acid antibodies with gold nanoparticles without compromising biological activity

1.11 Scope and assumptions

This project forms part of a larger project under leadership of Dr Yolandy Lemmer – a co-supervisor of this MSc. As such this MSc worked towards the realisation of a full working diagnostic, but did not aim to complete this in its entirety.

This was an exploratory project exploring the possible pitfalls and opportunities for the development of a POC LFT for the diagnosis of TB using lipid antigen (MA) to capture the biomarker antibodies of TB patients.

The focus of this work was not a methodological development to be applied in other cases or a theoretical study to determine the basis for observed phenomena. This project had a practical end in mind focusing on improvisation and optimisation.

The development was limited to the well-established field of LFTs as the paper-based diagnostic and investigated mainly the format proposed above. Further antibody or biomarker selection was not attempted, nor any development of new reagents.

There are various components of the LFT that can be investigated and optimised. These options were not exhaustively explored. Basic options were investigated for membrane, blocker and running buffers. A standard anti-chicken antibody was used for the control line.

The proposed competitive binding format and working methodology for this test is based on a similar principle to an optical biosensor patented previously by the group. The work on this project explored the feasibility of the proposed test.

1.12 Chapter outlines

The work done on this project has been described in three chapters with a concluding discussion.

Chapter 2 will introduce the custom developed reagents to be used in MALIA as well as the rationale for their use. The work described in this chapter will provide evidence for the functionality of these reagents.

Chapter 3 will introduce LFT technology and its historic use in the diagnosis of TB. The choice to develop another immuno-chromatic assay for TB will be discussed. This chapter will describe the work towards development of MALIA with focus on objective 1.

Chapter 4 will describe the evaluation of the gold nanoparticle labelled gallibodies (objective 2) and the evaluation of the functionality thereof and the alternatives explored.

Finally the concluding discussion in chapter 5 will discuss the overall findings of this work and the feasibility of the proposed diagnostic.

Chapter 2: Detection of mycolic acid by custom developed anti-mycolic acid antibodies

2.1 Introduction

Qualified biomarkers can be used to diagnose patients, predict treatment outcomes or monitor pathogenesis of an illness [31]. These are valuable tools in the diagnostic field and a starting point for diagnostic development. Many of the tuberculosis (TB) diagnostics described in chapter 1 rely on detection of the *Mycobacterium tuberculosis* (Mtb) bacteria itself or its deoxy-ribonucleic acid (DNA) in patient specimens (sputum culture, GeneXpert). Tests such as the interferon gamma release assay or the tuberculin skin test detect immune responses to TB, however, with various limitations as previously described herein.

Wallis *et al.* [31] define the need for identification of biomarkers in three crucial categories for TB: [a] "…in patients with active disease, to predict durable (non-relapsing) treatment success; [b] in patients with latent *M. tuberculosis* infection, to indicate reactivation risk and predict treatment success; and [c] in people other than those with active disease, to indicate protection from tuberculosis by new vaccines." A more recent review by Goletti *et al.* [60] still reports these gaps and reviews the current research in this field.

Previous work in our group suggests that antibodies to the Mtb antigen mycolic acid (MA) could serve as an ideal biomarker for active TB diagnosis. This is because these antibodies are produced independent of T-cells (and so are unaffected by human immuno-deficiency virus (HIV) infection), appear at the onset of disease and are short-lived [58]. The proposed diagnostic method will detect these antibodies in patient serum in a competitive format (figure 1.4).

This chapter will briefly describe some of the current research toward the search for active TB biomarker(s) that are useful for point of care (POC) diagnosis (often sero-diagnostic biomarkers) followed by a detailed rationale for the use of MA antigen for the diagnostic to be developed for this project.

2.1.1 Antigens for serodiagnosis of TB

Chegou *et al.* [61] investigated host biomarkers in 716 patients from various African countries with symptoms of TB and identified a TB specific "bio signature" consisting of seven serum proteins regardless of HIV status. They have patented this bio signature with the intention to develop a user friendly diagnostic for TB [61–63]. In a similar multiplex approach Khaliq *et al.* [64] developed a high-throughput microbead suspension array immunoassay combining 11 Mtb antigens for diagnosis of active TB from patient serum (from venous blood).

Tiwari *et al.* [65] used purified proteins from an active TB culture to develop a "cocktail" of secretory proteins for use in a TB diagnostic ELISA (enzyme linked immuno sorbent assay). They report excellent specificity and sensitivity (>98%) of diagnosis using these protein antigens [65].

One of the unusual reagents to be used in the proposed diagnostic is the lipid antigen MA. Current serodiagnostic tests (for any illness/condition) use mostly protein (recombinant or native) antigens to capture and detect patient antibodies (see for example [66–68]).

An exception is the glycolipid, lipoarabinomannan (LAM). As discussed in chapter 1 (section 1.4.5) LAM is a cell wall component of mycobacteria and is detectable in the urine of patients with active TB infection. However, the Alere™ Determine™ TB LAM Ag test (LF-LAM) is recommended for use only in diagnosing TB in "seriously ill" HIV positive patients with low CD4 cell counts [32].

Jones *et al.* [69] report the use of different combinations of synthetic MAs linked to trehalose in an ELISA based methodology to diagnose TB using serum samples from the TDR (Special programme for Research and Training in Tropical Diseases) TB specimen bank. They have patented the preparation of these sugar ester MA derivatives as well as their use as antigens [70], however, the methodology is not field deployable. On the basis of their results it appears that MA based serodiagnosis would be valid [69].

2.1.2 Mycolic acids as antigens

MAs are highly hydrophobic, wax like, long-chain (C70 – C90) fatty acids that are a unique component of mycobacterial cell walls [71,72]. Isoniazid, one of the first line anti-TB drugs, targets MA synthesis showing the essential role these molecules play in Mtb survival [4].

MAs are present in all mycobacteria in various forms – secreted as free MAs, bound to sugar molecules on the cell wall such as penta-arabinose or as extractable esters with trehalose, glucose or glycerol [73]. These are known as mycolate esters. There are three major subclasses of (free) MA– alpha-; keto- and methoxy-MA in Mtb, according to the functional groups on their mero-mycolate chains [73].

The extreme hydrophobicity of MAs does not preclude antigenicity. Beckman *et al.* [74] described the presentation of lipid antigens (specifically MA) by CD1 on antigen presenting cells, thus providing a mechanism for specific anti-MA antibody production. This work was done using MA extracted (using chloroform-methanol) from Mtb cultures and purified by chromatography [74]. This work by Beckman and colleagues laid the ground work to show that MAs are immunogenic.

Pan *et al.* [75] first described the MA class specificity of anti-Mtb cord factor antibodies, reporting a stronger reaction for methoxy MA than others. As with Beckman *et al.* [74] this work was done using chloroform-methanol extracted MAs from Mtb cultures and purified using thin layer chromatography. The serum dilutions for these tests were very low – 40 – 160 times suggesting the possibility of low avidity or non-specific binding. The results showed preferential binding of sera (1:160) to methoxy-MA instead of alpha and keto-MA with a negative control of palmitic acid methyl ester, a straight-chain C16 fatty acid [75]. The authors also report no binding to a shorter chain MA (C44 – 46) and from this suggest specific recognition of the branched long chain length in addition to the functional groups [75]. Despite the use of a fatty acid negative control the authors expressed surprise at the immunogenicity of MA-esters because of their extreme hydrophobicity and non-resemblance to normal protein and carbohydrate antigens [75].

Lipid antigen interaction with antibody is known to be stereo-specific in the case of cholesterol [76]. In the case of MA interaction with specific anti-MA antibodies this is complicated as different classes and subclasses of the molecules exist in nature as a heterogeneous mixture. In order to satisfactorily prove the class and subclass specificity of anti-MA antibodies, stereo-controlled synthetic MAs had to be produced and then tested against anti-MA antibodies using an appropriate MA-like molecule (long chain, wax etc.) as negative control.

This (synthetic production of stereo-controlled MAs – alpha, methoxy and keto) was achieved by Al Dulayymi, Baird and colleagues [77–79] and allowed for further testing of anti-MA antibodies to determine class and subclass specificity. This development also allowed for the elucidation of the structure function relationship of MA in TB pathogenesis and growth. Smet *et al.* [80] recently showed that the cis/trans nature of the MA functional groups affect the immuno-stimulatory activity of MAs. The stereo controlled synthetic production also allowed for a slightly altered version of a functional, antigenic MA to be produced for use as a negative control by blocking of a functional group on alpha MA.

Beukes *et al.* [81] demonstrated the varying antigenicities of the different synthetically produced MAs (and their various stereoisomers) with methoxy MA once again showing the strongest response. However, the natural MA mixture best distinguished TB positive (human) sera from TB negative sera. This then required the consistent production of MA from Mtb culture purification – a complicated procedure as MA composition changes with varying culture conditions. The standardisation of conditions to produce natural MA mixtures of consistent composition was achieved by Ndlandla in the course of her doctoral research [58] and reported in [82]. This protocol was used for the isolation of MAs used for this study.

The use of MA as an antigen is further complicated by its functional resemblance to cholesterol. The natural MA mix conformation appears to have functional resemblance to cholesterol indicated by binding of the MA mix by Amphotericin B (a known cholesterol binding compound) and cross-reactivity of monoclonal anti-MA antibodies with cholesterol [83]. This is important to consider as anti-cholesterol antibodies are known to be present in human sera [84,85] – potentially hampering the specificity of MA based serodiagnosis. Beukes *et al.* [81] also developed monoclonal scFvs (antigen binding antibody fragments) that were specific to MA, specific to cholesterol or specific to both MA and cholesterol.

Chan *et al.*[86] similarly produced monoclonal antibodies to MAs from a human antibody gene library, however no cholesterol cross-reactivity was found in this library. This study did, however, corroborate the preferred binding of anti-MA antibodies to methoxy-MA [86].

MA has also been shown to be involved in the elicitation of the innate immune response [87]. Importantly Schleicher *et al.* [88] reported that the anti-MA response measured by ELISA was not significantly different in HIV negative versus HIV positive patients. This study concluded that a lack of resolution existed in this method to distinguish between healthy individuals and TB patients [88]. The consistency of the antibody response to MA in HIV positive and negative patients is consistent with the finding that the production of antibodies to MA is T-cell independent (carried out by the CD1b lipid antigen presenting cells [74]) because T-cells are targeted by HIV infection.

Ndlandla [58] selected more stable scFvs from a chicken antibody gene library, with similar specificities to those produced by Beukes and colleagues as described above, however a cholesterol (only) specific scFv was not isolated. These scFvs also had different specificities among the chemically synthetic subclasses of MA. These scFvs were converted to chicken antibodies (gallibodies) by Heena Ranchod in the course of her doctoral research [59,89,90]. The gallibodies can be stably expressed in a human cell line and purified from the culture media by a nickel column chromatography protocol. These custom developed gallibodies will be used for the development of the proposed diagnostic.

Ranchod *et al.* [91] also analysed the ability of the developed gallibodies to bind MA in ELISA using a natural mixture of MAs from Sigma to coat the plate. The developed gallibodies were used as primary antibodies and detected using a horse radish peroxidase (HRP)-conjugated anti-chicken IgG (Fc): HRP antibody. The results showed varying sensitivities between the developed recombinant antibodies. This ELISA protocol was used to benchmark the functionality of the purified gallibodies before their use in this study.

2.1.3 Anti-mycolic acid antibodies as biomarkers for TB

The failures of current diagnostics for TB and the need for a POC test provide some rationale for the development of this diagnostic. The specificity and magnitude of the immune response against MA provides the platform for the detection of anti-MA antibodies. However, it remains to be demonstrated convincingly that anti-MA antibodies are excellent biomarkers for active TB infection in a feasible, high throughput diagnostic test.

Theoretically, anti-MA antibodies may prove to be good biomarkers for active TB as they seem to form part of the innate immune response. In the innate immune response antibodies with lower affinities to multiple antigens are produced – these are called natural antibodies [92]. This response is induced immediately upon introduction of the pathogen and peaks in one to two weeks [92]. Natural antibodies are produced by B1 cells and mainly in a T-cell independent manner [92]. This means that the antibodies will appear with onset of the disease, be independent of HIV-affected T-cells and subside as soon as the bacterial count is brought under control by chemotherapy. This bodes well for the use of natural antibodies in serodiagnosis.

In contrast, the adaptive immune response is characterised by continued prevalence of high affinity antibodies produced by antibody secreting B2-cells with T-cell help. These antibodies persist long after the infection is cleared and are also maintained as memory cells to guard against future infection [92]. These properties mean that the presence of B2-cell derived antibodies cannot distinguish between previous and current infections, nor vaccination, making their use quite limited for diagnosis of active disease.

Due to their role in the innate immune response, natural antibodies recognise various evolutionarily conserved molecules, including lipids such as cholesterol, phospholipids and cardiolipins [93]. TB patients produce anti-lipid antibodies which decrease upon the commencement of treatment [88,93,94]. This is consistent with the knowledge that natural antibodies form part of the initial immune response and are by nature short-lived. This implies that tracking of anti-lipid antibodies (such as anti-MA antibodies) may indicate treatment success and thus allow for the quick detection of drug-resistant disease – a special concern in TB diagnosis.

Furthermore, it has been explained that production of anti-lipid antibodies requires CD1 antigen presenting cells and is therefore T-cell independent [74]. HIV infection destroys/dampens T-cells and the dependent adaptive antibody response. Therefore serodiagnosis of TB in HIV infected patients is challenging, as most diagnostics measure the immune response that is widely affected by T-cell destruction. However, a T-cell independent antibody response would not be similarly affected and would remain stable in spite of HIV

infection as demonstrated for the case of anti-MA antibodies in TB patients by Schleicher *et al.* [88].

MA presentation on CD1 happens on the CD1b family member, which does not occur in rodents such as mice and rats. However, guinea pigs, chickens and humans express CD1b, which is essential for presentation of MA [58]. Guinea pigs are the preferred non-human mammal model for the characterisation of anti-MA antibodies as they can present with chronic TB, similar to humans, whereas mice and rats can only manifest acute TB upon infection with Mtb [58]. Ndlandla's study using guinea pig sera showed that anti-MA antibodies behave like natural antibodies. The anti-MA antibodies were detected within one week of infection and were not detectable in latently infected animals (by inhalation of air extracted from patient wards in a TB hospital). These findings are significant as they provide the means to: (1) Effectively diagnose patients with active TB, (2) periodically monitor high-risk individuals such as health care workers for TB infection, and (3) a possible means for determining treatment success, as anti-MA antibodies will persist in the case of treatment failure.

Detection of anti-MA antibodies is complex as these are naturally low affinity antibodies that tend towards lower sensitivity of detection. Traditional antibody detection techniques, such as ELISA, rely on the high affinity of antibodies to antigen. The use of MA ELISA was shown to lack sensitivity to diagnose TB [88].

2.1.4 Detection of anti-mycolic acid antibodies in serum

Biosensor technology is perfectly suited to the detection of low affinity interactions. This technology translates the interaction between biological "sensing" or recognition molecules – such as antibodies and their antigens – to an electronic signal. With biosensor technology the binding and subsequent accumulation of the analyte can be sensitively traced to gain information about the kinetics and thermodynamics of interaction [95,96].

Thanyani and colleagues [96,97] reported on the successful application of optical biosensor technology to the detection of anti-MA antibodies. They reported an inhibition methodology where the TB patient sera could be inhibited from binding to the immobilised MA in the biosensor by MA containing liposomes (i.e. the liposome MA outcompetes the immobilised MA for binding to anti-MA antibodies in sera) [97]. The authors report a trial of the diagnostic biosensor using 61 patient sera samples spread across HIV positive, negative and TB positive and negative patients. The overall specificity of the assay was 48.4% and sensitivity was 86.7% [97]. However these data include the population of TB "negative", HIV positive patients for whom sputum culture (which was used to determine the TB status of the samples) could be incorrect, as follow up was not possible with these patients [97]. When this cohort is removed

the specificity improves to 76.9%. The assay is predicted to perform well in the TB HIV co-infected patients [97].

The proposed diagnostic will attempt to replicate the competitive format of this biosensor for a POC deployable test that does not require electricity. The competitive format will serve to address the low affinity of the target anti-MA antibodies, while the lateral flow immuno-chromatography construct of the intended diagnostic device will cut the cost and facilitate high throughput capacity to the test.

2.1.5 Chapter outline

The work described in this chapter will introduce the custom developed reagents to be used for the proposed diagnostic. The sources of the reagents used will be discussed and the initial benchmark tests to demonstrate the functionality of these reagents described.

2.2 Materials and methods

2.2.1 Materials

Unless otherwise specified salts and reagents were procured from Sigma (USA). Three types of casein were used – biochemical reagent casein 'Carbohydrate and Fatty Acid Free' from Calbiochem, EMD Biosciences (USA), sports supplemental casein (SSC) from Scientific Sports Nutrition™ and casein hydrolysate (LP0041) from Oxoid (UK). The goat anti-chicken IgG (Fc): HRP and goat anti-chicken IgG (Fc) was procured from Bio-Rad. Nitrocellulose membrane (FF80HP) was procured from Whatman™, GE Healthcare (UK). TMB for blots was procured from Invitrogen™ (USA).

2.2.1.1 Custom developed monoclonal antibody

Custom engineered monoclonal antibodies developed using a chicken gene library and cloned into a IgY like scaffold (termed gallibodies) prepared by Heena Ranchod's PhD study [59] were used throughout this study. Ilse Du Preez, Arthessa Ragavaloo and Mosa Molatseli also prepared gallibodies as described below for this study (as part of the work for the larger project of which this MSc formed part).

Three clones (numbered 12, 16 and 18) were used initially. These clones were selected for their stability during prolonged storage and for their varying binding specificities to the three different MA classes and closely related cholesterol. These gallibodies were engineered into two types of bivalent IgY formats, one a theoretically flexible C_H1-4 construct (figure 2.1A, C_H denotes constant heavy domain) and the other a truncated and hypothetically more rigid C_H2-4 type (figure 2.1B). This then resulted in six gallibodies in total [91].

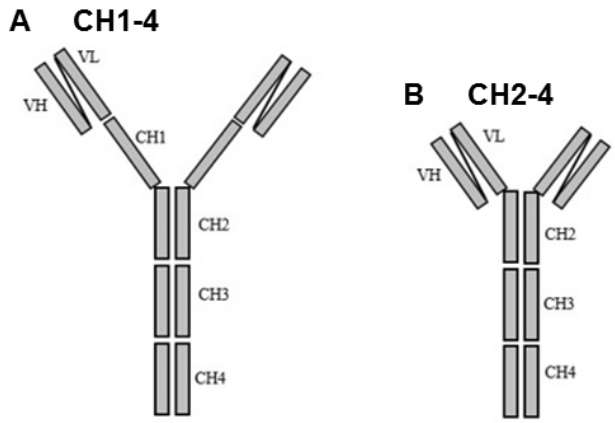

Figure 2.1: Structures of the two types of vectors used for the gallibody engineering. A: C_H1-4 and B: C_H2-4. C_H – constant heavy chain. Adapted from Greunke *et al.* [89] by Ranchod [91].

Throughout the gallibodies are referred to by their number and their type as follows, for example: 12-1 refers to clone number 12, the C_H1-4 vector. All six gallibodies were used for some experiments but for the most part gallibody 18-2 or 12-2 was used (as indicated). The sensitivity of the gallibodies was shown to be in a similar range in previous work [91].

The gallibodies were expressed in human embryonic kidney cells, purified from the culture media and concentrated in 0.1 M Borate buffer of pH 7.4. The quality control process for the expressed and purified antibodies included a Bradford assay to determine concentration and an MA ELISA [91] to determine functionality. All batches of gallibodies used were tested in this way to confirm activity.

2.2.1.2 Self-isolated mycolic acid

MAs used were a natural mixture isolated from late stage mycobacterial growth (Ndlandla *et al.*, 2016) and purified by the counter current distribution method described by Goodrum *et al.* [98]. This was done by post-graduate colleagues at the University of Pretoria – Mosa Molatseli and Arthessa Ragavaloo. MA was stored in solid phase or dissolved in freshly distilled hexane in brown glass vials at 4°C.

2.2.2 Enzyme Linked Immuno Sorbent Assay

The ELISA protocol used to benchmark the quality of the purified gallibodies used casein, hereinafter referred to as biochemical reagent casein (BRC), dissolved in 0.1 M phosphate buffered saline (PBS) as a blocker at a concentration 2% w/v pH 7 [91].

Sports nutritional supplement casein (hereinafter referred to as Sports Supplement casein, SSC) was investigated as a replacement for the pure casein due to the restrictions on the import of bovine milk products into South Africa. According to the label this product contains the following ingredients: Micellar casein enriched (92%) milk protein isolate, flavouring, guar

extract (thickener), sodium chloride, soya lecithin (emulsifier) and sucralose (non-nutritive sweetener). The composition per 100 grams is described as follows: energy 1425 kJ, protein 74 g, glycaemic carbohydrates 8.3 g of which total sugar 6.3 g, total fat 2 g of which saturated fat 1.3 g, fibre 1.7 g, sodium 0.217 g. For protein supplementation for athletes', use of the product at approximately 15% (w/v) concentration (~30 g in 200 mL) is recommended.

SSC was compared with bovine casein (BRC). The label for BRC lists the components as follows: casein 96%, glucose 0.05%, lactose 0.05%, free acid 0.1% and fats 0.1%. To prepare the blocking buffers the appropriate mass was weighed out and solubilised overnight in half of the required final volume of 0.1 M PBS (pH 7.4). The following day the volume was adjusted to the correct percentage (w/v) casein concentration in 0.1 M PBS and the pH adjusted to pH 7 using 3 M NaOH. The SSC required a small amount of pH adjustment to pH 7 using 8 M HCl, while the BRC required adjustment using 3 M NaOH up to pH 7.

Direct and indirect ELISA were used to compare the different sources of casein (figure 2.2). In the first configuration (figure 2.2 A), a direct ELISA was carried out in which the plate was coated with gallibody (antigen, green circle) and incubated with the HRP-conjugated anti-chicken IgG (Fc): HRP antibody. In the indirect ELISA configuration (figure 2.2B), MA was coated on the plate, the gallibody was used as the primary antibody and 'indirectly' indicated by the anti-chicken IgG (Fc): HRP antibody. Visualisation of binding is achieved by a colour substrate conversion by the conjugated enzyme – HRP in this application.

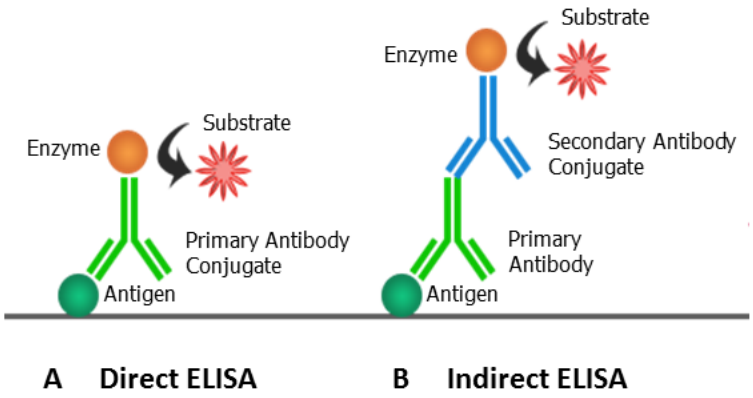

Figure 2.2: Schematic of direct and indirect ELISA. Direct ELISAs are used to detect antigen by using an enzyme conjugated antibody directly on the antigen coated plate. Indirect ELISA detects the binding of the primary antibody to the antigen by the use of an enzyme conjugated secondary antibody specific to the primary antibody. Adapted from Boster Biological Technology [99].

For the direct ELISA the gallibody was diluted in 0.1 M borate buffer (pH 7.4) and 100 µL per well used to coat a NUNC™ Maxisorp plate overnight at 2 – 8°C. The following day the liquid was flicked out and the wells washed three times using 300 µL of 0.1 M PBS/0.1% (v/v) Tween 20 (wash buffer). Each well was blocked for two hours at room temperature with 300 µL of 4%

casein in 0.1 M PBS pH 7 (blocking buffer). Following the blocking step, wells were washed three times with wash buffer as stated above. The coated gallibody was incubated for one hour with 50 µL goat anti-chicken IgG (Fc): HRP diluted 1:1000 in blocking buffer with 0.1% (v/v) Tween 20 added (dilution buffer). Unbound antibodies were removed by washing the wells with wash buffer. The reaction was developed by the addition of 50 µL of TMB (3, 3', 5, 5' tetramethylbenzidine) substrate for five minutes before stopping the reaction with 50 µL of 2 M H_2SO_4. Absorbance was measured at 450 nm using a plate reader (BioTek® PowerWave HT).

For the indirect ELISA NUNC™ Maxisorp plates were coated with a 0.25 mg/mL solution of MA in freshly distilled n-hexane or hexane alone as a background control (50 µL per well, using a glass Hamilton® syringe). Hexane was allowed to evaporate at room temperature. The indirect ELISA was carried out as the direct ELISA except after blocking and washing the wells an additional incubation step was inserted as follows. Wells were incubated for one hour with 50 µL of gallibody diluted to different concentrations in the dilution buffer described above. Unbound antibodies were removed, and the protocol carried out as described above.

Due to variability of results induced by the use of supplemental sports casein another alternative was tested – casein hydrolysate. This is a nitrogenous media additive that is produced by reacting casein with hydrochloric acid followed by neutralisation with sodium hydroxide. The conditions are controlled to produce a 2% solution that has a pH of 7 [100]. For this reason, the 4% solution used for this study did not require pH adjustment. The protocol for the indirect ELISA above was followed but replacing the casein in the blocking and dilution buffers with 4% casein hydrolysate (CasH, w/v).

2.2.3 Immunoblot tests

Blot tests were carried out to confirm that coating MA onto nitrocellulose does not render the MA non-antigenic. This was a specially adapted protocol that did not use blotting transfer methods. For the blot tests, circles (diameter ~ 6 mm) of nitrocellulose membrane were prepared by use of a paper punch. Nitrocellulose membrane discs were stuck by their plastic backing to well bottoms in a 96 well plate using double sided tape. A 1 µL volume of 0.25 mg/mL MA in n-hexane, n-hexane alone, 0.5 mg/mL goat anti-chicken IgG (Fc) in PBS or PBS alone was spotted onto the membrane circles inside the wells. The membranes were dried for at least 30 minutes at room temperature before use.

The ELISA protocol (section 2.2.2) was followed with the following changes/details. Biochemical reagent casein was used at 4% (w/v) as the blocking buffer. For the dilution buffer 2% casein (BRC) was used with 0.05% (v/v) Tween 20. For the final step before signal generation, each wash step was left in the wells for two minutes on an orbital shaker at 200

revolutions per minute (rpm). Finally, TMB solution for blots was used to develop the spots followed by two five minute washing steps with 300 µL deionised water per well on an orbital shaker at 200 rpm. The plates were photographed to record the results.

2.3 Results and discussion

After purification the anti-MA activity of the gallibodies was confirmed by ELISA on MA coated 96-well plates (section 2.2.2). In this ELISA, blocking was achieved with a casein solution [91]. Due to the difficulty of importing casein into South Africa an alternative source was tested, namely Scientific Sports Nutrition's (SSC) "Micellar Casein Protein" – a supplement used in high intensity training athletes' diets. This source was compared to Biochemical Reagent Casein (BRC) obtained from Calbiochem in a direct ELISA with coated gallibody. The results are shown in figure 2.3.

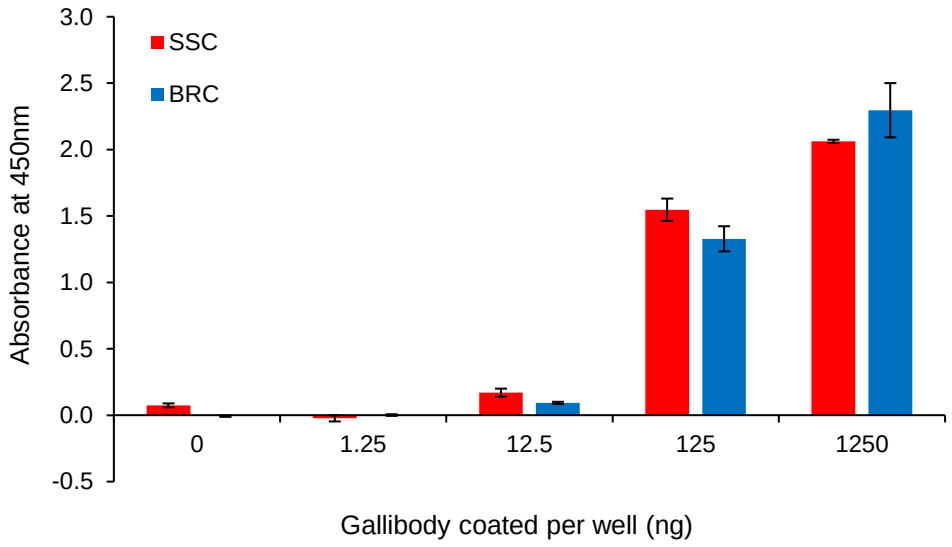

Figure 2.3: Direct ELISA to compare sports supplement and biochemical reagent casein blockers by titration of antibody coating concentration. Anti-chicken IgG (Fc):horse radish peroxidase conjugate at a concentration of 1 µg/mL was incubated on a dilution range of coated gallibody 18-2 wells blocked with 4% (w/v) sports supplement casein (SSC, red) or biochemical reagent casein (BRC, blue) in 0.1 M PBS. Average (bar heights) and standard deviation (error bars) of four wells are shown with average of 4 blank wells subtracted. Not corrected for background signal.

In the direct ELISA (figure 2.3) no significant difference was observed using different blocking buffers under the conditions tested. This comparison was also done on an indirect ELISA with coated MA and the gallibodies used as the primary antibody for which the results are shown in figure 2.4.

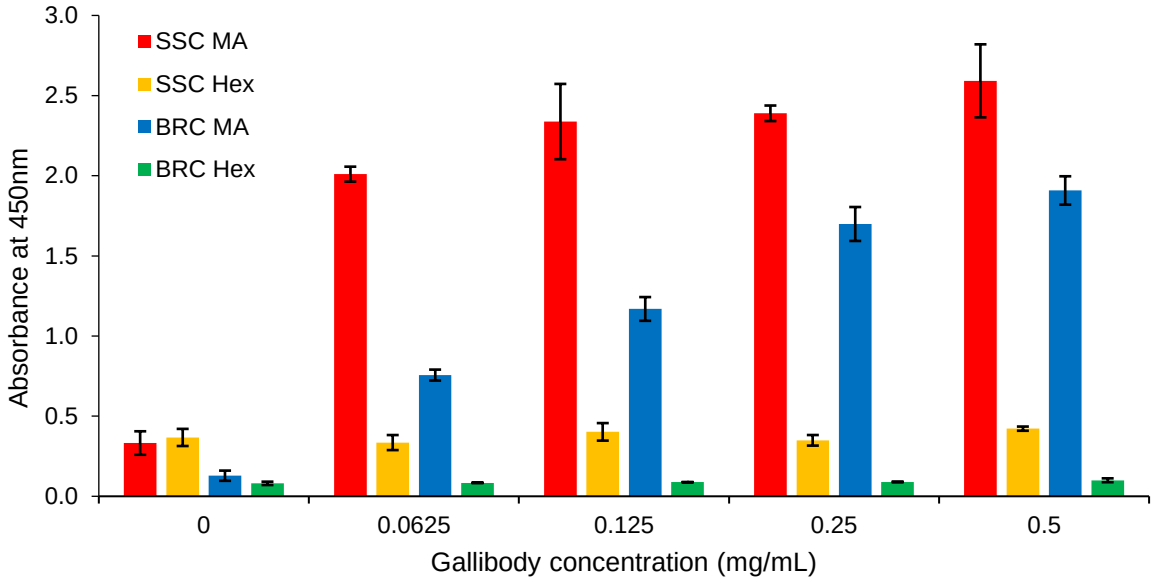

Figure 2.4: Indirect ELISA to compare sports supplement and biochemical reagent casein blockers for detection of gallibodies on MA coated plate Increasing concentrations of gallibody 12-1 incubated on coated MA in hexane (0.25 mg/mL, MA) or hexane only (Hex) coated wells blocked with 4% (w/v) sports supplement casein (SSC, MA red and Hex yellow) or biochemical reagent casein (BRC, MA blue and Hex green) in 0.1 M PBS. Average (bar heights) and standard deviation (error bars) of four wells are shown. Not corrected for background signal.

A significant difference in MA signal between the different blocking buffers was observed in the indirect ELISA – figure 2.4. In both direct and indirect ELISA the background signal when using SSC was higher than that obtained when using BRC see '0' columns in figure 2.3 and 2.4. The p value (calculated using the student's t-test) in both cases was much less than 0.05 indicating a significant difference between the BRC and SSC background values. However, the MA binding signal (figure 2.4) remained high at decreasing primary antibody concentration for longer when wells were blocked with SSC rather than with BRC. The BRC MA signal (blue bars) started to reduce significantly at 0.125 mg/mL (compared to 0.25 mg/mL p value = 0.0004) whereas the SSC MA signal (red bars) remained comparably high even at 0.0625 mg/mL (compared to 0.125 mg/mL p value = 0.055). This may be due to the additives present in the SSC which could affect the reaction kinetics. Blocker formulations are known to influence ELISA results [101].

These results indicate that the use of SSC casein as a blocker and dilution buffer improves the sensitivity of MA binding by gallibody 12-1.

The increased variability of the results for SSC in comparison to that found for BRC (note standard deviation at 0.5 and 0.125 mg/mL bars in figure 2.4) could have been due to the un-dissolvable solids (fibre) and other additives present in SSC (section 2.2.2). Furthermore concern was raised about the long term supply consistency of the sports supplement casein. To overcome these concerns alternative sources of casein without additives were explored. A

4% solution of casein hydrolysate (CasH) was prepared and used as a blocker in ELISA in the same way as the biochemical reagent casein used in the experiment from which figure 2.4 was derived. The results are shown in figure 2.5.

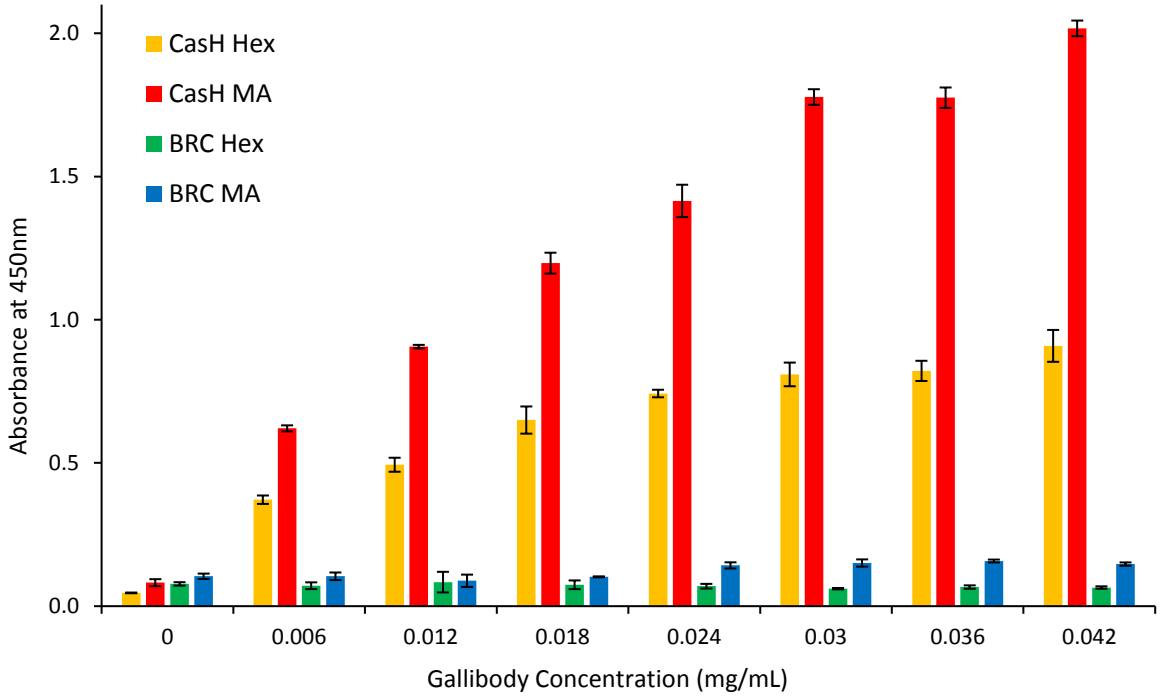

Figure 2.5: Indirect ELISA to compare casein hydrolysate and biochemical reagent casein as blockers for detection of gallibodies on MA coated plate Increasing concentrations of gallibody 12-2 incubated on coated MA in hexane (0.25 mg/mL, MA) or hexane only (Hex) coated wells blocked with 4% (w/v) casein hydrolysate (CasH, MA red and Hex yellow) or biochemical reagent casein (BRC, MA blue and Hex green) in 0.1 M PBS. Average (bar heights) and standard deviation (error bars) of four wells are shown. Not corrected for background signal.

It is known that acid hydrolysis separates proteins into their constituent amino acids. This makes the functional groups of the amino acids available producing a protein solution that has very different properties from the native protein solution. It is feasible that the presence of free amino acids changes the blocking effect of this solution compared to the native solution (BRC) seen in figure 2.5. The sensitive detection of MA was achieved with a reduced amount of gallibody (significant but reducing MA signal observed across concentration range tested for CasH but not for BRC, compare red and blue bars). However, the background signal for CasH was significantly higher than the background achieved using BRC across all the gallibody concentrations tested except 0 mg/mL (compare yellow to green bars, figure 2.5).

Taken together, these results (figure 2.3 – 2.5) show that casein hydrolysate can be used as a more readily available and consistent source of casein for the blocking step in the MA-ELISA, giving possibly more sensitive detection. However, these results are insufficient to characterise the differences conclusively or draw collective conclusions about the activity of

the gallibodies under these conditions. Titration of a wider range of primary antibody concentrations with all six gallibodies are required. This development was not the focus of this work and so was not attempted.

These results also confirm the detection of MA using the custom developed gallibodies as shown previously [91].

In order to test the antigenicity of the MA when blotted on nitrocellulose a blot test was performed with a similar protocol to the indirect ELISA followed (section 2.2.3). MA dissolved in hexane, hexane alone, control anti-chicken antibody and 0.1 M PBS was spotted separately onto nitrocellulose discs (diameter ~ 6 mm) fixed into each well of the plate using double sided tape. Photographs of the plate are shown in figure 2.6.

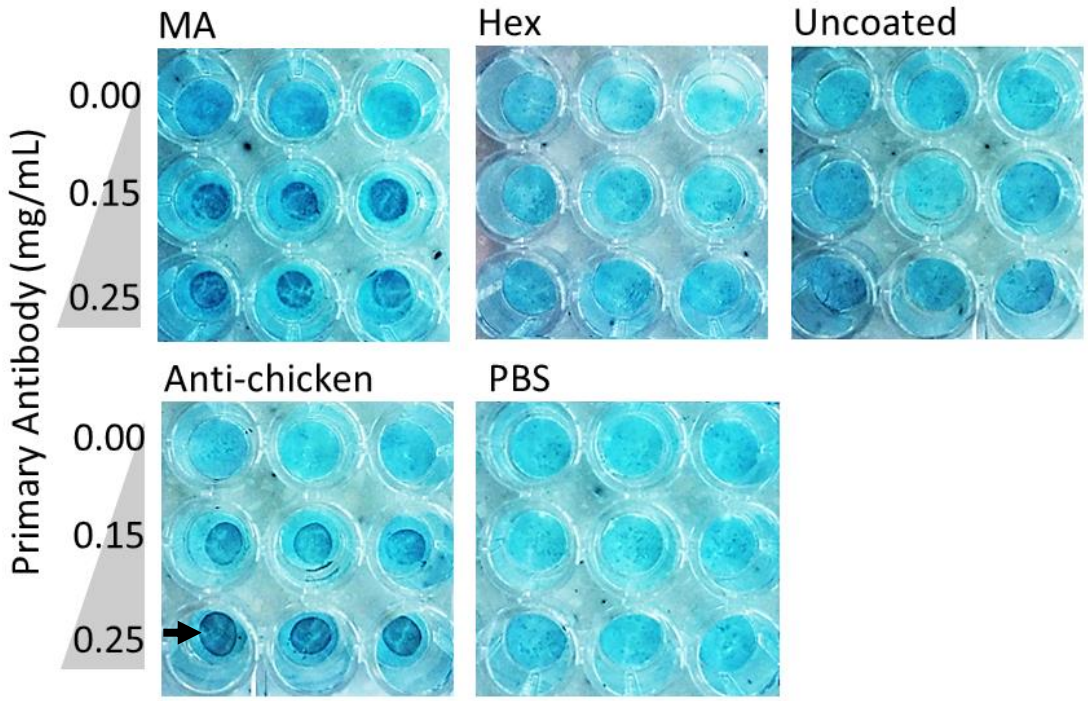

Figure 2.6: Immunoblot test to determine antigenicity of MA spotted on nitrocellulose membrane. Two concentrations of gallibody 18-2 and buffer alone was incubated on MA in hexane (0.25 mg/mL), hexane, anti-chicken IgG (Fc) antibody (0.5 mg/mL) and 0.1 M PBS spotted in triplicate on nitrocellulose membrane discs (~ 6 mm diameter) and pasted into wells using double sided tape. Cropped photographs of sections the plate after development are shown. Example of signal spot indicated by black arrow.

The results from the blot test showed that MA spotted onto nitrocellulose is antigenic at 0.25 mg/mL concentration (darker spots top left corner, figure 2.6). A faint non-specific signal on the MA was visible in the wells without primary antibody (0.00), however the positive signal was far stronger at gallibody concentrations of 0.15 and 0.25 mg/mL. The positive control (anti-chicken IgG (Fc) antibody) showed an increasing signal for increasing gallibody concentration with no non-specific binding (bottom left, figure 2.6). The negative controls (hexane only and PBS) as well as the uncoated control showed no detectable signal.

The MA signals in figure 2.6 indicate that MA is antigenic when spotted onto nitrocellulose membrane. This result was taken as representative of all six gallibodies. Previous work in the group (unpublished) using a different blot technique (requiring more reagent) showed similar results for all the developed gallibodies.

2.4 Conclusion

This chapter described the rationale (section 2.1), preparation protocol (section 2.2.1) and functionality (figures 2.3 – 2.6) of the custom developed and unusual reagents for the proposed diagnostic, i.e. the recombinant gallibodies and natural mixture of MA.

The identification of an alternative source of casein (figure 2.5) for use as a blocker and dilution buffer in ELISA to detect MA is significant as this solves the problem of the import restrictions on bovine milk products in to South Africa.

Pre-screening of antigen/antibody relationships in ELISA and blot assays before lateral flow test (LFT) development is useful, though not necessarily predictive of performance in LFT, because of the entirely different conditions provided by the formats for the antibody/antigen interaction to take place [102].

The binding of MA by the custom-developed gallibodies shown in the ELISA and blot test signals (figures 2.3 – 2.6) would be the same antibody/antigen interaction on the test line in the case of a negative patient sample and may predict the possibility of a signal on the test line. The detection of the relatively weak anti-lipid interaction by ELISA and blot tests that have vigorous washing steps, but long interaction times to counter this, was significant and will be expanded on in the context of later results. Subsequent chapters will describe the work towards capturing this gallibody/MA interaction into a detectable LFT signal.

Chapter 3: Lateral flow test development

3.1 Introduction

Lateral flow test (LFT) technology has been successfully applied in several point of care (POC) diagnostics. The historically unsuccessful and unadvised application of LFT technology in the diagnosis of tuberculosis (TB) and the reasons therefore are explained below, followed by a rationale for why this technology was chosen for the proposed TB diagnostic. The considerations for development of LFTs are outlined and some recent updates to this literature described.

3.1.1 Lateral flow test format

The most commonly used and understood LFT is the pregnancy test. The principal aim of the test is to rapidly detect an analyte in a sample by an immunoreaction (antibody – antigen interaction) resulting in a visible line or symbol indicating a positive test result without having to rely on electricity or other technology for measuring the extent of the reaction.

LFTs have a fairly standard architecture consisting of a sample and conjugate pad, usually glass fibre, overlapping a test membrane, usually nitrocellulose, with an absorbent wick on the furthest end. These components are held in place by an adhesive backing card (figure 3.1) [103]. Commercially available LFTs are usually in 5 mm wide strips placed in plastic holders that have a sample port and a result viewing "window" as illustrated in figure 3.3B. The sample is introduced onto the sample pad and drawn "up" the test by the capillary force and absorption by the wick [103].

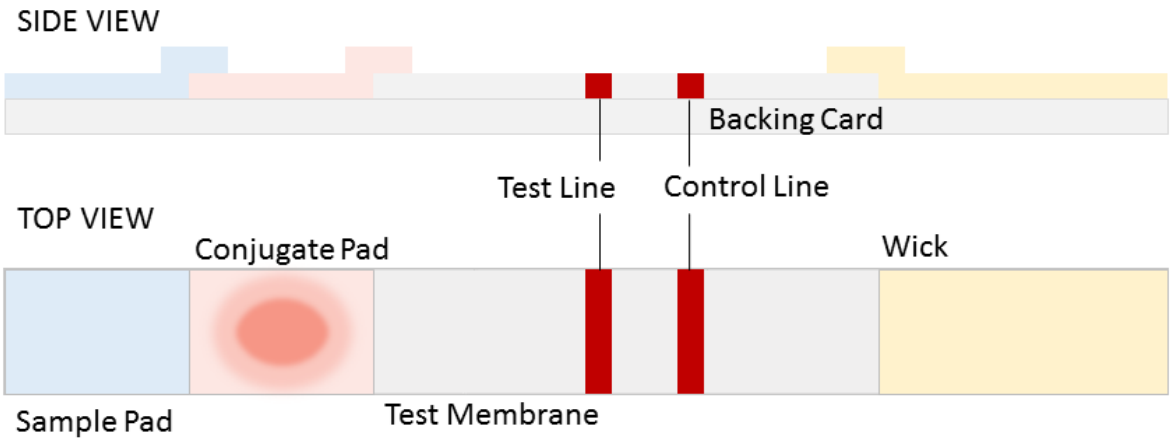

Figure 3.1: The standard lateral flow test format.

Analyte detection is achieved by constructing a test using either the sandwich or competitive formats [103]. In the sandwich format the analyte present in the sample (usually a large molecule with multiple antigenic sites) binds labelled antibodies dried in the conjugate pad and then this

complex is captured on the test line usually by additional anti-analyte antibodies forming a sandwich [103]. The excess labelled antibodies are captured by anti-antibody molecules on the control line (figure 3.2A) [103]. In the competitive format an analyte homologue (for example a monoclonal mouse antibody to a disease antigen) can be labelled and dried in the conjugate pad with an analyte binding molecule as the test line (e.g. the disease antigen) and homologue (only) binding molecule at the control line (e.g. anti-mouse antibody) [103]. If analyte is present in the sample, labelled and unlabelled analyte will compete to bind at the test line, thereby reducing or removing the test signal (figure 3.2B) [103]. This latter competitive format most closely resembles the format for the proposed diagnostic.

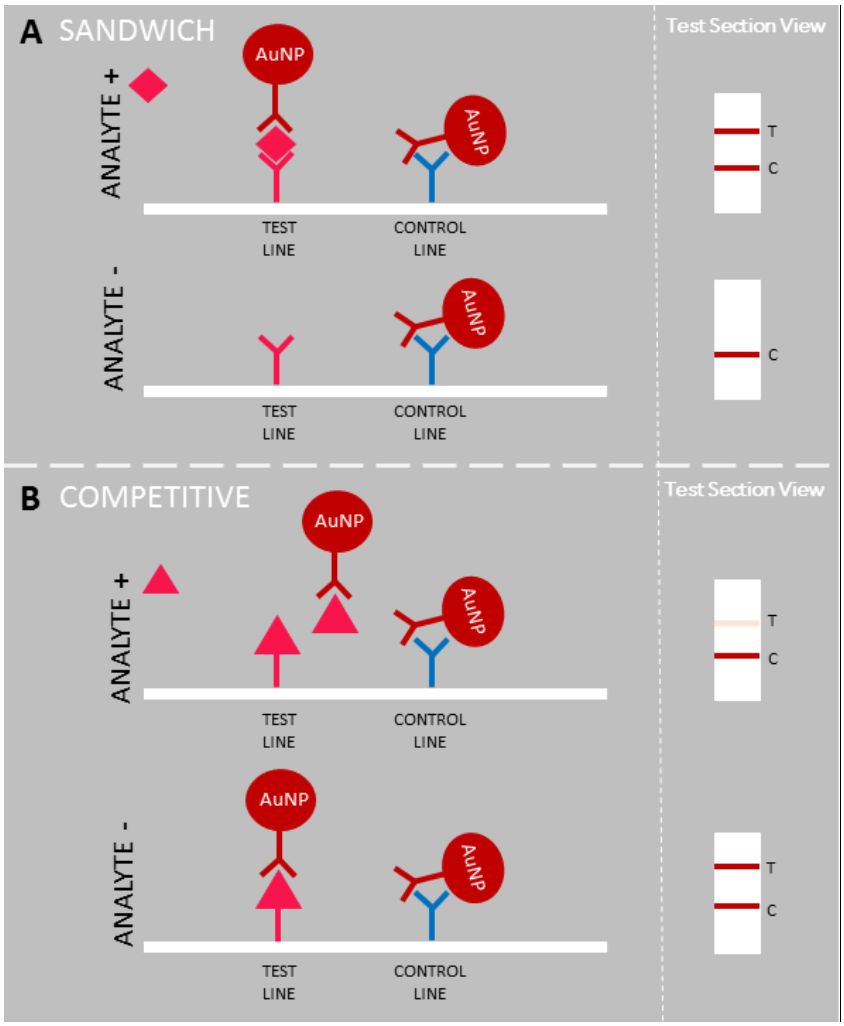

Figure 3.2: Mode of action of the sandwich (A) and competitive (B) formats of the lateral flow immunoassay.

3.1.2 A case study of a successful lateral flow test

Relative to the TB epidemic the human immuno-deficiency virus (HIV) epidemic is under better control in spite of the lack of a cure for the disease. This is partially because of an extremely effective and scalable diagnostic usable at the POC [104]. The test detects the presence of HIV antigens and anti-HIV antibodies (individually or simultaneously depending on the test) in

patient blood that can be non-invasively obtained through a finger prick [105]. The screening test can be administered at the health post level and does not require electricity or laboratory technicians [105]. World Health Organisation (WHO) guidelines advise that the test be carried out by health professionals in relative privacy to ensure relevant patient counselling and follow up [105]. A positive rapid HIV screening test is usually confirmed (as part of a HIV burden specific decision matrix) by a relatively straight-forward laboratory assay based on similar antigen/antibody detection principles to the rapid tests [105].

The rapid test for HIV has shown high (> 95%) specificity and sensitivity since the introduction of the test in the 1980s [106]. The major progress of the diagnostic has been in reducing the negative window period between infection and seroconversion (the production of antibodies to the virus) [106]. Because diagnosis with HIV is an irreversible event (there is no cure) even better accuracy has come to be expected with 100% sensitivity (no false negatives) and near perfect (99.5%) specificity (hardly any false positives) in the most recent evaluation [106].

The test development history is depicted in figure 3.3A. The first generation of rapid HIV tests detected antibodies to HIV using viral lysate as the antigen on the test region of the test [106]. These tests showed relatively high false positive rates but good sensitivity [106]. The second generation tests used synthetic antigens to improve the specificity of the assays. Both of these versions used labelled antibody conjugates to detect the patient antibodies bound to the viral lysate/antigens in the test region [106]. Third generation assays use labelled antigen conjugates further improving the specificity by allowing detection of all the patient's anti-HIV antibodies (not just those to which the antibody conjugates could bind) [106]. In the fourth generation of tests both antibodies and antigens are detected by the use of bound antibody and antigen as well as labelled antibody and antigen, thereby increasing the chances of binding HIV specific antigens and antibodies [106]. In the fifth generation of HIV screening tests, HIV-1 and HIV-2 are individually detected (figure 3.3B), however, significant cross-reactivity is reported [106].

A

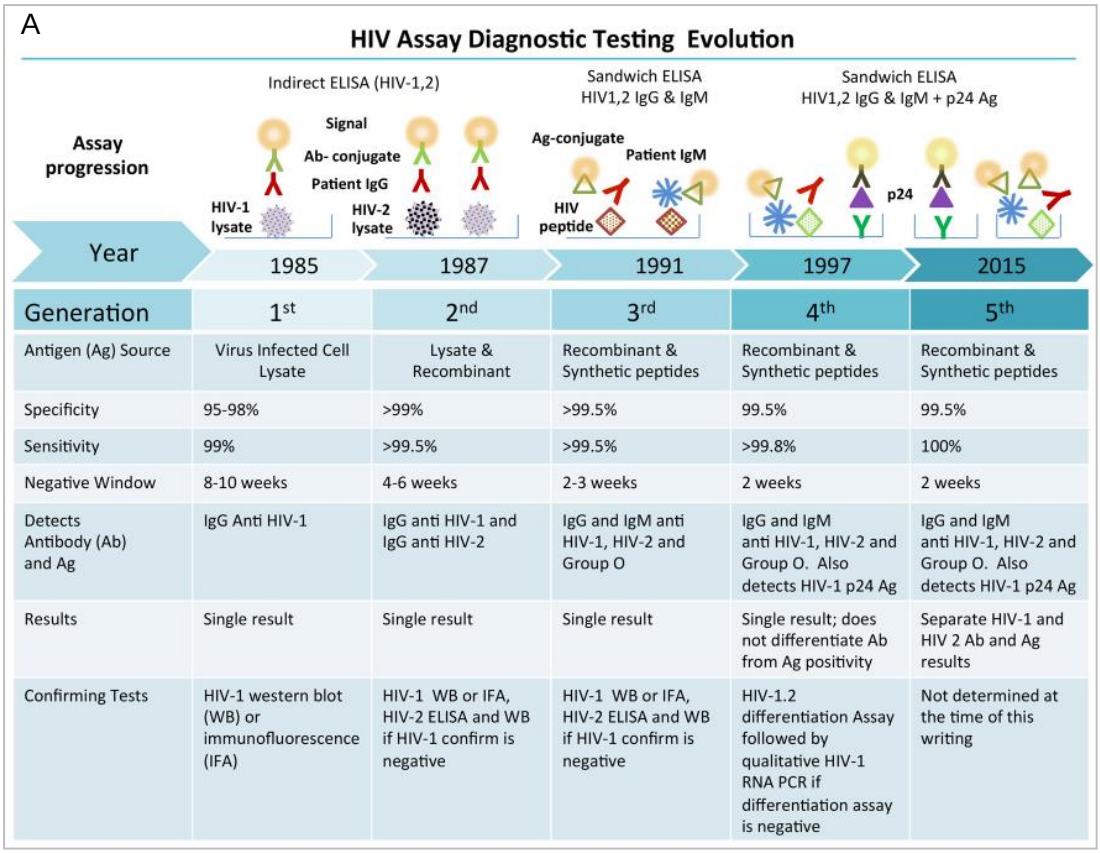

Generation	1st	2nd	3rd	4th	5th
Antigen (Ag) Source	Virus Infected Cell Lysate	Lysate & Recombinant	Recombinant & Synthetic peptides	Recombinant & Synthetic peptides	Recombinant & Synthetic peptides
Specificity	95-98%	>99%	>99.5%	99.5%	99.5%
Sensitivity	99%	>99.5%	>99.5%	>99.8%	100%
Negative Window	8-10 weeks	4-6 weeks	2-3 weeks	2 weeks	2 weeks
Detects Antibody (Ab) and Ag	IgG Anti HIV-1	IgG anti HIV-1 and IgG anti HIV-2	IgG and IgM anti HIV-1, HIV-2 and Group O	IgG and IgM anti HIV-1, HIV-2 and Group O. Also detects HIV-1 p24 Ag	IgG and IgM anti HIV-1, HIV-2 and Group O. Also detects HIV-1 p24 Ag
Results	Single result	Single result	Single result	Single result; does not differentiate Ab from Ag positivity	Separate HIV-1 and HIV 2 Ab and Ag results
Confirming Tests	HIV-1 western blot (WB) or immunofluorescence (IFA)	HIV-1 WB or IFA, HIV-2 ELISA and WB if HIV-1 confirm is negative	HIV-1 WB or IFA, HIV-2 ELISA and WB if HIV-1 confirm is negative	HIV-1.2 differentiation Assay followed by qualitative HIV-1 RNA PCR if differentiation assay is negative	Not determined at the time of this writing

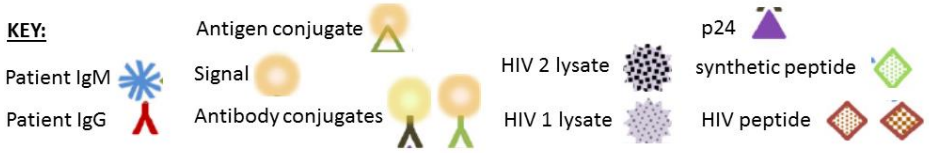

B

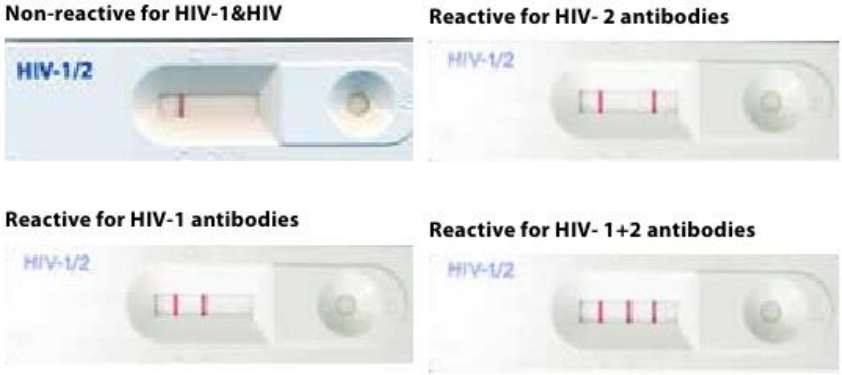

Figure 3.3 A: Schematic representation of the progressive development of the Rapid HIV test taken from Alexander [106] **B: Example of test results for a fifth generation rapid HIV test.** From the package insert for the SD BIOLINE HIV-1/2-3.0 (Standard Diagnostics INC.) submitted to reported by the WHO [105].

The major and obvious advantage of the use of rapid tests is that patients can learn their results and commence treatment in the first visit – drastically reducing the number of patients lost to follow up [104]. This then has invaluable use in preventing further transmission of the disease as patients can be advised on how to reduce the risk of transmission to partners and

healthcare workers exposed to bodily fluids. In addition, expectant HIV positive mothers can then be timeously enrolled in prophylactic anti-retroviral therapy to prevent mother-to-child transmission of the virus [104,107,108].

The improvement of the test to detect HIV antigens (from the 3rd generation) allows for diagnosis of the disease during the acute (early) phase of the infection when the transmission rate is much higher than usual, thus further reducing the spread of HIV [55,104]. Overall the impact of early, rapid diagnosis of HIV has had an enormous impact on limiting the spread of the disease and a similar test for TB could conceivably have a large impact to improve the management of the TB epidemic.

3.1.3 Lateral flow tests for TB

Due to the success of the rapid HIV diagnostic and the wide applicability and acceptability of the LFT format, several TB diagnostics based on the same principles were developed and marketed. Despite the evidence of low accuracy [109] these tests were widely used in developing countries – most notably in India [110,111] – leading to the WHO releasing a policy statement effectively condemning their use [112].

This section will explain the methodology of tests and what could be discovered about their manufacture and the reasons for their failures in sensitivity and specificity.

The commercial lateral flow TB serodiagnosis tests were comprehensively tested in a laboratory trial conducted by the WHO in 2008, using 355 archived patient samples whose TB status were confirmed or excluded by smear microscopy, culture, chest x-rays and clinical follow up [20]. The commercial serodiagnostic tests that were evaluated all detected the presence of anti-mycobacterial antibodies in patient sera, but the nature of the antigens or even the antigen type (protein, lipid etc.) were often not disclosed [20]. Tests were chosen for evaluation that were simple and rapid, meaning that they required a one or two step process to perform, required minimal equipment and training and provided easily interpretable results in less than 30 minutes [20].

The results of the evaluation indicated that none of the tests performed better than smear microscopy and when combined with it yielded an unacceptable false positive rate (42%) [20]. The tests have low and inconsistent sensitivity (0 – 0.6) and relatively low and highly variable specificity (0.53 – 0.99) as shown in figure 3.4 [20,112]. The reasons for this poor performance may be because TB antigens resemble those of many other human pathogens and the antigenic targets of antibodies generated toward the bacteria vary widely among patients [88,113]. These factors would limit the sensitivity and so the overall performance of the tests. Dheda *et al.* [114] suggested that the interaction of multiple cell types and pathways involved in the innate

immune response to TB provide mechanisms for the lack of immunodiagnostic evidence (specificity) for infection.

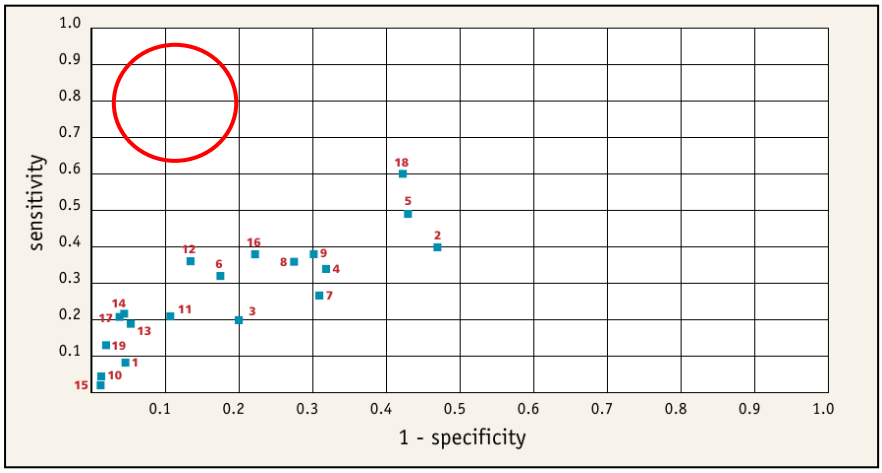

Figure 3.4: Receiver operating characteristic curve showing the specificity and sensitivity scores of the 19 commercial rapid tests for the diagnosis of pulmonary TB. (n = 355) Numbers indicate different tests. Tests with good overall performance would appear in the upper left hand quadrant of the chart (red circle).Taken from Laboratory-based evaluation of 19 commercially available rapid diagnostic tests for TB [20].

The evaluation also assessed the operational characteristics of the tests by having the operators fill in a questionnaire evaluating every test on: the clarity of the kit instructions, the technical complexity, and the ease of interpretation of results and whether or not the kit provided all the equipment required. None of the tests obtained perfect scores in any area but overall the diagnostics scored well on the technical complexity with 12 out of the 19 scoring "very easy" making them appropriate for use at the POC [20]. This is a key strength of the LFT format and so an accurate test with a similar format could be well used.

Interestingly, a thorough patent assignee search of all the manufacturers included in the evaluation above yielded minimal results. Only one manufacturer is still holding a patent on a serological TB test and that for the diagnosis of TB in non-primate mammals [115]. This patent, published in 2006 in the US and held by Chembio Diagnostic Systems Inc. appears to be the same test as used in the above trial given the dates – see number six in figure 3.4 above. The inventors published an article in September 2007 describing a trial of its use in non-human primates with excellent specificity and sensitivity claimed (99 and 90% respectively) [68].

3.1.4 Why another attempt at a lateral flow test for TB?

Despite the trade-offs in sensitivity and specificity, LFTs and paper based diagnostics in general have significant advantages in terms of affordability, user-friendliness, rapidity and deliverability over more complex microfluidic solutions [49]. These trade-offs and their applicability to health care settings are demonstrated in figure 3.5.

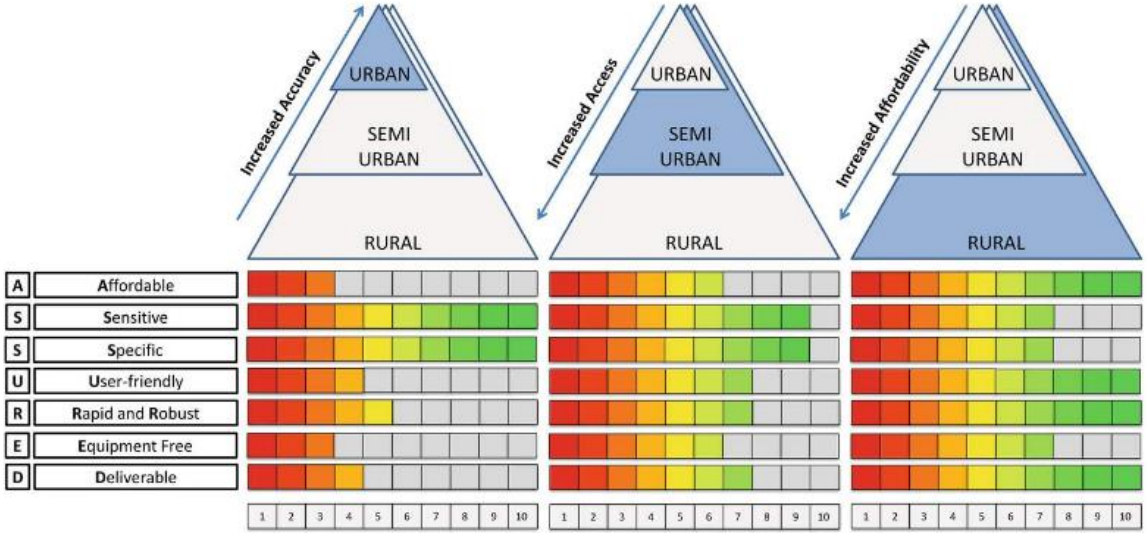

Figure 3.5: WHO ASSURED criteria for POC diagnostics: peak feature trade-off in resource constrained healthcare settings. Target/acceptable criterion score for diagnostics deployed in urban (increased accuracy expected), semi-urban (increased access provided) or rural (increased affordability required) settings are given using a red-yellow-green scale scoring system where red is low and green high. Taken from Land *et al.* [49]

LFT type tests also already have wide market and clinician acceptance due to their successful application in the HIV epidemic as described above. Given the specific gap in TB diagnosis at the POC and the requirement of low cost in this epidemic, these trade-offs are considered acceptable if the sensitivity is ideally greater than or equal to 80% in HIV positive patients or at least better than sputum microscopy [51].

This project aims to determine whether the science applied by Thanyani *et al.* [97] to the biosensor based diagnosis of TB and the reagents developed and demonstrated on enzyme linked immuno sorbent assay (ELISA) by Ndlandla *et al.* [82] and Ranchod *et al.* [91] can be used in an LFT test. Competitive strategies like that proposed for MALIA (mycolate antibodies lateral flow immunoassay) are commonly used on LFTs [103].

3.1.5 Lateral flow tests development considerations

ELISA can be used to characterise antibody/antigen relationships for use in LFT as done by Kumar [116]. However, the affinity required for a visible signal in LFT is much higher because of the short interaction time: effectively one to six seconds on the test line in conjunction with the requirement of overcoming the force of the flow [102]. In ELISA, the antigen/ primary antibody interaction occurs over the course of an hour, without mixing. However, the binding must withstand the forces of the several wash steps following each addition to the test.

LFTs further differ substantially from ELISA in most essential characteristics – substrate, reaction conditions, reaction kinetics and visualisation of the interaction. The effect of these

differences will be explored as the interaction between the MA and the custom developed gallibodies has been demonstrated in ELISA and blot tests (chapter 2).

Some of the major advantages of the use of LFT technology is the maturity and the subsequent widely accepted use of such assays; i.e. the market presence [117]. However, this occasionally leads to the false perception that because the technology is easy to use (and widely used) it is simple to develop. The very age of the technology contributes to the complexity – with many parts requiring extensive optimisation and customisation based on the choice of the reagents [118].

Each component of a LFT requires optimisation. There are several aspects to be considered at every step. Naturally the aim is to develop a test using the least complicated manufacturing process that will be sensitive and specific, show minimal background, use minimal reagents e.g. antibodies and have a strong colour reaction for ease of interpretation.

One of the major overarching considerations that affects numerous aspects of the test and is affected by numerous aspects, is the reaction kinetics of the test [119]. This is primarily influenced by the flow rate of reagent solution over or in the membrane [119]. If the flow rate of the membrane is fast the sensitivity, overall assay time, background 'streaking' and (antigen – antibody binding) reaction rate decreases [119]. Reagent volumes increase as the flow rate increases. The flow rate is determined mostly by the membrane properties – such as pore size and electrostatic interactions, but external factors can change the membrane properties for example blocking reagents [119]. In addition, the properties of the sample (viscosity etc.) as well as the labels used (size, charge etc.) will also affect the flow rate [119]. The flow rate also slows down as the liquid front moves through the membrane, due to decreasing capillary force [119]. A large pore size will increase the flow rate, but also increases the amount of reagent required to produce a strong signal [119]. All of these elements require optimisation to allow for the best antibody-antigen/ analyte-bio-recognition molecule interaction time [119].

As described above there are many properties of nitrocellulose membranes to take in to account but there are also completely different substrate options. One of these is Fusion 5, a proprietary glass fibre based substrate developed to replace all the components (sample and conjugate pads as well as nitrocellulose) of the LFT [120]. There is also a move to use more traditional paper types (i.e. cellulose/cotton based) for LFT development because of their advantages of strength, environmental friendliness and cost over that of nitrocellulose [121]. Substrate choice may be investigated using the flow throw method. In this format the liquid flows vertically through the test spot into the wick behind as opposed to laterally 'up' the test through the capillary channels of the membrane in LFT.

The choice of buffer system for the test is essential. The running buffer and blocking buffer can be considered separately or the blocking reagents can be included in the running buffer or even dried in to the sample pad. This may affect the shelf-life of the test as the membrane is still able to react with the environment [119]. Various reagents can be used to block the membrane (thus preventing streaking) such as bovine serum albumin (BSA), milk powder or poly-vinyl alcohol in addition to the buffering system such as phosphate, Tris, borate etc. [122].

To carefully control the sensitivity of the LFT the volume and concentration of the recognition reagents – usually antibodies – must be considered. This includes the amount of labelled conjugate to dry in the conjugate pad and the amount of antibody/other reagent to immobilise on the test and control lines [122]. Excess capture reagent in the test and control regions increases the likelihood of non-specific binding – potentially causing false positives and also could create steric hindrance, thus decreasing the efficiency of the binding [122]. Naturally an increased amount of labelled conjugate would increase the colour intensity of the test line. However, excess reagent here would simply be wasted as it would flow into the wick [122].

A major determining factor in the sensitivity and specificity of a LFT is the choice of labelled bio-recognition element. Overwhelmingly, antibodies are used for this purpose – specifically monoclonal antibodies – because producing stable polyclonal antibodies with sufficient specificity is difficult [103]. Specific polyclonal antibodies can be produced in chicken egg yolk by immunising egg laying hens. These are often referred to as IgY molecules. These molecules resemble IgG molecules but have several advantages such as native storage stability and increased hydrophobicity (ensuring more stable labelling) [123]. Because of the distance of relationship to humans and other mammals the cross-reactivity with various samples is reduced [123]. The gallibodies used in this study are recombinant engineered antibodies developed from a chicken gene library as described in section 2.2.1.1.

In addition various coloured detection reagents are available for labels, such as latex beads, magnetic particles, quantum dots or carbon nanotubes. Gold nanoparticles have good optical properties and are widely used, making protocols for their conjugation to antibodies and optimisation thereof well understood [103]. This will be discussed further in chapter 4.

Many lesser factors influence and are influenced by these global considerations, all of which could have a significant effect on the functioning of the final test. These include manufacturing conditions and techniques that will not be discussed here as they feature mainly in scaled up production of LFTs. This section has broadly contextualised the space and scope of early LFT development.

3.1.6 Use of lipids, liposomes and lipoidal antigens in lateral flow tests

One of the major challenges for the development of this test is around the use of a lipid antigen test line for a competitive assay. Because mycolic acid (MA) is hydrophobic, the usual protocols used to immobilise proteins (hydrophilic) on the hydrophilic (due to treatment with surfactant) nitrocellulose membrane will not work. In addition, as MA is not soluble in aqueous buffers, solvent compatibility with LFT manufacturing materials and equipment is a challenge. Related cases from literature will be described in this section.

Bührer-Sékula *et al.* [124] developed a LFT to diagnose leprosy by the detection of antibodies to the *Mycobacterium leprae* phenolic glycolipid-1. A semisynthetic tri-saccharide molecule was conjugated with BSA for use as the test line antigen to "present" the mycobacterium specific glycolipid [124]. This molecule would be hydrophilic and the presence of BSA protein would then allow for normal striping and drying protocols to be used for formation of the test line. Patient antibodies would then recognise and bind to this molecule on the test line which would in turn be bound by nanogold-labelled anti-human antibodies forming a red test line.

Such an approach would not be effective for use with MA antigen, as it is not a glycolipid. Cord factor, a MA containing trehalose, is known to give strong patient antibody binding signals [75], but is known to give false positives, i.e. too low specificity to be of practical use in TB diagnosis [125]. Jones *et al.* [69] compared natural trehalose-mycolate with synthetic MA-trehalose preparations. They reported the likely usefulness of seven different synthetic MA-trehalose antigens for diagnosis in an ELISA protocol [69].

A similar challenge of lipid immobilisation was experienced in the development of a LFT for syphilis – a sexually transmitted infection caused by the bacterium *Treponema pallidum*. The immune response to this bacterium involves the production of mostly anti-lipoidal antibodies because of the release of lipoidal material from host cell destruction and possibly from the bacteria. Conjugation of Treponemal lipid antigens results in a loss of antigenicity. Castro *et al.* [126] patented a method to bind these antigens to nitrocellulose using anchor antibody fragments. This was effective as they used a complex of the lipoidal antigens, thus implying the availability of multiple antigenic sites [126]. Such an approach would be unlikely to maintain the antigenicity of the MA.

So-called liposome based LFTs use dye-filled liposomes conjugated to protein or other antigens as the labelled conjugate molecules that allow visualisation at the test line [127]. These then do not involve the use of lipid antigens as the capture molecules immobilised on the test line itself.

Liposomes have been used as carriers of MA for immobilization as antigens on sensor surfaces in the biosensor anti-MA antibody detection device [95]. However, the maximum amount of MA that could be reproducibly included in the liposomes made without cholesterol was 500 µg of MA per mL [95]. This concentration would likely be too low and not sufficiently antigenically available to produce a visible signal on a LFT. Furthermore, the hydrophobicity of MA will may lead to reluctance to bind to the hydrophilic membrane.

Bahadır and Sezgintürk [103] reviewed over 200 publications describing LFT development without a single use of a lipid-antigen as the test line bio-recognition element mentioned. The use of BSA as an antigen carrier molecule was mentioned under the discussion of competitive formats. Because of this, challenges were expected in relation to the immobilisation of the MA on the nitrocellulose.

3.1.7 Chapter outline

In this chapter work is described towards detection of an anti-MA spot by custom developed, labelled anti-MA gallibodies on the LFT. This interaction represents the negative signal for the proposed diagnostic described in figure 1.4.

3.2 Materials and Methods

3.2.1 Materials

Unless otherwise specified salts and reagents were procured from Sigma (USA). Custom developed reagents as described in section 2.2.1 were also applied here. For the gold-labelled conjugate, colloidal gold (40nm) was procured from DCN^{DX} (USA); Hyclone ™ BSA fraction V from GE Healthcare (USA); dibasic sodium carbonate at 0.5 M from Fluka (UK). MES (2-(N-morpholino) ethanesulfonic acid) was procured from Calbiochem EMD Biosciences (USA) and Emplura® ethanol from EMD Millipore Corporation (Germany).

The materials for the LFT manufacture were as follows: goat anti-chicken IgG (Fc) from Bio-Rad; cellulose fibre sample pads and glass fibre conjugate pads from Millipore (USA); Invitrogen membrane blocking solution from Life technologies™ (USA) and backing cards from Kenosha C.V. (Netherlands). Alternative paper substrates: Fusion 5, Chromatography paper (grade 1 CHR), and grade CF3 (CF denotes cellulose fibre) were procured from Whatman™, GE Healthcare (UK). Alternative nitrocellulose membranes (as listed) were procured from Sartorius Stedim biotech (Germany).

3.2.2 Salt test to assess the conjugate stability

A stable conjugate with sufficient antibody to coat the 40 nm gold particle will be indicated by the red-pink colour of the colloidal gold being maintained upon addition of salt. An unstable conjugate is indicated by a purple colour due to aggregation of the gold nanoparticles [128].

Increasing gallibody concentrations diluted in 0.1 M borate buffer (pH 7.4) were added to 1 mL colloidal gold (40 nm) in plastic tubes. Colloidal gold was supplied at an optical density (OD) of 1 at 522 nm absorption and pH 5.2. The gold nanoparticle sol was adjusted to ~ pH 6, 7, 8 and 9 using 0.2 M dibasic sodium carbonate. Tubes were inverted once gently before incubation for 30 minutes at room temperature (RT). Following incubation, 100 µL of 10% (w/v) sodium chloride in 0.1 M borate buffer (pH 7.4) was added, the tube was inverted once more and the colour of the solution observed. The control test contained borate buffer (pH 7.4) as a substitution for the gallibody.

The second lowest concentration that gave a stable red colour was selected for test manufacture to prevent working with a conjugate that was on the border between stable and unstable. Following these experiments, a gallibody concentration of 0.04 mg/mL was chosen for subsequent conjugations as this concentration showed a pink (and therefore stable) conjugate. A pH of 6 was chosen for subsequent conjugations as this showed stable conjugation (pink conjugate) at the lowest concentrations. This test was done initially to determine pH and concentration required for stable conjugation in the test manufacture. The use of this test for conjugate evaluation is presented in chapter 4.

3.2.3 Gold labelled gallibody conjugate preparation

Basic conditions for conjugation and test manufacture were learned in our research group during the development of a LFT for the detection of *E. coli* in waste water described in [116,129,130]. The method for test manufacture and variations tested for each of the parameters are described.

During LFT manufacture, gallibody labelled gold conjugates were used at an OD of ~10 at 522 nm (OD 10 is an approximation based on the 10-fold concentration of gold supplied at OD 1). The final volume of gold (OD 10) required equals the total number of tests multiplied by 3 µL per test. This volume was multiplied by 10 to determine the volume of OD 1 gold required. The amount of gallibody to use was then determined using the following formula:

$$C_1V_1 = C_2V_2$$

Where C_1= the starting concentration of the gallibody, V_1 = the volume of gallibody solution to be added (unknown), C_2= the concentration of gallibody required determined by the salt test (0.04 mg/mL) and V_2 = 10 times the final volume of conjugate required. The gallibody was

added directly to the gold in a plastic tube, the tube was inverted once and the conjugation process was allowed to occur at RT for 30 minutes.

Following the incubation, an equal volume (to the gold volume) of BSA at a concentration of 21 mg/mL (w/v) in 0.1 M borate buffer (pH 7.4) was added and left at ~4°C overnight. The purpose of BSA was to block the open sites on the gold nanoparticle and to further stabilise the gold labelled gallibody conjugate. The following day the gold labelled conjugate was centrifuged at 13 000 x g for 15 minutes in a bench top centrifuge using a soft stop function. The supernatant was removed before re-suspending the pellet and checking the remaining volume using a pipette. The final volume of the conjugate, as determined above, was then made up using a 15% w/v sucrose solution in borate buffer (pH 7.4). This gold nanoparticle-gallibody complex is referred to as the conjugate – the application of which will be described below.

3.2.4 Lateral flow test manufacture

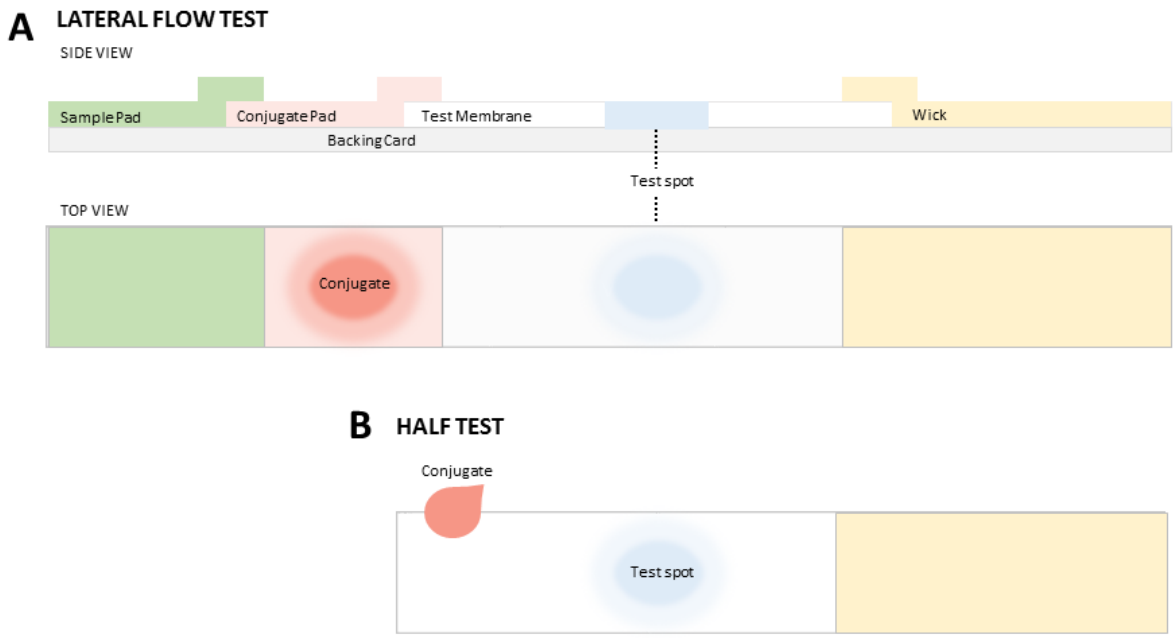

Figure 3.6: Composition of the lateral flow test (A) and the half test (B). The final assembly of the lateral flow test (A) and the half test (B) components are presented as described. Conjugate refers to gold labelled gallibodies. Test spot indicates approximate location of spotted antibody, MA or negative control solvents/diluents. Colours are not realistic.

Glass fibre conjugate pads were blocked by immersion in membrane blocking solution. The conjugate pads were then blotted dry by rolling with a rolling pin between 2 layers of paper roller towel. These were then dried at 37°C for one hour. Three microliters of conjugate were spotted onto the conjugate pads at 1 cm marked intervals. The spotted conjugate pads were then dried at 37°C for a further 30 minutes (as labelled figure 3.6A).

Nitrocellulose membrane 25 mm in width was affixed onto the centre portion of 30 cm long adhesive plastic backing cards.

MA antigen was used as described in section 2.2.1.2. MA antigen dissolved in freshly distilled hexane served as the test spot. The negative test comprised of freshly distilled hexane without MA. Three spots of 1 µL were spotted on top of each other to concentrate the MA used at a concentration of 1 mg in 3 mL hexane.

The positive control contained polyclonal goat anti-chicken IgG (Fc) diluted in 0.1 M phosphate buffered saline (PBS) pH 7.4. A 1 µL volume of the antibody at 0.5 mg/mL in 0.1 M PBS (pH 7.4) or buffer alone was spotted onto the membrane. Successful binding of the same anti-chicken antibody conjugated to horse radish peroxidase (HRP) to the monoclonal gallibodies in ELISA was previously shown during gallibody characterisation studies [91]. The capture agents and corresponding diluent controls were spotted onto the nitrocellulose membrane/s at marked intervals before being dried for at least 30 minutes at RT.

Following this, the membranes were blocked using the membrane blocking solution. The blocking solution was pipetted directly onto the membrane and allowed to wet the entire length of the membrane before the excess liquid was shaken off the surface. The remaining excess solution was then blotted off using a double layer of paper roller towel. Following this the membranes were left at RT for at least 2 hours to dry.

Tests were assembled as follows: cellulose fibre sample pads were used as the wick and placed at the top end of the adhesive backing card with ~2 mm overlap on the nitrocellulose membrane. The spotted conjugate pad was placed along the opposite end of the nitrocellulose (aligned via the interval markings, figure 3.7) on the adhesive backing card with ~1 mm overlap. An additional unblocked glass fibre conjugate pad was used as the sample pad, placed with ~1 mm overlap on the conjugate pad. The assembled test card was then cut in to strips of approximately 0.5 cm ensuring that none of the visible conjugate spot was cut off and wide enough to include the entire test spot (not visible).

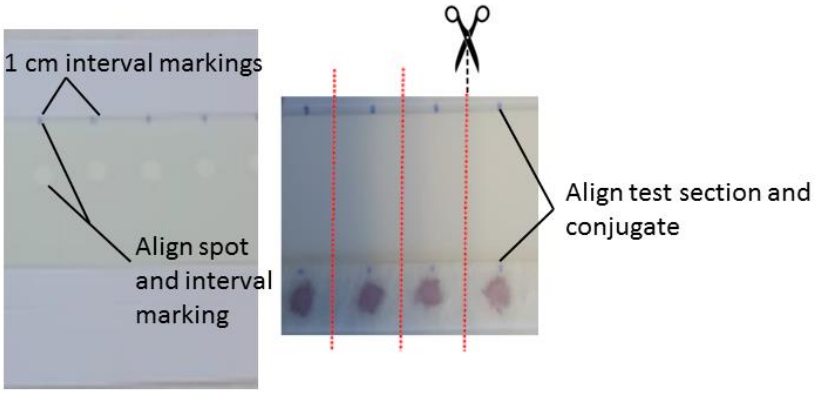

Figure 3.7: Test manufacture alignment process. Required alignment of the test spot and spotted conjugate before cutting is shown. Figure adapted from internal protocol prepared by Shavon David.

The tests were run with 200 µL borate buffer (pH 7.4) in an upright position in clear plastic tubes. Tests were run for a minimum of 15 minutes until the wick was completely saturated. For half tests, figure 3.6B above, three microliters of conjugate was spotted directly onto the nitrocellulose before dropping the test in 200 µL borate buffer (pH 7.4). In addition to borate, MES at 0.01 M (pH 7), phosphate buffer (PB, dibasic at 0.036 M, pH 9.1) and PBS (0.1 M, pH 7.4) were explored as alternative running solutions. The tests were scanned on a HP Scanjet 2400 flatbed scanner to record the results.

3.2.5 Phosphomolybdic acid staining

Phosphomolybdic acid (PMoA) staining is commonly used for staining thin layer chromatography membranes to detect lipids [131]. PMoA was prepared in ethanol at a concentration of 10% (w/v). The stain was applied to the nitrocellulose membrane after the tests were run with buffer to assess whether MA was present on the membrane. PMoA was dispensed into a petri dish to cover the bottom (~ 5 mL) and the dry LFTs, with wick and sample/conjugate pads removed, were dipped into the solution. The corner of the test was touched onto the petri dish rim to draw off the excess stain. The tests were then developed in an oven at 60°C on a wire mesh tray for 8 minutes. The tests were scanned on a HP Scanjet 2400 flatbed scanner to record the results.

3.2.6 Alternative substrate investigation

Four UniSart membranes with different flow speeds and thicknesses (as given in table 3.1) were compared to the FF80HP nitrocellulose membrane from GE Healthcare.

Different paper substrates (i.e. alternatives to nitrocellulose membrane) were tested in the flow through format. The flow through format is described in figure 3.8.

The following substrates were tested: Fusion 5, a glass fibre based proprietary material [120]; Chromatography number 1 (grade 1 CHR), a commonly used paper type in paper microfluidics [132] and Grade CF3 a highly pure cotton linter paper.

For the flow through tests, MA, anti-chicken antibody (positive control), hexane and PBS (negative controls) were each spotted onto the different substrate types using a 2 µL volume for the anti-chicken IgG (Fc) antibody (at 0.5 mg/mL) and PBS or a 3 x 2 µL volume for the MA (at 1 mg/mL) and hexane. The spots were dried for at least 30 minutes at RT. Following spotting, the substrate squares (1 cm x 1 cm) were blocked using the commercial Invitrogen blocker by pipetting blocker solution onto the squares until completely wet. Wet squares were left for 10 minutes at RT before blotting between two layers of paper roller towel and then allowed to dry at RT for a further two hours at least. Dry squares were placed on top of a square of wick (~2 cm x 1 cm) and 3 µL of the gold conjugate was pipetted directly onto the test spot. The test was then washed to remove non-specific binding by pipetting 200 – 500 µL of 0.1 M borate buffer (pH 7.4) over the spot in 50 µL increments.

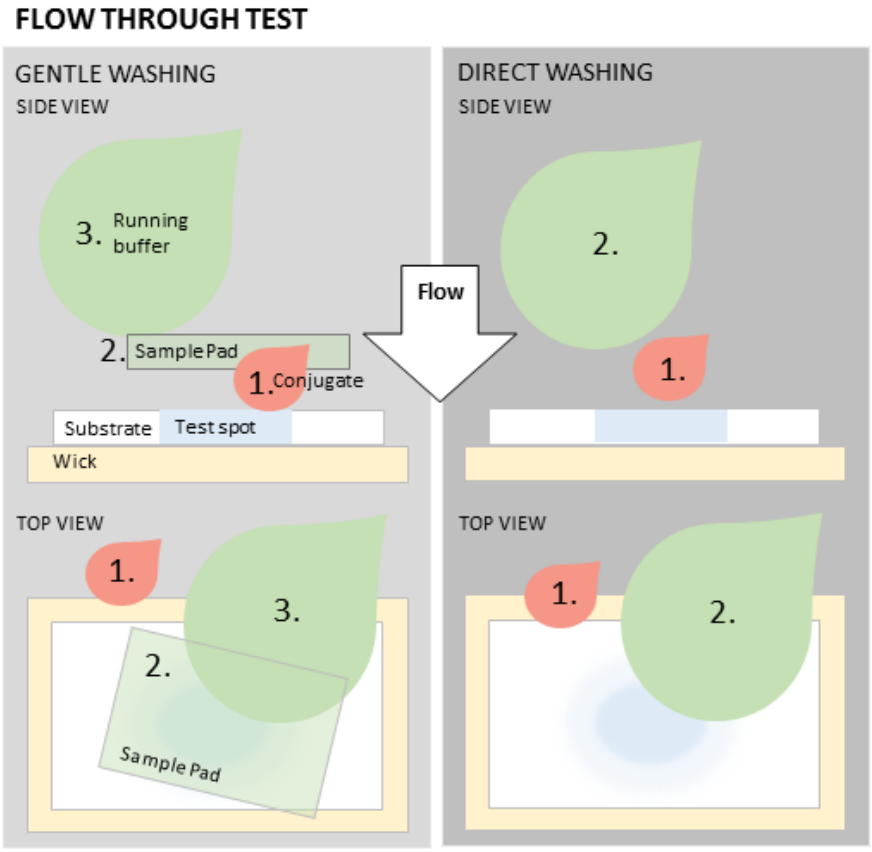

Figure 3.8: Composition and steps followed for the flow through test format. Two configurations of the flow through test were tried – with gentle washing done through a sample pad (left) or using direct washing (right). Conjugate refers to gold labelled gallibodies. Test spot indicates approximate location of spotted antibody, MA or negative control solvents. Colours are not realistic. Numbers denote the order of addition.

Two different configurations were tested as shown in figure 3.8. The first variation the washing step was done by directly pipetting buffer onto the spotted conjugate (figure 3.8, right). In the second, the washing was done by placing a square (1 cm x 1 cm) of the glass fibre conjugate pad over the test and then pipetting the buffer onto that (figure 3.8, left). This was done to make the washing process gentler and thus possibly allow the low binding affinity anti-MA gallibodies to remain bound. Both of these configurations were tested with and without overnight binding of the conjugate. Test squares were scanned on a HP Scanjet 2400 flatbed scanner to record the results.

3.2.7 Alternative blocker investigation

Casein solutions (as tested in chapter 2) were also investigated as possible blockers of the nitrocellulose membrane for the LFT. For these tests 0.025% (w/v) biochemical reagent casein (BRC), scientific sports casein (SSC) and casein hydrolysate (casH) blockers (section 2.2.2) were compared to the commercial membrane blocking solution (Invitrogen, Life technologies, USA) used above. Casein blocker solutions were prepared as in section 2.2.2 and membranes blocked as described in section 3.2.4.

3.3 Results and discussion

In early work, LFTs were manufactured using basic conditions similar to those used for a test to detect *E. coli* developed in the group and described in the thesis by Govindasamy [129]. Figure 3.9 shows photographs of these early attempts. MA in hexane was spotted on nitrocellulose membrane. Also spotted were hexane, a control anti-chicken IgG (Fc) antibody diluted in 0.1 M PBS and PBS as a negative control. Spots were probed with gold labelled gallibody 18-2 conjugate.

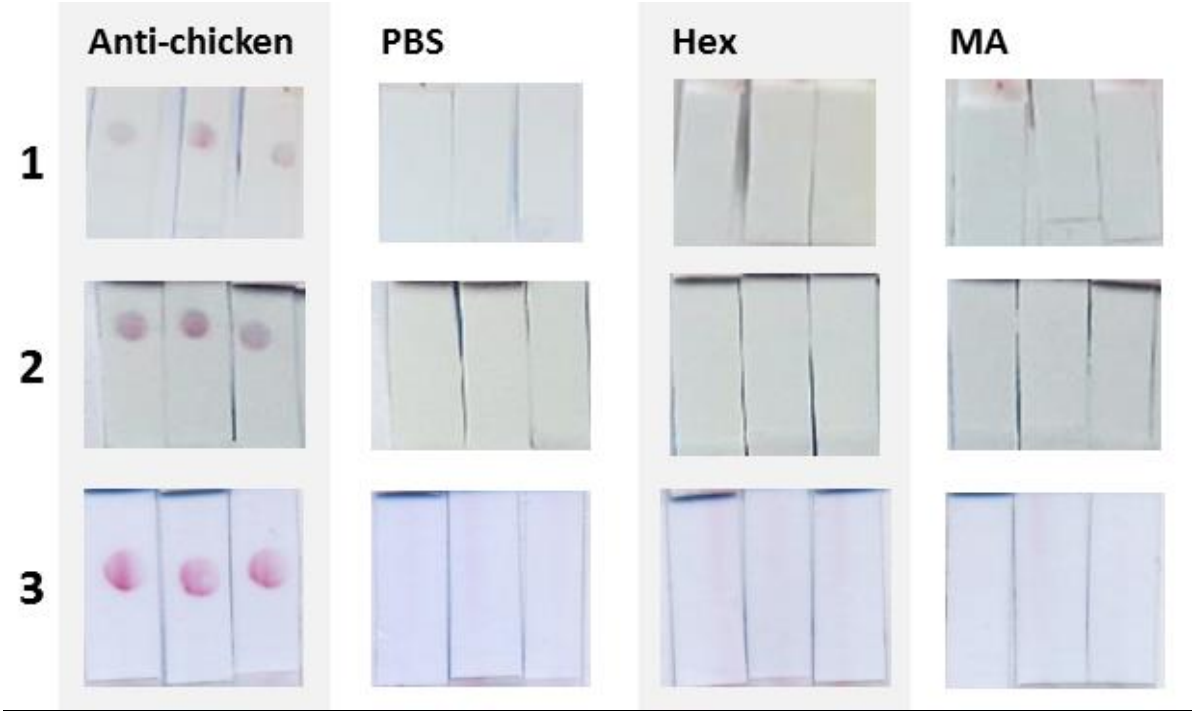

Figure 3.9: Examples of unsuccessful detection of coated MA by gold labelled gallibody conjugate. A 3 µL volume of gold labelled gallibody 18-2 in the LFT format was used to probe anti-chicken IgG (Fc) antibody (positive control), MA (test), PBS and Hexane (negative controls) spotted on nitrocellulose. Cropped photographs of the test section of three replicate experiments (1, 2 and 3) are shown.

The conjugated gallibodies are bound by the anti-chicken IgG (Fc) antibody giving a clear signal (figure 3.9). This antibody was chosen as the control because successful binding of the same anti-chicken IgG (Fc) antibody labelled with HRP to the gallibodies in ELISA was previously shown during characterisation studies [91] and chapter 2. In figure 3.9 no background signal is seen on the negative controls of PBS (the anti-chicken IgG (Fc) antibody diluent) or the hexane (the MA solvent). No conjugate signal is visible on the tests spotted with MA. The binding of MA by the custom developed gallibodies as shown in the ELISA and blot test signals (chapter 2) was not visible on the LFT (no anti-MA signal). This binding is the anticipated active interaction on the test line in the case of a negative patient sample and is the key signal for the development of MALIA. The absence of this signal will be explored and options investigated to allow ideal conditions for its formation.

3.3.1 Probing of absence of anti-mycolic acid gallibody signal on the test line

The blot test shown in the previous chapter (figure 2.6) confirmed the antigenicity of MA when spotted on nitrocellulose. However, it is possible that the MA is washed off the membrane during the flow of the LFT. The presence of the MA on the nitrocellulose after running the test was confirmed using a PMoA staining procedure that is used to stain lipids (section 3.2.5). This method was adapted from that used for thin layer chromatography visualisation of

cholesterol and bile salts [131]. Oven drying of the test after blocking (during manufacture) was also compared to air drying. Selected results of staining experiments are shown in figure 3.10.

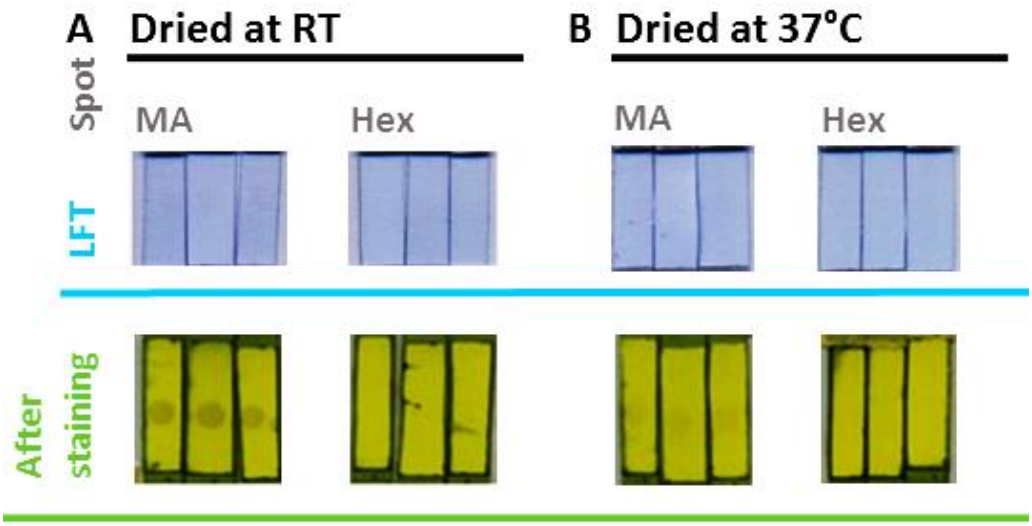

Figure 3.10: Phosphomolybdic acid staining to confirm presence of MA on nitrocellulose. Lateral flow tests prepared by drying at room temperature (RT) (A) or at 37°C (B). After spotting and blocking they were tested with gold labelled gallibody 18-2 conjugate in the LFT format. Test membranes were stained with phoshomolybdic acid (PMoA). Cropped scans of the test sections are shown after running (top) and after staining (bottom).

The staining confirmed the presence of MA on the test spots (figure 3.10 bottom tests) after running and showed stronger stained MA signal for tests dried at ambient conditions (A) rather than those dried at 37°C (B). Antigen and blocker drying conditions will require optimisation again in the developed test because this result only assumed a workable condition that may not be optimal for obtaining a gold labelled gallibody conjugate anti-MA signal.

Despite initial fears that the MA would prove difficult to immobilise on nitrocellulose in an antigenic form, PMoA staining results showed that the MA was present on the nitrocellulose (figure 3.10). As previous results using the same spotting technique showed, it is still antigenic (figure 2.6). As outlined in the introduction of this chapter, there are substantial differences, between the conditions in ELISA and LFT and there are many variables in LFT format that can influence the final result. Subsequently these variables were explored to attempt to find a combination that would allow for the formation of a visible gold labelled gallibody conjugate signal on the MA spot.

3.3.2 Alternative substrate investigation

Nitrocellulose is commonly used for LFTs, however, not all nitrocellulose membranes are the same [133]. A commonly reported variable is the flow speed of the membrane. The flow speed is measured as the seconds taken for an aqueous liquid front to move 40 mm ‘up’ the membrane. A faster flow rate will result in less interaction time of the labelled gallibodies with

the spotted MA or anti-chicken control, which may influence signal formation. This is especially important as the gallibodies have a relatively low affinity for their antigen as can be seen from the high concentration of gallibody required to obtain signals in ELISA [91], comparable to that observed with anti-MA antibodies in human TB patient sera [88].

Additionally, different nitrocellulose membrane manufacturers use different surfactants which are added at different stages of the manufacturing process [134]. To explore the possible effects of this, nitrocellulose membranes from Sartorius Stedim with varying flow speeds were tested and compared to the FF80HP membrane manufactured by GE Healthcare (figure 3.11).

Manufacturer provided flow speeds and thickness of the membranes tested are listed in table 3.1. The membranes are named for their average expected flow speed (s/40mm).

Table 3.1: Nitrocellulose membrane properties

Manufacturer	Membrane name	Flow speed (s/40mm)	Thickness (µm)
GE	FF80HP	60 – 100	200
Sartorius Stedim	UniSart™ CN 95	90 – 135	240 – 270
Sartorius Stedim	UniSart™ CN 150	90 – 180	240 – 280
Sartorius Stedim	UniSart™ CN 140	140 – 165	225 – 250
Sartorius Stedim	UniSart™ CN 110	110	200

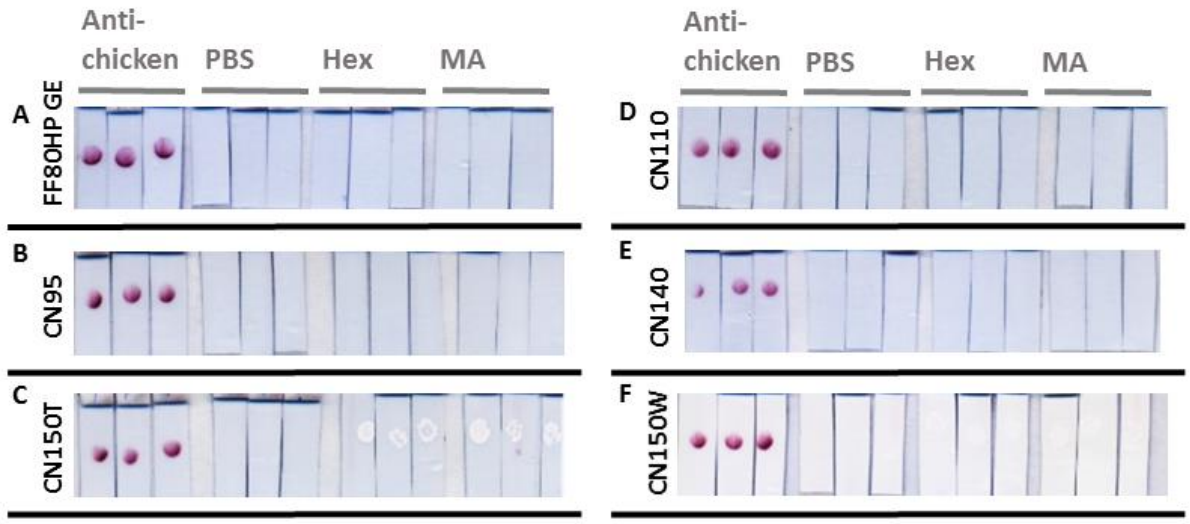

Figure 3.11: Nitrocellulose membrane investigation to compare the effect of membrane properties on gold labelled gallibody conjugate binding. Lateral flow tests were prepared using six different membranes (A – F) of varying flow speed and thickness. Spotted MA, hexane, anti-chicken IgG (Fc) antibody and 0.1 M PBS were probed with gold labelled gallibody 18-2 conjugate in the LFT format. Membrane names (denoting average flow speed) appear to the left of each series of tests. The 'T' and 'W' in CN150T/ CN150W denote the colour of the membrane backing as white or transparent. Cropped scans of the test section of three replicate tests are shown.

In terms of the anti-chicken IgG (Fc) antibody positive control signal intensities, the differences of thickness and flow speed do not appear to have made a difference (figure 3.11). However, it was observed that the white backed membrane CN150W gave excellent contrast, allowing the signal to appear brighter (figure 3.11F). It is worth noting that clear surface disturbed spots are visible for the CN150 membranes (figure 3.11C) spotted with MA or hexane (less visible for the white backed membrane). As this membrane has the slowest reported flow speed, these surface disturbed spots may be caused by the slow interaction of the aqueous flow front with the spotted hydrophobic solvent/lipid. Membrane flow speed choice will need to be revisited in the optimisation process of the test once the basic specifications for visible gold labelled gallibody-MA interaction are determined.

Membrane properties such as thickness and flow speed can have significant effects on the signal intensity and shape of the test spot or line. During spotting/striping, membranes with faster flow speed will produce larger more diffuse spots/ wider lines as the reagent will diffuse further into the paper before drying. [134] This effect was not visible in the above result. In addition the flow speed during running affects the amount of reaction time for the labelled probe with the spotted capture agent, this was demonstrated by Lee *et al.* [135]. Literature suggests that lower flow rates improves sensitivity [136]. This flow speed is affected by the membrane properties as well as the properties of the running buffer and blocking. [134] The first of these, the membrane properties, did not allow the formation of an anti-MA signal, nor did they appear to affect the intensity of the control signal.

Three completely different substrates (i.e. not types of nitrocellulose) were investigated using a flow through test format described in section 3.2.6 and figure 3.8. These substrates were: Fusion 5, a glass fibre based proprietary material from GE [120]; Chromatography number 1, a commonly used paper type in paper microfluidics [132] and CF3 (a highly pure cotton linter paper). In this format MA, hexane, anti-chicken IgG (Fc) antibody or 0.1 M PBS was spotted onto paper squares, dried and blocked as with nitrocellulose. To run the tests, a square of wick was placed underneath and 3 µL gallibody 18-2 gold conjugate pipetted onto the test followed by washing with an excess of borate buffer. Results are shown in figures 3.12 and 3.13.

In this format other parameters could also be manipulated to potentially encourage the formation of a specific anti-MA signal. The first of these is the interaction time of the conjugate with the antigen spot. Longer interaction was tested based on the ELISA protocol where the gallibody has one hour to interact with the coated MA. Therefore it could be possible that a longer interaction time may be required for binding of the low affinity gallibody to MA. The tests with overnight interaction with the conjugate are labelled ‘washed: next day’ in figure 3.12 and

3.13. These tests showed higher background signal as observed visually than those washed immediately. The anti-MA signal was not visibly darker than the controls however the anti-chicken IgG (Fc) control signals were.

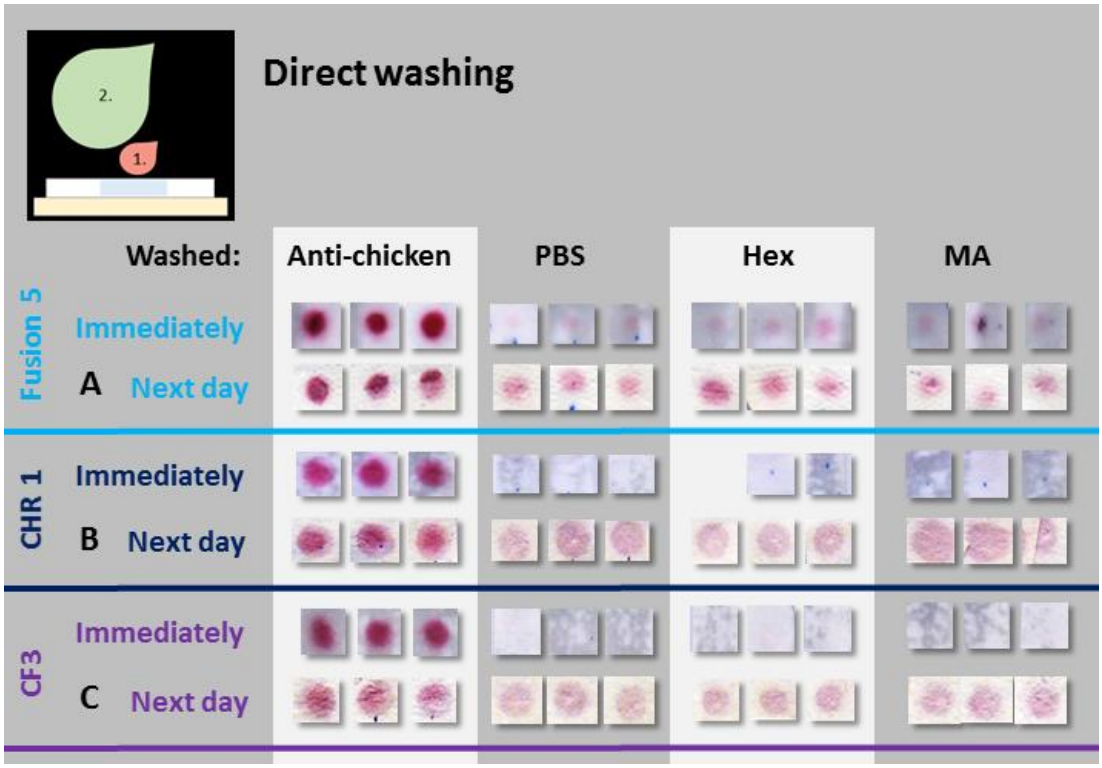

Figure 3.12: Flow through tests using direct washing comparing the effect of paper type and reaction time on signal intensity. Flow through tests were carried out on Fusion 5 (A, light blue), Chromatography CHR 1 (B, dark blue) and CF3 (C, purple) as substrates. In this experiment gold labelled gallibody 18-2 conjugate was spotted onto the prepared tests and washed by pipetting buffer directly over this - either immediately after or the next day (as indicated). See figure 3.8 for schematic principle of the test. Cropped scans of the test section of three replicate tests are shown.

It was hypothesized that the direct washing off of the conjugate by pipetting buffer onto the MA spots may disrupt any low affinity binding. To test this, the washing of the conjugate was made gentler by pipetting the buffer onto a sample pad placed on top of the test rather than directly onto the test (figure 3.13). This did not result in a specific heightened signal for the MA spot.

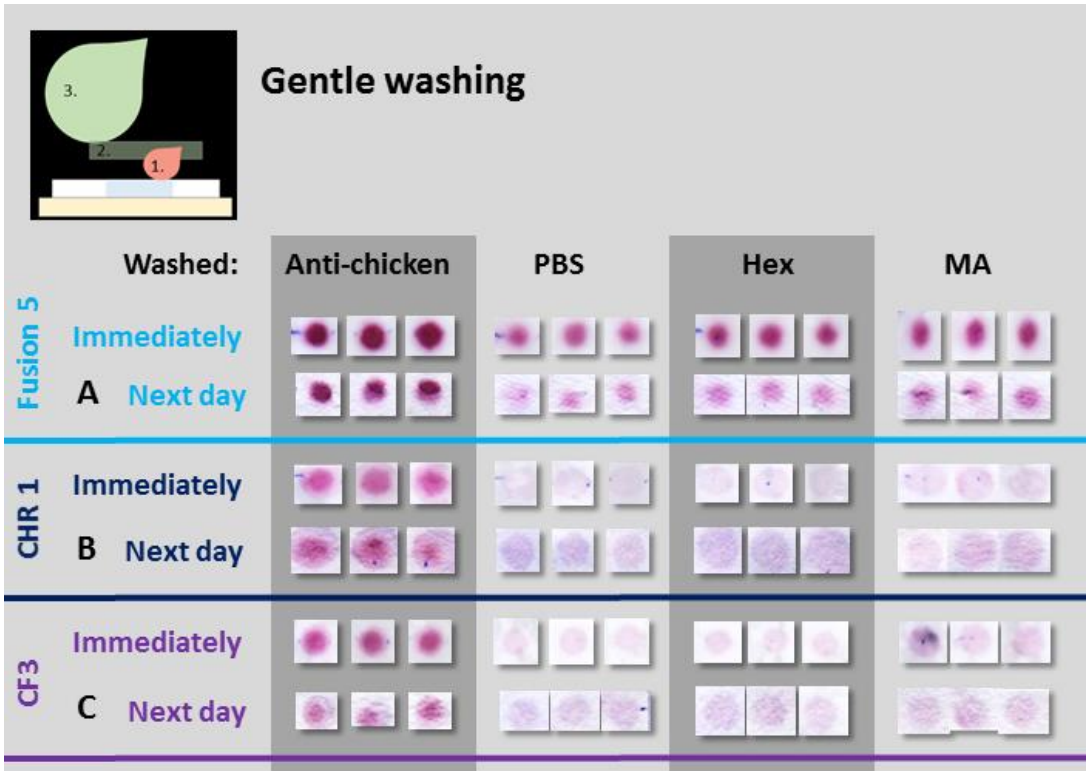

Figure 3.13: Flow through tests with gentle washing comparing the effect of paper type and reaction time on signal intensity. Flow through tests were carried out on Fusion 5 (A, light blue), Chromatography CHR 1 (B, dark blue) and CF3 (C, purple) as substrates. Tests were washed indirectly by pipetting wash buffer through a glass fiber sample pad instead of directly onto the spot, either immediately after or the next day (as indicated). Cropped scans of the test section of three replicate tests are shown.

The positive control anti-chicken IgG (Fc) antibody signal was visibly stronger than the others for all experiments on all paper types tested as expected. The fusion 5 substrate produced the most intense positive control signals, however the background (PBS/hex signal) was also commensurately darker (figures 3.12 and 3.13). The Chromatography 1 and CF3 paper types performed similarly in terms of signal intensities and background.

The alternative substrates and membranes tested did not allow for the formation of an anti-MA gallibody signal. Membrane/substrate properties will still require optimisation once the correct conditions are determined to obtain this signal. Furthermore the adaptation of the method to reduce the force of the washing step (figure 3.13) did not allow for the formation of a specific signal on the MA spot.

3.3.3 Membrane blocker investigation

On LFTs the choice of blocker has a significant effect on the running of the test, affecting flow speed and consequently reaction kinetics by changing the properties of the membrane [133]. The ELISA protocol with casein as the blocker shows gallibody binding to the coated MA. The different casein sources previously tested in ELISA (section 2.3) were also applied as blocking

agents on the nitrocellulose membrane during LFT manufacture and compared to the commercial Invitrogen blocker (figure 3.14).

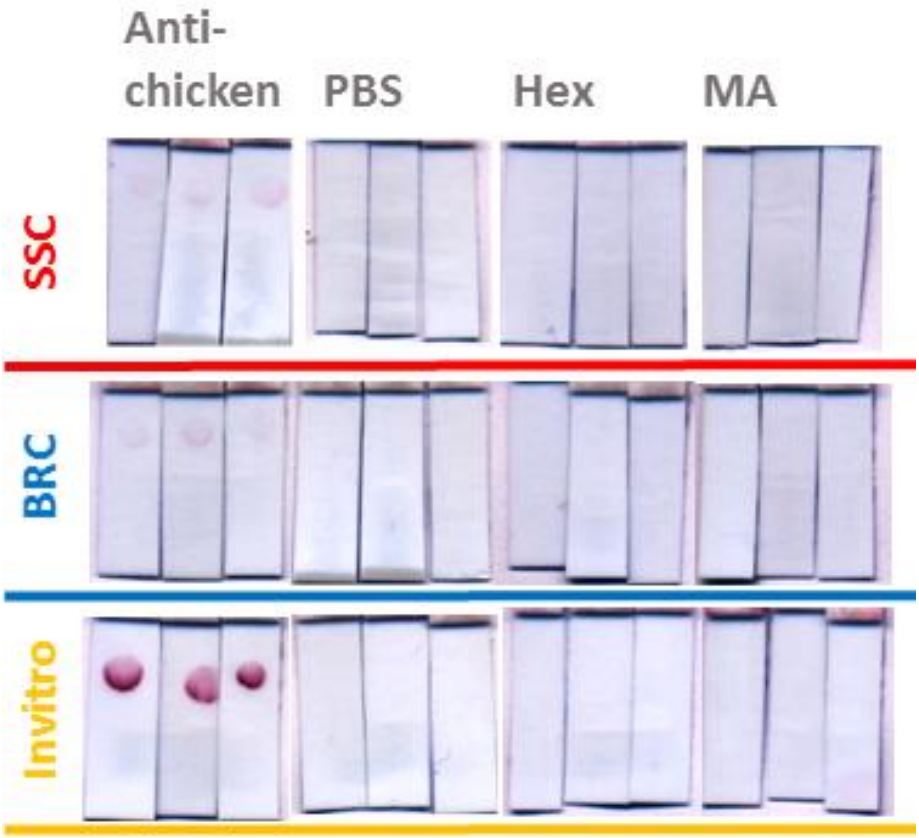

Figure 3.14: Half tests comparing commercial Invitrogen blocker to casein blockers by gold labelled gallibody conjugate binding. Half tests were prepared using three different blockers denoted as follows: 'SSC', red – sports supplement casein; 'BRC', purple – biochemical reagent casein and 'Invitro', yellow – Invitrogen commercial blocker. Casein blockers were used at a concentration of 0.025% (w/v) prepared in 0.1 M borate buffer and pH adjusted to 7. Tests were probed with 3 µL of gold labelled gallibody 18-2 conjugate spotted directly onto the membrane before running in 0.1 M borate buffer. Cropped scans of the test section of three replicate tests are shown.

The casein blocked tests showed much fainter positive anti-chicken IgG (Fc) antibody control signals than the Invitrogen blocked tests (figure 3.14). It was observed (data not shown) that the casein blocked tests showed a significantly slower flow rate than the Invitrogen blocked tests. This follows as the casein would block the pores in the nitrocellulose and thus slow down the flow [134]. Lutz *et al.* [137] applied a sugar solution to slow down flow in paper based devices due a similar effect [137]. However, in the case of sugar on paper the pore blocking is reversible as sugar dissolves in the presence of the running buffer. Protein based blockers interact with and bind to the membrane and so cause different effects. It is likely that the change in reaction kinetics and conditions caused by the casein blocking affected the binding of the gold labelled gallibody to the spotted antibody control. A similar effect of flow speed reduction (caused by

addition of BSA to the running buffer) on signal intensity was observed by Preechakasedkit *et al.* [138].

The casein hydrolysate that was previously tested on ELISA (chapter 2) was also tested as a membrane blocker using the same method as applied in figure 3.14 above but on a LFT format. The results are shown in figure 3.15.

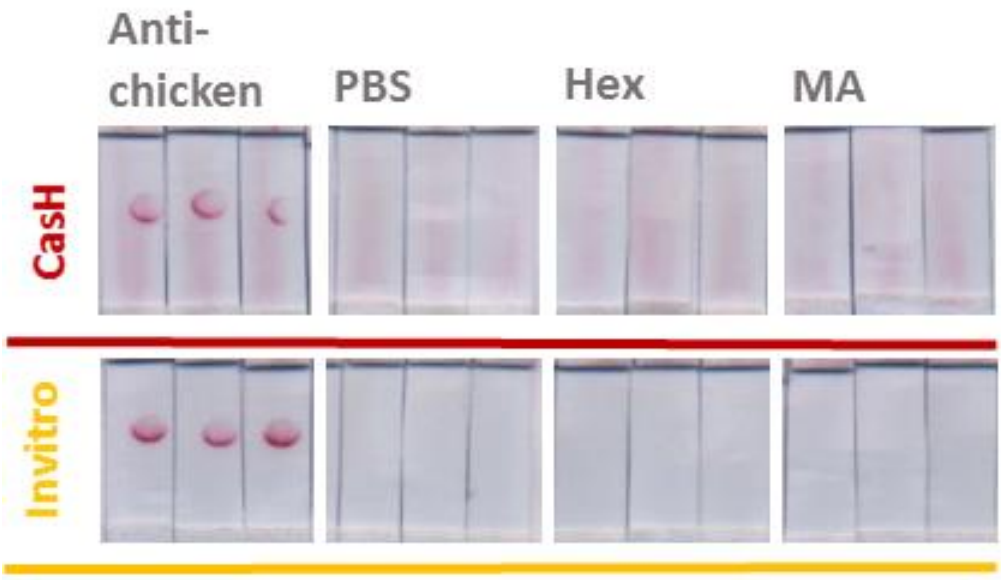

Figure 3.15: LFTs comparing commercial Invitrogen blocker to casein hydrolysate by gold labelled gallibody conjugate binding. Lateral flow tests were prepared using 'casH', maroon – casein hydrolysate and 'Invitro', yellow – Invitrogen commercial blocker. Casein hydrolysate was used at a concentration of 0.025% (w/v) prepared in 0.1 M PBS buffer. Tests were probed with 3 µL of gold labelled gallibody 18-2 conjugate spotted directly onto the membrane before running in 0.1 M borate buffer. Cropped scans of the test section of three replicate tests are shown.

The anti-chicken IgG (Fc) control signal is slightly less for the casein hydrolysate blocker than for the commercial blocker, however the hydrolysate tests (figure 3.15, 'casH') showed a background staining/'streaking' effect indicative of insufficient blocking of non-specific binding sites on the nitrocellulose [139]. No anti-MA signal was visible.

It is clear from the changes in signal intensity of the control anti-chicken IgG (Fc) signal that membrane blocking has a significant impact in LFT performance. However, the use of casein as a blocker does not allow for the formation of an anti-MA signal.

3.3.4 Running buffer investigation

The running buffer used was investigated as it is the same buffer that the gallibodies are purified in and in which they are known to be stable and active (from ELISA results). Three other buffers were chosen that are in use in the lab in applications similar to this. Dibasic phosphate buffer (PB) is used as the running buffer in the *E.coli* detection test developed in

our research group; MES buffer is used as an alternative gallibody purification buffer for application of the gallibodies in kit labelling strategies and PBS is used in the ELISA to characterise the functionality of the gallibodies. These buffers (at the concentrations and pH otherwise used) were tested as running buffers for half tests spotted with anti-chicken IgG (Fc) control antibody and MA, and their solvents PBS and hexane as previously described. Spots were probed with gallibody 18-2 conjugated to gold (figure 3.16) and BSA conjugated to gold as a non-specific control (result not shown).

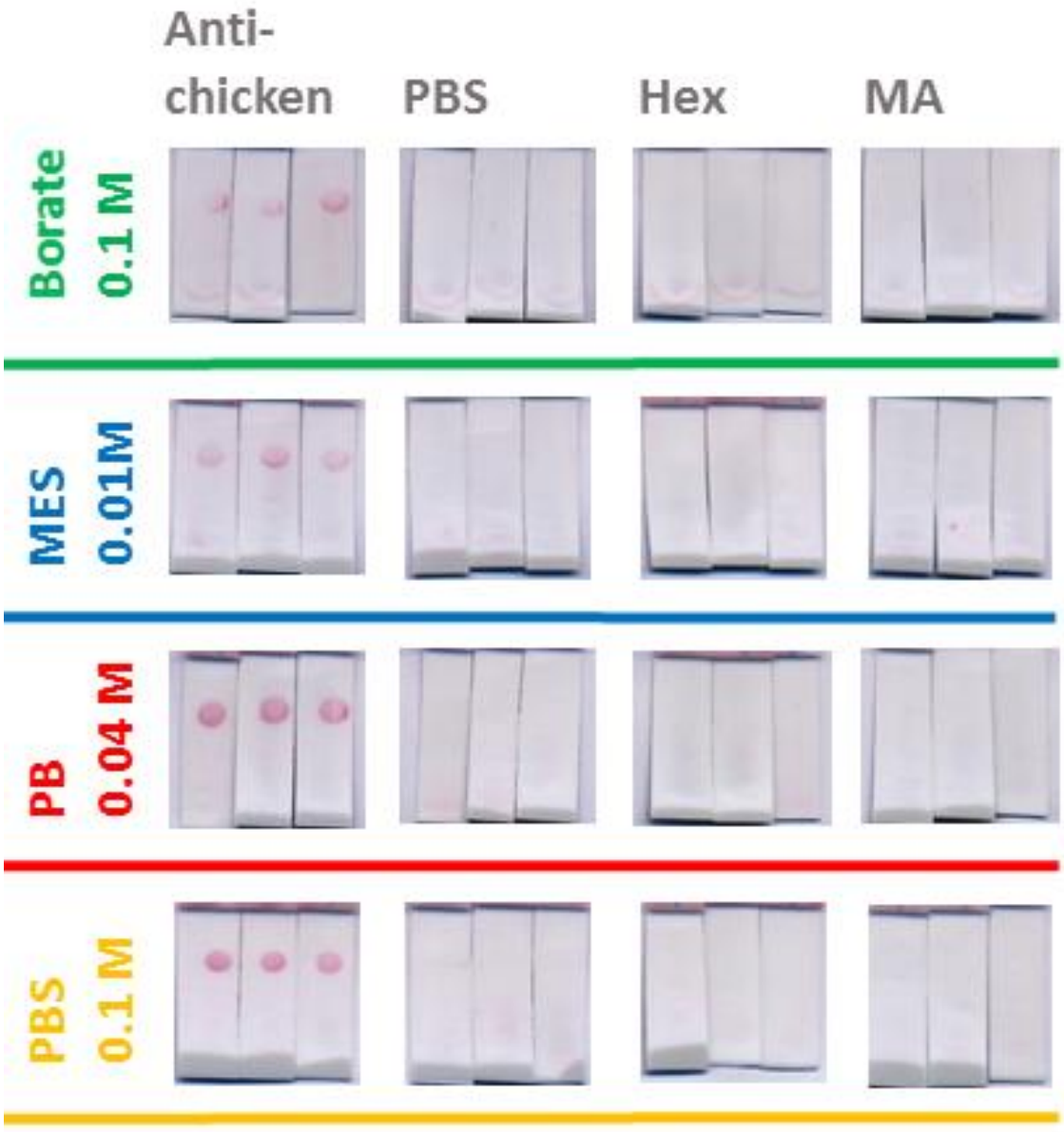

Figure 3.16: Half tests comparing different running buffers by gold labelled gallibody conjugate binding. Half tests were prepared and run in 200 µL of either borate buffer (green), MES buffer (blue), dibasic phosphate buffer (PB, red) or phosphate buffered saline (PBS, yellow). Tests were probed with 3 µL of gold labelled gallibody 18-2 conjugate spotted directly onto the membrane before running. Cropped scans of the test section of three replicate tests are shown.

As with the choice of membrane blocker, the choice of running buffer appears to have an intense impact on the intensity of the anti-chicken IgG (Fc) control signal, with PB (figure 3.16, red) giving the best signal intensity. The BSA conjugate tests (not shown) showed no background signal in any of the running buffers, indicating that the anti-chicken IgG (Fc) signal seen is not as a result of non-specific binding due to denaturation of the gallibody (on the gold) or the spotted anti-chicken IgG (Fc) antibody in the different buffers used.

These running buffers have different molarities and pHs which can affect the folding state of the spotted MA and anti-chicken IgG (Fc) antibody as well as the gold labelled gallibody. The running buffers tested here are unlikely to have affected flow speed as they are all aqueous buffers with similar viscosity. Higher viscosity buffers (sometimes used when blocker is added in the running buffer) also affects flow speed and thus test performance [138].

3.4 Conclusion

This chapter introduced LFT technology and presented a defence for its choice to convert TB diagnostic biosensor technology previously developed [97] to a POC usable device to diagnose active TB.

The explorative work towards the detection of MA spotted on nitrocellulose by gold labelled gallibodies is presented. MA was shown to remain immobilised on the tests by PMoA staining (figure 3.10) although it was not detected by the gold labelled 18-2 gallibody using basic conditions (figure 3.9), nor when conditions such as substrate (figures 3.11 – 3.13), blocker (figure 3.14 – 3.15) or running buffer (figure 3.16) were varied.

The custom developed gallibodies successfully bind MA in ELISA and blot tests that have similar protocols (chapter 2). This binding is not seen on the LFT format (chapter 3). LFTs differ substantially from ELISA in most essential characteristics – substrate, reaction conditions and kinetics, and visualisation of the interaction. The differences in substrate, reaction conditions and kinetics have been partially explored in the tests presented here. The differences in visualisation of antibody/antigen interaction i.e. gold labelled gallibody vs enzyme linked secondary antibody/tetramethylbenzidine reaction remain to be explored. In the following chapter the functionality of gold-labelled gallibody probe will be evaluated using various methods and alternatives explored.

Chapter 4: Labelled gallibody evaluation and alternatives

4.1 Introduction

In chapter 3 various options were explored to produce the optimal conditions for measuring the interaction of gold labelled gallibody conjugates to immobilised mycolic acid (MA) in the lateral flow format. In this chapter antibodies conjugated to colloidal gold nanoparticles and their use as bio-recognition elements and labels in lateral flow tests (LFT) are introduced. The gold labelled gallibody conjugate is evaluated in terms of the conditions required for the conjugation and the effect of conjugation on the gallibody functionality.

4.1.1 Antibodies

For the proposed LFT, custom developed anti-MA monoclonal antibodies, termed gallibodies, were developed as previously described [91]. These gallibodies were investigated for use as the labelled bio-recognition element on the LFT. The basic structure of antibodies and antibody/antigen binding thermodynamics will be briefly discussed below as this pertains to the evaluation and proposed use of these gallibodies.

The basic structure of antibodies is conserved among different species. Antibodies are made up of four protein chains – two heavy and two light – and take on a Y shaped structure. A detailed representation of the basic structure of a mammalian antibody is given in figure 4.1, annotated with the commonly used nomenclature for the various regions. The Fc (fragment crystallisable) region forms the trunk of the Y shape and the Fab region (fragment antigen binding) form the arms of the Y shape [140]. The two heavy chains span the Fab and Fc region with a flexible hinge region in the centre. Each have four domains, one variable (V_H) and three constant (C_H1-3) [140]. The light chains each consist of a variable (V_L) and constant (C_L) domain [140]. The structure of the recombinant gallibodies used in this study (slightly different from the mammalian antibody shown here) are shown earlier in the text in figure 2.1. The antigen binding site is formed at the tips of the Fab region on both the heavy and light chains by sites called the complementarity determining regions (CDRs, [140]).

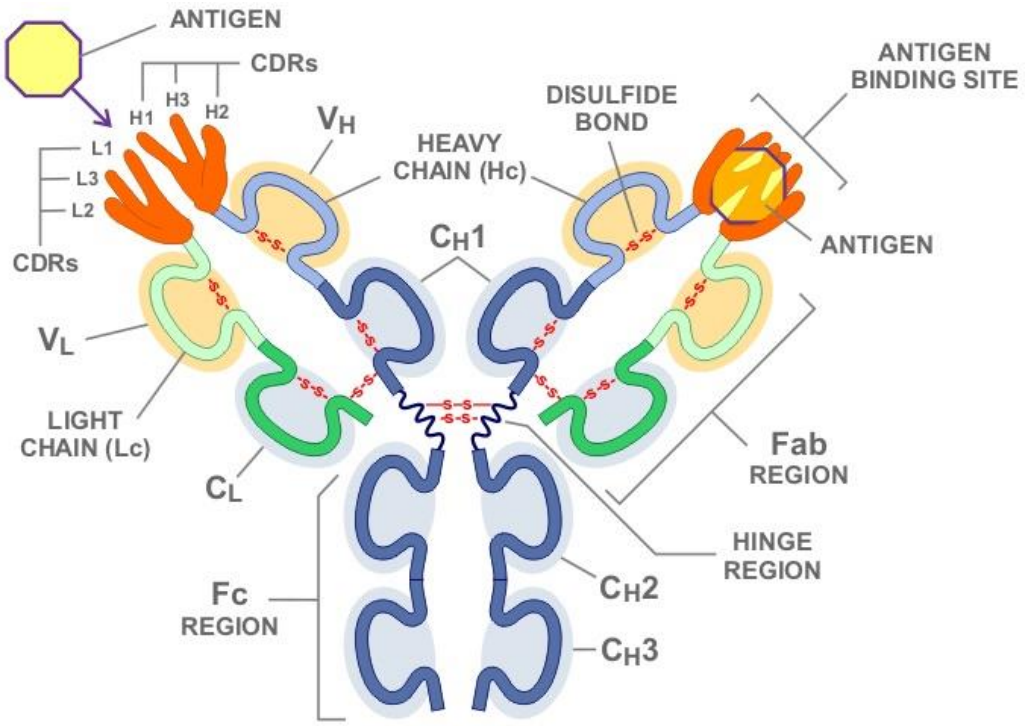

Figure 4.1: Labelled representation of the structure of an antibody. Abbreviations: Fc = fragment crystallisable; C_H1, 2, 3 = constant heavy domains; C_L = constant light domain; Fab = fragment antigen binding; V_L = variable light domain; V_H = variable heavy domain; CDR = complementarity determining region; L1 – 3 = Light chain regions; H1 – 3 = Heavy chain regions. Taken from The School of Biomedical Sciences Wiki, Newcastle University [141].

Biomolecular interactions are described by thermodynamics and reaction kinetics. The thermodynamics of reversible antibody/antigen interactions are defined by affinity and avidity and can be described by the mass action law [142,143]. At equilibrium, the dissociation constant (K_D, also referred to as the binding affinity) is equal to the ratio between the concentrations of dissociated antibody (Ab) and antigen (Ag) and the associated complex of the two [142,143]. This relationship is described by the equation:

$$K_D = {[Ab][Ag]}/{[AbAg]}$$

The association constant (K_A) is naturally the inverse of this relationship. The units for these values are then molarity (M) and M^{-1} respectively [142,143].

When talking about affinity a definition for avidity must also be given. Avidity relates affinity to the valency of an antibody, i.e. the number of antigen binding sites [143,144]. This is also called the functional affinity. The greater the avidity the greater the affinity will appear, but affinity is defined by the strength of the binding only between a single antigen binding site and its antigen [143,144]. While the basic structure of an antibody has two binding sites (figure 4.1), mammalian antibodies occur in different classes, some of which are multivalent with four or ten available

binding sites (figure 4.2) [140]. Naturally, increased valency will usually increase the avidity of an antibody for its antigen [143,144].

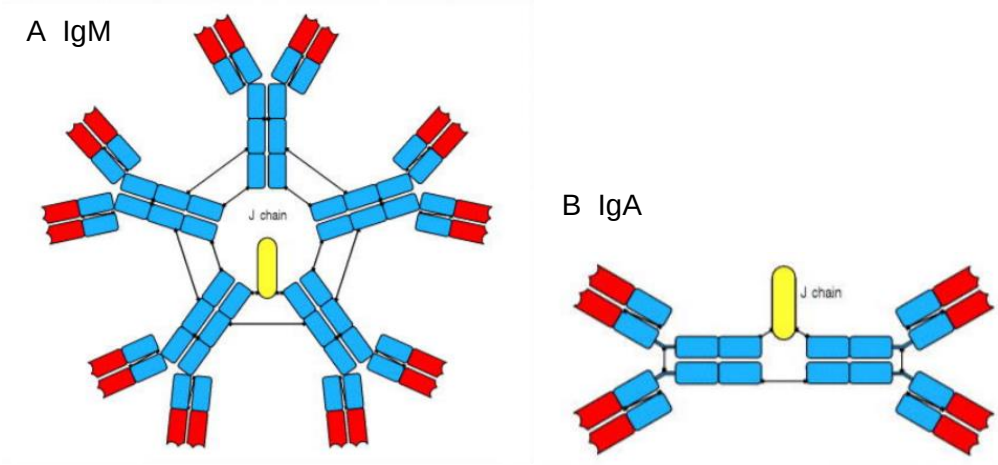

Figure 4.2: Multivalent antibody immunoglobulin (Ig) isotypes. (A) IgM with ten antigen binding sites and (B) IgA with four antigen binding sites. Taken from Janeway *et al.* [140].

The range of binding affinities measured from antibodies produced *in vivo* is 10^{-10} – 10^{-3} M^{-1}. Values lower than 10^{-10} M^{-1} are achieved by engineered interactions, e.g. with the biotin/ streptavidin (the standard for nature's highest binding affinity) in the 10^{-14} M^{-1} range [143]. The definition of a "weak" binding affinity depends on the context in which this is discussed, however affinity constants in the range of 10^{-10} – 10^{-8} M^{-1} are considered strong, for example protein G (a commonly used antibody binding protein) binds human antibody with a K_D of 10^{-8} M [143]. Definitely weak interactions range from 10^{-5} – 10^{-3} M^{-1} for the one antigen to one binding site interaction, however multi-valence can improve the functional affinity (avidity) 100 – 1000 fold [143].

Anti-lipid antibodies are typically of low affinity [145]. The competitive model of MALIA (mycolate antibodies lateral flow immunoassay) is aimed at overcoming the difficulty of detecting the low affinity anti-MA antibodies in the serum. However, there are also challenges associated with the use of low affinity antibodies as the labelled bio-recognition agent in LFT. In MALIA the labelled monoclonal anti-MA antibodies will bind the MA on the test line and in the presence of positive tuberculosis (TB) patient serum this binding should be reduced due to competition for binding by unlabelled serum anti-MA antibodies. It is thus essential that the affinity of the labelled antibodies is less than that of the serum antibodies but still high enough to sufficiently bind the MA for a visible negative test line.

Further challenges exist due to the cholesteroid nature of MA [83] and the presence of anti-cholesterol antibodies in patient sera [85] that may cross-react. The gallibodies then need to outcompete the serum anti-cholesterol antibodies for binding to MA but not the anti-MA antibodies. This then also serves to limit the cross-reactivity of the test that would occur in the

case of direct detection. The six developed gallibodies with varying specificities and sensitivities can then be combined or selected for to choose the ideal competitor for MALIA [91].

Colloidal gold nanoparticles are commonly used as a label for antibodies on LFTs, due to their superior optical properties. In LFT the application of gold nanoparticles as a label is very common, with excellent performance reported [103].

4.1.2 Colloidal gold nanoparticles

Colloids are formed when very small particles of an insoluble substance disperse in a liquid [146]. The size of particles that are used in this definition range from 1 nm – 1 µm in diameter. At less than 1 nm particle "dispersions" would be indistinguishable from solutions [146]. Protein and other macromolecule solutions then fall into the range of colloid solutions or dispersions [146]. Colloids are interchangeably called colloidal dispersions, suspensions/sols or solutions.

Spheroid colloidal gold suspensions can be easily produced by the reduction of chloroauric acid ($HAuCl_4$) [128]. The average size of the particles can be manipulated by changing the power and concentration of the reducing agent [128]. Colloidal gold has a number of favourable properties such as: biocompatibility, ease and cheapness of production and the adaptability of the size of particles that can easily be labelled with biological probes [128].

The optical properties of colloidal gold suspensions are their true attraction. Colloidal gold suspensions have an intense red colour (pictured in figure 4.3) due to their plasmon resonance [147]. The surface plasmon resonance (SPR) band of colloidal gold nanoparticles occurs in the visible light range of wavelengths (figure 4.4) [148]. SPR refers to the cooperative fluctuation of the free (or conducting) electrons across the particle due to the resonant excitation by the received photons [147].

Figure 4.3: Bright red colour of differently sized colloidal gold nanoparticle suspensions. From Ojea-Jiménez and Puntes [149] and own image (40 nm).

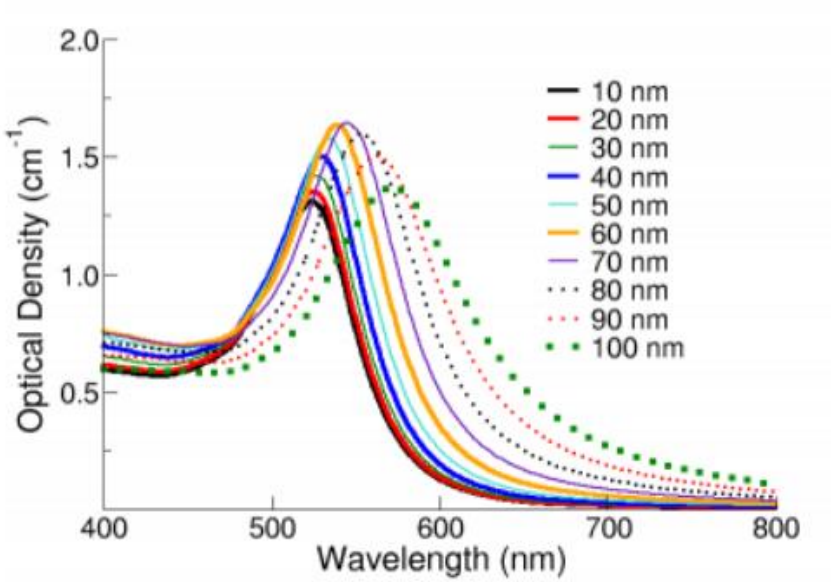

Figure 4.4: Visible absorbance spectra of colloidal gold nanoparticles of varying sizes. Taken from nanoComposix [148]**.**

Anything that affects the surface charge density of the nanoparticles, such as particle size and shape, will affect the SPR and thus the visible colour of the particle suspension (figure 4.4) [148]. This phenomenon is used to characterise the conjugation of the particles to macromolecules and to monitor the stability of the colloid. If unstable, aggregation occurs and the SPR band shifts or the maximum is lost if aggregation is severe [148].

Colloidal suspensions characteristically have a high particle surface area to liquid volume ratio – as such the interactions at the surface-liquid interface play a major role in the stability of a colloid [146]. The electrical double layer is a term that describes the two parallel charge layers that occur at the solid liquid interface [146]. In the case of a positively charged particle, negative ions in the medium will be attracted to it. These negative ions are also subject to thermal motion and so the charge concentration is high close to the particle and decreases with increasing distance into the medium (figure 4.5) [146]. The higher the ion concentration in the medium the denser the charge concentration close to the particle (figure 4.5, dashed line) [146].

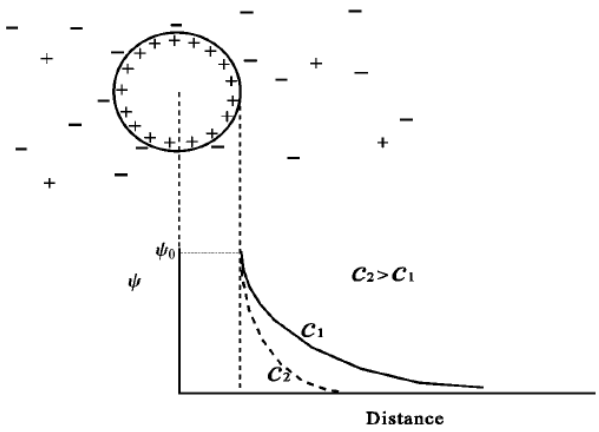

Figure 4.5: Graphical representation of the electrical double layer describing the electrostatic potential (ψ) near a charged colloidal particle. Dashed line represents higher ionic strength (C2). Taken from Hunter [146].

The Derjaguin, Landau, Verwey, and Overbeek (DLVO) theory describes the effect of the electrical double layer and Van der Waals forces on colloidal stability. Essentially the theory explains that attractive van der Waals forces that would cause aggregation of the particles in suspension are prevented by an energy barrier caused by electrostatic and steric forces. [146,150,151] Three scenarios for colloid stabilisation are represented in figure 4.6 – electrostatic (A), steric (B) and electro-steric (C).

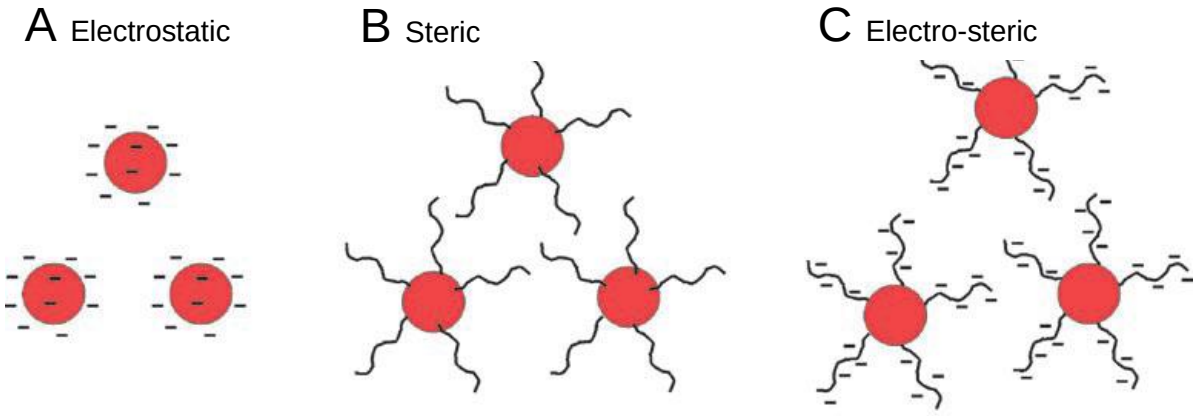

Figure 4.6: Colloidal suspension stabilisation strategies. (A) Electrostatic: electrical double layers formed due to charges on surface – particles repel each other (B) Steric: polymers coated on the surface of particles prevent close interaction and aggregation and (C) Electro-steric: charged polymers on surface prevent interaction of particles through steric and electrostatic (charge repulsion) means. Taken from Zhao *et al.*[152].

Electrostatic stabilisation (figure 4.6A) is most commonly in force in aqueous colloidal gold suspensions. Citrate ions (commonly used during the production of gold nanoparticles) form ion 'caps' on the surface and keep the nanoparticles from aggregating by electrical double layer formation [128,153]. This method is sensitive to high ionic strength, which suppresses the double layer and in extreme cases (high salt concentrations) causes aggregation [146,153].

The steric stabilisation effect (figure 4.6B) is what keeps gold labelled protein conjugates stable [146]. In this scenario macromolecules, for example protein such as bovine serum albumin (BSA) [154] or polymers such as poly-ethylene glycol (PEG) [155], coat the nanoparticles and prevent the dominance of Van der Waals forces. As the coated particles approach each other the steric hindrance of the polymers discourages closer interaction. Particles prepared by this method are less sensitive to salt concentration but rely on adequate coating of the particles – i.e. a sufficiently thick and consistent layer all around the particles [146,152].

The third stabilisation scenario – electro-steric (figure 4.6C) – is a combination of the previous two. This involves modification of particles with a charged polymer, usually deoxy ribonucleic acid (DNA) [152,153]. The interaction between conjugated polymers prevents aggregation by electrostatic repulsion between the charges and the steric hindrance of two interacting polymers [152,153].

The interactions required to stabilise colloidal suspensions are effectively exploited in the process to conjugate nanoparticles to biological probes such as antibodies, DNA or other relevant macromolecules. The process for developing stable gold conjugates will be described hereafter.

4.1.3 Colloidal gold conjugation

Colloidal gold can easily be conjugated to protein by passive means. Other strategies involve the use of an intermediate linker to aid in orientation of the conjugated protein such as a biotin/streptavidin mediated linkage [121]. Covalent attachment using chemical functionalisation is also a possible strategy [121]. Passive conjugation was the primary method pursued for this study.

The interaction with protein can be seen as a steric stabilisation of the nanoparticles as described above. The positive charges on the protein would interact with the negative charges on the surface of the citrate capped gold nanoparticle. This forms a polymer layer that if of sufficient thickness (determined by concentration added) will stabilise the sol against aggregation caused by high salt concentration [128,149]. The net charge of the protein can be manipulated by changing the pH of conjugation [149]. Depending on the iso-electric point of the protein, its surface charge will be changed affecting its interaction with the gold nanoparticle [149].

The aggregation of gold nanoparticle suspensions can be quantified spectrophotometrically by measuring the absorbance at 580 nm [156] or the loss of the plasmon resonance maximum peak at 520 nm [157]. As protein is bound to the nanoparticle surface the absorbance at 580 nm will decrease until reaching a plateau. This is represented effectively in figure 4.7 taken from

Byzova *et al.* [158]. Further stabilisation of conjugates after protein (of interest) binding is common by addition of polymers such PEG or BSA [128].

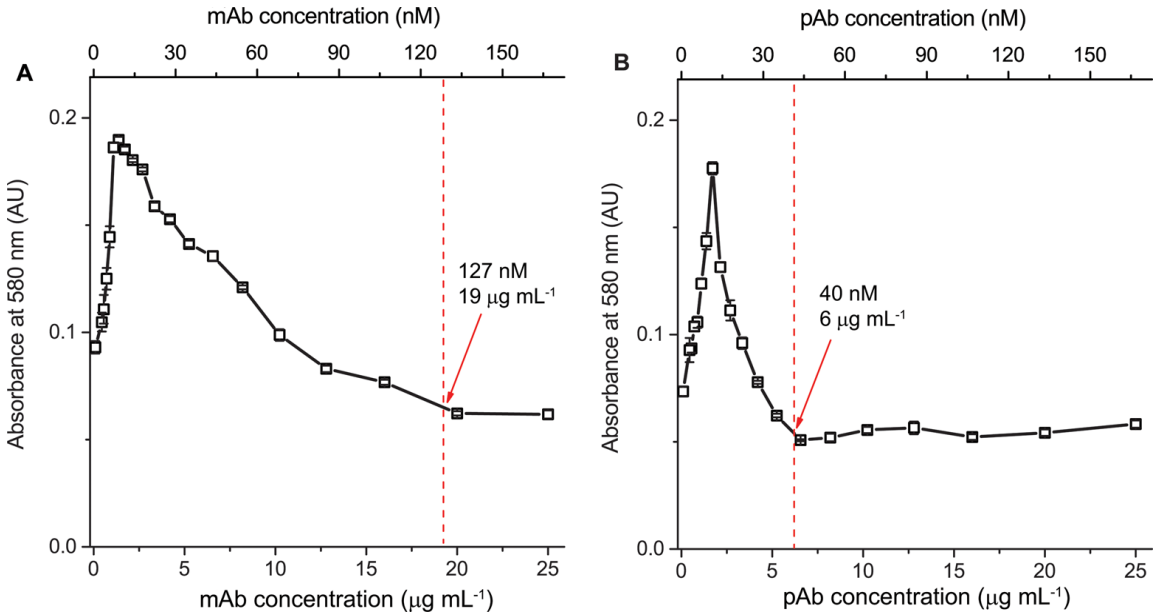

Figure 4.7. Flocculation curves (absorbance at 580 nm) for colloidal gold (25 nm) sols stabilised with increasing concentrations of monoclonal (A) or polyclonal (B) antibodies. Absorbance at 580 nm of gold labelled antibody conjugates in the presence of excess NaCl graphed. Red arrows indicate antibody concentrations at which gold is sufficiently coated to prevent aggregation upon the addition of NaCl. Taken from Byzova *et al.* [158].

To summarise, during the development and preparation of stable protein/gold conjugates three main parameters are considered, namely: the iso-electric point of the protein to be conjugated, the pH at which the adsorption occurs and the quantity of protein used [159]. For this application the iso-electric points (pI) of the gallibodies were not determined, but the conditions for conjugation optimised by testing a range of pH values for coating. The ideal conditions may be determined by observation of the SPR band of the colloidal gold conjugate (at ~520 nm) or the absorbance at 580 nm (flocculation curve).

4.1.4 Conjugate characterisation in literature

The use of Vis spectra to characterise the plasmon resonance shift of gold nanoparticles have been described above. Further methods to characterise the functionality of gold labelled antibody conjugates of specific relevance to the present study will be described hereafter.

4.1.4.1 Transmission Electron Microscopy

The labelling of antibodies with gold nanoparticles was initially developed for use in immunostaining techniques in histological and other similar studies [128]. The permanence of labelling with gold nanoparticles over chemical staining techniques that fade and fluorescent reporters that bleach over time are among some of the advantages [128]. Some examples of the

use of gold labelled proteins in transmission electron microscopy (TEM) are given in figure 4.8 from Horisberger and Rosset [157].

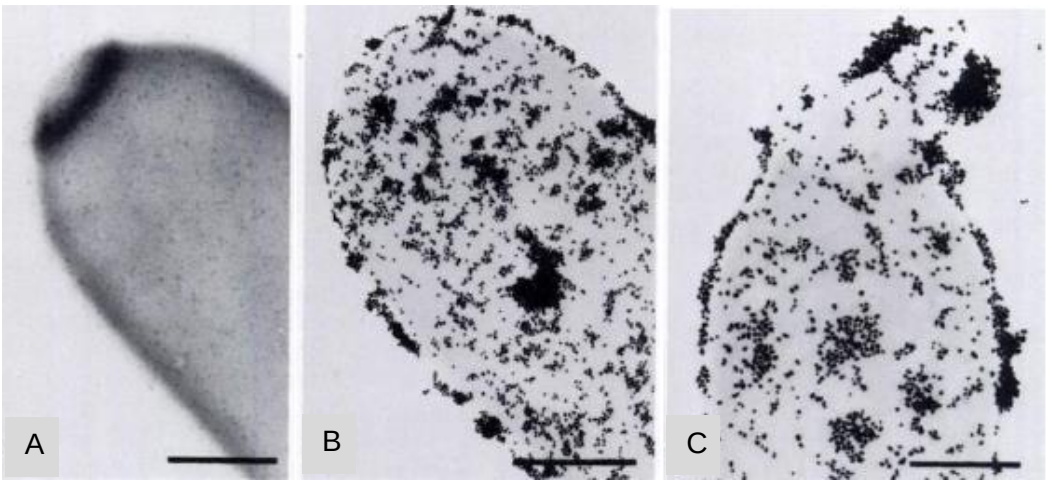

Figure 4.8: Examples (A, B and C) of TEM images using gold nanoparticle labelling to enhance visualisation. Yeast *Candida utilis* cell walls marked with three differently sized (A= 5.2; B= 18 and C= 31.5 nm) and stabilised gold labelled lectin (mannose binding concanavalin A) conjugates. Scale bar represents 1 µm. Taken from Horisberger and Rosset [157].

Furthermore, TEM is commonly used to confirm the size and shape of gold nanoparticles [138,160,161] after manufacturing and before conjugation. However, TEM has been applied to characterise the interaction of gold labelled antibodies by Potůčková *et al.* [162] using a sample preparation procedure similar to enzyme linked immunosorbent assay (ELISA) and by Singh *et al.* [163] using a simpler immobilisation strategy. Both groups were developing nanoparticle based immuno-PCR (polymerase chain reaction) to sensitively detect cytokines and a TB antigen respectively. Their applications of TEM to characterise the binding ability of gold labelled antibody conjugates will be discussed here.

Potůčková *et al.* [162] labelled 30 nm gold nanoparticles with polyclonal rabbit anti-murine interleukin- 3 antibodies, stem cell factor (SCF) or BSA. These conjugates were allowed to settle on poly-L-lysine coated nickel grids. The grids were washed after ten minutes with phosphate buffered saline (PBS) and blocked for 15 minutes with BSA in PBS before washing again [162]. To confirm the presence of antibodies on the gold nanoparticles the authors purchased 5 nm size gold nanoparticles labelled with anti-rabbit IgG antibodies and incubated these on the coated grids for 30 minutes. Following this the grids were washed three times for five minutes each with BSA in PBS before fixing with glutaraldehyde. These grids were washed finally with deionised water and viewed using a TEM at 60 kV [162]. Figure 4.9A shows the ‘rosettes’ formed by the binding of the rabbit polyclonal antibody on the 30 nm nanoparticle by the anti-rabbit IgG antibody on the 5 nm nanoparticles. Figure 4.9B shows the negative

control – 30 nm nanoparticles conjugated to BSA that were similarly treated (but not bound) by the anti-rabbit IgG antibodies on the 5 nm nanoparticles [162].

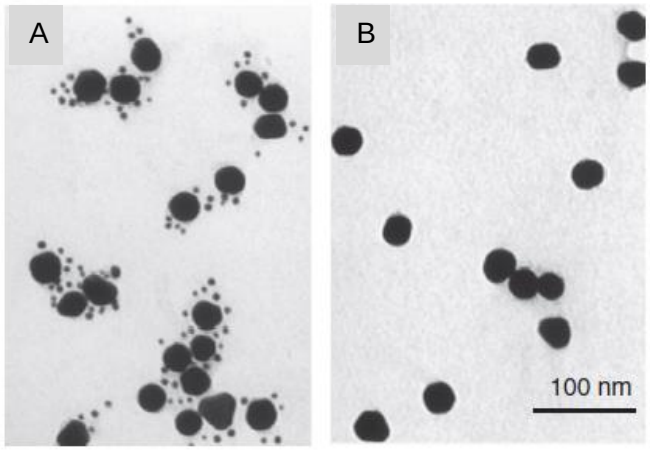

Figure 4.9: TEM visualisation of binding of differently sized gold labelled antibody conjugates in ELISA-like protocol. A: Polyclonal rabbit antibody conjugated to 30 nm (large) gold nanoparticles bound by anti-rabbit IgG antibodies conjugated to 5 nm (small) gold nanoparticles. B: BSA conjugated to 30 nm gold nanoparticles remain unbound by anti-rabbit Ig antibodies conjugated to 5 nm gold nanoparticles. Taken from Potůčková *et al.* [162].

Singh *et al.* [163] labelled 20 nm gold nanoparticles with rabbit anti-TB antibodies and incubated them with 60 nm gold nanoparticles labelled with anti-rabbit IgG antibodies. These were imaged with TEM "after washing" [163]. BSA labelled gold was used as a control as well as unlabelled gold nanoparticles incubated with each of the labelled samples for one hour at RT [163]. Figure 4.10 shows the TEM images from this study [163]. Figure 4.10B and C shows interaction of the two differently sized gold nanoparticle conjugates labelled with rabbit antibody and an anti-rabbit IgG antibody respectively. The controls show no interaction due to non-specific binding with BSA (D) or between two sizes of uncoated gold nanoparticles (E) or one size of coated and one of uncoated nanoparticles (F) or 60 nm gold nanoparticles alone (A) [163].

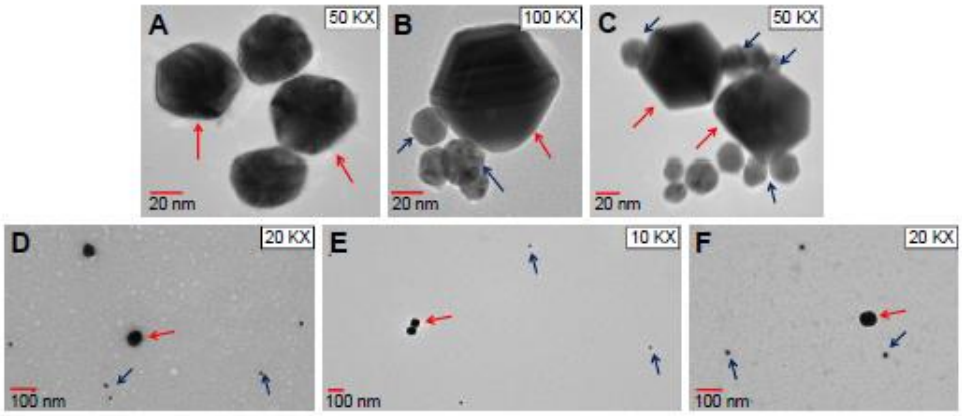

Figure 4.10: TEM visualisation of binding of differently sized gold labelled antibody conjugates incubated in liquid. A: Uncoated 60 nm gold nanoparticles. B and C: 20 nm gold labelled rabbit antibody conjugate incubated with anti-rabbit IgG antibodies conjugated to 60 nm gold nanoparticles. D: 20 nm gold labelled BSA incubated with 60 nm gold labelled anti-rabbit IgG antibodies. E: unconjugated 20 nm gold nanoparticles incubated with unconjugated 60 nm gold nanoparticles. F: 20 nm gold labelled rabbit antibody conjugate incubated with unconjugated 60 nm gold nanoparticles. Red arrows indicate 60 nm particles. Blue arrows indicate 20 nm particles. Taken from Singh *et al.* [163].

These articles demonstrate the effective use of TEM to confirm the binding of functional secondary to recognisable primary antibodies when conjugated to different sizes of gold nanoparticles. However, this procedure is relatively novel and so the use of a commonly used technique such ELISA to characterise the functionality of antibodies conjugated to gold nanoparticles is also described. Furthermore, the ability of the primary antibody to bind its antigen when conjugated was not confirmed in these studies.

4.1.4.2 Enzyme Linked Immuno Sorbent Assay

ELISA is commonly used to characterise the binding of antibody antigen pairs [142,143]. In ELISA antigen is commonly coated in a microtiter plate and the antibody of interest incubated on the coated and blocked plate for an hour. To detect whether the primary antibody has bound to the antigen, a secondary anti-antibody, labelled with an enzyme that produces colour from a substrate, is used. Between coating, blocking, primary incubation and secondary incubation are triplicate wash steps using a buffer containing a mild detergent such as Tween 20.

Tripathi and Driskell [164] applied an ELISA type of assay to the characterisation of conjugate. In their test they conjugated an anti-horse radish peroxidase (HRP) antibody onto gold nanoparticles. They then quantified the amount left in the supernatant (obtained during conjugate preparation, to remove excess protein) in a Bradford assay to determine the amount of protein not bound to the gold nanoparticles [164]. Excess HRP was added to the conjugates and allowed to saturate the anti-HRP conjugated to the gold nanoparticles and the substrate added to quantify the bound antibody. They used this to show that anti-HRP antibody conjugates mediated with protein A allowed for more active anti-HRP antibody coating

because of oriented immobilisation [164]. Sotnikov *et al.* [165] similarly used the supernatant to infer the amount of protein bound to the gold nanoparticles by measuring the activity of the unbound protein in ELISA [165].

To apply 'standard' plate based ELISA to the characterisation of gold labelled antibody conjugates, the primary antibody is replaced with the gold labelled antibody conjugate and the rest of the protocol followed as usual. Thus in order to visualise the binding of the conjugate, the interaction between the coated antigen and the gold labelled antibody must withstand the wash steps. Furthermore, the conjugated antibody must remain able to bind its antigen and remain recognisable by the secondary antibody despite the presence of the gold nanoparticle. This then is a useful experiment to confirm the presence and activity of conjugated antibodies.

During their study Byzova *et al.* [158] effectively used ELISA to characterise gold labelled monoclonal and polyclonal antibody conjugates. They used ELISA to partially characterise the effect of using different concentrations of antibody to prepare the conjugates. The binding affinities calculated using this method differed for the conjugates prepared at different concentrations of antibody [158].

The gold labelled antibodies tested using ELISA described above are high affinity antibodies. The 'worst' performing of the monoclonal antibodies' conjugates tested by Byzova *et al.* [158] had an affinity (K_D) of ~10^{-9} M and the worst performing of the polyclonal conjugate ~10^{-10} M. Both of these dissociation constant values fall in the range of high affinity relationships discussed earlier. These ELISA data effectively show that conjugation to gold nanoparticles (25 nm and 20 nm respectively) did not render the antibodies unable to bind their antigens and antibodies were still available to be bound by enzyme labelled anti-antibodies. ELISA is therefore an effective method to functionally characterise gold labelled antibody conjugates.

4.1.4.3 Dynamic Light Scattering

Dynamic light scattering (DLS) measures the intensity of light scattered by particles in suspension under the influence of Brownian motion and uses this information to infer the size of the particle (actually a sphere of the same diameter) [166]. Larger particles are known to move slowly and small particles more quickly [166].

Data from the DLS instrument can be presented in several ways using various algorithms and theories to convert between them [166]. The most basic data obtained from a DLS instrument is the correlation curve. This function gives the correlation of the present measured intensity information from the sample to the initial intensity as a function of time [166]. This data is then converted using various algorithms and instrument constants to the intensity size distribution [166]. This plot gives the relative intensity of the scattered light (%) to a given size bin. This

distribution can then be converted to a volume distribution using Mie theory and the refractive index of the material in the dispersant [166]. This gives the percentage of the volume contributed by the different size bins. Finally the volume distribution can be used to determine the number distribution - giving the relative (%) of the number of particles in the size bins [166]. However, the number distribution is rarely used as small errors in the measurements will translate to very large errors in this distribution [166].

The excellent ability of gold nanoparticles to enhance light scattering due to their optical properties has been exploited in a number of assays such as DLS. Furthermore the accuracy of DLS measurements of particle size allows its application to sensitive and time-linked tracking of gold nanoparticle aggregation caused by the interaction of conjugated proteins, DNA or other molecules [167].

Jans *et al.* [168] effectively demonstrated the use of DLS to study the conjugation of proteins to gold nanoparticles and the subsequent interaction of gold labelled protein conjugates. The conjugation of proteins to gold nanoparticles is observed by the increase in the hydrodynamic diameter of the protein (as measured by DLS) by two times the diameter of the protein on its own. This also gives information about the orientation of the conjugated protein as can be seen in figure 4.11. Byzova *et al.* [158] and Tam *et al.* [169] used the same logic to infer the orientations of their conjugated antibodies.

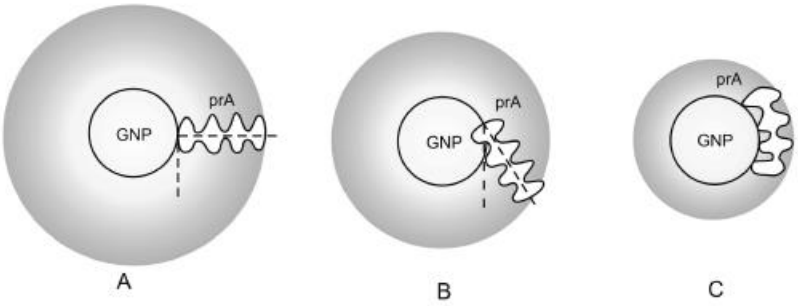

Figure 4.11: The effect of protein orientation on hydrodynamic diameter of conjugates. Three possible orientations of the elongated protein A (prA) on the gold nanoparticle (GNP) are given in A, B and C changing the final radius of the conjugated particle. Taken from Jans *et al.* [168].

Furthermore, Jans *et al.* [168] used gold labelled protein A conjugate and DLS to study the interaction of the conjugated protein A for its target – human IgG. For these studies the change in particle size is plotted as a function of time or alternatively as a function of human IgG concentration [168]. This data supports the known ability of each protein A molecule to bind two or more IgGs with high affinity, thus allowing almost direct observation of biomolecular binding [168].

DLS is most commonly used to confirm the size of manufactured gold nanoparticles as measured on TEM or the size increase after conjugation [158,169] and is not commonly applied to the characterisation of the functionality or binding ability of gold nanoparticle conjugates.

4.1.5 Chapter outline

In this chapter the conclusions that can be drawn from the anti-chicken IgG (Fc) control signal on the LFT and the conditions of the gold labelling of the gallibodies will be investigated. The functional binding ability of the conjugated gallibodies will be explored using various methods.

4.2 Materials and methods

4.2.1 Materials

For the ELISA, conjugate and LFT manufacture materials were used as listed in section 2.2.1 and 3.2.1. Unless otherwise specified salts and reagents were procured from Sigma (USA). Kwik-Stik™ *E. coli* O157:H7 (American type culture collection® 700728) was procured from ThermoScientific (USA) and sub-cultured on nutrient agar before use; McFarland equivalence turbidity standard from Remel, Lenexa (USA); Nutrient Agar and Tryptone Soya Broth from Oxoid (UK); Bactrace™ polyclonal goat anti-*E. coli* O157:H7 and anti-goat IgG (Fc): HRP from Kirkegaard & Perry Laboratories (USA).

4.2.2 Anti-chicken IgG (Fc) antibody controls

The specificity of the anti-chicken IgG (Fc) antibody control to gold labelled gallibody conjugate was explored using all six gallibodies produced by Ranchod *et al.* [91], i.e. the three clones 12, 16 and 18 each expressed in two scaffolds C_H1-4 and the shorter C_H2-4 (details in section 2.2.1.1). These are hereinafter abbreviated as follows: 12-1, 12-2, 16-1, 16-2, 18-1 and 18-2. In 12-1, the 12 is the clone number and the -1 refers to the C_H1-4 scaffold.

Conjugates were prepared with all six gallibodies according to the methods described in section 3.2.3. A concentration of 0.04 mg/mL gallibody (in 0.1 M borate buffer at pH 7.4) was used and added to pH 6 colloidal gold at an optical density (OD) of 1. These conjugates were probed with anti-chicken IgG (Fc) antibody and 0.1 M PBS (pH 7.4) coated on the nitrocellulose as described in section 3.2.4.

The specificity of the anti-chicken IgG (Fc) signal was probed by titrating the concentration of the anti-chicken IgG (Fc) antibody down from the supplied concentration of 1 mg/mL by dilution in 0.1 M PBS to 0.5, 0.2 and 0.1 mg/mL before spotting. Gold-labelled gallibody 18-2 conjugate was used to probe this.

To confirm that the anti-chicken IgG (Fc) antibody was not reacting non-specifically with the conjugate blocker, gold was also conjugated to bovine serum albumin (BSA) at 0.04 mg/mL (w/v) BSA instead of the gallibody. The same process was followed as in section 3.2.3. This gold labelled BSA conjugate was probed against immobilised anti-chicken IgG (Fc) antibody at a concentration of 0.5 mg/mL as described in section 3.2.4.

4.2.3 Visible spectrum salt tests

Previously a salt test was carried out (section 3.2.2) to determine conditions for conjugation of the gallibody to gold nanoparticles. These tests used visual observation to determine optimal gallibody concentration and colloidal gold pH values for conjugation well within the stable area of the conjugation titration curve. In order to further explore conjugate stability, salt tests were carried out according to the protocol in Hermanson [128] as follows: Increasing concentrations of gallibody (0 – 0.04 mg/mL) were added directly to 250 µL of colloidal gold. Tubes were gently inverted once before incubation for 30 minutes at RT. Following incubation 250 µL of 10% (w/v) sodium chloride in 0.1 M borate buffer pH 7.4 was added. The tube was inverted before absorbance measurement across the visible wavelength spectrum of conjugates with NaCl added measured (390 – 700 nm, every 10 nm) using a Biotek™ Powerwave HT microplate reader. Gallibody 12-2 was used for these tests.

The aggregation/stabilisation of the gold sol can be observed by measurement of the absorbance at 580 nm. A decrease in absorbance is observed as the sol is stabilised by protein. Common practice is to conjugate the gold with the protein concentration corresponding to the minimum absorbance at 580 nm plus 10 – 20% more of the protein [128,157,170]. At this protein/ antibody concentration the gold nanoparticles will be completely coated.

The pH at which maximum protein adsorption to nanogold will occur is usually at or near the iso-electric point (pI) of the protein to be conjugated [128,159]. Optimal pH for conjugation for the gallibody 12-2 was determined by carrying out the salt test described above at varying pH values (5.2, 6, 7, 8 and 9) of the colloidal gold sol. The supplied colloidal gold sol (pH ~ 5.2) was adjusted to ~ pH 6, 7, 8 and 9 using 0.2 M dibasic sodium carbonate. At the optimal pH of the gold less antibody will be required to stabilise the conjugation. This means that the minimum absorbance at 580 nm will correspond to a lower concentration of gallibody for the optimal pH compared to that for a sub-optimal pH.

In order to determine whether gold labelled gallibody retains its ability to bind to MA the conjugate was characterised using three methods different from lateral flow based detection.

4.2.4 Enzyme Linked Immuno Sorbent Assay using gold labelled conjugate

To confirm the use of ELISA to functionally characterise gold labelled conjugates a system test was carried out using gold labelled anti-*E. coli* conjugate known to successfully bind *E. coli* on LFT (appendix A) and unconjugated in ELISA [116]. This protocol is based on that carried out by Kumar [116].

For the system test ELISA, *E. coli* O157:H7 was coated as follows. Bacteria were grown on nutrient agar overnight at 37°C, scraped off the plate and suspended in 0.1 M PBS to a concentration of 10^8 colony forming units (CFU) per mL. This concentration was determined by comparing the OD at 625 nm to the McFarland standard [171]. A 100 µL volume of this bacterial suspension (0.1 M PBS coated as a negative) was used to coat a NUNC-Maxisorp™ plate overnight at 2 – 8°C.

The following day the liquid was flicked out and the wells washed three times using 300 µL of 0.1 M PBS/0.1% (v/v) Tween 20 (wash buffer). Each well was blocked for two hours at RT with 300 µL of 4% casein hydrolysate in 0.1 M PBS adjusted to pH 7 (blocking buffer). Following the blocking step, wells were again washed three times as above.

For the primary antibody Bactrace™ polyclonal goat anti-*E. coli* O157:H7 antibody was used. This antibody was diluted to 0.05 mg/mL in blocking buffer with 0.1% (v/v) Tween 20 added (dilution buffer). A similar concentration was used by Kumar [116]. For the test the antibody was conjugated to gold nanoparticles as described in section 3.2.3 at a concentration of 0.01 mg/mL to OD 1 colloidal gold suspension at a pH of 9. This conjugate has been optimised in the group to successfully detect *E. coli* bacteria on LFT (appendix A). For negative controls dilution buffer and gold labelled BSA conjugate at OD 5 was used. A 50 µL volume of diluted antibody or gold labelled antibody conjugate (at OD 5) was incubated on the wells for an hour at RT. Following incubation, liquid was flicked from the wells and the wells were washed three times as before.

Following this the wells were incubated for one hour with 50 µL anti-goat IgG (Fc): HRP at 1 µg/mL in dilution buffer. Unbound antibodies were removed by washing the wells as before. The reaction was developed by the addition of 50 µL of tetramethylbenzidine substrate for 1.5 minutes before stopping the reaction with 50 µL of 2 M H_2SO_4. Absorbance was measured at 450 nm using a plate reader (BioTek® PowerWave HT).

On the LFTs gold labelled gallibody conjugate was consistently bound by anti-chicken IgG (Fc) antibody (for example figure 3.9). For this reason a control sandwich ELISA test was carried out in which wells were coated with the same anti-chicken IgG (Fc) antibody as used for the LFTs (section 3.2.4) as a positive control. A 100 µL volume of antibody at 10 µg/mL in

0.1 M PBS (PBS as the negative control) was used to coat a NUNC-Maxisorp™ plate overnight at 2 – 8°C. The sandwich ELISA was carried out as described for the indirect ELISA described above using different primary and secondary antibodies. For the primary antibody, gallibody 12-2 was conjugated to gold as described in section 3.2.3 using a concentration of 0.04 mg/mL to OD 1 gold at a pH of 6. The conjugate was used at OD 5 on the anti-chicken IgG (Fc) or PBS coated wells and compared to gallibody diluted to 0.2 mg/mL in dilution buffer. As described in section 2.2.2, goat anti-chicken IgG (Fc): HRP antibody was used as the secondary antibody.

For the test, the binding of MA by gold labelled gallibody conjugate was investigated. MA in hexane or hexane alone was coated as for the indirect ELISA as described in section 2.2.2. For the primary antibody, two concentrations of gallibody and gold labelled gallibody conjugate were used: 0.04 mg/mL/ OD 1 conjugate and 0.2 mg/mL/ OD 5 conjugate. Dilution buffer or gold labelled BSA conjugate (at OD 5) were used as negative controls. A further negative control was included using an engineered unrelated IgY gallibody provided by Susan Wemmer of the Agricultural Research Council – Onderstepoort Veterinary Institute. These gallibodies were raised against the HSP65 protein antigen of *Mycobacterium bovis* and also expressed on the C_H2- 4 scaffold as described by Wemmer *et al.* [90]. This gallibody was conjugated to gold at a concentration of 0.04 mg/mL to OD 1 gold at pH 6. The gold labelled unrelated gallibody conjugate was used at OD 5 and the gallibody alone diluted to 0.2 mg/mL in 0.1 M PBS at pH 7.4.

4.2.5 Dynamic Light Scattering

DLS was used to explore the association of MA with gold labelled gallibody conjugate without any washing or mixing steps. Measurements were taken at 25°C using a Zetasizer Nano ZS (Malvern, USA) and a folded capillary tube (DTS 1070). The instrument software default settings (to ensure optimal laser attenuation, number of measurement repeats etc.) were used.

Empty $poly_{DL}$-lactic-co-glycolic acid (PLGA) nanoparticles and PLGA nanoparticles containing MA prepared by Dr Yolandy Lemmer and Dr Heena Ranchod and (particles prepared in the same way) shown to be antigenic in Lemmer *et al.* [172] were used. Nanoparticles were suspended in 0.1 M borate buffer (pH 7.4) at a concentration of 2 mg/mL. Nanoparticle suspensions were incubated with gold labelled gallibody 18-2 and BSA conjugates (OD 10, as prepared according to section 3.2.3) in a 1:1 volume ratio for at least one hour.

To measure, nanoparticle suspensions were further diluted in deionised water to concentrations of 2 µg/mL or 10 µg/mL (1 or 5 µL of 2 mg/mL nanoparticle suspension prepared above added to 1 mL deionised water). Similarly 5, 3 or 1 µL volumes of OD 10 conjugate and 100, 50, 20 and 10 µL volumes of OD 1 uncoated gold were added to 1 mL of

ultrapure deionised water. The concentrations of the gold nanoparticles were not known and are spoken of in terms of OD at 525 nm. This is a relative term based on the concentration of the supplied OD 1 colloidal gold nanoparticle solution during conjugate preparation by centrifugation and resuspension. For the incubated samples 3 µL (of the 1:1 ratio mixture of gold labelled OD 10 conjugate and the 2 mg/mL PLGA nanoparticle suspension) was added to 1 mL water before measurement. A further control where a volume of 50 µL of uncoated OD 1 gold was interacted with 5 µL of MA nanoparticle suspension (2 mg/mL) was also measured.

For the data analysis, percentage intensity measurements from the DLS instrument were used exclusively. This is because dielectric constants cannot be determined for mixtures of materials (PLGA nanoparticles with gold nanoparticles etc.) and these constants are required to accurately determine the volume distribution. The data presented herein was used and is presented as exploratory work, not as a method development.

4.2.6 Transmission Electron Microscopy

TEM was used to visualise the interaction of gold labelled gallibody conjugate with antigenic PLGA nanoparticles containing MA. A simple sample preparation strategy was employed similar to that described in Singh *et al.* [163]. The interaction between gold labelled anti-*E. coli* conjugate and whole *E. coli* bacteria was used as a system test.

For the system test *E. coli* O157:H7 was incubated in Tryptone Soya broth for 16 hours at 37°C. A 2 mL volume of culture was centrifuged in a bench top centrifuge at 5000 x g for ten minutes. The supernatant was discarded and the pellet re-suspended in 0.04 M dibasic phosphate buffer pH 9.1 to a concentration of ~9 x 10^8 CFU/mL according to the McFarland standard [171]. Bacterial suspension was incubated with gold labelled anti-*E. coli* conjugate (as used in section 4.2.4) in a 1:1 volume ratio for one hour. Gold labelled gallibody and BSA conjugates were also incubated with bacteria as negative controls.

For the test empty PLGA nanoparticles and PLGA nanoparticles containing MA were used (prepared as for DLS in section 4.2.5). These nanoparticles are visible in TEM without coating as white circles [172]. Nanoparticles were suspended in 0.1 M borate buffer (pH 7.4) at a concentration of 2 mg/mL. Nanoparticles were incubated with gold labelled gallibody and BSA conjugates in a 1:1 volume ratio for at least one hour.

To visualise, a 3 µL volume of sample was pipetted onto smooth carbon or formvar (a resin coating) coated copper grids prepared by Dr James Wesley-Smith at Sefako Makgatho University and allowed to settle. Excess liquid was blotted off by touching the side of the drop to filter paper. Grids were air dried before imaging using a JEOL JEM-1010 TEM (JEOL,

Japan) by Dr James Wesley-Smith at Sefako Makgatho University at 100kV. Bacterial suspension, nanoparticles and gold labelled conjugates were all prepared as individual samples as well, for comparison.

4.3 Results and discussion

4.3.1 Gold conjugate evaluation

4.3.1.1 The binding of gold labelled gallibody by anti-chicken IgG (Fc) antibody

The control spot for MALIA is formed by coating with anti-chicken IgG (Fc) antibody that would bind the gold labelled gallibody during the flow reaction. In a test with both test and control lines this signal confirms that test has run to completion and confirms that conjugate has passed over the test line.

For the custom developed gallibodies it is known that they are recognised by the anti-chicken IgG (Fc): HRP as this was shown by ELISA [59]. Due to the lack of binding of the gold labelled gallibody to immobilised MA, the anti-chicken IgG (Fc) control spot was used to partially characterise the conjugate. However, it is important to note that this is not the key signal for MALIA.

The immobilised control anti-chicken IgG (Fc) antibody (without the HRP conjugated) was titrated down from the supplied concentration of 1 mg/mL and probed with a constant amount of gold labelled gallibody 18-2 conjugate (figure 4.12).

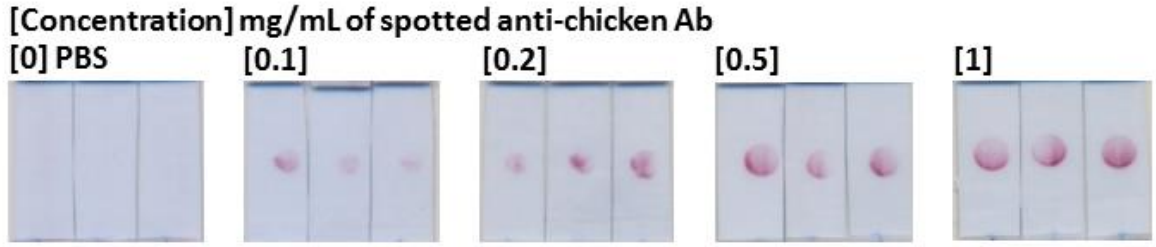

Figure 4.12: LFTs comparing the signal intensity of gold labelled gallibody conjugate at a concentration range of immobilised anti-chicken IgG (Fc) antibodies. Increasing concentrations of goat anti-chicken IgG (Fc) antibody in PBS were coated on the nitrocellulose and probed using gold labelled gallibody 18-2 conjugate (at 0.04 mg/mL to OD 1 gold at pH 6) in the LFT format. A flatbed scanner was used to image the test results. Test sections shown were cropped from a single image.

The size of the control spot decreases with decreasing coating concentration (figure 4.12 right to left). This can be explained by decreasing amounts of anti-chicken IgG (Fc) antibody being available to bind the gold labelled gallibody conjugate. The appearance of the semi-circle spot in the centre of the [0.5] set of tests is due to the way the LFT was manufactured. The coating

concentration of 0.5 mg/mL was selected for subsequent work as this showed a similarly intense signal to the 1 mg/mL coating concentration.

BSA was used as a blocker in the manufacturing of the gallibody conjugate. To confirm that the control signal was not due to the binding of the BSA blocker on the conjugate by the coated anti-chicken IgG (Fc) antibody (at a concentration of 0.5 mg/mL), a gold labelled BSA conjugate was prepared and tested instead of the gold labelled gallibody in the half test format (figure 4.13).

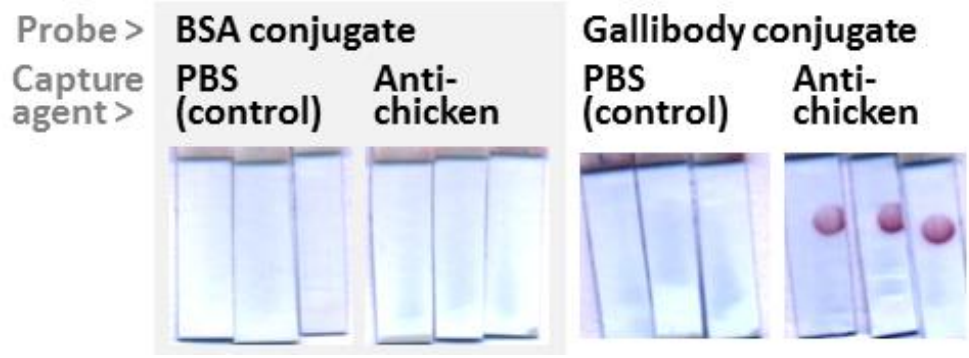

Figure 4.13: Half tests to compare binding of immobilised anti-chicken IgG (Fc) antibodies by gold labelled gallibody 18-2 and BSA conjugates. Gold labelled gallibody 18-2 and BSA conjugates were prepared at a concentration of 0.04 mg/mL to OD 1 gold at pH 6. This was used to probe anti-chicken IgG (Fc) antibody coated on nitrocellulose at a concentration of 0.5 mg/mL using the half test format. A flatbed scanner was used to image the test results. Test sections for each conjugate were cropped from single images.

Substitution of the gallibody with BSA on the nanogold did not yield a signal when exposed to the immobilised anti-chicken IgG (Fc) antibody (figure 4.13) showing that nanogold conjugated to BSA does not interact with the control antibody.

As previously described in section 2.2.1 three clones (with different variable amino acid sequences) of gallibodies were identified with specific MA binding activity and these were engineered into two scaffolds making six gallibodies in total (figure 2.1). The Fc regions of all six gallibodies are then the same and so it was expected they would be similarly recognised by the anti-Fc anti-chicken IgG (Fc) antibody. Gold labelled gallibody conjugates were made with all six gallibodies to investigate this (figure 4.14).

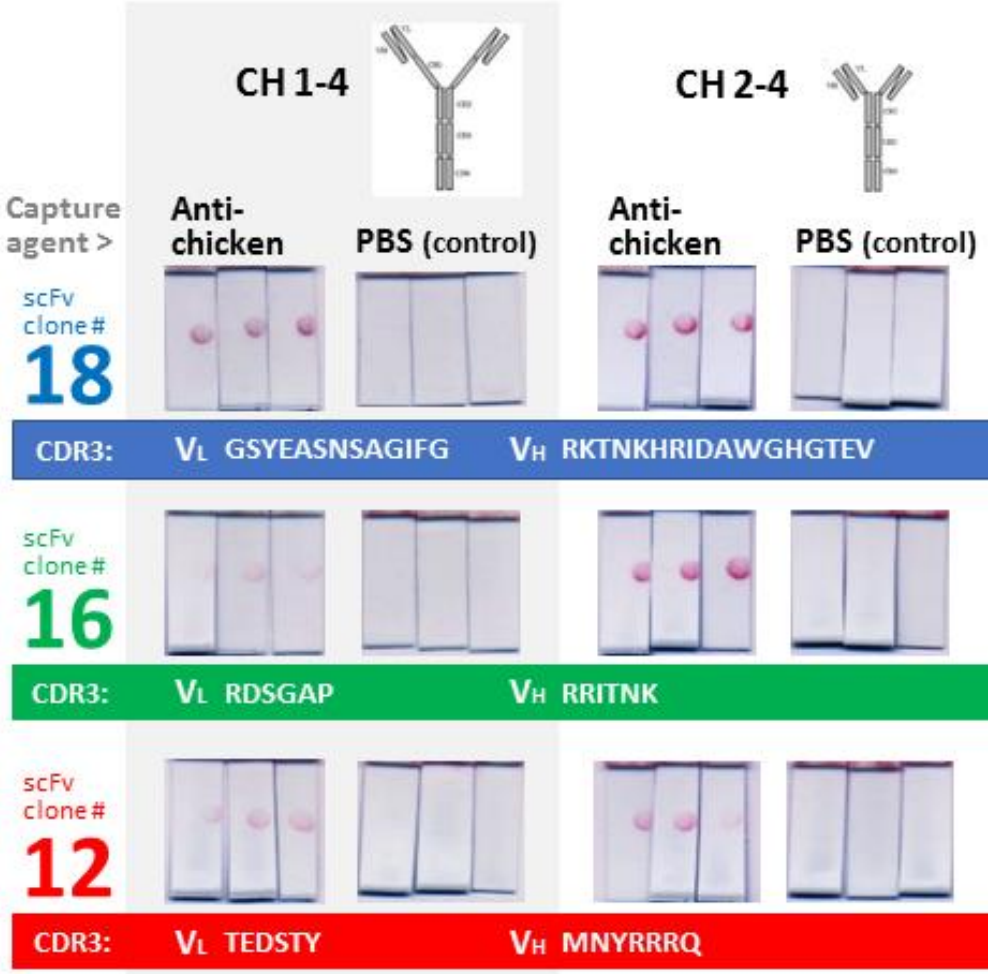

Figure 4.14: Half tests comparing the signals obtained on immobilised anti-chicken IgG (Fc) antibodies and PBS using all six gallibodies conjugated to gold. Gallibodies 12-1, 12-2, 16-1, 16-2, 18-1 and 18-2 were conjugated to gold at a concentration of 0.04 mg/mL to OD 1 gold at pH 6. This was used to probe anti-chicken IgG (Fc) antibody coated on nitrocellulose at a concentration of 0.5 mg/mL with PBS as the negative control using the half test format. Blue, green and red bars separate different clones (18, 16 and 12 respectively) and contain the amino acid sequences of the complementarity determining region 3 (CDR3) regions of the gallibodies, V_L- variable light, V_H- variable heavy [91]. Those engineered into the bivalent format C_H1-4 are shown on the left and those in C_H2-4 are shown on the right. A flatbed scanner was used to image the test results. Test sections shown were cropped from a single image.

Contrary to expectation the control anti-chicken IgG (Fc) antibody binds the different gold labelled gallibodies differently. In general the signal intensity is darker for the C_H2-4 gallibodies (figure 4.14 right). The differences may be explained by the C_H2-4 constructs having Fc fragments that are differently orientated to provide more sites where the anti-chicken IgG (Fc) antibodies can bind. The slightly lesser binding of 12 C_H2-4 (figure 4.14, bottom) compared to the 16 C_H2-4 and 18 C_H2-4 (figure 4.14, middle and top) may be due to the differences in the CDR3 regions, allowing for varying interactions with the gold nanoparticles. The difference between the signals on the replicate tests for 12-2 are likely a consequence of differences in the manual manufacturing process such as the cutting or the conjugate spotting as described

in section 3.2.4. The orientation of the gallibody on the gold nanoparticle would have a significant influence on the signal intensity [173]. Three different possibilities for orientation of the Y shaped gallibody are represented in figure 4.15. The scFv antigen binding region of the gallibody will be called the Fab region for ease.

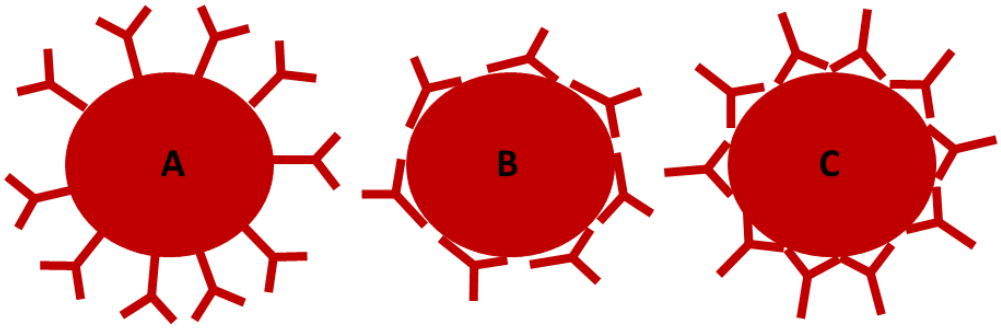

Figure 4.15: Two dimensional representation of possible orientations of gallibody conjugated to gold nanoparticles. A: Fc region interacting with the nanoparticle, leaving the Fab region free to interact with the antigen. B: Side-on interaction of the gallibody with the nanoparticle requiring theoretically less gallibody to coat the particle. C: Fab region interaction with the gold nanoparticle leaving the Fc region free to be bound. Abbreviations: Fc = fragment crystallisable Fab = fragment antigen binding

The C_H2-4 scaffold may allow for improved orientation of the interaction of the gallibody with the gold nanoparticle. Given that the anti-chicken IgG (Fc) antibody is an anti-Fc antibody, 'improved' orientation for recognition by this antibody would be that shown in figure 4.15 C, although this orientation would not allow optimal interaction of the Fab region with the MA antigen. Both A and C would allow more gallibody per nanoparticle than the orientation in B. The higher signal intensity obtained with the C_H2-4 gallibodies may also be explained as the C_H2-4 scaffold is smaller than the C_H1-4 scaffold, allowing the conjugation of more gallibody per gold nanoparticle. If the most common orientation is as in B, a smaller gallibody would have more molecules bound per particle than a larger one. However this difference in size is probably too small to have such a large impact as observed in figure 4.14. A combination of some or all of these effects is likely.

From the results in figure 4.14 it appears that C_H2-4 constructs provide stronger signal intensity for the control line for MALIA. Ranchod *et al.* [91] also indicated more sensitive antigen (MA) detection by the C_H2-4 constructs. [91] From this it was decided to use C_H2-4 gallibodies for further MALIA development. Minor differences in signal intensity were observed (figure 4.14) between the C_H2-4 constructs of the three clones (12, 16 and 18) with any of these suitable for further studies.

4.3.1.2 The effect of coating conditions on gold labelled gallibody

The Vis spectrum analysis of gold nanoparticles and conjugates is a common characterisation step [138,160,161] with an expected shift in the plasmon resonance band (maximal absorbance)

when gold is conjugated to a protein [160,163]. To confirm the stability of the conjugate, varying concentrations of gallibody 12-2 were added directly to gold and allowed to conjugate at RT. Following this, an excess (10%) NaCl solution was added and the Vis absorbance spectrum measured (390 – 700 nm, every 10 nm). If the gold nanoparticles are not sufficiently coated with protein they will aggregate, turning purple in colour and the plasmon resonance band will collapse. Figure 4.16 shows the Vis absorbance spectra of uncoated gold nanoparticles without NaCl added (gold alone, red), with NaCl added (uncoated, aggregated gold, blue) and conjugated to 5 µg/mL of gallibody 12-2 (sufficiently coated gold, black).

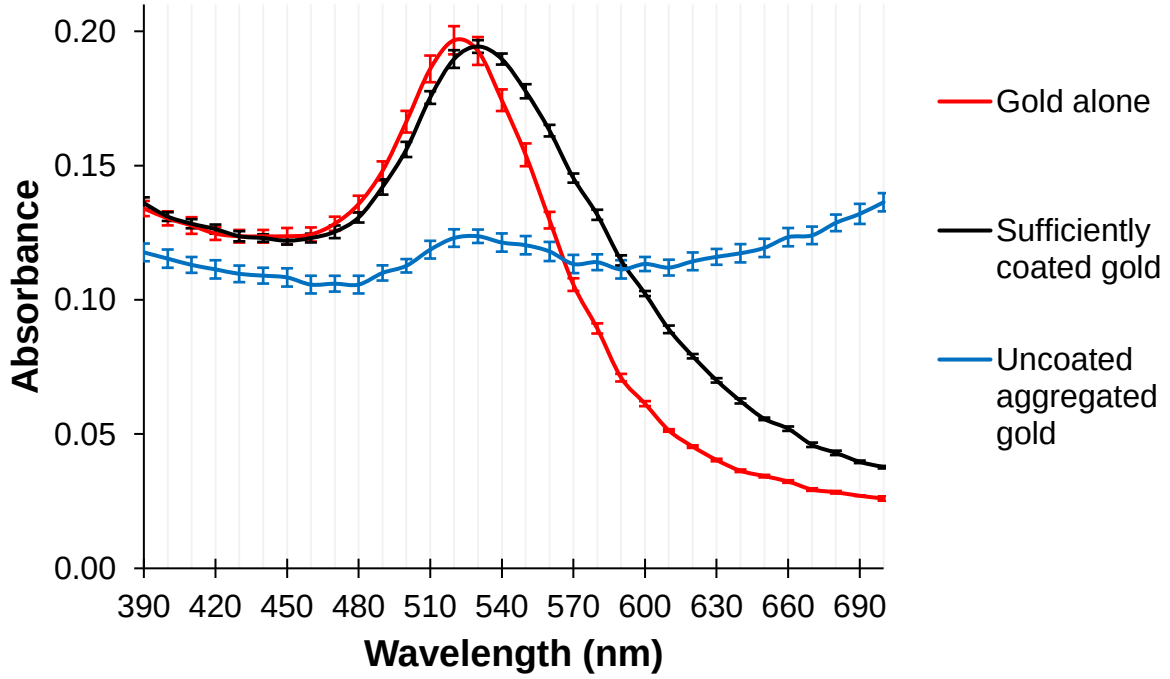

Figure 4.16: Visible wavelength absorbance spectra showing surface plasmon resonance bands of three conditions of colloidal gold suspensions: stable, conjugated to gallibody and aggregated. Absorbance at 390 – 700 nm is shown for uncoated gold nanoparticles without NaCl added (gold alone, red), with NaCl added (uncoated aggregated gold, blue) and conjugated to 5 µg/mL of gallibody 12-2 (sufficiently coated gold, black). The standard deviation of three replicate wells shown.

The expected shift in plasmon resonance occurred from 520 to 530 nm (figure 4.16, red and black) upon conjugation of the gold to gallibody [160]. Uncoated gold aggregated upon the addition of salt, causing the loss of the plasmon resonance band.

Figure 4.17 shows the Vis absorbance curves for gold labelled gallibody conjugates using 1, 1.5, 10 and 40 µg/mL concentrations of gallibody after addition of NaCl. At 10 and 40 µg/mL (figure 4.17C and D) gold particles are sufficiently coated and the plasmon resonance peak is maintained, whereas at 1 and 1.5 µg/mL (figure 4.17A and B) the addition of NaCl caused the aggregation of the gold and the loss of the plasmon resonance band.

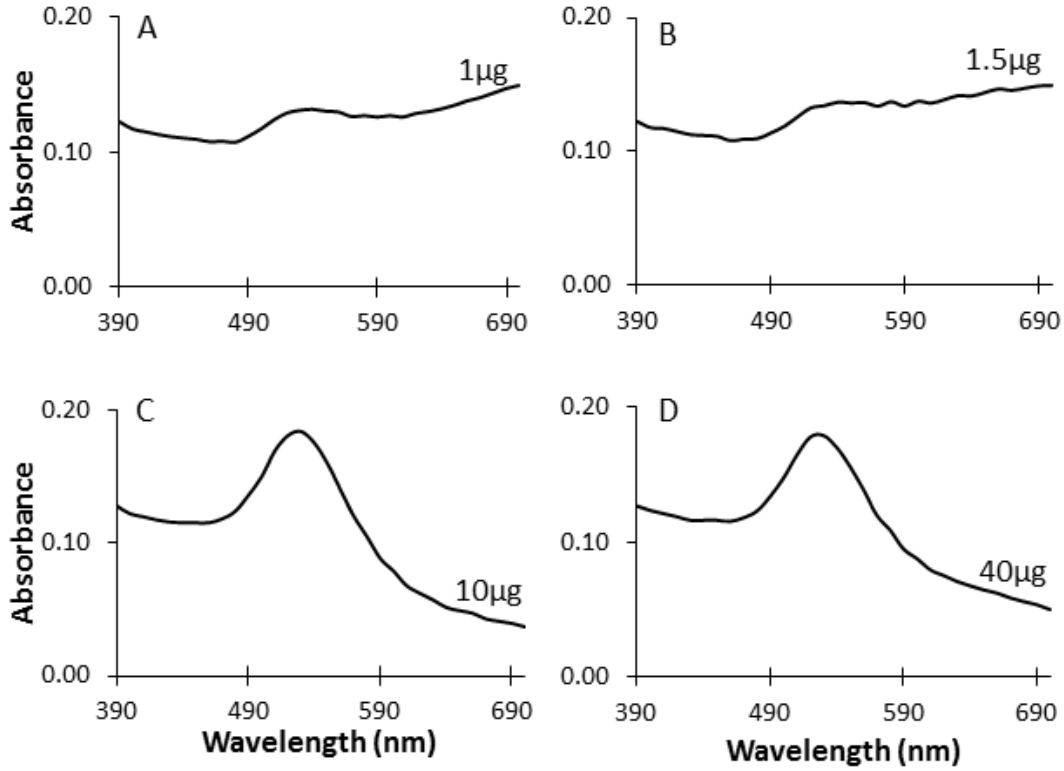

Figure 4.17: Visible wavelength absorbance spectra showing surface plasmon resonance bands of colloidal gold conjugated to a range of gallibody 12-2 concentrations: 1(A), 1.5(B), 10(C), 40(D) µg/mL. Absorbance at 390 – 700 nm are shown for gold labelled gallibody 12-2 conjugates prepared with four concentrations of gallibody, after the addition of excess NaCl.

The use of Vis spectra to observe aggregation and make conclusions about the shape of colloidal gold conjugates and nanoparticles alone is documented [161,174,175]. If the gold nanoparticles are not sufficiently coated with protein the NaCl ions force their aggregation due to the shielding of repulsive forces. This is seen by a visual colour change and the loss of the plasmon resonance band. This effect is clear in figure 4.17A and B where 1 and 1.5 µg/mL of gallibody are insufficient to completely coat the nanoparticles. The Vis spectra maintain their shape (plasmon resonance peak at ~530 nm) at both 10 and 40 µg/mL of gallibody shown in figure 4.17C and D, compared to the gold alone shown in figure 4.16 (red).

Previously (section 3.2.2) the visual observation of the 'redness' of the conjugates was used to determine whether it was stable. The red colour intensity equates to the maximal absorbance wavelength ~520 nm as can be observed in figure 4.16. The gold is supplied at an OD of 1 at 522 nm (provided by the manufacturer as the maximal absorbance wavelength). Horisberger and Rosset [157] used absorbance at 520 nm to determine conjugate stability. As the conjugate stabilises, the absorbance value at 520 nm will increase until plateauing at a certain concentration of gallibody. In the traditional use of the salt test, the absorbance is recorded at 580 nm as a measurement of the aggregation of the gold nanoparticles [128,158]. At

580 nm the minimum absorbance value indicates a stable conjugate. These analyses (absorbance at 580 and 520 nm) were carried out at varied concentrations of gallibody 12-2 with results shown in figure 4.18. Included above the 520 nm graph (red) are pictures of the gold labelled gallibody 12-2 conjugates at the indicated concentrations, after interaction with excess NaCl. Below the 580 nm graph (blue) are scanned images of half tests with immobilised anti-chicken IgG (Fc) antibody and probed with gold labelled gallibody conjugates prepared at the gallibody concentrations indicated.

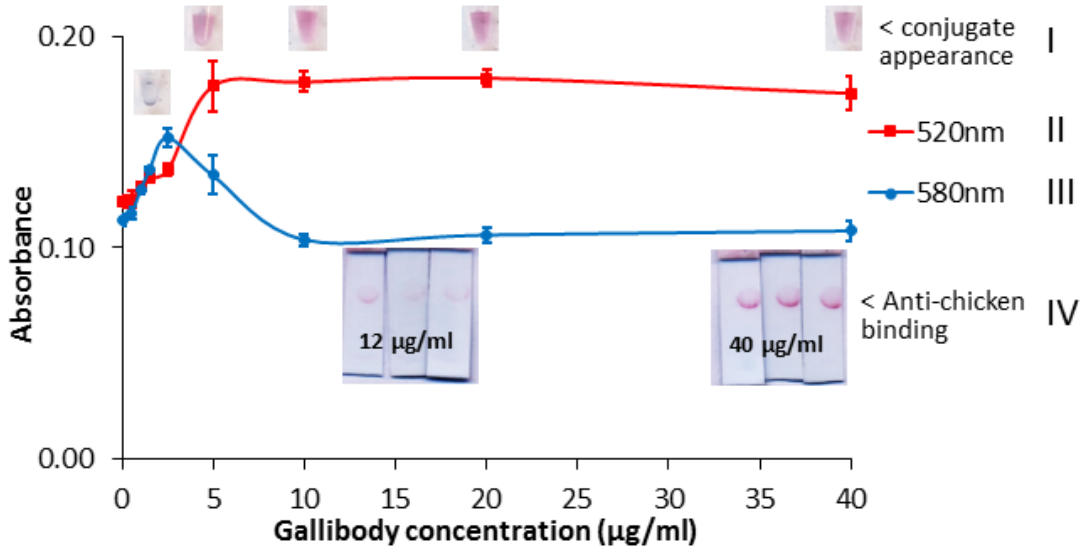

Figure 4.18: Gold labelled gallibody 12-2 conjugate stability at varying gallibody concentration shown by: (I) conjugate colour after NaCl addition, absorbance curves at (II) 520 nm the plasmon resonance wavelength and at (III) 580 nm as an indicator of flocculation, and (IV) binding by immobilised anti-chicken IgG (Fc) antibodies. Absorbance at 520 nm (red) or 580 nm (blue) are shown for gold labelled gallibody 12-2 conjugates prepared with increasing concentrations from 0 – 40 µg/mL of gallibody (added to OD 1 gold at pH 6) after the addition of excess NaCl. The standard deviations of three replicate experiments with three wells each are shown. Pictures above the 520 nm curve are of the appearance of the conjugates after the addition of NaCl. Scanned, cropped images of half tests coated with 0.5 µg/mL anti-chicken IgG (Fc) antibody and probed with gold labelled gallibody conjugates prepared at 12 µg/mL and 40 µg/mL are shown beneath the 580 nm curve.

The colour of the conjugate remained red from 5 – 40 µg/mL (figure 4.18I). At 2.5 µg/mL the colour of the conjugate had collapsed due to aggregation of the gold nanoparticles. In figure 4.18II the 520 nm curve absorbance increased until a gallibody concentration of 5 µg/mL and then plateaued, decreasing slightly at 40 µg/mL. From this the stabilising concentration of gallibody 12-2 appears to be 5 µg/mL also confirmed by the pink/red colour (indicating no aggregation) of the pictured conjugate above. The shape of the Vis spectrum graph (of the same conjugate of a gallibody concentration of 5 µg/mL) shown in figure 4.16 (black) also supports this.

For the 580 nm curve (figure 4.18III), a peak is formed at 2.5 µg/mL with the minimum absorbance at 10 µg/mL before stabilising at concentrations higher than this. Hermanson [128] recommends that the concentration of antibody/protein corresponding to the minimum absorbance at 580 nm with 10 – 20% more antibody added will produce sufficiently stable conjugate based on work done by De Mey *et al.* [170] and Horisberger and Rosset [157]. At concentrations higher than this, excess antibody may be leached off as was shown to be the case for protein A conjugates [176]. In addition, during the centrifugation and resuspension steps in conjugate manufacture excess, unbound antibody is removed and therefore wasted. Using this method the stabilising concentration of gallibody 12-2 appears to be 10 µg/mL to be used at 12 µg/mL.

Tokuyasu [177] and Tinglu *et al.*[178] showed that conjugates produced with excess antibody allow the formation of darker signals in immunohistochemistry techniques for electron microscopy in the 1980s. In contrast, Byzova *et al.* [158] more recently showed that superior conjugates (producing better signal intensity on LFT) are produced using the concentration of antibody corresponding to the peak of the 580 nm curve. This would be a lower concentration than that determined by the Hermanson [128] recommendation. Because the antibody is often a large contributor to the cost of the LFT reduction of the amount of antibody used on the test could be an advantage by reducing the cost per test [102].

As can be seen from the half tests in figure 4.18IV, better signal intensity was obtained when using the gold labelled gallibody conjugate at a gallibody concentration of 40 µg/mL rather than 12 µg/mL. This result is thus similar to the observation of Tokuyasu [177] and Tinglu *et al.*[178] and contradictory to that made by Byzova *et al.* [158] and the recommendation of Hermanson [128]*.* A possible explanation for this relates to the orientation of the gallibodies on the gold nanoparticles. The lower concentration of gallibody may sufficiently coat the gold nanoparticles and give a stable conjugate, if they are mostly in the orientation shown in figure 4.15B. At the higher concentration the gallibodies may be coating the nanogold in a more upright formation as shown in 4.15A and C. More gallibody would thus be available for binding by the immobilised anti-chicken IgG (Fc) antibody, thus increasing the signal.

Besides the concentration of the protein to be conjugated, the other factors that have important impact on the production of optimal conjugates are the pH of the conjugation and the pI of the protein to be conjugated [128]. Optimal conjugation occurs at or near the pI of the protein. The gold nanoparticle sol was adjusted from the supplied pH of 5.2 to 6, 7, 8 and 9 and conjugation performed at varying concentrations of gallibody at all these pH values. At the optimal pH less gallibody is required to stably coat the gold nanoparticles in the salt test. Figure 4.19 shows the Vis spectra for four concentrations of gallibody at all the pH values tested (I), the

absorbance at 520 nm (IIA) and 580 nm (IIB) and scanned images of half tests (III) with immobilised anti-chicken IgG (Fc) antibody and probed with gold labelled gallibody conjugates prepared at the pH values indicated at a concentration of 40 µg/mL gallibody to OD 1 gold.

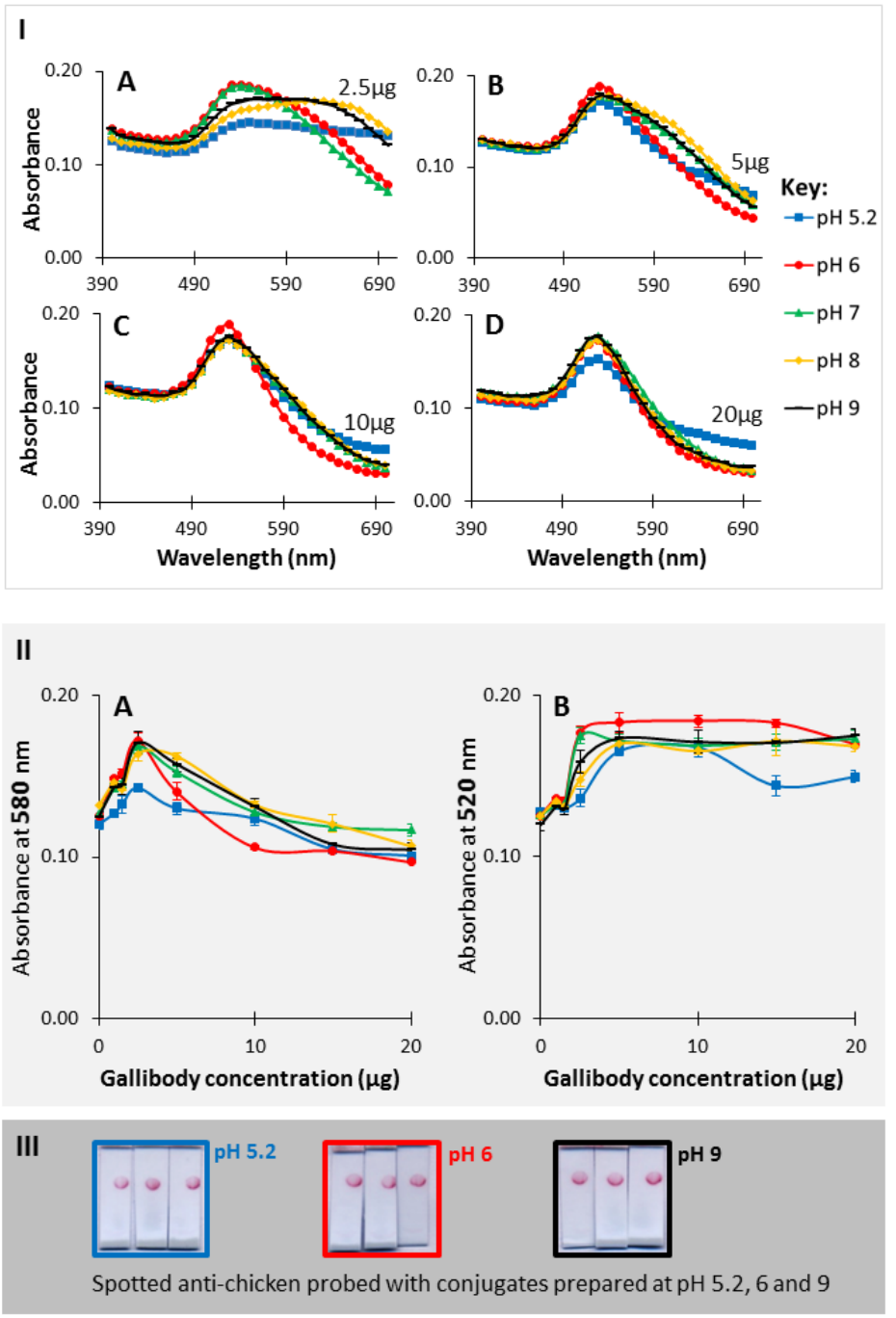

Figure 4.19: Gold labelled gallibody conjugate stability at varying pH shown by: (I) visible wavelength absorbance spectra at a range of gallibody 12-2 concentrations; (II) absorbance curves at 580 nm and 520 nm at varying gallibody 12-2 concentration and (III) binding of immobilised anti-chicken IgG (Fc) antibodies by gold labelled gallibody 18-2 conjugates. (I) Absorbance at 390 – 700 nm for gold labelled gallibody conjugates prepared at pH 5.2 (blue), 6 (red), 7 (green), 8 (yellow) and 9 (black) at concentrations of 2.5(A), 5(B), 10(C) and 20(D) µg/mL gallibody after the addition of excess NaCl. Colour key for pH is maintained for II and III in the figure. **(II)** Absorbance curves at 580 (A) or 520 (B) nm for gold labelled gallibody conjugates prepared at pH 5.2 (blue), 6 (red), 7 (green), 8 (yellow) and 9 (black) with increasing concentrations of gallibody (from 0 – 20 µg/mL) after the addition of excess NaCl. The standard deviations of measurements from three wells are shown. **(III)** Scanned images of half tests with anti-chicken IgG (Fc) antibody coated at a concentration of 0.5 mg/mL and probed with gold labelled gallibody 18-2 conjugates prepared at a concentration of 40 µg/mL gallibody to OD 1 gold (at the pH values indicated).

From figure 4.19I conjugations performed at pH 6 and 7 maintained plasmon resonance bands at the lowest concentration (A, 2.5 µg/mL) of gallibody, with pH 6 gold maintaining an absorbance spectra that most closely fits that of gold alone in all concentrations shown. In figure 4.19IIA the pH 6 (red) curve reaches the minimum point (indicating stable concentration) at a lower concentration than the other pH values. In figure 4.19IIB the pH 6 graphs reaches maximum absorbance at 2.5 µg/mL and then remains at this absorbance. Thus, from the Vis spectra, and the curves at 520 and 580 nm (figure 4.19I and II) it appears that using colloidal gold at a pH of 6 produces stable conjugates at the lowest concentrations of gallibody when interpreted as described above for figures 4.17 and 4.18. However, the variation of pH of the colloidal gold does not affect signal intensity on immobilised anti-chicken IgG (Fc) when gallibody 18-2 is conjugated to gold nanoparticles at 40 µg/mL (figure 4.19III). From this data a pH of 6 for optimal gallibody conjugation supported the results in section 3.2.2, obtained by visual observation of salt test conjugations. It is important to note that conjugates used in figure 4.19III were not prepared at the minimum concentration (shown in figure 4.19I and II, of 10 µg/mL or less), but rather at 40 µg/mL as shown to give superior signal intensity from the concentration titration in figure 4.18 as previously (section 4.3.1.2) explained.

The production of nanogold conjugates with antibodies has been used for the detection of specific molecular entities in various tissues by electron microscopy since the 1970s [128]. Therefore, protocols describing methods to obtain stable nanogold/ antibody conjugates are well established. However, in the current application the antibodies to be labelled were custom developed and rather unusual in that they are anti-lipid antigen rather than anti-protein antigen binding antibodies. The early work to characterise nanogold/ antibody interactions upon which these protocols are based, used anti-protein antibodies or protein antigens [159]. It is possible that the immobilisation of the gallibodies to the gold may render them unable to bind to their antigen, MA, despite being recognisable by the control anti-chicken IgG (Fc) antibody. It is therefore required to confirm that the gallibodies are still able to bind to MA after conjugation to gold. As early indications (as in figure 3.9) already indicate loss of MA binding activity of gallibodies in LFT, the biological activity determination of the gallibody gold conjugates had to be determined with different immunoassay technologies, such as ELISA.

4.3.2 Functional characterisation of gold labelled gallibody conjugate

4.3.2.1 Conjugate interaction with MA coated on a microtiter plate – ELISA

Byzova *et al.* [158] used ELISA to functionally characterize gold labelled polyclonal and monoclonal antibodies. In this ELISA the gold labelled antibody conjugate is incubated on the antigen coated plate as the primary antibody and detection of conjugate binding achieved by binding of a secondary enzyme labelled anti-antibody.

To confirm the ability of this method to characterise the binding ability of gold labelled antibody conjugate a system test was carried out using a high affinity antibody/antigen system known to work on both ELISA [116] and LFT (Appendix A). The results are shown in figure 4.20A. In this ELISA live *E.coli* bacteria suspended in 0.1 M PBS buffer were coated in the 96 well plate overnight with PBS as the negative coating control. The wells were then incubated with polyclonal goat anti-*E. coli* antibody, dilution buffer, gold labelled goat anti-*E. coli* conjugate and gold labelled BSA conjugate. An anti-goat IgG (Fc): HRP antibody was used as the secondary antibody. The results, with a stylised figure of the reaction scheme are given in figure 4.20 A and B, respectively.

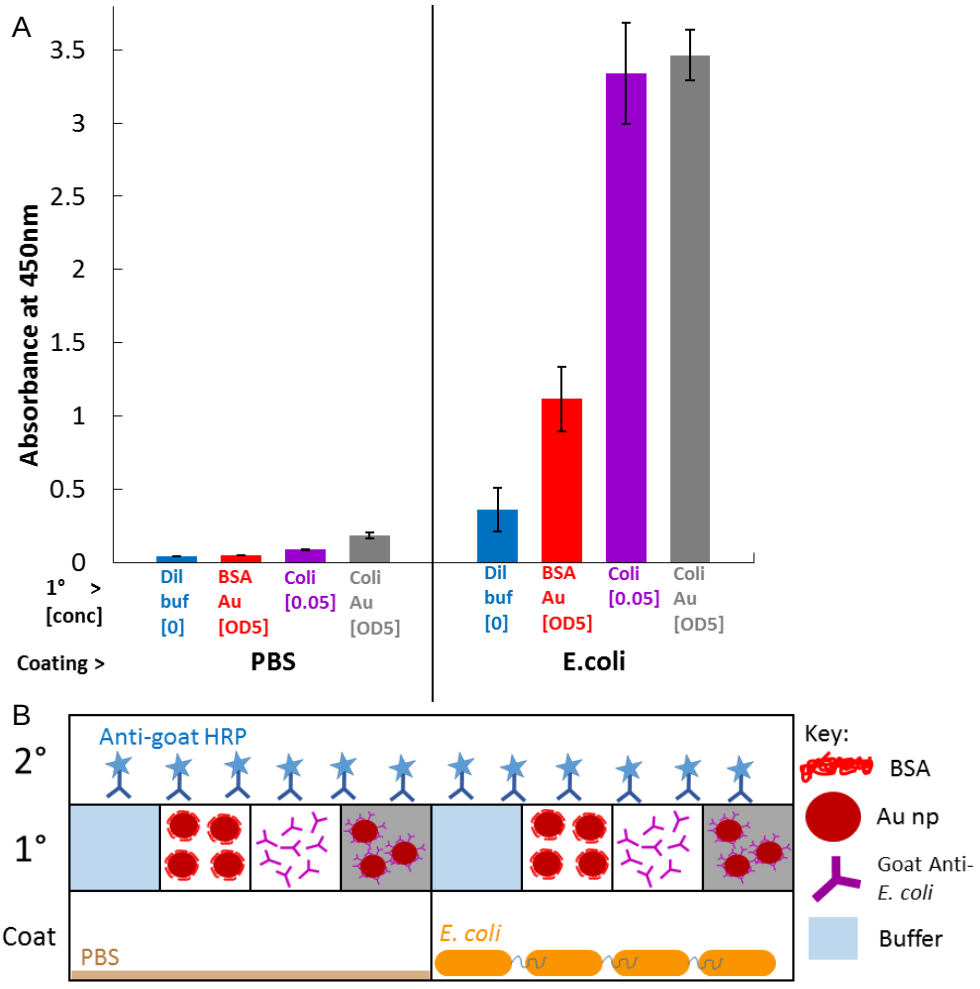

Figure 4.20: Indirect ELISA system test using *E. coli* as antigen with gold labelled anti-*E. coli* antibody conjugate and anti-*E. coli* antibodies as primary antibody to establish the method of antibody functionality determination after gold conjugation. A: Signal (A450nm) results of ELISA. B: schematic representation of the ELISA system and set-up with controls. A 100 µL volume of 10^8 CFU/mL *E. coli* in PBS or PBS only was coated, indicated in bottom 'coat' row in B. Wells were incubated with buffer only (Dil buf blue), BSA conjugate (BSA Au red), goat anti-*E. coli* antibody alone (Coli purple), anti-*E. coli* Ig conjugate (Coli Au grey) left to right (as according to the '1°' row in B) with concentrations indicated in square brackets in mg/mL or optical density (OD). HRP-linked anti-goat IgG antibodies at fixed concentration were added as indicated in '2°'. Average signal strength (bar heights) and standard deviation (error bars) of three wells are shown. Not corrected for background signal.

The result in figure 4.20 shows minimal signal for PBS coated wells. Both gold conjugated (purple bar) and unconjugated (grey bar) goat anti-*E. coli* antibody bound the coated *E. coli* (right). A background signal is visible with gold labelled BSA conjugate (red bar, right). No significant difference in *E. coli* binding ability for the conjugated (grey bar, right) vs unconjugated (purple bar, right) polyclonal antibody was observed (p value = 0.96). The amount of antibody per well (0.05 mg/mL) was calculated assuming that all of the antibody added to the OD 1 gold sol (0.01 mg/mL) would bind to and remain on the gold, even after centrifugation and resuspension to a concentration of OD 5 (during conjugate preparation). The data in figure 4.20 indicates that gold conjugation does not impair the ability of the goat anti-*E. coli* antibody to bind its antigen, nor is it no longer recognisable by the anti-goat IgG (Fc): HRP antibody. The system is thus effective and workable for this study.

In addition to the system test an additional set of controls was added to probe whether the gold labelled gallibody would still be recognised by the anti-chicken IgG (Fc) antibody in ELISA. The anti-chicken IgG (Fc) antibody does successfully bind the gold labelled gallibody conjugate on LFT (figure 4.12 – 4.14). For this experiment the gallibody (or gold labelled gallibody conjugate) would be bound by the coated anti-chicken IgG (Fc) antibody and then again by the HRP-labelled version of the same polyclonal anti-chicken IgG (Fc) antibody. The results are shown in figure 4.21A with a stylised figure of the reaction scheme in figure 4.21B.

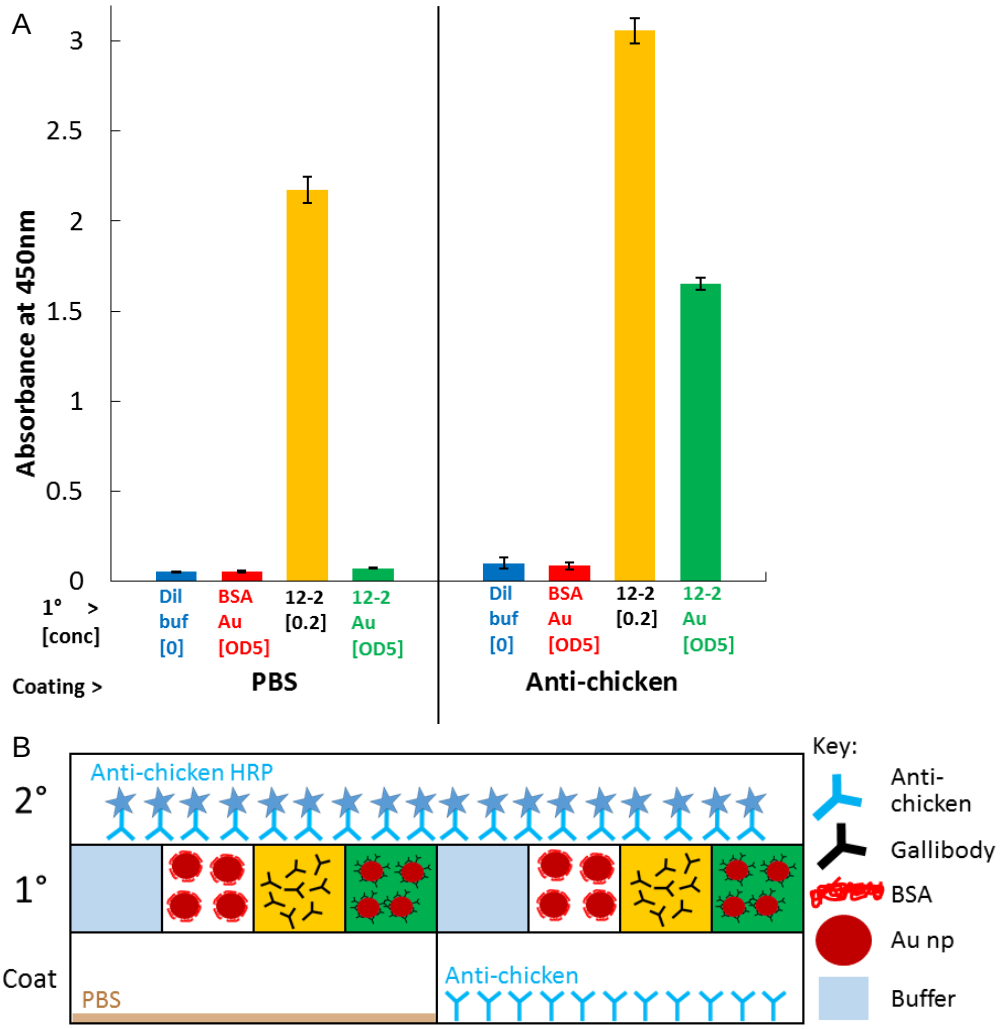

Figure 4.21: Sandwich ELISA control test using anti-chicken IgG (Fc) antibody as capture antibody with gold labelled gallibody 12-2 conjugate or gallibody 12-2 as antigen to be detected to confirm anti-chicken IgG (Fc) binding of gallibody after conjugation. A: Signal (A450nm) results of ELISA B: schematic representation of ELISA system and set-up with controls. Anti-chicken IgG (Fc) antibody in PBS or PBS only was coated, indicated in bottom 'coat' row in B. Wells were incubated with buffer only (Dil buf blue), BSA conjugate (BSA Au red), gallibody 12-2 alone (12-2 black), gallibody 12-2 conjugate (12-2 Au green) left to right '1°' row in B with concentrations indicated in square brackets in mg/mL or optical density (OD). HRP-linked anti-chicken IgG (Fc) antibodies at fixed concentration were added as indicated in '2° in B. Average (bar heights) and standard deviation (error bars) of three wells are shown. Not corrected for background signal.

In figure 4.21 minimal signal is seen for PBS coated wells (left), except for gallibody which non-specifically bound non-coated (PBS) wells (yellow bar, left). The amount of gallibody used for these assays (0.2 mg/mL) is far above the optimal amount for MA ELISA (~0.04 mg/mL) as shown in chapter 2 (figure 2.5) but was chosen to be comparable to OD 5 conjugate concentration. This excess may be the reason for the high background (PBS coated) signal for the gallibody alone (yellow bar left). Significant binding of both the gold labelled gallibody conjugate (green bar, right) and the unconjugated gallibody (yellow bar, right) by the coated anti-chicken IgG (Fc) antibody is evident from the absorbance signals in figure 4.21. However,

if the non-specific PBS binding signals are subtracted the signal for the conjugate would appear stronger than the unconjugated gallibody. The background signal of gallibody on hexane has previously been shown to be high (figure 2.5). Regardless of this background the binding of the gold labelled gallibody conjugate by the anti-chicken IgG (Fc) antibody is clear (green bar, right). This result confirms that from the LFT results (immobilised anti-chicken IgG (Fc) antibody signals seen in figures 3.9, 3.11, 3.14, 3.15, 3.16, 4.12, 4.13 and 4.14).

From Ranchod *et al.* [91] and the results presented in chapter 2 the ability of the custom developed gallibodies to bind MA is established. However, once conjugated to gold and probed with MA in a LFT format, this binding was no longer evident (chapter 3, figure 3.9). To test the MA binding ability of the gold labelled gallibody conjugate MA was coated in a 96 well plate as previously described (section 4.2.4) and probed with two concentrations of gold labelled gallibody conjugate and unconjugated gallibody. An unrelated gallibody control was also included (conjugated and unconjugated) (figure 4.22).

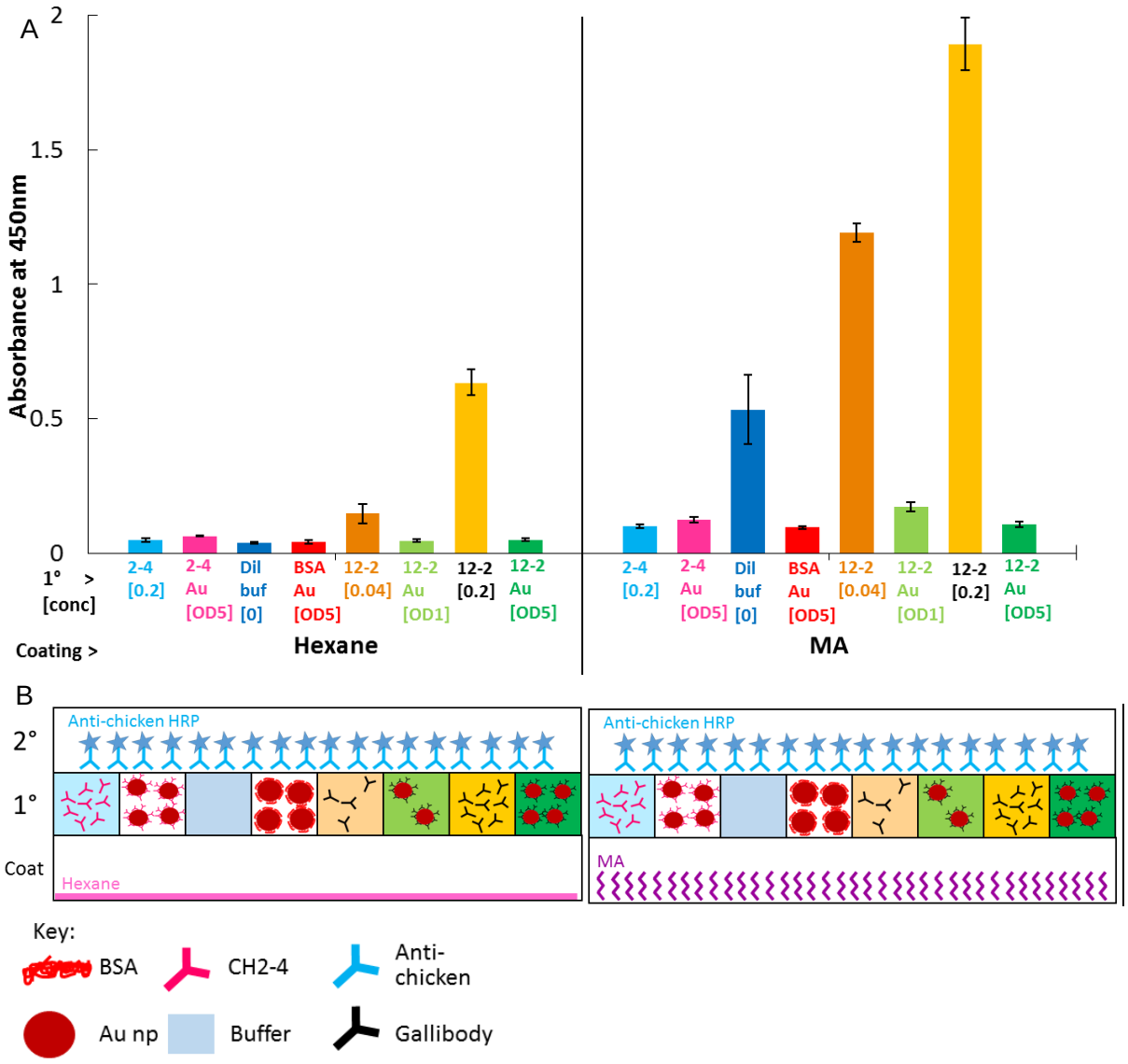

Figure 4.22: Indirect ELISA test using MA as antigen with gold labelled gallibody 12-2 conjugate or gallibody 12-2 as primary antibody to determine MA binding functionality of gallibody after conjugation. A: Signal (A450nm) results of ELISA B: schematic representation of ELISA system and set-up with controls. MA in hexane (0.25 mg/mL) or hexane only was coated, indicated in bottom 'coat' row in B. Wells were incubated with unrelated gallibody only (C_H2-4 light blue), unrelated gallibody conjugate (C_H2-4 Au pink), buffer only (Dil buf blue), BSA conjugate (BSA Au red), two concentrations of gallibody 12-2 alone (12-2 orange and black)and two concentrations of gallibody 12-2 conjugate (12-2 Au light and dark green) '1°' row in B, with concentrations indicated in square brackets in mg/mL or optical density (OD). HRP-linked anti-chicken IgG (Fc) antibodies at fixed concentration were added as indicated in '2° in B. Average (bar heights) and standard deviation (error bars) of three wells are shown. Not corrected for background signal.

From figure 4.22, minimal signal is seen for hexane coated wells (left), except for gallibody at 0.2 mg/mL, which non-specifically bound the hexane coated wells (yellow bar, left). A similar background signal on PBS coated wells was seen in figure 4.21. Gold conjugated gallibody did not bind MA (light and dark green bars right), however the gallibody alone shows significant binding of MA at both concentrations tested (0.04 and 0.2 mg/mL, orange and yellow bars

respectively) as expected. A background signal was seen with dilution buffer showing some signal on MA (dark blue bar).

It is important to note that the affinity of the binding between the gallibody and MA is much lower than between the gallibody and the anti-chicken IgG (Fc) antibody. The former is an inherently weaker protein-lipid interaction between a monoclonal antibody and an unusual lipid antigen. The latter interaction is a much stronger protein-protein interaction and involves a polyclonal antibody to the conserved Fc portion which is maintained in the recombinant gallibody. There are therefore several possible reasons for the loss of MA binding ability by the gold labelled gallibody conjugate:

Firstly as alluded to in section 4.3.1.1 it is not known in which orientation the gallibodies are bound to the gold. It is therefore possible that the scFv antigen binding antibody regions (containing the MA antigen binding site) preferentially interact with the gold nanoparticle, rendering them unavailable to bind the MA (as in figure 4.15C). Some other effect of interaction with the gold nanoparticles may cause the gallibodies to slightly denature or otherwise change so that they lose their MA binding ability or drastically reduce it. While this is not reported for antibody-gold conjugates in general, it is important to remember that the gallibodies are unusual anti-lipid binding antibodies. Also, as these are monoclonal antibodies, if there is any specific disruption of the gallibody (due to amino acid affinities etc.) the activity will be reduced for all the species in the sample. In the case of polyclonal antibodies, (as for the anti-chicken IgG (Fc) and the anti-*E. coli* interaction) several species may unfavourably interact, while still leaving plenty of species (and activity) intact.

Another possible explanation for the apparent loss of MA binding ability by the conjugated gallibody lies in the affinity of the interaction between the MA and the gallibody. This is a low affinity interaction unlike that of the anti-chicken IgG (Fc)/gallibody or anti-*E. coli /E. coli* interactions. The numerous and vigorous wash steps (during an ELISA assay) while the gallibody is bound to a ‘heavy’ gold nanoparticle may overcome the force of the gallibody/MA binding. This force could reduce/remove signal at every wash step.

The loss of the MA binding ability of the gallibody when conjugated to gold may then be as a result of the low affinity of that interaction being overcome by the experimental conditions in ELISA or as a result of a loss of function of the gallibody because of its conjugation to gold. To investigate this further characterisation of the gold labelled gallibody/MA interaction was done in a system without vigorous wash steps.

4.3.2.2 Conjugate interaction with MA nanoparticles – DLS

The interaction between the gold labelled gallibody conjugate and MA was explored using DLS. PLGA nanoparticles containing MA and empty PLGA nanoparticles were used that were the same as those developed for and confirmed as antigenic on electro impedance spectroscopy [95]. The particles were diluted in deionised water to a concentration of 2 µg/mL or 10 µg/mL before measurement in the Zetasizer Nano ZS (Malvern, USA). The volume of nanoparticle suspension diluted in 1 mL of deionised water is given in brackets in the legend of figure 4.23 and the peak size value in colour coded boxes. The instrument software converted the data into intensity distributions which are graphically displayed in figure 4.23.

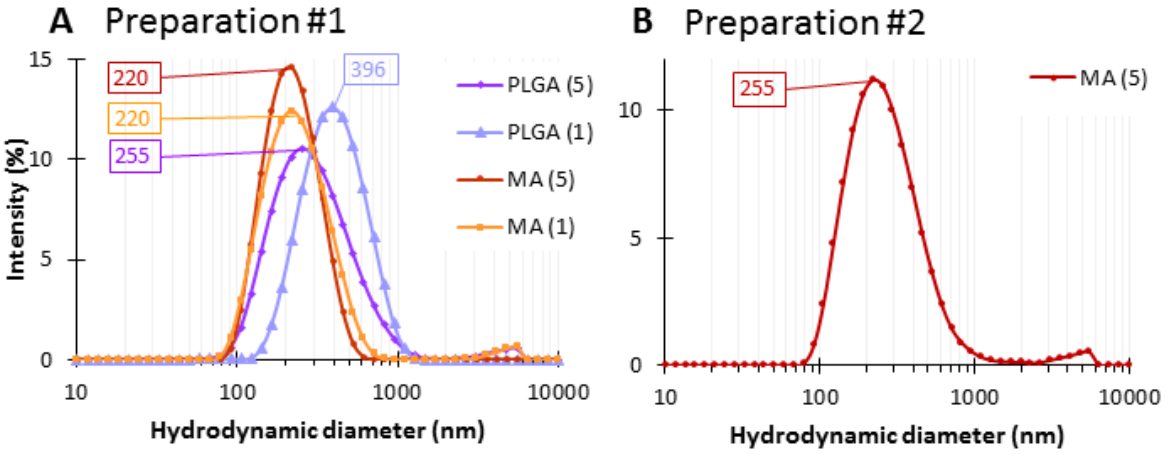

Figure 4.23: Hydrodynamic diameter distributions of PLGA nanoparticles with and without MA. Hydrodynamic diameters of two preparations (A and B) of nanoparticle suspensions at different concentrations were estimated using intensity distributions from DLS measurement. The volume of 2 mg/mL nanoparticle suspension diluted in 1 mL of deionised water is given in brackets in the legend. Peak values are given in colour coded boxes. Abbreviations: PLGA = poly$_{DL}$-lactic-co-glycolic acid (empty) nanoparticles; MA = mycolic acid PLGA nanoparticles. Measurements were taken at 25°C in a Zetasizer Nano ZS (Malvern, USA) with instrument software optimised settings. Shown is the average result of at least 3 repeat measurements with at least 12 replicate measurements each.

The results in figure 4.23 show approximate peak values for preparation number 1 PLGA (5) = 255 nm and PLGA (1) = 396 nm. A clear increase in particle size is observed upon dilution. It therefore appears that empty PLGA particles tend to dimerization at the lower concentration tested. MA containing nanoparticles however remained as monomers at both concentrations.

Hydrodynamic diameters of different concentrations of conjugates or colloidal gold alone were also estimated using intensity distributions from DLS measurement. As the conjugate is prepared at a concentration of OD 10, and the gold is supplied at an OD of 1, 1 µL of conjugate contains approximately the same number of particles as 10 µL of uncoated colloidal gold. Thus the concentration of particles in 1 µL of conjugate and 10 µL of uncoated colloidal gold in 1 mL of deionised water is comparable. The intensity distribution data is presented in figure 4.24.

The volume of conjugate or colloidal gold diluted in 1 mL of deionised water is given in brackets in the legend and the peak size value in colour coded boxes.

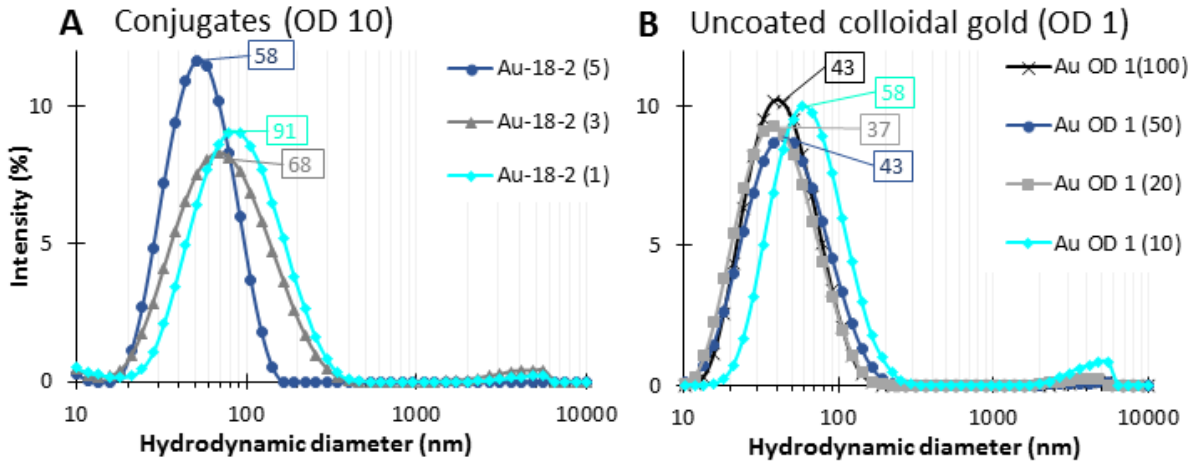

Figure 4.24: Hydrodynamic diameter distributions of various gold labelled gallibody 18-2 conjugates (A) and uncoated colloidal gold (B). Hydrodynamic diameters different concentrations of conjugates or colloidal gold alone were estimated using intensity distributions from DLS measurement. The volume of nanoparticle suspension diluted in 1 mL of deionised water is given in brackets in the legend. Peak values are given in colour coded boxes. Abbreviations: Au-18-2 = gold labelled gallibody 18-2 conjugate; Au = unconjugated gold nanoparticles; OD = optical density (absorbance) at 520 nm. Measurements were taken at 25°C in a Zetasizer Nano ZS (Malvern, USA) with instrument software optimised settings. Shown is the average result of at least 3 repeat measurements with at least 12 replicate measurements each.

The data in figure 4.24 represent a dynamic situation of particles in solution under the influence of Brownian motion. The shift in size between the measurement of the same nanoparticles at higher and lower concentrations appears to show that at lower concentration (1 or 10 µL for conjugates and uncoated gold respectively) the gold nanoparticles are more likely to associate as dimers. For the 5 µL volume Au-18-2 conjugates the peak diameter is around 58 nm, the 3 µL volume at 78 nm and the 1 µL volume at 91 nm. A clear increase in particle size is observed upon dilution. Similarly for the uncoated gold both the 100 µL, 50 µL and 20 µL volumes provide diameter peaks around 40 nm, while the 10 µL measured a diameter peak around 58 nm; indicating a clear increase in size with no other change than a decreased concentration in water.

Interesting to note is the change in diameter between the uncoated gold (figure 4.24B, 50 µL) and the 18-2 conjugated gold (figure 4.24B, 5 µL) from 43 nm to 58 nm, a difference of 15 nm. This is at the concentration where the size of the uncoated nanoparticles appears stable as monomers and similar to the manufacturer stated size of the gold nanoparticle of 40 nm. This is consistent with the observation of Jans *et al.* [168] about the diameter increase for citrate capped gold nanoparticles conjugated directly to IgG. They report a consistent increase of 15 – 20 nm as logical as a single antibody is 7 – 10 nm in diameter [168]. This 15 nm size

increase observed in figure 4.24 then confirms the conjugation of monomeric gallibody to the gold nanoparticle surface.

Finally, the 2 mg/mL suspensions of PLGA nanoparticles with and without MA were incubated in a 1:1 ratio with gold labelled 18-2 or BSA conjugate. Of this reaction mixture a volume of 3 µL was diluted in 1 mL of deionised water. Thus volumes of each in the 1 mL of deionised water was 1.5 µL. At similar dilution (1 µL in 1 mL instead of 1.5 µL) gold labelled 18-2 conjugate and the PLGA nanoparticles tend towards dimerization. This was concluded from the higher peak values of suspensions at similar concentration in figures 4.23A and 4.24A (light purple and light blue graphs respectively). In this experiment no wash steps or flow affects the interaction between the MA and the gold labelled conjugates. The intensity distribution data is presented in figure 4.25.

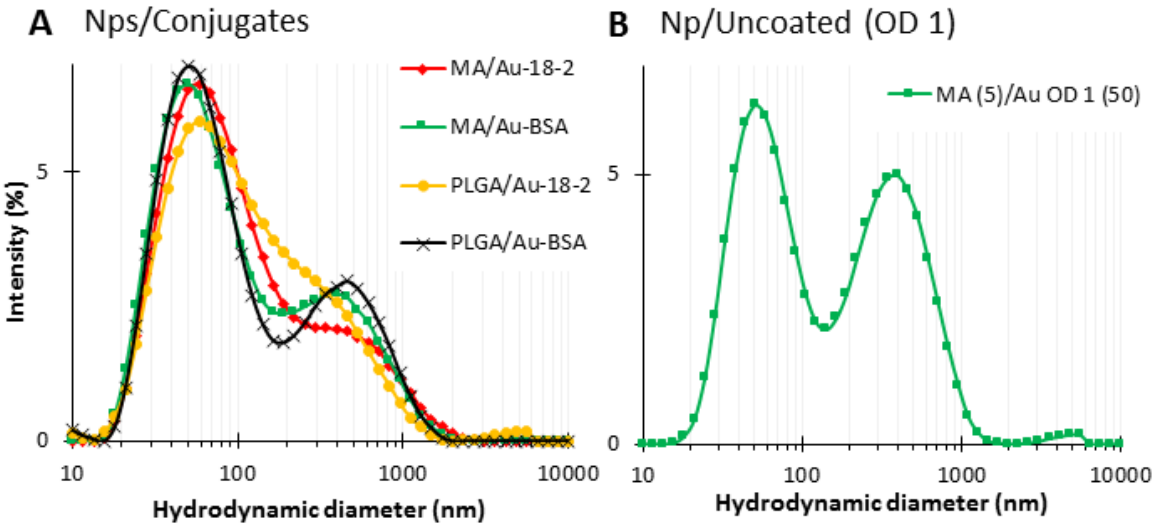

Figure 4.25: Hydrodynamic diameter distributions of gold labelled gallibody conjugates (A) and uncoated gold (B) incubated with PLGA nanoparticles with and without MA. Hydrodynamic diameters of A: 3 µL of conjugate and nanoparticles in a 1:1 ratio and B: 5 µL of 2 mg/mL suspension of MA nanoparticles (as measured in figure 4.23B) incubated with 50 µL of uncoated OD 1 gold nanoparticles (as measured in figure 4.24B) diluted in 1 mL deionised water were estimated using intensity distributions from DLS measurement. Abbreviations: PLGA = poly$_{DL}$-lactic-co-glycolic acid (empty) nanoparticles MA = mycolic acid PLGA nanoparticles; Au-18-2 = gold labelled gallibody 18-2 conjugate; Au-BSA = gold labelled BSA conjugate. Au = unconjugated gold nanoparticles; OD = optical density at 520 nm; Np = nanoparticle. Measurements were taken at 25°C in a Zetasizer Nano ZS (Malvern, USA) with instrument software optimised settings. Shown is the average result of at least three repeat measurements with at least 12 replicate measurements each.

The following null hypotheses were used to interpret the data from figure 4.25:

I. Both gold labelled BSA and gallibody conjugates bind non-specifically to empty PLGA nanoparticles.
II. Gold labelled gallibody conjugate binds empty PLGA nanoparticles and MA nanoparticles with equal strength.

The first hypothesis (I) is rejected as only gold labelled gallibody conjugate (figure 4.25A, yellow graph) appears to bind the PLGA particles, unlike the gold labelled BSA conjugate (figure 4.25A, black graph). This is drawn from the two distinct peaks formed by the PLGA/Au-BSA interaction rather than the more singular peak seen for the PLGA/Au-18-2 interaction. The black graph representing the interaction between the gold labelled BSA and the PLGA nanoparticles more definitely resembles that of the interaction between the uncoated gold and MA nanoparticles shown in figure 4.25B as a control for non-reaction. Both of these interactions (black and yellow graphs in figure 4.25A) would be non-specific (i.e. not antibody/antigen) interactions between the conjugates and the empty PLGA nanoparticles.

The second hypothesis (II) is rejected as gold labelled gallibody 18-2 appears to bind more closely to the MA nanoparticles (figure 4.25A, red graph) than the empty PLGA nanoparticles (figure 4.25A, yellow graph). This is drawn from the higher and more singular peak for the MA/Au-18-2 interaction (red) than the PLGA/Au-18-2 (yellow) interaction. It also appears that the gold labelled BSA conjugate preferentially binds the MA nanoparticles (figure 4.25A, MA/Au-BSA, green graph) rather than the empty nanoparticles (PLGA/Au-BSA black graph), although not to the same extent as observed with the interaction of gold-labelled 18-2 and MA-PLGA. Thus the activity of the gold labelled gallibody is in a better, but similarly small order of magnitude as the known binding of fatty acid (of which class of lipid molecules MA is an extreme example) by BSA [179].

The DLS data seem to suggest that conjugation of the gallibody does not completely destroy the MA binding activity of the gallibody to MA binding. However the remaining affinity of this interaction is low. In addition, the interference of non-specific binding of PLGA to gold-labelled 18-2 (yellow graph, figure 4.25) weakens the power of the DLS approach to make a convincing case for biological activity determination of antigen-antibody interaction.

Further evidence of the loss of MA binding activity from the gold labelling of the gallibody was gathered by observation of this interaction by transmission electron microscopy.

4.3.2.3 Conjugate interaction with MA nanoparticles – TEM

The interaction between gold labelled gallibody conjugates and PLGA nanoparticles with and without MA was visualised using TEM. As a starting point the nanoparticles from the same batch as used for the DLS experiments described in 4.3.2B were imaged on their own. A 3 µL volume of the 2 mg/mL nanoparticle suspension was dropped onto a carbon coated TEM grid and excess liquid drawn off with filter paper. The grid was air dried before visualisation in TEM. Representative images are shown in figure 4.26.

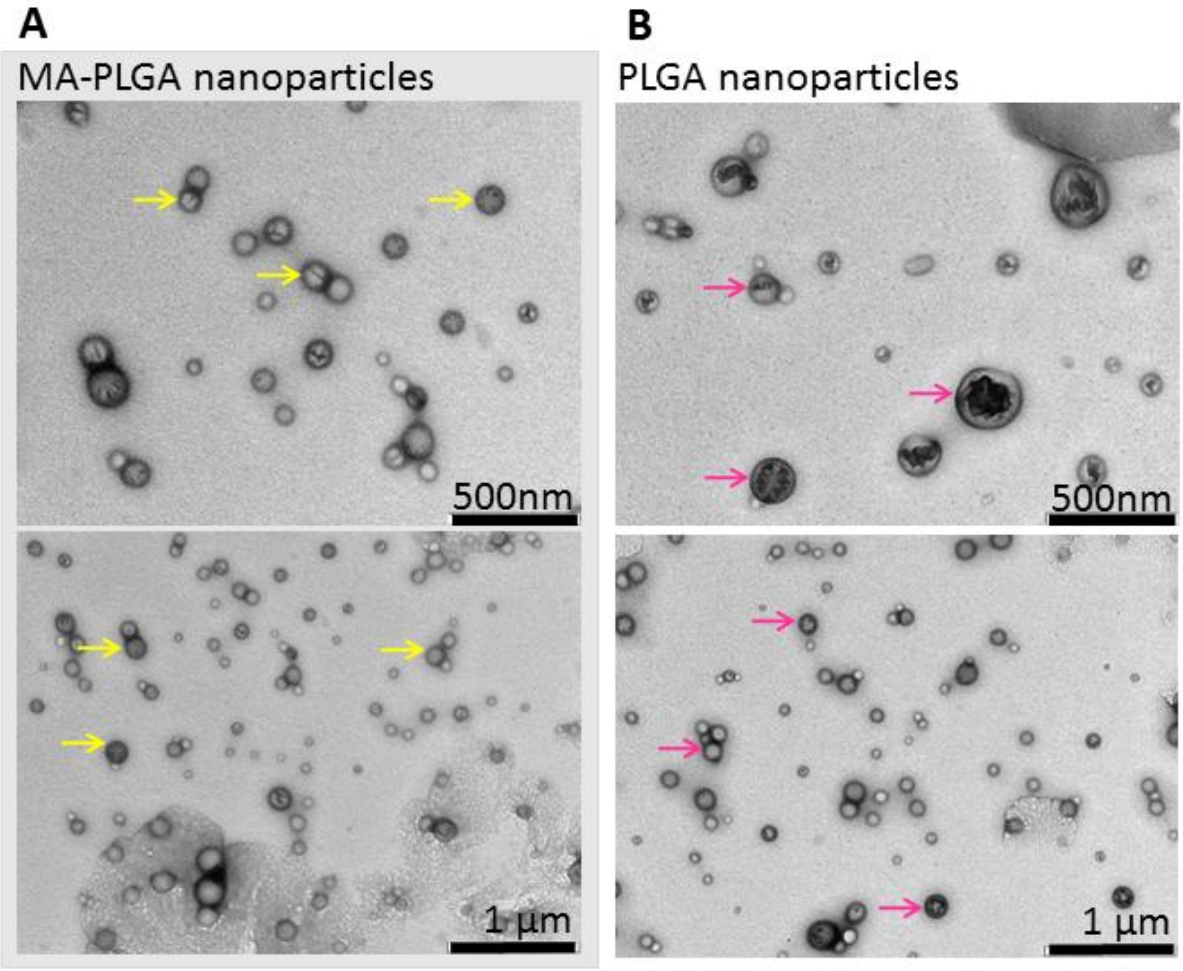

Figure 4.26: TEM images of PLGA nanoparticles with MA (A) and without (B). Representative MA-PLGA nanoparticles are indicated with yellow arrows (A) and PLGA nanoparticles with pink arrows (B). A 3 µL volume of a 2 mg/mL suspension of nanoparticles in 0.1 M borate buffer was used to coat a carbon coated grid.

From figure 4.26 the nanoparticles are clearly visible by themselves without coating or staining required. There is no visible difference between the particles with MA and those without. The particles present varying sizes and uniform spherical shape. The nanoparticles when imaged inside a eukaryotic cell by Lemmer *et al.* [172] were visible as white circles on a dark background whereas in the present images no background is given and so particles appear dark on a light background.

Figure 4.27 shows images of the gold labelled gallibody and BSA conjugates. A 3 µL volume of the conjugate (OD 10) was dropped onto the carbon coated grid and excess liquid drawn off and the grid air dried as before. Gold nanoparticles appear as small dark circles on a light field.

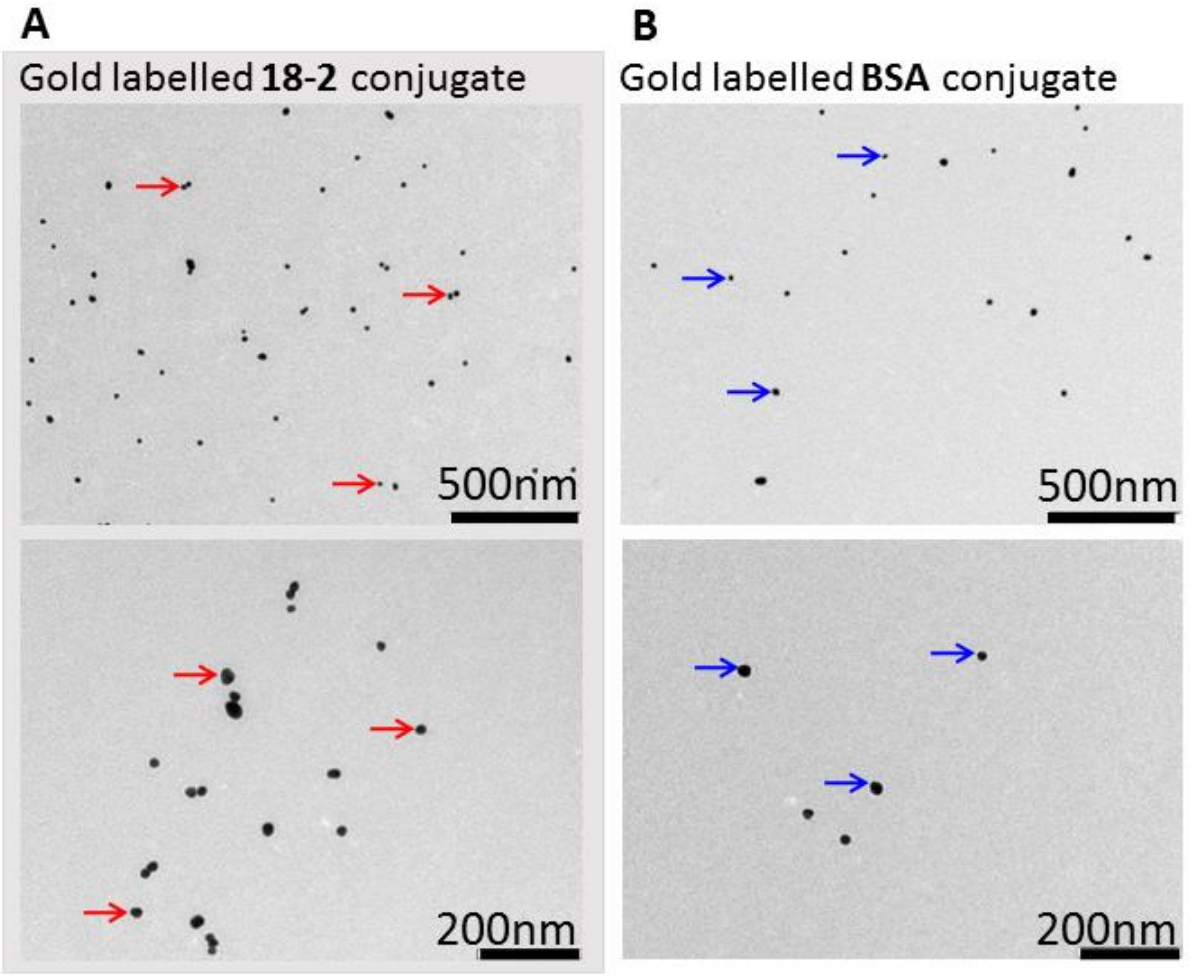

Figure 4.27: TEM images of gold labelled gallibody 18-2 (A) and BSA (B) conjugates. Representative gold conjugate nanoparticles are indicated with red arrows (A) for gallibody labelled and blue arrows (B) for BSA labelled gold nanoparticles. A 3 µL volume of OD 10 concentration of conjugate was used to coat a carbon coated grid.

Gold conjugates appear as expected (figure 4.27). Particles are of varying size but approximately in the expected range of 20 – 40 nm. No attempt was made to measure a statistically significant proportion of nanoparticles, however it was observed that particles were generally less than 40 nm in diameter. No visible difference between gold labelled BSA or gallibody conjugates is evident.

To observe the interaction between gold labelled gallibody conjugates and MA nanoparticles, gold labelled gallibody and BSA conjugates were incubated with 2 mg/mL suspensions of the nanoparticles in 1:1 ratios for at least one hour before preparation on TEM grids and imaged as previously described herein (section 4.2.6). Results are shown in figure 4.28.

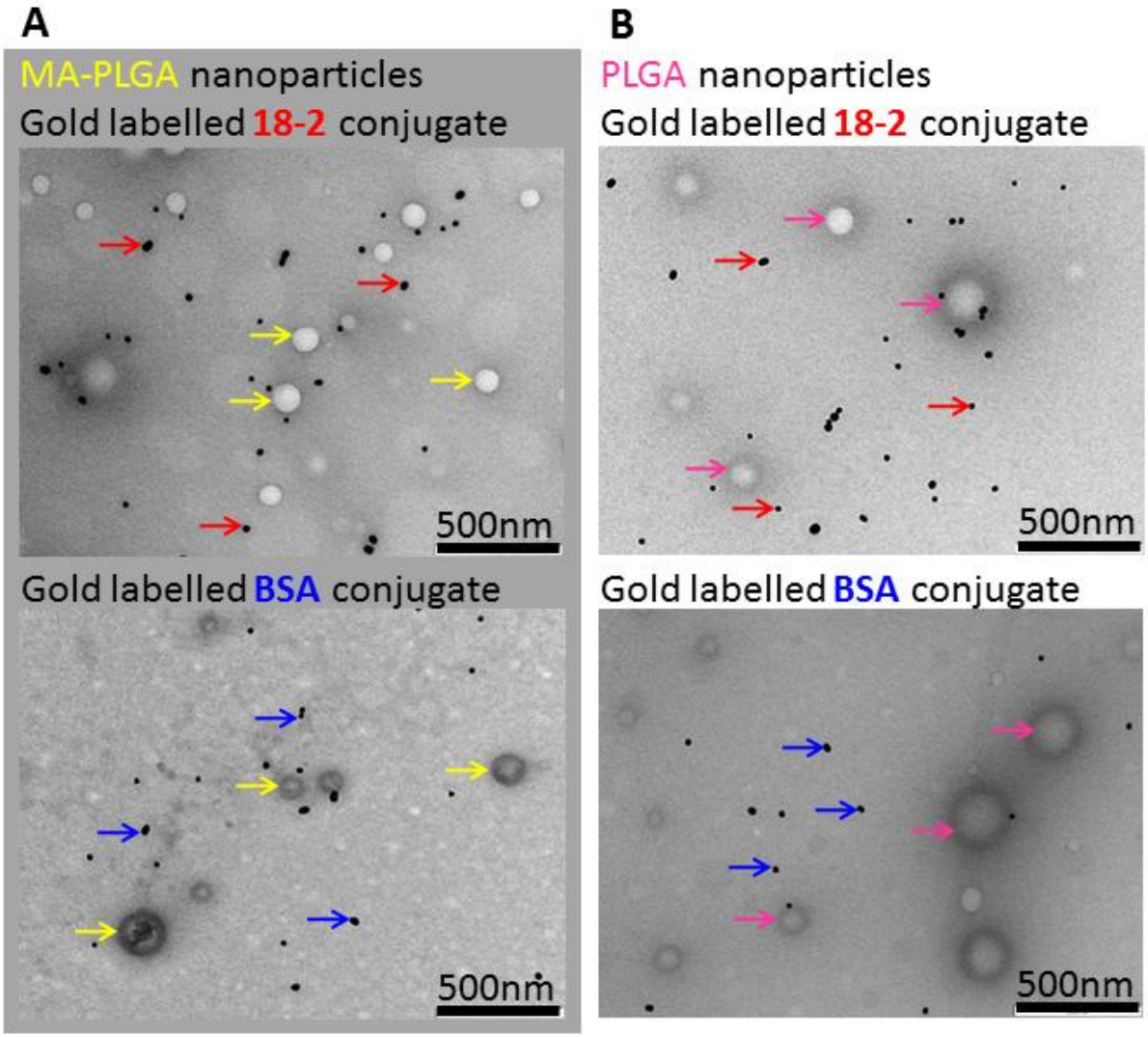

Figure 4.28: TEM images of gold labelled gallibody 18-2 (top) and BSA (bottom) conjugates incubated with MA-PLGA nanoparticles (A) and PLGA nanoparticles (B). Red arrows = 18-2 conjugate; yellow arrows = MA-PLGA nanoparticles; pink arrows = PLGA nanoparticles; blue arrows = BSA conjugate. A 3 µL volume of 1:1 mixed nanoparticle suspension and gold labelled conjugate was used to coat a carbon coated grid.

Due to the increase in contrast provided by the electron dense gold nanoparticles the PLGA nanoparticles appear lighter than when imaged by themselves in figure 4.26. There is no closer association of the gold labelled conjugates with the nanoparticles visible in figure 4.28. Clear interaction of two differing sizes of gold nanoparticles labelled with interacting antibody and antigen pairs was seen by Potůčková *et al.* and Singh *et al.* [162,163] as shown in figure 4.9 and 4.10 in section 4.1.4.1. This kind of observation of the antibody and antigen interaction was used to confirm the biological activity of the conjugated antibodies. The other gallibodies (12-1, 12-2, 16-1, 16-2 and 18-1) were also incubated and imaged as above with very similar images obtained (Appendix B). Thus from these data it appears that gold labelled gallibody is not able to bind MA-PLGA nanoparticles.

A system test was carried out using the same conjugate antibody/antigen system as was used in the ELISA system testing experiments (figure 4.20). For this test *E. coli* bacteria grown in liquid culture and re-suspended at a concentration 10^8 CFU/mL in phosphate buffer were imaged by themselves and incubated with gold labelled polyclonal anti-*E. coli* antibody conjugate. A 3 µL volume of the bacterial suspension; the conjugate at OD 10 or a 1:1 mixture of the two (incubated for one hour) was prepared as above before imaging. Figure 4.29 shows the conjugate as well as the bacteria imaged by themselves.

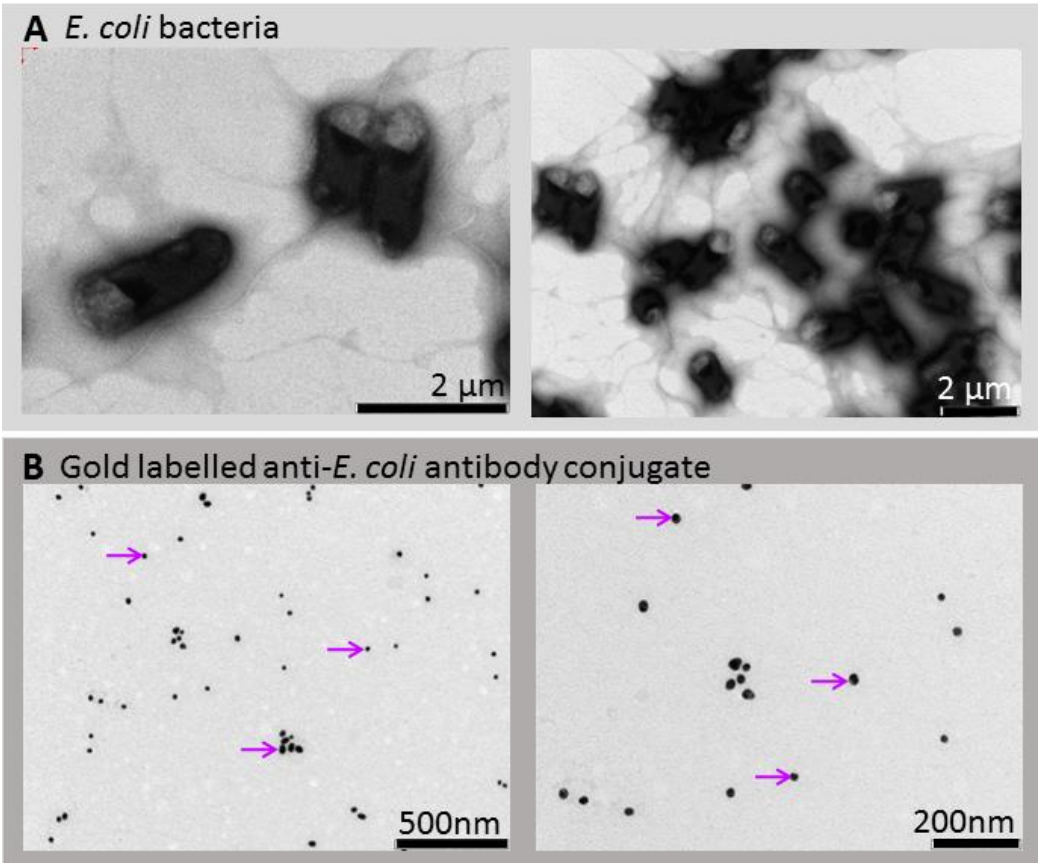

Figure 4.29: TEM images of *E. coli* bacteria (A) and gold labelled anti-*E.coli* antibody conjugate (B). (A) *E. coli* bacteria grown in liquid culture overnight and re-suspended in phosphate buffer at a concentration of 10^8 CFU/mL (B) Gold labelled polyclonal anti-*E. coli* antibody conjugate. Representative nanoparticles are labelled with purple arrows.

Bacteria of roughly the expected size (~2 µm long) and shape (roughly rod shaped) are seen in figure 4.29A with trailing flagella and an associated 'cloud' of media or some other matrix that appears darker than the background. The preservation of the structure of bacteria was not important for this experiment and so advanced sample preparation methods were not required. Gold labelled polyclonal anti-*E. coli* antibody conjugate appears as expected (figure 4.29B) with no notable aggregation visible.

The interaction of the bacterial suspension with gold labelled gallibody 18-2, BSA and anti-*E. coli* antibody conjugates are shown in figure 4.30.

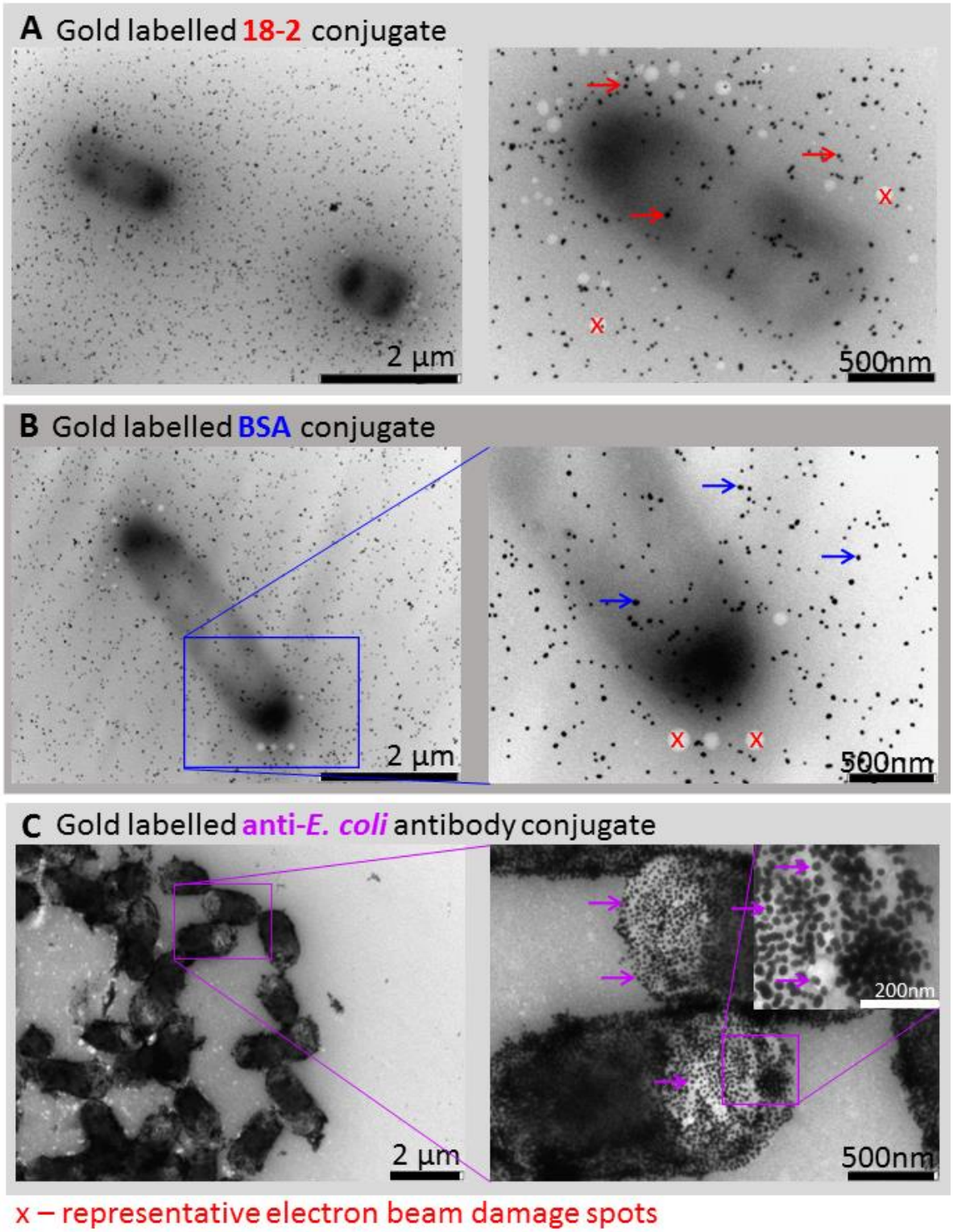

Figure 4.30: TEM images of *E. coli* bacteria incubated with gold labelled gallibody 18-2 conjugate (A); gold labelled BSA conjugate (B) and gold labelled anti-*E. coli* antibody conjugate (C). A 10^8 CFU/mL concentration of *E.coli* bacterial suspension incubated in a 1:1 ratio for one hour with gold labelled 18-2 conjugate (A, red arrows); BSA conjugate (B, blue arrows) and anti-*E. coli* antibody conjugate (C, purple arrows). White circles in A and B are caused by beam damage formed during imaging. Note the clear background in C (no black particles visible) and the clear association of gold nanoparticles on the surface of the bacteria, inset of higher magnification shows individual gold nanoparticles with specific conjugate interaction observed.

Clear interaction of the gold labelled anti-*E. coli* conjugate with the *E. coli* bacteria is visible in figure 4.30C. No non-specific binding of *E. coli* bacteria with gallibody 18-2 (figure 4.30A) or BSA (figure 4.30B) conjugates is observed. These images (figure 4.30C) resemble those obtained by Huang *et al.* [180] when visualising *Listeria monocytogenes* using a gold labelled monoclonal anti-*L. monocytogenes* antibody conjugate prepared and analysed by similar methods [180].

The positive results of the system test using the same incubation and TEM grid preparation strategy as for the PLGA nanoparticle experiments indicates that the lack of interaction seen with the MA nanoparticles with the gold labelled gallibody 18-2 conjugate, figure 4.28A top, is a relevant result. The lack of MA binding ability by gold labelled gallibody conjugate was also observed by ELISA (figure 4.22).

Taken together these results indicate a loss of MA binding functionality of the gallibodies when bound to gold nanoparticles using passive conjugation chemistry.

4.4 Conclusion

This chapter introduced antibodies, gold nanoparticles and the chemistry of the passive conjugation of proteins to gold nanoparticles and subsequent characterisation techniques. This was applied to the gold labelled gallibody conjugates under development for the proposed MALIA diagnostic.

The binding of the gold labelled gallibody by immobilised anti-chicken IgG (Fc) antibody was evaluated by titrating the coating concentration of the coated antibody (figure 4.12), comparing it to a BSA-only conjugate (4.13) and comparing the signals obtained when using all six gallibodies (4.14). From these results it is possible that the lack of MA signal on LFT (seen in chapter 3) is due to the orientation of the gallibody when conjugated to the gold nanoparticles.

The conjugation conditions (gallibody concentration – figure 4.18 and pH – figure 4.19) were investigated by using Vis spectroscopy. The effect of different concentrations of gallibody used in the conjugate preparation on the anti-chicken IgG (Fc) control signal was probed (figure 4.18). The stronger signal intensity for the higher concentration of gallibody supports the notion that the gallibody orientation plays a role in the efficacy of the conjugate. Complete coating of the gold nanoparticles is possible at a lower concentration indicated by the stability of the conjugate. At a higher concentration, more gallibody is coated on the gold nanoparticle, likely in a more upright conformation that is more easily recognisable by the coated anti-chicken IgG (Fc) antibody. The change in pH did not appear to greatly affect signal intensity at the optimal concentration level (figure 4.19C). However, a pH of 6 was seen to allow stable conjugation at the lowest concentrations of gallibody (figure 4.19A and B).

To further evaluate the labelled gallibody the ability of the gold labelled gallibody to bind MA was tested in ELISA (figure 4.22), DLS (figure 4.25) and TEM (figure 4.28). In ELISA the ability of gold labelled gallibody to bind MA was lost when compared to unlabelled gallibody (figure 4.22). However, gold labelled gallibody was still bound by coated anti-chicken IgG (Fc) antibody (figure 4.21) as was consistently seen on the LFT. In DLS some low affinity binding of the gold labelled gallibody with MA-PLGA nanoparticles was observed (figure 4.25), albeit in the same magnitude of BSA for binding MA – BSA is known to bind fatty acids [179]. No MA-PLGA nanoparticle interaction with gold labelled gallibody was seen in TEM (figure 4.28). Taken together these results indicate a loss of MA binding functionality of the gallibodies when bound to gold nanoparticles using passive conjugation chemistry.

From these results it appears that the gold-label visualisation system used in the proposed LFT (gold labelling of the gallibodies) does not allow visualisation of the binding of the MA by the gallibodies. MA binding activity is lost or greatly reduced upon labelling of the gallibodies with gold nanoparticles and if any activity remains, it is of too low affinity to withstand the capillary flow force.

Chapter 5: Concluding Discussion

"The foundation of [Tuberculosis, TB] infection control is early and rapid diagnosis, and proper management of TB patients"- this quote from the World Health Organisation's (WHO) policy on TB infection control indicates the potentially enormous impact that a rapid point-of-care (POC) diagnostic could have on the epidemic [12]. This policy document emphasizes the importance of reducing diagnostic delays and commencing treatment for positively identified patients as quickly as possible to limit transmission. This focus underlines the importance of effective diagnostics to control TB transmission. However, as previously outlined herein there are significant challenges and gaps associated with currently available diagnostics.

The aim of this MSc was to determine specifications required to manufacture a point of care, competitive lateral flow immunoassay that uses readily available, but highly specialised reagents. These specialised reagents relate to the choice of biomarker to be detected by the proposed diagnostic – anti-mycolic acid (MA) antibodies in TB patient sera. MA is a unique lipid antigen of mycobacteria and antibodies specific for this antigen are produced by a T- cell independent pathway and so their presence is unaffected by HIV infection [88]. Furthermore, work by Ndlandla [58] using a guinea pig TB infection model indicated that anti-MA antibodies are produced early upon infection and are short lived (so previous infection or exposure will not be detected). These features render anti-MA antibodies uniquely useful as a biomarker in the diagnosis of active TB as HIV and latent (asymptomatic) infections are major problems facing the resolution of the epidemic.

The work of Thanyani and colleagues [97] suggests that the detection of biomarker anti-MA antibodies for diagnosis of TB is valid. They developed the MARTI (mycolic acid antibodies real time inhibition) assay that successfully diagnosed TB serologically. Jones *et al.* [69] also showed that MA based serodiagnosis is valid using an ELISA based protocol and a synthetically produced MA-trehalose mixture.

For the proposed diagnostic, MA isolated from self-cultured *M. tuberculosis* according to conditions established by Ndlandla *et al.* [82] and purified according to the protocol of Goodrum *et al.* [98] was used. Beukes *et al.* [81] selected and expressed MA binding monoclonal scFvs (antigen binding antibody fragments) from a chicken antibody gene library. More stable scFvs were selected and expressed by Ndlandla [58] and were converted to IgY-like chicken antibodies (gallibodies) by Ranchod [59]. The gallibodies were expressed in a human cell line and purified from the culture media by a nickel column chromatography protocol for use in the proposed diagnostic. The MA binding ability of these reagents was demonstrated in ELISA using MA coated on microtiter plates by Ranchod *et al.* [91].

In the current study, the MA binding ability of the developed gallibodies was demonstrated again in chapter 2 using alternative casein blocker sources. Bacterial culture media supplement, casein hydrolysate, was shown to successfully replace biochemical reagent casein in the ELISA. This replacement is required due to import restrictions on bovine milk products into South Africa.

Lateral flow immunoassays/tests (LFTs) generally rely on the same antibody/antigen interaction as ELISAs. The visualisation of the binding that is achieved via an enzyme label (and substrate conversion) in ELISA is usually achieved by a colour label in LFT. The format for the diagnostic that was investigated for this MSc exploited the competitive lateral flow test strategy. This format was named MALIA, for mycolate antibodies lateral flow immunoassay.

In MALIA, MA antigen will be used on the test line and anti-chicken IgG (Fc) antibody on the control line. The custom developed gallibodies will be the labelled probe binding both the test and control line in the absence of competing anti-MA antibodies in the patient sera and only the control line in the presence of TB positive patient sera to produce a colour signal. This format is represented in figure 1.4. Many variables are relevant in the development of a lateral flow test even given the simplest of parameters. This project was focussed on making a practical contribution to the development of MALIA by investigating and evaluating methods to apply the novel gallibodies as the labelled recognition element and the unusual use of a lipid (MA) as the test line capture agent.

In chapter 3 the deposition of the MA antigen (lipid) test line and antibody (anti-chicken IgG (Fc) antibody) control line on various substrates and the adaptation of the conditions of the test was explored. The control interaction of spotted anti-chicken IgG (Fc) antibodies with the gold labelled gallibodies was consistently observed, but no MA/gallibody binding was visualised. The successful immobilisation of the MA on the LFT (tested after running of the test) was confirmed by phosphomolybdic acid staining. The immobilisation of the MA on the nitrocellulose was achieved by spotting of the MA dissolved in freshly distilled hexane- the same solvent as used to coat the plate for ELISA. While this technique is simple, hexane is not compatible with the bio-printing machinery commonly in use [181], which will prove a hurdle in larger scale manufacturing. The MA was shown to be antigenic when spotted in this way on nitrocellulose in an immunoblot test with a similar protocol to that of the ELISA (chapter 2). Various substrates, blockers and buffers were tested without resulting in an anti-MA signal on the LFT. These exploratory results support, but do not replace optimisation of the final test, as the conditions in which the required ‘negative’ (i.e. a TB negative sample) test signal is obtained (labelled gallibodies bound by coated MA) still remain to be determined.

For the labelling of the anti-MA gallibodies 40 nm gold nanoparticles were chosen. This labelling system is commonly used with excellent results [103] and was previously successfully used in the group for detection of *E. coli* in water sources [129]. Colloidal gold solutions have excellent optical properties driving their selection as labels for LFTs. The labelling of the recombinant monoclonal chicken anti-MA gallibodies with gold nanoparticles without compromising biological activity of MA binding ability was evaluated and described in chapter 4.

Initial characterisation was done by probing the gold labelled gallibody conjugate with coated control anti-chicken IgG (Fc) antibody on the LFT and using Visible light range spectroscopy of conjugates prepared under various conditions. The results from these tests suggested that the orientation of the gallibody on the gold nanoparticle influences the binding of the conjugate by the anti-chicken IgG (Fc) antibody and thus the signal intensity. The anti-chicken antibody used is an anti-Fc antibody that binds the conserved region of the antibody, the trunk of the Y shape. The scFv antigen binding (Fab) region may then be unavailable due to close association with the gold nanoparticle or some other disruption. Thus, a gold labelled gallibody conjugate that is successfully bound by the anti-chicken IgG (Fc) antibody does not give information about whether binding of MA is still possible and/or likely.

The passive conjugation of proteins to colloidal gold nanoparticles is usually sufficient for direct application to LFT. The ability of the gold labelled gallibody conjugate to bind MA coated on a polystyrene plate (in ELISA) or in PLGA nanoparticles (on TEM and DLS) was investigated to determine whether the biological activity of the gallibodies was not compromised by conjugation. System tests using gold labelled anti-*E. coli* antibody conjugate and *E. coli* in ELISA and visualisation on TEM showed clear *E. coli* binding ability of the gold conjugated anti-*E. coli* antibodies. ELISA experiments did not show conserved MA binding ability by the conjugated versus unconjugated gallibodies, despite the finding that anti-chicken IgG (Fc) antibody binding by gold labelled gallibody conjugate was observed in ELISA as well as on LFT. These results suggest that the primary biological activity of the gallibody is lost upon conjugation to the gold nanoparticles. This loss of biological activity may be because the MA/gallibody binding (a lipid/protein interaction) has a low affinity, unlike the interaction of the anti-chicken IgG (Fc) antibody with a gallibody or that of *E. coli* with anti-*E. coli* antibodies (protein/protein interactions). In ELISA this relatively low affinity of interaction may be overcome by the wash steps in the protocol when the heavy laden gold labelled gallibodies are subjected to repeated wash steps. Without the gold nanoparticle labelling, the gallibody-MA interaction remained strong enough.

The TEM protocol to observe the interaction of the MA nanoparticles with the gold labelled gallibodies did not include any wash steps, but a similar loss in activity was observed. The MA nanoparticle/gold labelled gallibody conjugate interaction was further studied using DLS. DLS relies on light scattering and Brownian motion to determine the size of particles. The DLS data suggested a slight binding, with an energy of association similarly small to that of BSA to fatty acid. These observations were drawn from analysis of the number, corresponding particle size and distinctness of the peaks in the intensity size distribution of gold conjugate/MA nanoparticle mixtures. This conclusion is weakened by the non-specific interaction between the empty PLGA nanoparticles and the gold labelled gallibody conjugate. Nevertheless, the DLS approach served as a novel way to find indications of a much weakened biological MA binding ability of the gallibodies with their target antigen after conjugation to gold.

MALIA attempts the detection of low affinity anti-MA antibodies in TB patient serum in a simpler and faster way than was achieved with the evanescent field biosensor based diagnostic demonstrated by Thanyani *et al.* [97]. Evanescent field biosensors are recommended to characterise low affinity antibody-antigen interactions [96,143]. The competitive format of MALIA was developed to address the low affinity of the targeted antibodies and their tendency to cross-react with cholesterol [83]. It now appears that the affinity of the anti-MA gallibodies is crucially affected by commonly applied gold-labelling procedures. Antibodies are known to have a conserved Y shaped structure with two binding sites (i.e. a valency of two). Increased valency can increase the functional affinity of antibodies. This format may still be feasible if the gallibodies are re-engineered to increase their functional affinity by increasing the valency of the gallibodies. These re-engineered gallibodies may then conserve more biological activity when labelled. It is important to note that MALIA relies on the binding of the labelled monoclonal antibodies to the immobilised MA being outcompeted by the serum anti-MA antibodies that have a known low affinity, but not by the ubiquitously present anti-cholesterol antibodies. As such an increased functional affinity of the gallibodies may impact both the binding activity to MA, as well as its intended displacement by serum antibodies in ways that cannot be predicted at this stage.

The results reported herein suggest that the biological activity of the gallibodies is adversely affected by labelling with gold nanoparticles. Many more possibilities exist for labelling of the gallibodies that have not been attempted. These involve the use of linkers such as biotin/streptavidin, covalent attachment chemistries and alternative labels such as cellulose nanobeads and quantum dots. Given the sensitivity of the gallibodies to the comparatively gentle passive labelling system tested herein, it seems unlikely that strategies like these which require the application of functionalisation chemicals as well as centrifugation or sonication steps will be successful. However, workable alternatives may still be possible.

A further interesting idea to pursue is to invert the test by labelling the antigen and immobilising the gallibodies on the test line. Sotnikov *et al.* [182] suggested that this inverted format may improve sensitivity compared to the more traditional scheme (labelled antibody, immobilised antigen) and allow better detection of low affinity antibodies to TB in patient serum. MA liposomes [95,97] and MA nanoparticles [172] that have been similarly used in several projects in the group could feasibly be adapted for use in a LFT. In this scheme the anti-MA gallibodies would be immobilised on the test line and coloured MA nanoparticles or dye-filled liposomes (with a biotin or some other label) could be used as the recognition element. In the case of a negative test the MA nanoparticles or liposomes would be bound by the gallibodies on the test line and a streptavidin control line. In the presence of anti-MA antibodies in patient sera (a positive test) the patient antibodies would saturate the MA on the nanoparticles or liposomes and prevent their binding to the immobilised anti-MA gallibodies. This format bears a close resemblance to the MARTI test, while applying the specificity of the gallibodies to provide a potentially more robust and deliverable test.

The potential impact of a POC test such as MALIA on the millions of people affected by and exposed to the TB epidemic cannot be overstated. A rapid diagnostic would reduce the time to treatment commencement improving patient prognosis and aid in prevention of transmission, reducing the burden of disease. It would also allow regular screening of high risk populations such as healthcare and mine workers further minimising the spread of TB. This kind of potential impact means that work towards such a test cannot be abandoned in the face of unexpected challenges discovered in the course of this research. This work has made a critical contribution in the assessment of the feasibility and pitfalls in the development of a non-standard LFT applying a lipid antigen and specially developed recombinant antibodies namely the MALIA POC diagnostic test for TB. These results have led to several feasible avenues of investigation, herein outlined, to pursue to actualise this critically important technology.

6. References

(1) Hershkovitz, I.; Donoghue, H. D.; Minnikin, D. E.; May, H.; Lee, O. Y.-C.; Feldman, M.; Galili, E.; Spigelman, M.; Rothschild, B. M.; Bar-Gal, G. K. Tuberculosis origin: the neolithic scenario. *Tuberculosis* **2015**, *95*, S122–S126. https://doi.org/10.1016/j.tube.2015.02.021.

(2) World Health Organisation. Global tuberculosis report 2018. Geneva: World Health Organisation September 18, 2018.

(3) Drain, P. K.; Bajema, K. L.; Dowdy, D.; Dheda, K.; Naidoo, K.; Schumacher, S. G.; Ma, S.; Meermeier, E.; Lewinsohn, D. M.; Sherman, D. R. Incipient and subclinical tuberculosis: a clinical review of early stages and progression of infection. *Clin. Microbiol. Rev.* **2018**, *31* (4), e00021-18. https://doi.org/10.1128/CMR.00021-18.

(4) Delogu, G.; Sali, M.; Fadda, G. The biology of Mycobacterium tuberculosis infection. *Mediterr. J. Hematol. Infect. Dis.* **2013**, *5* (1), e2013070. https://doi.org/doi:10.4084/MJHID.2013.070.

(5) South African National Department of Health, TB DOTS Strategy Coordination. National tuberculosis management guidelines 2014. South African National Department of Health 2014.

(6) South African National Department of Health. Management of drug-resistant tuberculosis policy guidelines. South African National Department of Health August 2011.

(7) Houben, R. M. G. J.; Dodd, P. J. The global burden of latent tuberculosis infection: a re-estimation using mathematical modelling. *PLOS Med.* **2016**, *13* (10), e1002152. https://doi.org/10.1371/journal.pmed.1002152.

(8) Weiner, J.; Maertzdorf, J.; Sutherland, J. S.; Duffy, F. J.; Thompson, E.; Suliman, S.; McEwen, G.; Thiel, B.; Parida, S. K.; Zyla, J.; Hanekom, W.A.; Mohney, R.P.; Boom, W.H.; Mayanja-Kizza, H.; Howe, R.; Dockrell H.M.; Ottenhoff, T.H.M.; Scriba, T.J.; Zak, D.E.; Walzl, G.; Kaufmann, S.H.E. Metabolite changes in blood predict the onset of tuberculosis. *Nature Commun.* **2018**, *9* (1), 5208. https://doi.org/10.1038/s41467-018-07635-7.

(9) World Health Organisation. Use of tuberculosis interferon-gamma release assays (IGRAs) in low-and middle-income countries: policy statement. Geneva: World Health Organisation 2011.

(10) World Health Organisation. WHO | Tuberculosis vaccine development http://www.who.int/immunization/research/development/tuberculosis/en/ (accessed Jan 18, 2019).

(11) World Health Organisation. Latent tuberculosis infection updated and consolidated guidelines for programmatic management. Geneva: World Health Organization 2018.

(12) World Health Organisation. WHO Policy on TB infection control in healthcare facilities, congregate settings and households. Geneva: World Health Organisation 2009.

(13) Casey, H.; Smith, A.; Parker, L.; Dipper, M.; Gould, T. Pulmonary tuberculosis in a South African regional emergency centre: can infection control be improved to lower the risk of nosocomial transmission? *S. Afr. Med. J.* **2015**, *105* (10), 862–865. https://doi.org/10.7196/SAMJnew.8329.

(14) Farley, J. E.; Tudor, C.; Mphahlele, M.; Franz, K.; Perrin, N. A.; Dorman, S.; Van der Walt, M. A National infection control evaluation of drug-resistant tuberculosis hospitals in South Africa. *Int. J. Tuberc. Lung Dis.* **2012**, *16* (1). https://doi.org/10.5588/ijtld.10.0791.

(15) Claassens, M. M.; van Schalkwyk, C.; du Toit, E.; Roest, E.; Lombard, C. J.; Enarson, D. A.; Beyers, N.; Borgdorff, M. W. Tuberculosis in healthcare workers and infection control measures at primary healthcare facilities in South Africa. *PloS One* **2013**, *8* (10), e76272. https://doi.org/10.1371/journal.pone.0076272.

(16) World Health Organisation. Implementing tuberculosis diagnostics: policy framework. Geneva: World Health Organisation 2015.

(17) Stinson, K. W.; Eisenach, K.; Kayes, S.; Matsumoto, M.; Siddiqi, S.; Nakashima, S.; Hashizume, H.; Timm, J.; Morrisey, A.; Mendoza, M.; Mathai, P. *Mycobacteriology laboratory manual*, 1st ed.; Global Laboratory Initiative: Japan, 2014.

(18) Meyer, A. J.; Atuheire, C.; Worodria, W.; Kizito, S.; Katamba, A.; Sanyu, I.; Andama, A.; Ayakaka, I.; Cattamanchi, A.; Bwanga, F.; Huang, L.; Davis, J.L. Sputum quality and diagnostic performance of GeneXpert MTB/RIF among smear-negative adults

with presumed tuberculosis in Uganda. *PloS One* **2017**, *12* (7), e0180572. https://doi.org/10.1371/journal.pone.0180572.

(19) Siddiqi, S. H.; Rusch-Gerdes, S. *MGIT procedure manual for BACTEC MGIT 960 TB system*; Foundation for Innovative New Diagnostics, 2006.

(20) UNICEF/UNDP/World Bank/WHO; Special Programme for Research &Training in Tropical Diseases. Laboratory-based evaluation of 19 commercially available rapid diagnostic tests for tuberculosis. Geneva: World Health Organisation 2008.

(21) World Health Organisation. Global tuberculosis report 2016. Geneva: World Health Organisation 2016.

(22) Caulfield, A. J.; Wengenack, N. L. Diagnosis of active tuberculosis disease: from microscopy to molecular techniques. *J. Clin. Tuberc. Mycobact. Dis.* **2016**, *4*. https://doi.org/10.1016/j.jctube.2016.05.005.

(23) Bisognin, F.; Lombardi, G.; Lombardo, D.; Re, M. C.; Monte, P. D. Improvement of Mycobacterium tuberculosis detection by Xpert MTB/RIF Ultra: a head-to-head comparison on Xpert-negative samples. *PloS One* **2018**, *13* (8), e0201934. https://doi.org/10.1371/journal.pone.0201934.

(24) Steingart, K. R.; Sohn, H.; Schiller, I.; Kloda, L. A.; Boehme, C. C.; Pai, M.; Dendukuri, N. Xpert MTB/RIF assay for pulmonary tuberculosis and rifampicin resistance in adults. *Cochrane Database Syst. Rev.* **2013**, *1* (1).

(25) FIND. Report for WHO – A multicentre non-inferiority diagnostic accuracy study of the Ultra assay compared to the Xpert MTB/RIF assay. Foundation for Innovative New Diagnostics February 2017.

(26) World Health Organisation. WHO meeting report of a technical expert consultation: non-inferiority analysis of Xpert MTB/RIF Ultra compared to Xpert MTB/RIF. Geneva: World Health Organisation January 20, 2017.

(27) Sabi, I.; Rachow, A.; Mapamba, D.; Clowes, P.; Ntinginya, N. E.; Sasamalo, M.; Kamwela, L.; Haraka, F.; Hoelscher, M.; Paris, D. H.; Saathoff, E.; Reither, K. Xpert MTB/RIF Ultra assay for the diagnosis of pulmonary tuberculosis in children: a multicentre comparative accuracy study. *J. Infect.* **2018**, *77* (4), 321–327. https://doi.org/10.1016/j.jinf.2018.07.002.

(28) Theron, G.; Venter, R.; Smith, L.; Esmail, A.; Randall, P.; Sood, V.; Oelfese, S.; Calligaro, G.; Warren, R.; Dheda, K. False-positive Xpert MTB/RIF results in retested patients with previous tuberculosis: frequency, profile, and prospective clinical outcomes. *J. Clin. Microbiol.* **2018**, *56* (3). https://doi.org/10.1128/JCM.01696-17.

(29) Acuña-Villaorduña, C.; Orikiriza, P.; Nyehangane, D.; White, L. F.; Mwanga-Amumpaire, J.; Kim, S.; Bonnet, M.; Fennelly, K. P.; Boum, Y.; Jones-López, E. C. Effect of previous treatment and sputum quality on diagnostic accuracy of Xpert ® MTB/RIF. *Int. J. Tuberc. Lung Dis.* **2017**, *21* (4), 389–397. https://doi.org/10.5588/ijtld.16.0785.

(30) Dorman, S. E.; Schumacher, S. G.; Alland, D.; Nabeta, P.; Armstrong, D. T.; King, B.; Hall, S. L.; Chakravorty, S.; Cirillo, D. M.; Tukvadze, N.; Bablishvili, N.; Stevens, W.; Scott, L.; Rodrigues, C.; Kazi, M.I.; Joloba, M.; Nakiyingi, L.; Nicol, M.P.; Ghebrekristos, Y.; Anyango, I.; Murithi, W.; Dietze, R.; Lyrio Peres, R.; Skrahina, A.; Auchynka, V.; Chopra, K.K.; Hanif, M.; Liu, X.; Yuan, X.; Boehme, C.C.; Ellner, J.J.; Denkinger, C.M.; on behalf of the study team. Xpert MTB/RIF Ultra for detection of Mycobacterium tuberculosis and rifampicin resistance: a prospective multicentre diagnostic accuracy study. *Lancet Infect. Dis.* **2018**, *18* (1), 76–84. https://doi.org/10.1016/S1473-3099(17)30691-6.

(31) Wallis, R. S.; Pai, M.; Menzies, D.; Doherty, T. M.; Walzl, G.; Perkins, M. D.; Zumla, A. biomarkers and diagnostics for tuberculosis: progress, needs, and translation into practice. *Lancet* **2010**, *375* (9729), 1920–1937.

(32) World Health Organisation. The use of lateral flow urine lipoarabinomannan assay (LF-LAM) for the diagnosis and screening of active tuberculosis in people living with HIV: policy guidance. Geneva: World Health Organisation 2015.

(33) Boyles, T. H.; Griesel, R.; Stewart, A.; Mendelson, M.; Maartens, G. Incremental yield and cost of urine determine TB-LAM and sputum induction in seriously ill adults with HIV. *Int. J. Infect. Dis.* **2018**, *75*, 67–73. https://doi.org/10.1016/j.ijid.2018.08.005.

(34) Harries, A. D.; Kumar, A. M. V. Challenges and progress with diagnosing pulmonary tuberculosis in low- and middle-income countries. *Diagnostics* **2018**, *8* (4), 78. https://doi.org/10.3390/diagnostics8040078.

(35) Creswell, J.; Qin, Z. Z.; Gurung, R.; Lamichhane, B.; Yadav, D. K.; Prasai, M. K.; Bista, N.; Adhikari, L. M.; Rai, B.; Sudrungrot, S. The performance and yield of tuberculosis testing algorithms using microscopy, chest x-ray, and Xpert MTB/RIF. *J. Clin. Tuberc. Mycobact. Dis.* **2019**, *14*, 1–6. https://doi.org/10.1016/j.jctube.2018.11.002.

(36) Whitworth, H. S.; Badhan, A.; Boakye, A. A.; Takwoingi, Y.; Rees-Roberts, M.; Partlett, C.; Lambie, H.; Innes, J.; Cooke, G.; Lipman, M.; Conlon, C.; Macallan, D.; Chua, F.; Post, F.; Wiselka, M.; Woltmann, G.; Deeks, J.J.; Kon, O.M.; Lalvani, A. Clinical utility of existing and second-generation interferon-γ release assays for diagnostic evaluation of tuberculosis: an observational cohort study. *Lancet Infect. Dis.* **2019**, *19* (2), 193–202. https://doi.org/10.1016/S1473-3099(18)30613-3.

(37) Division of Tuberculosis Elimination. CDC | TB | Latent tuberculosis infection – diagnosis of latent TB infection https://www.cdc.gov/tb/publications/ltbi/diagnosis.htm (accessed Sep 11, 2017).

(38) Clayden, P.; Chou, L.; Collins, S.; Harrington, M.; Jefferys, R.; Jimenez, E.; Morgan, S.; Swan, T.; Syed, J.; Wingfield, C. TAG 2010 pipeline report: HIV, tuberculosis, and viral hepatitis: drugs, diagnostics, vaccines, immune-based therapies, and preventive technologies in development. Treatment Action Group September 2010.

(39) National Health Laboratory Service. GeneXpert MTB/RIF progress report December 2014. http://www.nhls.ac.za/assets/files/GeneXpert%20Progress%20Report%20December%202014%20Final.pdf (accessed Jun 20, 2019).

(40) National Health Laboratory Service National Priority Programmes. GeneXpert MTB/RIF national report December 2018. http://www.nhls.ac.za/assets/files/GeneXpert%20Progress%20Report%20December%202014%20Final.pdf (accessed Jun 20, 2019).

(41) McCarthy, K.; Fielding, K.; Churchyard, G. J.; Grant, A. D. Empiric tuberculosis treatment in South African primary healthcare facilities – for whom, where, when and why: implications for the development of tuberculosis diagnostic tests. *PloS One* **2018**, *13* (1), e0191608. https://doi.org/10.1371/journal.pone.0191608.

(42) MacPherson, P.; Houben, R. M.; Glynn, J. R.; Corbett, E. L.; Kranzer, K. Pre-treatment loss to follow-up in tuberculosis patients in low- and lower-middle-income

countries and high-burden countries: a systematic review and meta-analysis. *Bull. World Health Organ.* **2014**, *92* (2), 126–138. https://doi.org/10.2471/BLT.13.124800.

(43) Mwansa-Kambafwile, J.; Maitshotlo, B.; Black, A. Microbiologically confirmed tuberculosis: factors associated with pre-treatment loss to follow-up, and time to treatment initiation. *PloS One* **2017**, *12* (1), e0168659. https://doi.org/10.1371/journal.pone.0168659.

(44) Podewils, L. J.; Bantubani, N.; Bristow, C.; Bronner, L. E.; Peters, A.; Pym, A.; Mametja, L. D. Completeness and reliability of the Republic of South Africa national tuberculosis (TB) surveillance system. *BMC Public Health* **2015**, *15*. https://doi.org/10.1186/s12889-015-2117-3.

(45) Claassens, M. M.; du Toit, E.; Dunbar, R.; Lombard, C.; Enarson, D. A.; Beyers, N.; Borgdorff, M. W. Tuberculosis patients in primary care do not start treatment. What role do health system delays play? *Int. J. Tuberc. Lung Dis.* **2013**, *17* (5), 603–607. https://doi.org/10.5588/ijtld.12.0505.

(46) Engel, N.; Davids, M.; Blankvoort, N.; Pai, N. P.; Dheda, K.; Pai, M. Compounding diagnostic delays: a qualitative study of point-of-care testing in South Africa. *Trop. Med. Int. Health* **2015**, *20* (4), 493–500. https://doi.org/10.1111/tmi.12450.

(47) Sullivan, B. J.; Esmaili, B. E.; Cunningham, C. K. Barriers to initiating tuberculosis treatment in Sub-Saharan Africa: a systematic review focused on children and youth. *Glob. Health Action* **2017**, *10* (1). https://doi.org/10.1080/16549716.2017.1290317.

(48) Mugauri, H.; Shewade, H. D.; Dlodlo, R. A.; Hove, S.; Sibanda, E. Bacteriologically confirmed pulmonary tuberculosis patients: loss to follow-up, death and delay before treatment initiation in Bulawayo, Zimbabwe from 2012–2016. *Int. J. Infect. Dis.* **2018**, *76*, 6–13. https://doi.org/10.1016/j.ijid.2018.07.012.

(49) Land, K. J.; Smith, S.; Peeling, R. W. Unmet diagnostics needs for the developing world. In *Paper-based diagnostics current status and future applications*; Springer Nature: Switzerland, 2018; pp 1–22.

(50) World Health Organisation. High priority target product profiles for new tuberculosis diagnostics: report of a consensus meeting, 28-29 April 2014, Geneva, Switzerland. Geneva: World Health Organisation April 29, 2014.

(51) Denkinger, C. M.; Kik, S. V.; Cirillo, D. M.; Casenghi, M.; Shinnick, T.; Weyer, K.; Gilpin, C.; Boehme, C. C.; Schito, M.; Kimerling, M.; Pai, M. Defining the needs for next generation assays for tuberculosis. *J. Infect. Dis.* **2015**, *211* (suppl_2), S29–S38.

(52) Land, K. J.; Boeras, D. I.; Chen, X.-S.; Ramsay, A. R.; Peeling, R. W. REASSURED diagnostics to inform disease control strategies, strengthen health systems and improve patient outcomes. *Nature Microbiol.* **2019**, *4* (1), 46–54. https://doi.org/10.1038/s41564-018-0295-3.

(53) Mabey, D.; Peeling, R. W.; Ustianowski, A.; Perkins, M. D. Tropical infectious diseases: diagnostics for the developing world. *Nature Rev. Microbiol.* **2004**, *2* (3), 231–240. https://doi.org/10.1038/nrmicro841.

(54) Gift, T. L.; Pate, M. S.; Hook, E. W.; Kassler, W. J. The rapid test paradox: when fewer cases detected lead to more cases treated: a decision analysis of tests for Chlamydia trachomatis. *Sex. Transm. Dis.* **1999**, *26* (4), 232–240.

(55) Branson, B. M. The future of HIV testing. *J. Acquir. Immune Defic. Syndr.* **2010**, *55*, S102-105. https://doi.org/10.1097/QAI.0b013e3181fbca44.

(56) Johnson, M. Cepheid to launch GeneXpert Edge for decentralized testing while Omni remains delayed https://webcache.googleusercontent.com/search?q=cache:5-M8b8sweAcJ:https://www.genomeweb.com/pcr/cepheid-launch-genexpert-edge-decentralized-testing-while-omni-remains-delayed+&cd=4&hl=en&ct=clnk&gl=za#.XEcQ_lUzapo (accessed Jan 22, 2019).

(57) finddx.org/dx-pipeline-status/. Dx pipeline status https://www.finddx.org/dx-pipeline-status/ (accessed Feb 1, 2019).

(58) Ndlandla, F. Diagnostic antibody biomarkers of tuberculosis characterized by natural and chemically synthetic mycolic acid antigens. PhD thesis, University of Pretoria, 2016.

(59) Ranchod, H. Novel recombinant anti-mycolic acid immunoglobulin tools for improved understanding and management of tuberculosis. PhD thesis, University of Pretoria, 2018.

(60) Goletti, D.; Lee, M.-R.; Wang, J.-Y.; Walter, N.; Tom H. M. Ottenhoff. Update on tuberculosis biomarkers: from correlates of risk, to correlates of active disease and of

cure from disease. *Respirology* **2018**, *23*, 455–466. https://doi.org/10.1111/resp.13272.

(61) Chegou, N. N.; Sutherland, J. S.; Malherbe, S.; Crampin, A. C.; Corstjens, P. L. A. M.; Geluk, A.; Mayanja-Kizza, H.; Loxton, A. G.; van der Spuy, G.; Stanley, K.; Kotzé, L.A.; van der Vyver, M.; Rosenkrands, I.; Kidd, M.; van Helden, P.D.; Dockrell, H.M.; Ottenhoff, T.H.M.; Kaufmann, S.H.E.; Walzl, G. Diagnostic performance of a seven-marker serum protein biosignature for the diagnosis of active TB disease in African primary healthcare clinic attendees with signs and symptoms suggestive of TB. *Thorax* **2016**, *71* (9), 785–794. https://doi.org/10.1136/thoraxjnl-2015-207999.

(62) Chegou, N. N.; Walzl, G.; Mihret, A. Method for diagnosing tuberculosis. WO2015/128830A1, September 3, 2015.

(63) Walzl, G. New, quick TB test developed in SA http://www.health24.com/Medical/Tuberculosis/Testing/new-quick-tb-test-developed-in-sa-20160512 (accessed Sep 12, 2017).

(64) Khaliq, A.; Ravindran, R.; Hussainy, S. F.; Krishnan, V. V.; Ambreen, A.; Yusuf, N. W.; Irum, S.; Rashid, A.; Jamil, M.; Zaffar, F.; Chaudhry, M.N.; Gupta, P.K.; Akhtar, M.W.; Khan, I.H. Field evaluation of a blood based test for active tuberculosis in endemic settings. *PLoS ONE* **2017**, *12* (4), e0173359. https://doi.org/10.1371/journal.pone.0173359.

(65) Tiwari, D.; Tiwari, R.; Chandra, R.; Bisen, P.; Haque, S. Efficient ELISA for diagnosis of active tuberculosis employing a cocktail of secretory proteins of Mycobacterium tuberculosis. *Folia Biol. (Praha)* **2014**, *60* (1), 10.

(66) AHC Media. A blood test for TB? Well, maybe this time https://www.ahcmedia.com/articles/65900-a-blood-test-for-tb-well-maybe-this-time (accessed Sep 11, 2017).

(67) Standard Diagnostics Inc. SD BIOLINE TB Ag MPT64 rapid ordering information http://www.standardia.com/en/home/product/Rapid_Diagnostic_Test/TB_Ag_MPT64.html (accessed Sep 12, 2017).

(68) Lyashchenko, K. P.; Greenwald, R.; Esfandiari, J.; Greenwald, D.; Nacy, C. A.; Gibson, S.; Didier, P. J.; Washington, M.; Szczerba, P.; Motzel, S.; Handt, L.; Pollock, J.M.; McNair, J.; Andersen, P.; Langermans, J.A.M.; Verreck, F.; Ervin, S.; Ervin, F.; McCombs, C. PrimaTB STAT-PAK Assay, a novel, rapid lateral flow test for

tuberculosis in nonhuman primates. *Clin. Vaccine Immunol.* **2007**, *14* (9), 1158–1164. https://doi.org/10.1128/CVI.00230-07.

(69) Jones, A.; Pitts, M.; Al Dulayymi, J. R.; Gibbons, J.; Ramsay, A.; Goletti, D.; Gwenin, C. D.; Baird, M. S. New synthetic lipid antigens for rapid serological diagnosis of tuberculosis. *PloS One* **2017**, *12* (8), e0181414.

(70) Baird, M. S.; Gwenin, C. D.; Jones, A. Method and kit for detection of Mycobacteria. WO 2016/024118 A1, February 18, 2016.

(71) Barry III, C. E.; Lee, R. E.; Mdluli, K.; Sampson, A. E.; Schroeder, B. G.; Slayden, R. A.; Yuan, Y. Mycolic acids: structure, biosynthesis and physiological functions. *Prog. Lipid Res.* **1998**, *37* (2–3), 143–179. https://doi.org/10.1016/S0163-7827(98)00008-3.

(72) Brennan, P. J. Structure, function, and biogenesis of the cell wall of Mycobacterium tuberculosis. *Tuberculosis* **2003**, *83* (1), 91–97. https://doi.org/10.1016/S1472-9792(02)00089-6.

(73) Minnikin, D. E. Lipids: complex lipids, their chemistry, biosynthesis and roles. In *The biology of the Mycobacteria*; Academic Press Inc.: London, UK, 1982; Vol. 1, pp 95 – 185.

(74) Beckman, E. M.; Porcelli, S. A.; Morita, C. T.; Behar, S. M.; Furlong, S. T.; Brenner, M. B. Recognition of a lipid antigen by CD1-restricted (alpha)(beta)(positive) T-cells. *Nature* **1994**, *372* (6507), 691–694.

(75) Pan, J.; Fujiwara, N.; Oka, S.; Maekura, R.; Ogura, T.; Yano, I. Anti-cord factor (trehalose 6,6′-dimycolate) IgG antibody in tuberculosis patients recognizes mycolic acid subclasses. *Microbiol. Immunol.* **1999**, *43* (9), 863–869. https://doi.org/10.1111/j.1348-0421.1999.tb01221.x.

(76) Izhaky, D.; Addadi, L. Stereoselective interactions of a specialized antibody with cholesterol and epi-cholesterol monolayers. *Chem. – Eur. J.* **2000**, *6* (5), 869–874. https://doi.org/10.1002/(SICI)1521-3765(20000303)6:5<869::AID-CHEM869>3.0.CO;2-L.

(77) Al Dulayymi, J. R.; Baird, M. S.; Roberts, E.; Deysel, M.; Verschoor, J. The first syntheses of single enantiomers of the major methoxy-mycolic acid of Mycobacterium tuberculosis. *Tetrahedron* **2007**, *63* (12), 2571–2592. https://doi.org/10.1016/j.tet.2007.01.007.

(78) Al Dulayymi, J. R.; Baird, M. S.; Roberts, E. The synthesis of a single enantiomer of a major α-mycolic acid of M. tuberculosis. *Tetrahedron* **2005**, *61* (50), 11939–11951. https://doi.org/10.1016/j.tet.2005.09.056.

(79) Koza, G.; Theunissen, C.; Al Dulayymi, J. R.; Baird, M. S. The synthesis of single enantiomers of Mycobacterial keto-mycolic acids containing cis-cyclopropanes. *Tetrahedron* **2009**, *65* (49), 10214–10229. https://doi.org/10.1016/j.tet.2009.09.099.

(80) Smet, M.; Pollard, C.; De Beuckelaer, A.; Van Hoecke, L.; Vander Beken, S.; De Koker, S.; Al Dulayymi, J. R.; Huygen, K.; Verschoor, J.; Baird, M. S.; Grooten, J. Mycobacterium tuberculosis-associated synthetic mycolates differentially exert immune stimulatory adjuvant activity. *Eur. J. Immunol.* **2016**, *46* (9), 2149–2154. https://doi.org/10.1002/eji.201646357.

(81) Beukes, M.; Lemmer, Y.; Deysel, M.; Al Dulayymi, J. R.; Baird, M. S.; Koza, G.; Iglesias, M. M.; Rowles, R. R.; Theunissen, C.; Grooten, J.; Toschi, G.; Roberts, V.V.; Pilcher, L.A.; Van Wyngaardt, S.; Mathebula, N.S.; Balogun, M.O.; Stoltz, A.C.; Verschoor, J.A. Structure-function relationships of the antigenicity of mycolic acids in tuberculosis patients. *Chem. Phys. Lipids* **2010**, *163* (8), 800–808.

(82) Ndlandla, F.; Ejoh, V.; Stoltz, A.; Naicker, B.; Cromarty, A.; van Wyngaardt, S.; Khati, M.; Rotherham, L.; Lemmer, Y.; Niebuhr, J.; Baumeister, C.; Al Dulayymi, J.R.; Swai, H.; Baird, M.S.; Verschoor, J.A. Standardization of natural mycolic acid antigen composition and production for use in biomarker antibody detection to diagnose active tuberculosis. *J. Immunol. Methods* **2016**, *435*, 50–59.

(83) Benadie, Y.; Deysel, M.; Siko, D. G. R.; Roberts, V. V.; Van Wyngaardt, S.; Thanyani, S. T.; Sekanka, G.; Ten Bokum, A. M.; Collett, L. A.; Grooten, J.; Baird, M.S.; Verschoor, J.A. Cholesteroid nature of free mycolic acids from M. tuberculosis. *Chem. Phys. Lipids* **2008**, *152* (2), 95–103.

(84) Bíró, A.; Cervenak, L.; Balogh, A.; Lőrincz, A.; Uray, K.; Horváth, A.; Romics, L.; Matkó, J.; Füst, G.; László, G. Novel anti-cholesterol monoclonal immunoglobulin G antibodies as probes and potential modulators of membrane raft-dependent immune functions. *J. Lipid Res.* **2007**, *48* (1), 19–29. https://doi.org/10.1194/jlr.M600158-JLR200.

(85) Horváth, A.; Füst, G.; Horváth, I.; Vallus, G.; Duba, J.; Harcos, P.; Prohászka, Z.; Rajnavölgyi, É.; Jánoskuti, L.; Kovács, M.; Császár, A.; Romics, L.; Karádi, I. Anti-

cholesterol antibodies (ACHA) in patients with different atherosclerotic vascular diseases and healthy individuals. Characterization of human ACHA. *Atherosclerosis* **2001**, *156* (1), 185–192. https://doi.org/10.1016/S0021-9150(00)00630-4.

(86) Chan, C. E.; Zhao, B. Z.; Cazenave-Gassiot, A.; Pang, S.-W.; Bendt, A. K.; Wenk, M. R.; MacAry, P. A.; Hanson, B. J. Novel phage display-derived mycolic acid-specific antibodies with potential for tuberculosis diagnosis. *J. Lipid Res.* **2013**, *54* (10), 2924–2932.

(87) Korf, J.; Stoltz, A.; Verschoor, J.; De Baetselier, P.; Grooten, J. The Mycobacterium tuberculosis cell wall component mycolic acid elicits pathogen-associated host innate immune responses. *Eur. J. Immunol.* **2005**, *35* (3), 890–900.

(88) Schleicher, G. K.; Feldman, C.; Vermaak, Y.; Verschoor, J. A. Prevalence of anti-mycolic acid antibodies in patients with pulmonary tuberculosis co-infected with HIV. *Clin. Chem. Lab. Med.* **2002**, *40* (9), 882–887.

(89) Greunke, K.; Spillner, E.; Braren, I.; Seismann, H.; Kainz, S.; Hahn, U.; Grunwald, T.; Bredehorst, R. Bivalent monoclonal IgY antibody formats by conversion of recombinant antibody fragments. *J. Biotechnol.* **2006**, *124*, 446–456.

(90) Wemmer, S.; Mashau, C.; Fehrsen, J.; van Wyngaardt, W.; du Plessis, D. H. Chicken scFvs and bivalent scFv-CH fusions directed against HSP65 of Mycobacterium bovis. *Biologicals* **2010**, *38* (3), 407–414. https://doi.org/10.1016/j.biologicals.2010.02.002.

(91) Ranchod, H.; Ndlandla, F.; Lemmer, Y.; Beukes, M.; Niebuhr, J.; Al Dulayymi, J. R.; Wemmer, S.; Fehrsen, J.; Baird, M. S.; Verschoor, J. A. The antigenicity and cholesteroid nature of mycolic acids determined by recombinant chicken antibodies. *PLoS ONE* **2018**, *13* (8), e0200298.

(92) Manz, R. A.; Hauser, A. E.; Hiepe, F.; Radbruch, A. Maintenance of serum antibody levels. *Annu. Rev. Immunol.* **2005**, *23*, 367–386.

(93) Goodridge, A.; Cueva, C.; Lahiff, M.; Muzanye, G.; Johnson, J. L.; Nahid, P.; Riley, L. W. Anti-phospholipid antibody levels as biomarker for monitoring tuberculosis treatment response. *Tuberculosis* **2012**, *92* (3), 243–247. https://doi.org/10.1016/j.tube.2012.02.004.

(94) Fujita, Y. Diverse humoral immune responses and changes in IgG antibody levels against Mycobacterial lipid antigens in active tuberculosis. *Microbiology* **2005**, *151* (6), 2065–2074. https://doi.org/10.1099/mic.0.27790-0.

(95) Lemmer, Y.; Thanyani, S. T.; Vrey, P. J.; Driver, C. H. S.; Venter, L.; Van Wyngaardt, S.; Ten Bokum, A. M. C.; Ozoemena, K. I.; Pilcher, L. A.; Fernig, D. G.; Stoltz, A.C.; Swai, H.; Verschoor, J.A. Chapter five – detection of anti-mycolic acid antibodies by liposomal biosensors. *Methods Enzymol.* **2009**, *464*, 79–104.

(96) Thanyani, S. T. An assessment of two evanescent field biosensors in the development of an immunoassay for tuberculosis. PhD thesis, University of Pretoria, 2009.

(97) Thanyani, S. T.; Roberts, V.; Siko, D. G. R.; Vrey, P.; Verschoor, J. A. A novel application of affinity biosensor technology to detect antibodies to mycolic acid in tuberculosis patients. *J. Immunol. Methods* **2008**, *332* (1), 61–72.

(98) Goodrum, M. A.; Siko, D. G.; Niehues, T.; Eichelbauer, D.; Verschoor, J. A. Mycolic acids from Mycobacterium tuberculosis: purification by counter current distribution and T-cell stimulation. *Microbios* **2001**, *106* (413), 55–67.

(99) Boster Biological Technology. Four types of ELISA assay https://www.bosterbio.com/newsletter-archive/20170728-which-elisa (accessed Sep 15, 2018).

(100) Oxoid.com. LP0041, Casein hydrolysate (acid) | Oxoid – product detail http://www.oxoid.com/UK/blue/prod_detail/prod_detail.asp?pr=LP0041&c=UK&lang=EN (accessed Feb 6, 2019).

(101) Waritani, T.; Chang, J.; McKinney, B.; Terato, K. An ELISA protocol to improve the accuracy and reliability of serological antibody assays. *MethodsX* **2017**, *4*, 153–165. https://doi.org/10.1016/j.mex.2017.03.002.

(102) Brown, M. C. Chapter 4 Antibodies: key to a robust lateral flow immunoassay. In *Lateral Flow Immunoassay*; Humana Press: New York, 2009; pp 59–74.

(103) Bahadır, E. B.; Sezgintürk, M. K. Lateral flow assays: principles, designs and labels. *Trends Anal. Chem.* **2016**, *82*, 286–306. https://doi.org/10.1016/j.trac.2016.06.006.

(104) Wu, G.; Zaman, M. H. Low-cost tools for diagnosing and monitoring HIV infection in low-resource settings. *Bull. World Health Organ.* **2012**, *90* (12), 914–920.

(105) World Health Organisation. HIV assays: laboratory performance and other operational characteristics: rapid diagnostic tests (combined detection of HIV-1/2 antibodies and discriminatory detection of HIV-1 and HIV-2 antibodies): report 18. Geneva: World Health Organization 2015.

(106) Alexander, T. S. Human immunodeficiency virus diagnostic testing: 30 years of evolution. *Clin. Vaccine Immunol.* **2016**, *23* (4), 249–253. https://doi.org/10.1128/CVI.00053-16.

(107) Branson, B. M. Point of care rapid tests for HIV antibodies. *Lab. Med.* **2003**, *27* (7–8), 288–295.

(108) Bulterys, M.; Jamieson, D. J.; O'Sullivan, M. J.; Cohen, M. H.; Maupin, R.; Nesheim, S.; Webber, M. P.; Dyke, R. V.; Wiener, J.; Branson, B. M.; Study group for the mother – infant rapid intervention at delivery (MIRIAD). Rapid HIV-1 testing during labor: a multi-center study. *J. Am. Med. Assoc.* **2004**, *292* (2), 219–223. https://doi.org/10.1001/jama.292.2.219.

(109) Steingart, K. R.; Henry, M.; Laal, S.; Hopewell, P. C.; Ramsay, A.; Menzies, D.; Cunningham, J.; Weldingh, K.; Pai, M. Commercial serological antibody detection tests for the diagnosis of pulmonary tuberculosis: a systematic review. *PLoS Med.* **2007**, *4* (6), e202.

(110) Grenier, J.; Pinto, L.; Steingart, K. R.; Dowdy, D. W.; Ramsay, A.; Pai, M. Widespread use of serological tests for tuberculosis: data from 22 high-burden countries. *Eur. Respir. J.* **2012**, *39* (2), 500–502. https://doi.org/10.1183/09031936.00070611.

(111) Jaroslawski, S.; Pai, M. Why are inaccurate tuberculosis serological tests widely used in the Indian private healthcare sector? A root-cause analysis. *J. Epidemiol. Glob. Health* **2012**, *2* (1), 39–50.

(112) World Health Organisation. Commercial serodiagnostic tests for diagnosis of tuberculosis: policy statement. Geneva: World Health Organisation 2011.

(113) Okuda, Y.; Maekura, R.; Hirotani, A.; Kitada, S.; Yoshimura, K.; Hiraga, T.; Yamamoto, Y.; Itou, M.; Ogura, T.; Ogihara, T. Rapid serodiagnosis of active

pulmonary Mycobacterium tuberculosis by analysis of results from multiple antigen-specific tests. *J. Clin. Microbiol.* **2004**, *42* (3), 1136–1141.

(114) Dheda, K.; Schwander, S. K.; Zhu, B.; Zyl-Smit, R. N. V.; Zhang, Y. The immunology of tuberculosis: from bench to bedside. *Respirology* **2010**, *15* (3), 433–450. https://doi.org/10.1111/j.1440-1843.2010.01739.x.

(115) Lyashchenko, K.; Esfandiari, J.; McCombs, C. Assay for detecting tuberculosis in nonhuman primates. US8128941B2, March 6, 2012.

(116) Kumar, S. Antibody characterisation for the development of an E. coli immunosensor: a model system for water quality monitoring. MSc Thesis, University of Pretoria, 2014.

(117) *Lateral flow immunoassay*, 1st ed.; Wong, R., Tse, H., Eds.; Humana Press, 2009.

(118) Hsieh, H.; Dantzler, J.; Bernhard Weigl. Analytical tools to improve optimization procedures for lateral flow assays. *Diagnostics* **2017**, *7* (2), 29. https://doi.org/10.3390/diagnostics7020029.

(119) Bangs Laboratories, Inc. Lateral flow tests TechNote 303. Bangs Laboratories, Inc. March 20, 2013.

(120) Jones, K. Fusion 5: a new platform for lateral flow immunoassay tests. In *Lateral flow immunoassay*; Humana Press: New York, 2009; pp 115–129.

(121) Credou, J. Simple, biocompatible and robust modification of cellulose membranes for the eco^2-friendly preparation of immunoassay devices. PhD thesis, Ecole Polytechnique, 2014.

(122) Zeng, Q.; Mao, X.; Xu, H.; Wang, S.; Liu, G. Quantitative immuno-chromatographic strip biosensor for the detection of carcinoembryonic antigen tumor biomarker in human plasma. *Am. J. Biomed. Sci.* **2009**, 70–79. https://doi.org/10.5099/aj090100070.

(123) Zhang, L.; Li, D.; Liu, L.; Fang, J.; Xu, R.; Zhang, G. Development of a colloidal gold immuno-chromatographic strip for the rapid detection of soft-shelled turtle systemic septicemia spherical virus. *J. Virol. Methods* **2015**, *221*, 39–45. https://doi.org/10.1016/j.jviromet.2015.04.016.

(124) Bührer-Sékula, S.; Smits, H. L.; Gussenhoven, G. C.; Van Leeuwen, J.; Amador, S.; Fujiwara, T.; Klatser, P. R.; Oskam, L. Simple and fast lateral flow test for classification of leprosy patients and identification of contacts with high risk of developing leprosy. *J. Clin. Microbiol.* **2003**, *41* (5), 1991–1995.

(125) Julián, E.; Matas, L.; Pérez, A.; Alcaide, J.; Lanéelle, M.-A.; Luquin, M. Serodiagnosis of tuberculosis: comparison of immunoglobulin A (IgA) response to sulfolipid I with IgG and IgM responses to 2,3-Diacyltrehalose, 2,3,6-Triacyltrehalose, and cord factor antigens. *J. Clin. Microbiol.* **2002**, *40* (10), 3782–3788. https://doi.org/10.1128/JCM.40.10.3782-3788.2002.

(126) Castro, A., R.; George, R., W.; Pope, V. Methods, immunoassays and devices for detection of anti-lipoidal antibodies. WO 2007/002178 A2, January 4, 2007.

(127) Wen, H.-W.; Borejsza-Wysocki, W.; DeCory, T. R.; Durst, R. A. Development of a competitive liposome-based lateral flow assay for the rapid detection of the allergenic peanut protein Ara H1. *Anal. Bioanal. Chem.* **2005**, *382* (5), 1217–1226.

(128) Hermanson, G. T. Preparation of colloidal gold-labelled proteins. In *Bioconjugate techniques*; Academic Press: London, UK, 2008; pp 924–935.

(129) Govindasamy, K. The development of a paper based microfluidic device for the selective and sensitive determination of E. coli in water sources. MSc Thesis, University of Johannesburg, Johannesburg, South Africa, 2014.

(130) Govindasamy, K.; Potgieter, S.; Land, K. J.; Kumar, S. Method and device for detection of whole organism bacteria. WO 2015/181790 Al, March 12, 2015.

(131) Zarzycki, P.; Bartoszuk, M.; Radziwon, A. Optimization of TLC detection by phosphomolybdic acid staining for robust quantification of cholesterol and bile acids. *J. Planar Chromatogr. – Mod. TLC* **2006**, *19* (107), 52–57. https://doi.org/10.1556/JPC.19.2006.1.9.

(132) Sher, M.; Zhuang, R.; Demirci, U.; Asghar, W. Paper-based analytical devices for clinical diagnosis: recent advances in the fabrication techniques and sensing mechanisms. *Expert Rev. Mol. Diagn.* **2017**, *17* (4), 351–366. https://doi.org/10.1080/14737159.2017.1285228.

(133) O'Farrell, B. Evolution in lateral flow-based immunoassay systems. In *Lateral flow immunoassay*; Humana Press: New York, 2009; pp 1–35.

(134) Mansfield, M. A. The use of nitrocellulose membranes in lateral flow assays. In *Drugs of abuse: body fluid testing*; Forensic Science and Medicine; Humana Press: Totowa, NJ, 2005; pp 71–85.

(135) Lee, J.-Y.; Kim, Y. A.; Kim, M. Y.; Lee, Y. T.; Hammock, B. D.; Lee, H.-S. Importance of membrane selection in the development of immuno-chromatographic assays for low-molecular weight compounds. *Anal. Chim. Acta* **2012**, *757*, 69–74. https://doi.org/10.1016/j.aca.2012.10.052.

(136) Beloglazova, N. V.; Sobolev, A. M.; Tessier, M. D.; Hens, Z.; Goryacheva, I. Yu.; De Saeger, S. Fluorescently labelled multiplex lateral flow immunoassay based on cadmium-free quantum dots. *Methods* **2017**, *116*, 141–148. https://doi.org/10.1016/j.ymeth.2017.01.004.

(137) Lutz, B.; Liang, T.; Fu, E.; Ramachandran, S.; Kauffman, P.; Yager, P. Dissolvable fluidic time delays for programming multi-step assays in instrument-free paper diagnostics. *Lab. Chip* **2013**, *13* (14), 2840. https://doi.org/10.1039/c3lc50178g.

(138) Preechakasedkit, P.; Pinwattana, K.; Dungchai, W.; Siangproh, W.; Chaicumpa, W.; Tongtawe, P.; Chailapakul, O. Development of a one-step immuno-chromatographic strip test using gold nanoparticles for the rapid detection of Salmonella typhi in human serum. *Biosens. Bioelectron.* **2012**, *31* (1), 562–566. https://doi.org/10.1016/j.bios.2011.10.031.

(139) Mansfield, M. A. Nitrocellulose membranes for lateral flow immunoassays: a technical treatise. In *Lateral flow immunoassay*; Humana Press: New York, 2009; pp 95–113.

(140) Janeway, C. A.; Travers, P.; Walport, M.; Shlomchik, M. J. *Immunobiology*, 5th ed.; Garland Science: New York, 2001.

(141) The School of Biomedical Sciences Wiki, Newcastle University. Antibody https://teaching.ncl.ac.uk/bms/wiki/index.php/Antibody (accessed Mar 20, 2019).

(142) Berzofsky, J. A.; Berkower, I. J. Chapter 7 Antigen–antibody interactions and monoclonal antibodies. In *Fundamental Immunology*; Lippincott Williams & Wilkins, a Wolters Kluwer business: Philadelphia, USA, 2013; p 32.

(143) Strandh, M. Insights into weak affinity antibody-antigen interactions: studies using affinity chromatography and optical biosensor. PhD thesis, University of Kalmar, Kalmar, Sweden, 2000.

(144) Schroeder Jr, H. W.; Wald, D.; Greenspan, N. S. Chapter 5 Immunoglobulins: structure and function. In *Fundamental immunology*; Lippincott Williams & Wilkins, a Wolters Kluwer business: Philadelphia, USA, 2013.

(145) Wong-Baeza, C.; Reséndiz-Mora, A.; Donis-Maturano, L.; Wong-Baeza, I.; Zárate-Neira, L.; Yam-Puc, J. C.; Calderón-Amador, J.; Medina, Y.; Wong, C.; Baeza, I.; Zárate-Neira, L.; Yam-Puc, J. C.; Calderón-Amador, J.; Medina, Y.; Wong, C.; Baeza, I.; Flores-Romo, L. Anti-lipid IgG antibodies are produced via germinal centers in a murine model resembling human lupus. *Front. Immunol.* **2016**, *7*. https://doi.org/10.3389/fimmu.2016.00396.

(146) Hunter, R., J. *Foundations of colloid science*, 2nd ed.; Oxford University Press Inc., 2004.

(147) Avvakumova, S. Gold nanoconjugates: preparation, characterisation and biological applications. PhD thesis, Università degli Studi di Milano, Milan, Italy, 2012.

(148) nanoComposix. Optical properties https://nanocomposix.com/pages/gold-nanoparticles-optical-properties (accessed Nov 27, 2018).

(149) Ojea-Jiménez, I.; Puntes, V. Instability of cationic gold nanoparticle bioconjugates: the role of citrate ions. *J. Am. Chem. Soc.* **2009**, *131* (37), 13320–13327. https://doi.org/10.1021/ja902894s.

(150) Derjaguin, B.; Landau, L. Theory of the stability of strongly charged lyophobic sols and of the adhesion of strongly charged particles in solutions of electrolytes. *Acta Physicochim. URSS* **1941**, *14* (1), 633–662. https://doi.org/10.1016/0079-6816(93)90013-L.

(151) Verwey, E. J. W.; Overbeek, J. Th. G. *Theory of the stability of lyophobic colloids: the interaction of sol particles having an electric double layer.*, 1st ed.; Elsevier: Amsterdam, 1948.

(152) Zhao, W.; Brook, M. A.; Li, Y. Design of gold nanoparticle-based colorimetric biosensing assays. *ChemBioChem* **2008**, *9* (15), 2363–2371. https://doi.org/10.1002/cbic.200800282.

(153) Capek, I. Dispersions based on noble metal nanoparticles-DNA conjugates. *Adv. Colloid Interface Sci.* **2011**, *163* (2), 123–143. https://doi.org/10.1016/j.cis.2011.02.007.

(154) Kaufman, E. D.; Belyea, J.; Johnson, M. C.; Nicholson, Z. M.; Ricks, J. L.; Shah, P. K.; Bayless, M.; Pettersson, T.; Feldotö, Z.; Blomberg, E.; Claesson, P.; Franzen, S. Probing protein adsorption onto mercapto-undecanoic acid stabilized gold nanoparticles and surfaces by quartz crystal microbalance and ζ-potential measurements. *Langmuir* **2007**, *23* (11), 6053–6062. https://doi.org/10.1021/la063725a.

(155) Qian, X.; Peng, X.-H.; Ansari, D. O.; Yin-Goen, Q.; Chen, G. Z.; Shin, D. M.; Yang, L.; Young, A. N.; Wang, M. D.; Nie, S. In vivo tumor targeting and spectroscopic detection with surface-enhanced raman nanoparticle tags. *Nature Biotechnol.* **2008**, *26* (1), 83–90. https://doi.org/10.1038/nbt1377.

(156) Horisberger, M.; Rosset, J.; Bauer, H. Colloidal gold granules as markers for cell surface receptors in the scanning electron microscope. *Experientia* **1975**, *31* (10), 1147–1149. https://doi.org/10.1007/BF02326761.

(157) Horisberger, M.; Rosset, J. Colloidal gold, a useful marker for transmission and scanning electron microscopy. *J. Histochem. Cytochem.* **1977**, *25* (4), 295–305. https://doi.org/10.1177/25.4.323352.

(158) Byzova, N. A.; Safenkova, I. V.; Slutskaya, E. S.; Zherdev, A. V.; Dzantiev, B. B. Less is more: a comparison of antibody-gold nanoparticle conjugates of different ratios. *Bioconjug. Chem.* **2017**, *28* (11), 2737–2746. https://doi.org/10.1021/acs.bioconjchem.7b00489.

(159) Geoghegan, W. D. The effect of three variables on adsorption of rabbit IgG to colloidal gold. *J. Histochem. Cytochem.* **1988**, *36* (4), 401–407.

(160) Hou, W.; Wang, S.; Wang, X.; Han, X.; Fan, H.; Cao, S.; Yue, J.; Wang, Q.; Jiang, W.; Ding, C.; Yu, S. Development of colloidal gold immuno-chromatographic strips for detection of Riemerella anatipestifer. *PLoS ONE* **2015**, *10* (3), e0122952. https://doi.org/10.1371/journal.pone.0122952.

(161) Shim, J.-Y.; Gupta, V. K. Reversible aggregation of gold nanoparticles induced by pH dependent conformational transitions of a self-assembled polypeptide. *J. Colloid Interface Sci.* **2007**, *316* (2), 977–983. https://doi.org/10.1016/j.jcis.2007.08.021.

(162) Potůčková, L.; Franko, F.; Bambousková, M.; Dráber, P. Rapid and sensitive detection of cytokines using functionalized gold nanoparticle-based immuno-PCR, comparison with immuno-PCR and ELISA. *J. Immunol. Methods* **2011**, *371* (1), 38–47. https://doi.org/10.1016/j.jim.2011.06.012.

(163) Singh, N.; Dahiya, B.; Radhakrishnan, V. S.; Prasad, T.; Mehta, P. K. Detection of Mycobacterium tuberculosis purified ESAT-6 (Rv3875) by magnetic bead-coupled gold nanoparticle-based immuno-PCR assay. *Int. J. Nanomedicine* **2018**, *13*, 8523–8535. https://doi.org/10.2147/IJN.S181052.

(164) Tripathi, K.; Driskell, J. D. Quantifying bound and active antibodies conjugated to gold nanoparticles: a comprehensive and robust approach to evaluate immobilization chemistry. *ACS Omega* **2018**, *3* (7), 8253–8259. https://doi.org/10.1021/acsomega.8b00591.

(165) Sotnikov, D. V.; Radchenko, A. S.; Zherdev, A. V.; Dzantiev, B. B. Determination of the composition and functional activity of the conjugates of colloidal gold and antibodies. *Eurasian J. Anal. Chem.* **2017**, *11* (3), 169–179.

(166) Malvern. Zetasizer Nano series user manual. Malvern Instruments Ltd. April 2013.

(167) Liu, X.; Huo, Q. A washing-free and amplification-free one-step homogeneous assay for protein detection using gold nanoparticle probes and dynamic light scattering. *J. Immunol. Methods* **2009**, *349* (1–2), 38–44. https://doi.org/10.1016/j.jim.2009.07.015.

(168) Jans, H.; Liu, X.; Austin, L.; Maes, G.; Huo, Q. Dynamic light scattering as a powerful tool for gold nanoparticle bioconjugation and biomolecular binding studies. *Anal. Chem.* **2009**, *81* (22), 9425–9432. https://doi.org/10.1021/ac901822w.

(169) Tam, J. O.; de Puig, H.; Yen, C.; Bosch, I.; Gómez-Márquez, J.; Clavet, C.; Hamad-Schifferli, K.; Gehrke, L. A comparison of nanoparticle-antibody conjugation strategies in sandwich immunoassays. *J. Immunoassay Immunochem.* **2017**, *38* (4), 355–377. https://doi.org/10.1080/15321819.2016.1269338.

(170) De Mey, J.; Moeremans, M.; Geuens, G.; Nuydens, R.; De Brabander, M. High Resolution light and electron microscopic localization of tubulin with the IGS (immuno gold staining) method. *Cell Biol. Int. Rep.* **1981**, *5* (9), 889–899. https://doi.org/10.1016/0309-1651(81)90204-6.

(171) McFarland, J. The nephelometer: an instrument for estimating the number of bacteria in suspensions used for calculating the opsonic index and for vaccines. *J. Am. Med. Assoc.* **1907**, *49* (14), 1176–1178. https://doi.org/10.1001/jama.1907.25320140022001f.

(172) Lemmer, Y.; Kalombo, L.; Pietersen, R.-D.; Jones, A. T.; Semete-Makokotlela, B.; Van Wyngaardt, S.; Ramalapa, B.; Stoltz, A. C.; Baker, B.; Verschoor, J. A.; Swai, H.; de Chastellier, C. Mycolic acids, a promising mycobacterial ligand for targeting of nanoencapsulated drugs in tuberculosis. *J. Controlled Release* **2015**, *211*, 94–104.

(173) Dávalos-Pantoja, L.; Ortega-Vinuesa, J. L.; Bastos-González, D.; Hidalgo-Álvarez, R. Colloidal stability of IgG- and IgY-coated latex microspheres. *Colloids Surf. B Biointerfaces* **2001**, *20* (2), 165–175. https://doi.org/10.1016/S0927-7765(00)00189-2.

(174) Bankar, A.; Joshi, B.; Ravi Kumar, A.; Zinjarde, S. Banana peel extract mediated synthesis of gold nanoparticles. *Colloids Surf. B Biointerfaces* **2010**, *80* (1), 45–50. https://doi.org/10.1016/j.colsurfb.2010.05.029.

(175) Zimbone, M.; Calcagno, L.; Messina, G.; Baeri, P.; Compagnini, G. Dynamic light scattering and UV–Vis spectroscopy of gold nanoparticles solution. *Mater. Lett.* **2011**, *65* (19–20), 2906–2909. https://doi.org/10.1016/j.matlet.2011.06.054.

(176) Horisberger, M.; Clerc, M. F. Labelling of colloidal gold with protein A: a quantitative study. *Histochemistry* **1985**, *82* (3), 219–223. https://doi.org/10.1007/BF00501398.

(177) Tokuyasu, K. T. Present state of Immunocryoultramicrotomy. *J. Histochem. Cytochem.* **1983**, *31* (1A_suppl), 164–167. https://doi.org/10.1177/31.1A_SUPPL.6186722.

(178) Tinglu, G.; Ghosh, A.; Ghosh, B. K. Subcellular localization of alkaline phosphatase in Bacillus licheniformis 749/C by immuno-electron microscopy with colloidal gold. *J. Bacteriol.* **1984**, *159* (2), 668–677.

(179) Spector, A. A.; John, K.; Fletcher, J. E. Binding of long-chain fatty acids to bovine serum albumin. *J. Lipid Res.* **1969**, *10* (1), 56–67.

(180) Huang, X.; Xu, Z.; Mao, Y.; Ji, Y.; Xu, H.; Xiong, Y.; Li, Y. Gold nanoparticle-based dynamic light scattering immunoassay for ultrasensitive detection of Listeria

monocytogenes in lettuces. *Biosens. Bioelectron.* **2015**, *66*, 184–190. https://doi.org/10.1016/j.bios.2014.11.016.

(181) BIODOT. BIODOT AD6000 system operating manual version 1.2. BIODOT September 2007.

(182) Sotnikov, D.; Zherdev, A.; Dzantiev, B. Theoretical and experimental comparison of different formats of immuno-chromatographic serodiagnostics. *Sensors* **2017**, *18* (2), 36. https://doi.org/10.3390/s18010036.

Appendix A

A1. LFT detection of *E. coli* 0157:H7 by gold labelled anti-*E. coli* antibody conjugate

The conditions and manufacture methods for this test are described in previous work in the group [129,130]. However, Bactrace™ polyclonal goat anti-*E.coli* O157:H7 (Kirkegaard & Perry Laboratories, USA) was used to conjugate to the gold nanoparticles (using the same conditions as for the original antibody).

This test follows a sandwich format in which anti-*E. coli* antibodies are striped onto the nitrocellulose and (different) anti-*E. coli* antibodies are labelled with gold nanoparticles and dried into the conjugate pad. The gold labelled antibodies will bind to the bacteria in the sample which has multiple antigenic sites and so will be bound on the test line forming a red line. In the absence of bacteria, no line will form. Results are shown in figure A1.

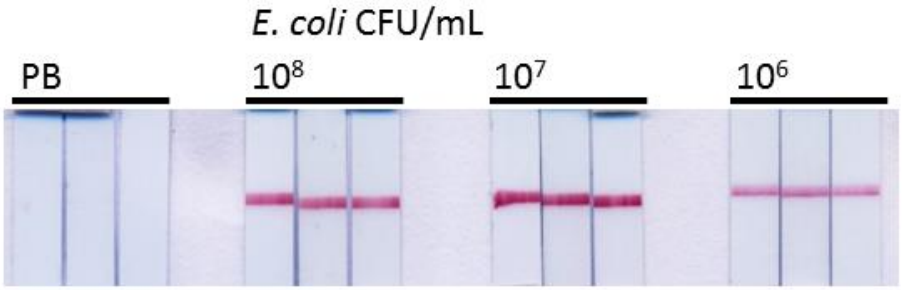

Figure A1: Detection of *E. coli* 0157:H7 by gold labelled anti-*E. coli* antibody conjugate. Three concentrations of E. coli bacterial suspension in dibasic phosphate buffer (PB) and PB alone were run on lateral flow tests with 1.5 µL of gold labelled anti-*E. coli* antibody conjugate (prepared at 0.01 mg/mL to OD 1 nanogold at pH 9, used at OD 10) dried in the conjugate pad. The strongest signal can be seen at a bacterial concentration of 10^7 colony forming units (CFU) per mL.

The darkest signal is visible at the middle concentration of bacteria tested. This phenomenon is discussed elsewhere [116]. For the present work, the relevant point is the effective detection of *E. coli* present in the sample.

Appendix B

B1. TEM images of conjugate interaction with MA nanoparticles

The interaction between gold labelled gallibody conjugates and PLGA nanoparticles with and without MA was visualised using TEM. The detailed sample preparation and imaging conditions are described in section 4.2.6. Herein are provided the TEM images of the gold labelled gallibody conjugates, and their interaction with PLGA nanoparticles with and without MA, for the remaining gallibodies not shown in the main text. Figure 4.26 shows the PLGA and PLGA-MA nanoparticles alone. Figure B1 shows the gold labelled gallibody conjugates on their own.

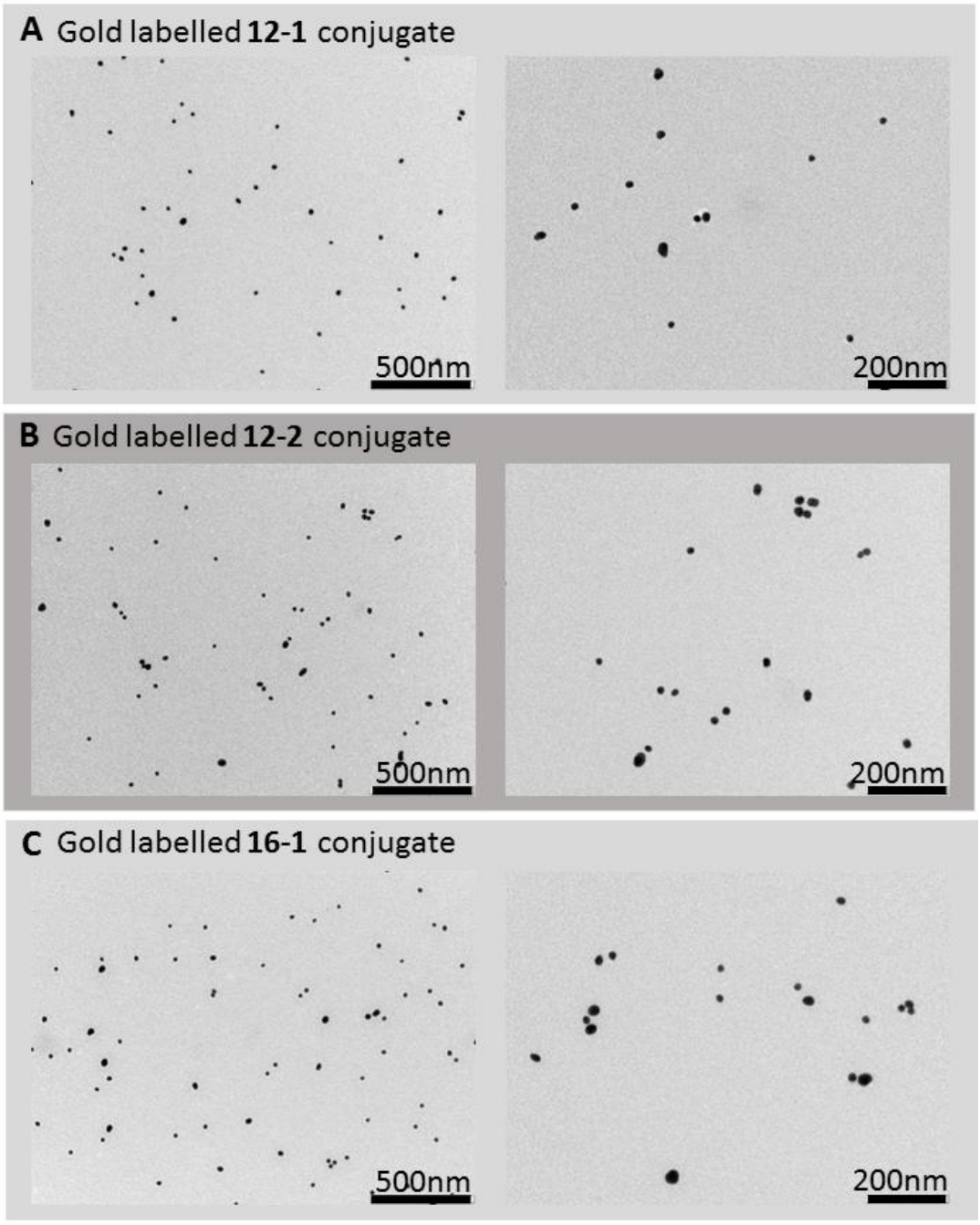

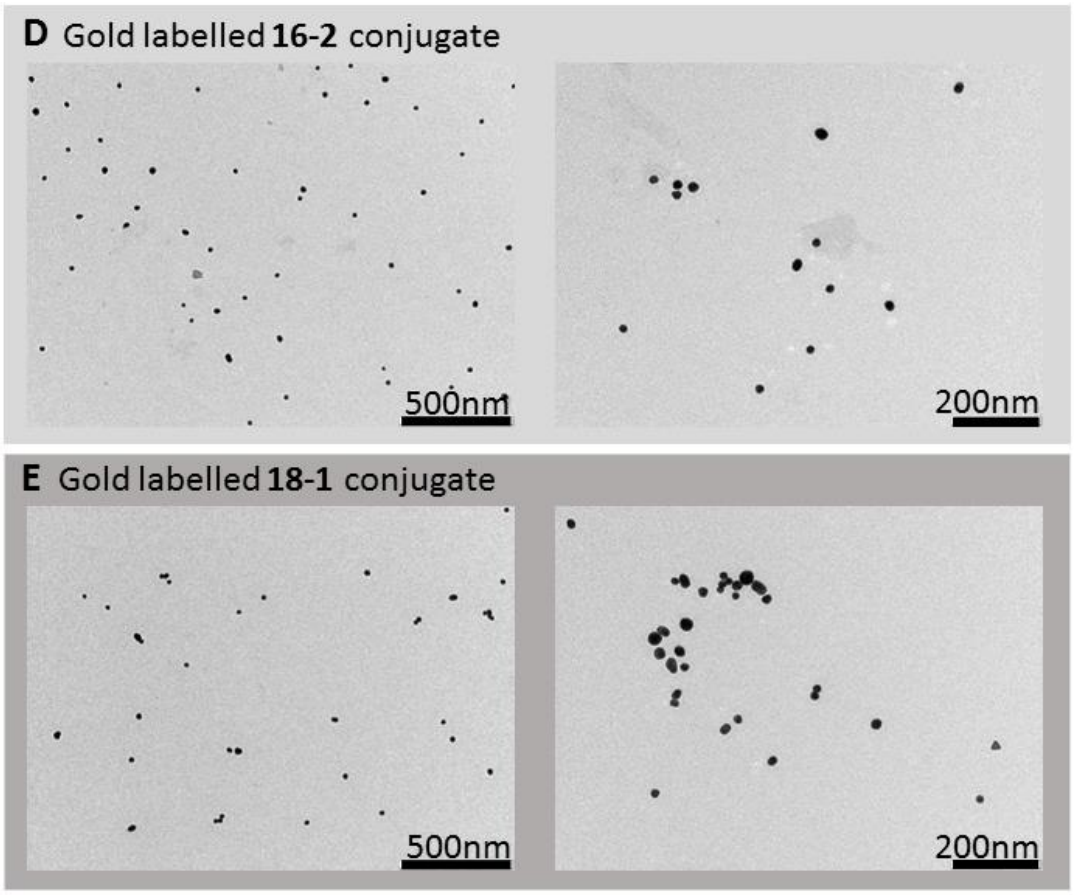

Figure B1: TEM images of gold labelled gallibody 12-1 (A), 12-2 (B), 16-1 (C), 16-2 (D) and 18-1 (E) conjugates. Gold nanoparticles conjugated to gallibodies as indicated are visible as black circles on a grey background. A 3 µL volume of OD 10 concentration of conjugate was used to coat a carbon coated grid.

As previously described in section 4.3.2.3 no discernible difference is observable between the conjugates of the different gallibodies, see also figure 4.27 for gold labelled gallibody 18- 2 and BSA conjugates. Figure B2 shows the interaction of these conjugates with PLGA nanoparticles without MA (Figure B2, left) and with MA (figure B2, right).

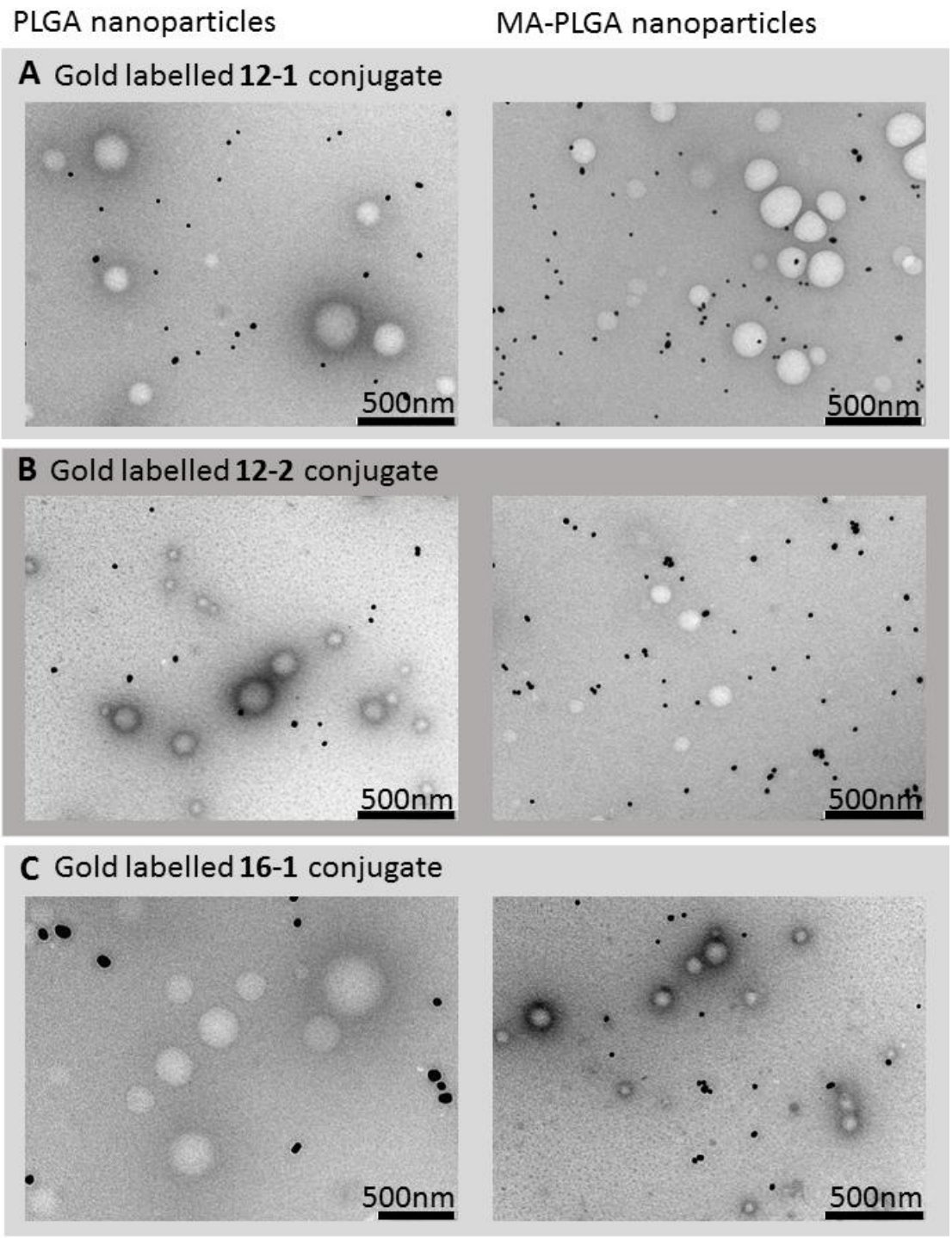
PLGA nanoparticles
MA-PLGA nanoparticles
A Gold labelled 12-1 conjugate
500nm
500nm
B Gold labelled 12-2 conjugate
500nm
500nm
C Gold labelled 16-1 conjugate
500nm
500nm

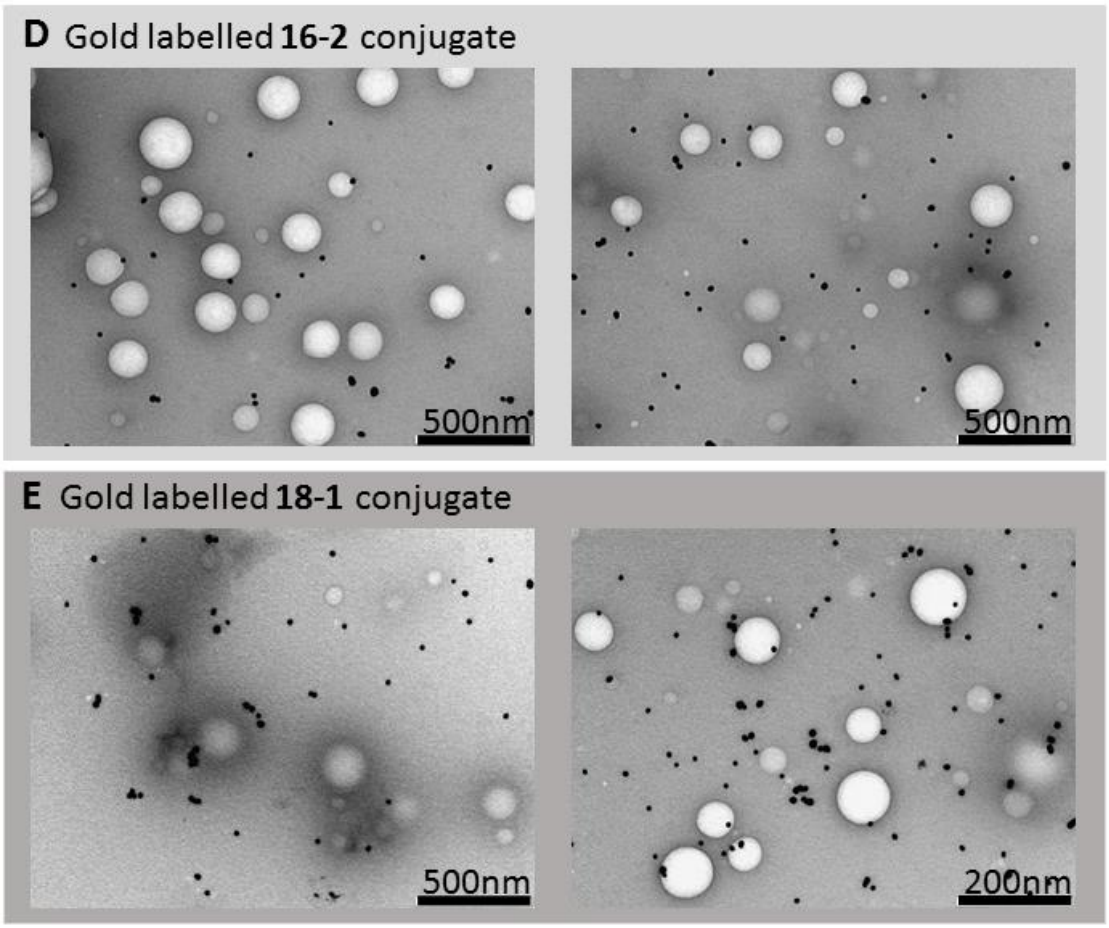

Figure B2: TEM images of gold labelled gallibody 12-1 (A), 12-2 (B), 16-1 (C), 16-2 (D) and 18-1 (E) conjugates incubated with MA-PLGA nanoparticles (right) and PLGA nanoparticles (left). PLGA nanoparticles are visible as white/lighter circles and gold nanoparticles conjugated to gallibodies as black circles on a grey background. A 3 µL volume of 1:1 mixed nanoparticle suspension and gold labelled conjugate was used to coat a carbon coated grid.

There is no closer association of the gold labelled conjugates with the MA containing PLGA nanoparticles. As discussed in section 4.3.2.3 no discernible difference is observable in the interaction of PLGA and PLGA-MA nanoparticles and the conjugates of the different gallibodies, see also figure 4.28 for gold labelled gallibody 18- 2 and BSA conjugates interacted with the PLGA nanoparticles. This data indicates that none of the gallibodies remain able to interact with MA-PLGA nanoparticles following conjugation.